Mandatory Declaration/Statements

Word Count of thesis: 51478

DECLARATION

This work has not previously been accepted in substance for any degree and is not being concurrently submitted in candidature for any degree.

Candidate name: **Pierre Lardeux**

Signature: 

Date: 16/07/2017

STATEMENT 1

This thesis is the result of my own investigations, except where otherwise stated. Where correction services have been used, the extent and nature of the correction is clearly marked in a footnote(s).

Other sources are acknowledged by footnotes giving explicit references. A bibliography is appended.

Signature: 

Date: 16/07/2017

STATEMENT 2

I hereby give consent for my thesis, if accepted, to be available for photocopying and for inter-library loan, and for the title and summary to be made available to outside organisations.

Signature: 

Date: 16/07/2017

PRIFYSGOL ABERYSTWYTH UNIVERSITY

Summary Sheet

This summary sheet should be completed after you have read the guidance notes. The completed sheet should be submitted by you to your Department/School/Institute at the time of submission of your work and the supporting documentation.

Candidate's Surname/Family Name	Lardeux
Candidate's Forenames (in full)	Pierre François Frédéric
Candidate for the Degree of	PhD
Academic year the work submitted for examination	2017

Summary / Abstract

Like in other mountain ranges around the world (the Southern Alps, the Himalayas and the Rockies), glaciers in the European Alps are a major source of fresh water for human usage and actively contribute to sea-level rise. Among European Alpine glaciers, this study shows that 12% are debris-covered, representing 54% in ice volume. Debris-covered glaciers are those presenting a layer of rock debris on their surface. This debris layer has an insulation effect on the glacier, which influences the response to climate change of this type of glacier. However, little is known about their long-term historical evolution and their future behaviour in the face of climate change. By directly comparing debris-covered glaciers and clean-ice glaciers at several different spatial and temporal scales, this study shows the large impact that debris-covered glaciers have on the Alpine cryosphere. On a glacier-wide scale, this study shows that, over 200 years, a debris-covered glacier (Glacier Noir in the French Alps) has retreated 21% less than an adjacent clean-ice glacier (Glacier Blanc) under the same climatic conditions (a temperature rise of minimum 2°C since the 1960s). On the scale of the European Alps, this study shows that debris-covered glaciers will extend the water supply of 145 million inhabitants. By the middle of the 21st century, debris-covered glaciers will contribute more than 22% of the total glacier runoff from the Alps, with a slower release than clean-ice glaciers. The importance of debris-covered glaciers in terms of behaviour and quantity could change the way they are represented in numerical models and could also change forecasts of the fate of glaciers in the European Alps under future climate scenarios.

Thesis submitted for the degree of Doctor of Philosophy (PhD)

July 2017

Debris-covered glaciers in the European Alps: from the glacier to the mountain range scale

Author: Pierre Lardeux

Supervised by: Prof. Neil Glasser

Dr. Tom Holt

Prof. Bryn Hubbard

Centre for Glaciology

Department of Geography and Earth Sciences

Aberystwyth University

Table of contents

Table of figures

Table of tables

ACKNOWLEDGEMENT

“No glaciers were harmed in the making of this PhD thesis."

First I would like to thank my parents for supporting me during these four years. ***Merci beaucoup Maman et Papa.***

Secondly I would like to thank my wife Patricia for helping in every aspect of the PhD, from the moral and financial support to all the English corrections she gave me. By the way, I still have trouble with my plurals.

Then I would like to thank my supervisors: Neil, thanks for the supervision, the support and for coming on the field in the Alps; Tom and Bryn: Thank you for the supervision and the manuscript revisions.

Concerning the fieldwork, I would like to thank Steffan Griffiths and Helena Pomfret for the two weeks spent on Glacier Noir. I also thank Katie Miles for the month spent there. I told you so that you would do a PhD.

For the help on the logistics of the fieldwork, I thank Emmanuel Thibert from IRSTEA and Delphine Six from LGGE.

In “les Ecrins” National Park, I would like to thank all the personnel on the field (promise, we will try to not lose the car key again) and at the headquarters, especially Clotilde Sagot for all the follow-up. All fieldwork was conducted thanks to the activity authorisation 060/2014 of “Ecrins” National Park and was funded by the British Society for Geomorphology under the Postgraduate Research Grant programme and by the Department of Geography and Earth Sciences of Aberystwyth University under the Postgraduate Discretionary Research Fund programme.

The historical aerial images and some other geospatial products were provided by the French National Institute of Geographic and Forestry Information under an education and research licence. The meteorological data have been provided by Météo France under the education and research licence reference MF_FO_GESFI.

I wish to also thank all the people I met at the 2013 BSG Windsor workshop in the UK, at the 2014 IGS International Symposium on Contribution of Glaciers and Ice Sheets to Sea Level Change in Chamonix, France, at the 2015 IGU Moscow Regional Conference in Russia, at the 2015 AGU Fall Meeing in San Francisco, USA, and at the 2016 EGU General Assembly in Vienna, Austria. Especially the following (not in order): Brian Whalley, Bethan Davies, Ruth Mottram,

Pipa Whitehouse, Emmanuel LeMeur, Christian Vincent, Valentina Radic, Catriona Fyffe, Evan Miles, Pascal Buri, Martin Kirkbride, Tobias Bolch, Mauri Pelto, Simon Cook, Matt Westoby, Duncan Quincey, Lionel Benoit, Jacob Steiner, David Rounce, Etienne Berthier, Sarah Boon, Emilie Collier, Gwenn Flowers, Philip Harder, Flavien Beaud, Mike Hambrey, Walter Immerzeel, Melaine Le Roy, Joseph Shea, Ali Giese. Thanks for all the discussion, pints and laughs.

Special thanks to Matthias Huss and David Bahr for their advice on their respective studies.

Special thanks to Lindsey Nicholson for giving me the opportunity to be convener of the debris-covered glacier EGU session.

Special thanks to Jonathan Carrivick and Tristram Irvine-Fynn to be my examiners.

And finally, I would like to thank all my friends who supported all the craziness of the last four years: Stephen Jennings, Marie-Jeanne Royer, Stephen Brough, Xavier, Kevin et Lucie.

CHAPTER 1: Introduction

Context

In the face of climate change, the cryosphere represents the second largest contributor to sea-level rise (SLR) after thermal expansion of the oceans (IPCC, 2013). Between 2003 and 2010, the entire cryosphere (glaciers, ice caps and ice sheets and their peripheral glaciers) contributed 1.48 $mm.a^{-1}$ ± 0.26 to SLR (Jacob et al., 2012). Almost a third of this rise rate (0.41 $mm.a^{-1}$ ± 0.08) comes from mountain glaciers and ice caps, which is equivalent to the Antarctica ice sheet contribution (0.46 $mm.a^{-1}$ ± 0.20) and slightly less than that from the Greenland ice sheet (0.62 $mm.a^{-1}$ ± 0.02). These numbers show the importance of glaciers and ice caps for the consequences of climate change (Kerr, 2013). Indeed, glacier and ice cap contribution to SLR is predicted to increase for the 21st century, potentially adding 0.098 m ± 0.002 total by 2100 (Radić and Hock, 2011).

Additionally, glaciers are considered in many areas worldwide as the main source of fresh water, directly usable for human consumption. For example, the Himalayan glaciers are known as the water towers of Asia (Immerzeel et al., 2010).

Multiple studies (Le Meur et al., 2007, Clarke et al., 2015) have already shown that glaciers are extremely vulnerable to climate change, especially mountain glaciers, and that some mountain glaciers will ultimately disappear before the rest of the cryosphere. Part of the uncertainty in the estimation of the glaciers' contribution to SLR, cause of concern in some mountain regions (e.g. the Himalayas) is that the determination of their fate arises from their sheer number, diversity and local conditions, e.g. state of the surface or solar radiation (Pfeffer et al., 2014). One aspect of glaciers' diversity resides in the state of their surface: clean-ice or debris-covered. For example, Himalayan glaciers are commonly debris-covered (Immerzeel et al., 2014) and more than expected are also in the European Alps (Chapter 5).

According to (Kirkbride, 2011), a debris-covered glacier is "A glacier where part of the ablation zone has a continuous cover of supraglacial debris across its full width". Kirkbride adds that some authors consider that 50% minimum of the ablation area should be covered for the glacier to be defined as debris-covered. This percentage appears subjective as it seems that a debris layer of 40% of the ablation area will have major effects on the glacier behaviour similar to a debris layer of 50%. Consequently, only the full width coverage is retained here as a criterion for definition. As demonstrated in Chapter 5, this definition is not binary (debris-

covered or not) and other definitions can be found in the literature to cover the entire spectrum of ice masses with supraglacial debris (Davies et al., 2013).

Due to their characteristics and importance for humans, a better understanding of debris-covered glaciers' response to climate change is important to reduce the uncertainty they generate in SLR estimation. It is also important to study debris-covered glaciers as they can be found in almost every mountain range around the world (WGMS and NSIDC, 1989, updated 2012). The following table lists (non-exhaustively) some studies and locations.

CH1 – Table 1: Debris-covered glaciers location, example and associated studies.

Mountain Range	Example of glacier	Study
Alaska, USA	Sherman Glacier	Marangunic, 1972, Shugar et al., 2012
Andes, South America	Glaciar Exploradores	Aniya et al., 2007a, Aniya et al., 2007b, Janke et al., 2015
Asian High Mountains	Ngozumpa glacier	Benn et al., 2012, Nicholson and Racoviteanu, 2013, Juen et al., 2014, Banerjee and Shankar, 2014, Immerzeel et al., 2014, Collier et al., 2015, Anderson and Anderson, 2015, Rounce et al., 2015b, Herreid et al., 2015
Caucasus, East Europe/Central Asia	(Inventory)	Tielidze and Wheate, 2017
Dry Valleys, Antarctica	Mullins Glacier	Levy et al., 2006, Shean and Marchant, 2010, Mackay et al., 2014
European Alps, Europe	Miage glacier	Thomson et al., 2000, Mihalcea et al., 2008a, Caccianiga et al., 2011, Collier et al., 2014, Lardeux et al., 2015
Rockies, North America	Dome Glacier	Mattson, 2000
Southern Alps, New Zealand	Tasman Glacier	Anderson and Mackintosh, 2012, Haritashya et al., 2015, Kirkbride, 2000
Torngat Mountains, Canada	(Inventory)	Way et al., 2014

Despite all of these studies on the past and current behaviour of debris-covered glaciers, their response to climate change is still poorly understood. Debris-covered glaciers are, however, contributing to sea-level rise and are in some mountain ranges (e.g. the Himalayas) the main/only source of fresh water (Immerzeel et al., 2013) and surely to the uncertainty associated with glacier contribution and evolution. Part of this uncertainty lies with the potential disturbances in the hydrological system created by the debris layer compared to clean-ice glaciers (Fyffe, 2012, Miles et al., 2017). The debris layer can modify the spatial origin of the meltwater by creating differential melting on the surface of the glacier and ultimately creating supraglacial ponds or lakes, storing the meltwater until a breach. This breach can be in the ice and the water of the supraglacial pond/lake becomes en- or subglacial (Röhl, 2008). The breach can also happen through the debris layer, producing supra-debris channels instead of supraglacial channels, preventing the meltwater from being routed en- or subglacially (Sakai et al., 2000). Additionally, the debris can block certain channels (supra-, en- and subglacially) potentially re-routing or closing the hydrological system.

The simple presence of debris on the surface of a glacier has the potential to produce a large difference in the hydrological system of debris-covered glaciers compared to clean-ice glaciers (e.g. in the case of Glacier Noir and Glacier Blanc; Stott et al., 2003, Stott et al., 2004, Stott et al., 2006). Rock debris can also produce major differences in the geomorphological system of debris-covered glaciers. Compared to a clean-ice glacier, a debris-covered one carries a vast amount of sediment, creating features such as very large moraines (Lardeux et al., 2015) which in turn can create moraine-dammed lakes, posing major threats such as glacial lake outburst floods (Benn et al., 2012, Westoby et al., 2014). As such, studying debris-covered glaciers could be valuable to understand these geohazards and their associated potential human catastrophes.

The large amount of sediment carried by debris-covered glaciers and the associated massive features can also create confusion on the interpretation of paleo-features and their relation to paleo-climates. For example, this is the case in the interpretation of the Waiho Loop moraine in New Zealand (Santamaria Tovar et al., 2008, Shulmeister et al., 2009) where this feature has been misinterpreted as the results of a sudden climate change in the region, when it is potentially due to a rock avalanche on Franz Joseph Glacier. In the process, this glacier became – at least temporarily – debris-covered. A better understanding of the impact of a

debris layer on the behaviour of a glacier (i.e. advance or stagnation) could help to resolve similar cases around the world.

Finally, a better definition, detection (especially via satellite imaging) and description of debris-covered glaciers could help us understand the geomorphology of other planets. Indeed, debris-covered glaciers have similar geometrical characteristics to glacial-like features on Mars (Hubbard et al., 2014, Brough et al., 2016).The presence of potential debris-covered glaciers on another planet of the Solar System broadens the implications and the relevance of studies on this particular type of glacier.

Origins of debris-covered glaciers

Debris-covered glaciers are also named debris-mantled (Benn et al., 2001, Hambrey et al., 2008) or buried glaciers (Lliboutry, 1965) and should not be confused with rock glaciers, which are mainly rocks with interstitial ice (Østrem, 1971). However, both debris-covered and rock glaciers seem to be part of a continuum of ice masses with no debris (i.e. clean-ice glaciers) to rock debris masses with almost no ice (i.e. rock glaciers) or no ice at all (i.e. scree). This continuum includes a suite of ice-cored geomorphological features (Hamilton and Whalley, 1995, Davies et al., 2013): for example, ice-cored moraines or dead-ice moraines. It is not yet clear if those different features represent different evolutionary stages of a debris-covered glacier, starting with a clean-ice glacier with some debris and ending with a rock glacier with some ice.

While the origins of a debris-covered glacier remain unclear, the origins of the supraglacial debris have been clearly identified. The debris originate from three different sources: sub- and englacial sediments, rock falls and avalanches, and finally scree slopes. Due to the ice flow or the melting, bedrock debris that were mostly carried subglacially or in certain cases englacially, surface in the ablation area and then are carried supraglacially (De Blasio, 2014). Rock falls and avalanches can also be the origin of a sudden extended debris layer on a glacier surface. Due to the lower friction offered by the glacier surface, rock falls and avalanches on glaciers present larger extents and lower thicknesses than those landing on other terrain (Deline et al., 2015). Often rock avalanches are triggered by earthquakes (Marangunic, 1972, Shugar et al., 2012), and when landing, can trigger an advance of the glacier (Reznichenko et al., 2011). This type of avalanche-borne debris layer has been recognised in paleo-glacier

reconstructions (Carrasco et al., 2013). At higher elevation, where mountain sides present a lower extent above the glacier surface, snow avalanches provide debris, as they are mixed with ice and rock (Banerjee and Shankar, 2014). Finally, the last and possibly the most common source of debris for debris-covered glaciers is scree slopes surrounding the glacier (Vivian, 1967). In the Northern hemisphere, scree slopes providing debris are generally oriented southwest-facing (Nagai et al., 2013) where cryoclasty (frost weathering) is happening due to the strong freeze-thaw cycle of these slopes (Hales and Roering, 2005). Following the same principle, unconsolidated lateral moraines, which are collapsing after glacial retreat, can become a large source of debris on the surface of the glacier (Lardeux et al., 2015; Chapter 2).

Many studies focus on the direct effects created by this debris layer of different origins (Nakawo et al., 2000): i.e. the modification of the albedo by the debris (Azzoni et al., 2016), the insulation effect and its consequences (Juen et al., 2013), modification of the velocity (Haritashya et al., 2015), and hydrology of meltwater ponds (Röhl, 2008). All these effects of the debris layer require different methods of study. Debris-covered glaciers have already been observed and modelled using the following techniques:

- Physical modelling to quantify the insulation effect (Reznichenko et al., 2010);
- Numerical modelling to study the insulation effect (Evatt et al., 2015), the energy balance (Fyffe et al., 2014, Rounce et al., 2015), the mass balance (Rowan et al., 2015), specific ice movement such as ice cliffs back-wasting (Steiner et al., 2015), and debris transport (Wirbel et al., 2017);
- Field measurement of the insulation effect (Vincent et al., 2016), of meteorological parameters (Nicholson and Benn, 2013), of the debris thickness with ground penetrating radar (Shean and Marchant, 2010, Wu et al., 2013), and of volume loss (Brun et al., 2016);
- Remote sensing to estimate debris thickness (Mihalcea et al., 2008, Schauwecker et al., 2015, Sasaki et al., 2016), for evaluating the mass balance (Capt et al., 2016), and for estimating supraglacial ponds evolution (Miles et al., 2016).

Debris-covered glaciers are also studied from a biological point of view, as the debris layer represents its own ecosystem (Caccianiga et al., 2011).

Research questions, aims and objectives

Even on large glaciers, especially in the Himalayas, the scope of most studies is mainly local on both the spatial and temporal level, such as one part of the debris area and one melting season (Lejeune et al., 2013). To better understand the impact and importance of debris-covered glaciers more broadly, the present study looks at a larger scale as well as on a spatial scale (entire glacier and mountain range) and on a temporal scale (two centuries) in the European Alps. The research questions of this thesis are:

- Question A. Do debris-covered glaciers behave differently from clean-ice glaciers on the long-term and on the glacier-wide scale? If so, is it due to the debris layer?
- Question B. What is the importance of debris-covered glaciers at the mountain range scale, in the European Alps?
- Question C. In terms of method development, is Structure-from-Motion photogrammetry a viable technique at a landscape scale without specific fieldwork for glaciology?

Question A

Do debris-covered glaciers behave differently from clean-ice glaciers on the long-term and on the glacier-wide scale? If so, is it due to the debris layer?

To answer the first part of the question, two similar glaciers are needed with one debris-covered and the other clean-ice. These glaciers have to be close to one another, so they experience the same climatic conditions. Their size, orientation and elevation should be as similar as possible. Data series on these glaciers should be longer than 50 years to be considered long-term. One study site with two glaciers that fit these requirements is Glacier Noir (debris-covered) and Glacier Blanc (clean-ice) located in “les Ecrins” National Park in the French Alps. I reconstructed around 200 years of length and surface area variations for both glaciers plus around 60 years of elevation change. Additionally, it was possible to establish a 60-year time series for the velocity of Glacier Noir.

To answer the second part of the question, mass balance series would be ideal. Unfortunately, only a short time series (less than 20 years) exists for only one of the glaciers - Glacier Blanc. Therefore, an evaluation of the main glaciological controls that can explain long-term

behaviour difference is needed. These controls are: climate (assumed identical), micro-climate (no data), direct solar radiation (calculated), debris cover (extension mapped but scarce thickness data), bedrock topography (qualitatively known only at a former terminus position due to glacial recession), basal conditions (no data). The limited available data will force the conclusions of the role of the debris cover to be limited and considered only as clues on the origin of behavioural differences.

The objective for this part of the project is to establish time series of geometric changes that are precise and accurate for Glacier Noir and Glacier Blanc over a 200-year period. This corresponds to Chapter 4.

Question B

What is the importance of debris-covered glaciers at the mountain range scale in the European Alps?

The glaciological importance of debris-covered glaciers in the Alps could be determined by creating an inventory of the different type of glaciers (which need to be defined) present in the mountain range. Using the Randolph Glacier Inventory (Pfeffer et al., 2014), Google Earth imagery (©Google, 2015-2016) and dataset from Huss and Farinotti (2012), this inventory will give access to statistics including the number of glaciers of each type, glacial surface area and volume, average thickness and slope per type, etc. Even with this dataset, it would be difficult to scale-up the results used to answer question A, as many parameters are still unknown for every glacier in the Alps, such the basal conditions.

The human importance of debris-covered glaciers can be assessed by looking at the impact of this type of glacier on the fresh water runoff from the Alpine watersheds. As a first approach, a simple mathematical model combined with the data from Huss (2011) provides the contribution of debris-covered glaciers per watershed from 2008 to 2100.

The objective for this part of the project is to establish classification and an inventory of the different type of glaciers present in the European Alps. This corresponds to Chapter 5.

Question C

Is Structure-from-Motion (SfM) a viable technique at a landscape scale without fieldwork for glaciology?

To answer this methodological question, the limitation of SfM needs to be assessed on a small and well-determined glacial area. Using a small number of aerial images (2 to 9) as well as a small number of control points (5 to 10), I evaluated the impact on 2D georeferencing and on glaciological measurement such as terminus position. Then I conducted the landscape scale application using 7 to up to 149 images from different years between 1952 and 2013 with around 150 control points to produce orthoimages and DEM covering a 400km^2 area. Both the small and large scale SfM calculations were realised without any fieldwork.

The objective of this part of the project was to determine if that the combination of historical images with no fieldwork is a viable option for large scale glaciological studies. This corresponds to Chapter 3 and 4.

The answer to all three questions are discussed in Chapter 6.

Overview of this thesis

These research questions were suitable for the thesis to be written as a series of papers. Consequently, this manuscript is structured as follows:

- Chapter 2 is composed of two part, describing the field site:
    - An article published in Journal of Maps in 2015 (Lardeux et al., 2015).
    - Additional information concerning the field site itself and not only the map.
- Chapter 3 is composed of two parts to explain the different methods used:
    - An overall explanation of all the methods (remote sensing and fieldwork).
    - An article rejected by Journal of Glaciology in August 2017 and currently in revision (June 2018), which described and evaluated the new method developed to answer the above research question.

- Chapter 4 is an article rejected by Journal of Glaciology in September 2017 and currently in revision (June 2018), which concerned the geometric changes of Glacier Noir and Glacier Blanc over two centuries.
- Chapter 5 is an article rejected by Nature Geoscience in October 2017 and currently in revision (June 2018), concerning the debris-covered glacier inventory in the European Alps and their influence on the hydrological system and future water supply of this mountain range.
- Chapter 6 is the general discussion and conclusion of this thesis. As each article has its own discussion, this Chapter summarises conclusions for the entire project.
- A reference section for Chapters 1 and 6. Each article has its own reference section.
- the Appendix, grouping the published version of the Journal of Maps paper and additional fieldwork and modelling results, supplemental to the main body of work.

Each article has its own set of figures and tables. The mention in the text of these figures/tables is relative to each Chapter. However, in order to list all the figures and tables together, each caption has now the prefix "CHx - ", where x is the number of the Chapter. For example, in Chapter 2 "[…] *in the French Alps (Figure 1), Glacier Noir is […]*" refers to the Figure 1 of the Chapter 2 and the caption is "*CH2 - Figure 1: Overview map presenting […]*".

CHAPTER 2: Field site

Glaciological and geomorphological map of Glacier Noir and Glacier Blanc, French Alps

Published in Journal of Maps online on 17th June 2015

Lardeux, P., Glasser, N.F., Holt, T., & Hubbard, B. (2015). Glaciological and geomorphological map of Glacier Noir and Glacier Blanc, French Alps. *Journal of Maps, 12*(3), 582-596. doi:10.1080/17445647.2015.1054905

Print version: see Appendix [I]

Abstract

This paper presents and describes a glaciological and geomorphological map of Glacier Noir and Glacier Blanc, French Alps. Glacier Noir is a debris-covered glacier and is adjacent to Glacier Blanc, a clean-ice (debris-free) glacier. The glaciological and geomorphological evolution of Glacier Blanc is well-known, but the evolution of Glacier Noir is poorly understood, as is the case for many debris-covered glaciers globally, despite their importance in a number of mountain ranges around the world (e.g. European and Southern Alps, the Himalayas and the Rockies). The accompanying map was created by manually digitising aerial ortho-images and historical georeferenced photographs from 1952-2013. The main glacial and geomorphological features of both glaciers were mapped including: debris cover, crevasses, moraines, hummocky terrain and scree areas. Hydrological features (supra- and pro- glacial streams and meltwater ponds) were also mapped. The map illustrates the key differences between Glacier Noir and Glacier Blanc, and is important for understanding future glaciological and geomorphological changes.

Introduction

Mountain glaciers are currently contributing ~27 % of the observed global sea level rise with a large uncertainty of more than 20% (Jacob et al., 2012). Although the contribution of debris-free or clean-ice glaciers is well-known, debris-covered glaciers and their contribution are still poorly understood. Debris-covered, or debris-mantled glaciers, are those where part of the surface of the ablation area, is covered by a layer of rock debris including dust, ash and boulders of various sizes (Hambrey et al., 2008, Cogley et al., 2011, Singh et al., 2011).

Debris-covered glaciers represent ~5% of all mountain glaciers worldwide (WGMS and NSIDC, 1989, updated 2012) and the rate of sea-level rise attributed to them differs from clean-ice glaciers due to the insulating effect of the debris layer (Reznichenko et al., 2010). A better understanding of long-term glaciological processes on debris-covered glaciers is needed to reduce the uncertainty of their contribution to global sea level.

The debris layer on debris-covered glaciers derives from a number of sources, most notably valley-side rockfalls (Deline and Kirkbride, 2009). These rockfalls can be significant at the glacier-scale, such as is the case for the Black Rapids Glaciers (Shugar et al., 2012) and the

Sherman Glacier (Marangunic, 1972) rock avalanches. These rock avalanches form specific deposits characterised by the regular thickness of the debris layer and angular grains (Hewitt, 2009). Other sources of debris include collapsing lateral moraines (Hambrey and Ehrmann, 2004) and debris elevated from subglacial and englacial positions to supraglacial positions (Goodsell et al., 2005). The debris from these latter sources is more heterogeneous and may contain a mix of sub-angular to sub-rounded grains.

The supply of surface debris to the glacier's terminus has great control over the geomorphological processes occurring on and adjacent to that glacier (Reznichenko et al., 2011) and often results in the formation of very large geomorphological features, such as the Waiho Loop moraine in the Southern Alps, New Zealand (Tovar et al., 2008). From a glaciological point of view, the elevation of the snout of a debris-covered glacier would be lower than a similar clean-ice glacier. Specific glaciological and geomorphological dynamics of a debris-covered glacier are beginning to be considered in the interpretation of glaciated landscape and landforms (Reznichenko et al., 2012, Carrasco et al., 2013). Accurate interpretation and attribution of features to debris-covered glaciers can lead to re-interpretation of palaeo-climatic conditions contributing to their formation (Shulmeister et al., 2009, Vacco et al., 2010).

Here, a detailed map is presented in order to provide the basis for investigating the geomorphological context of, and relationships between, a debris-covered glacier (Glacier Noir) and an adjacent and morphometrically-similar clean-ice glacier (Glacier Blanc). This map will also help the re-interpretation of palaeo-landforms where debris-covered glaciers may have contributed to their formation.

Study site

Located in the Haute Vallée de St Pierre in the "Écrins" National Park (Parc National des Écrins) in the French Alps (Figure 1), Glacier Noir is a 4.5 km long debris-covered glacier with a surface area of 3.8 km². In contrast, the surface of adjacent Glacier Blanc is debris-free. Both glaciers were confluent in the Pré de Madame Carle field during the Little Ice Age (LIA, 16th to mid-19th century, [Mann, 2002]). Pré de Madame Carle was a grazing field before it was transformed into an outwash plain by the advance of the glacier during the LIA (Letreguilly and Reynaud, 1989).

Glacier Noir (44°54’58” N, 6°23’03” E) has an elevation range of 2200 to 3600 m and comprises a main trunk (2200 to 2900 m in elevation) of 1.1 km² (2.6 km long), orientated WSW-ENE with a single tributary (2500 to 3600 m in elevation) of 2.7 km² (3.2 km long), orientated SSW-NNE. The tributary is now an independent glacier - named here as Glacier Noir Sud - having separated from the main glacier between 2009 and 2013.

Glacier Blanc (44°56’25” N, 6°22’42” E) has an elevation range of 2500 to 4000 m and is 5.5 km long (4.8 km²), being orientated SW-NE in its upper section (3050 to 4000 m in elevation), which is relatively flat and then NW-SE in the steep crevassed area approaching its terminus (2500 to 3050 m in elevation). This main trunk is fed by six individual accumulation basins (cirques).

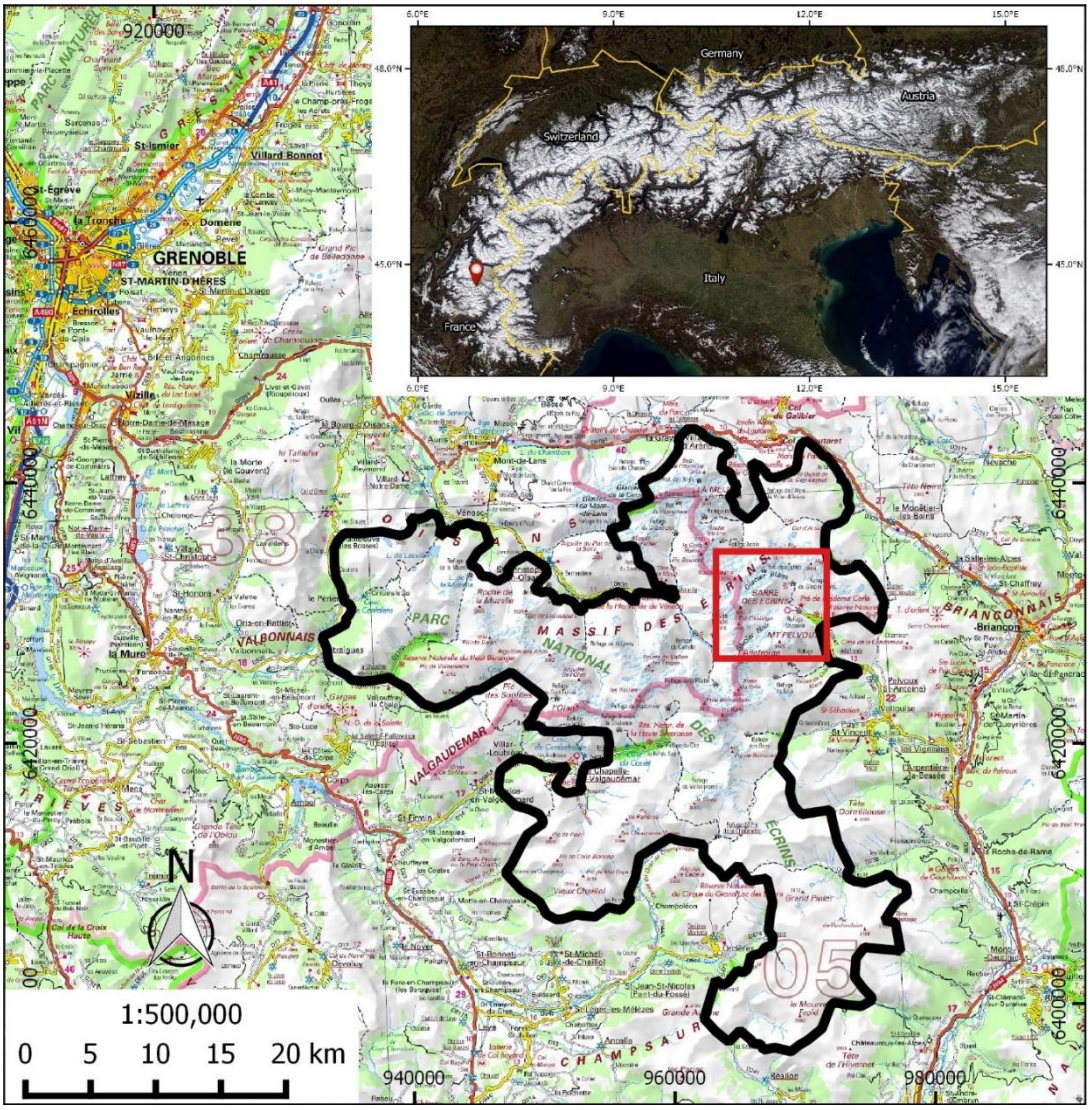

CH2 - Figure 1: Overview map presenting the position of the study site (red rectangle) in “Écrins” National Park (solid black line). *Background map: IGN ©SCANREGIONAL. Inset: location (red marker) of the study site in the European Alps. Background image: ©NASA.*

Both glaciers have attracted previous glaciological research, with Glacier Blanc being more widely studied (Allix, 1922, Allix, 1929, Vivian, 1967a, Letreguilly and Reynaud, 1989, Reynaud and Vincent, 2000, Rabatel et al., 2002, Reynaud and Vincent, 2002, Thibert et al., 2005, Rabatel et al., 2008, Rabatel et al., 2013), than Glacier Noir (Allix, 1922, Allix, 1929, Vivian, 1967b, Cossart et al., 2006, Stott and Mount, 2007, Mount and Stott, 2008). The most recent studies have focused on sediment transport in the proglacial stream at Glacier Noir (Stott and Mount studies) and on the variation of the equilibrium line altitude (ELA) at Glacier Blanc (Rabatel's studies) and its determination by optical remote sensing.

Data and methods

Data sources

Mapping was conducted by manually digitising aerial ortho-images (six RGB tiles of 5 km by 5 km with a 50 cm resolution) using QGIS software (Section 3.2). The National Institute of Geographic and Forestry Information (IGN) provided the ortho-images. These images are part of the French national database, ©BDORTHO, and were taken during summer 2013.

The toponymy comes from the IGN topographical map (Meije-Pelvoux 3436 ET), which is included in the database ©SCAN25. The scale of the map is 1:25000.

The dates of formation of the moraines are from various sources:

- A public engagement booklet edited by the "Écrins" National Park (Écrins, 2005) on the glaciers present in the park.
- Unpublished historical and archive documents owned by the "Écrins" National Park.
- Archived ortho-images and georeferenced aerial photographs extracted from the historical IGN database. This database is the compilation of previous versions of the ©BDORTHO, grouping aerial scenes from 1952 to 2009.

The archived ortho-images were also used for the photo-interpretation of moraines, which is sensitive to the position of shadows (Otto and Smith, 2013).

The interpretation of the ortho-images was verified and refined by direct field observation between mid-August and mid-September 2014, particularly where the ortho-images have

shadowed areas or other areas where a misinterpretation is possible. All ground-based photographs presented in this article and on the map were taken during the same period.

Software and digitising tools

All mapping and digitising was conducted in ©QGIS software (QGIS, 2014), a free and open source geographic information system. Multiple versionsof QGIS have been used (see Software Section below) as well as the updated versions of the following plugins:

- autoSaver plugin, for automatic saves of the work in progress
- Digitizing Tools plugin, for additional digitising options
- GdalTools plugin, for elevation data extraction
- Georeferencer GDAL plugin, for the georeferencing of the aerial images
- GPS Tools plugin, for the import of field data
- Multipart Split plugin, for better management of multiple features in the same layer

The map was designed using the composer module of QGIS. The ground-based photographs presented on the map were modified using ©Adobe Illustrator CS2.

The digitisation of the ortho-images was conducted within a scale range of 1:1000 to 1:10000, allowing a global view of each feature across the study site's large altitudinal range.

Map design

General principles

The mapped features are divided into four themes with additional background data: glaciological, geomorphological, hydrological and anthropogenic. The different colour schemes used are theme dependent. Glaciological features are depicted using only black and white colours. Geomorphological features are depicted in brown to yellow colours.In addition, vegetated features are presented in dark green. Hydrological features (ponds and streams) are depicted using different hues of blue. Although not essential to the map's principal purpose, anthropogenic features which provide important context (e.g. buildings) are depicted in grey. To bring contrast to the map, the background contour lines are depicted in light green.

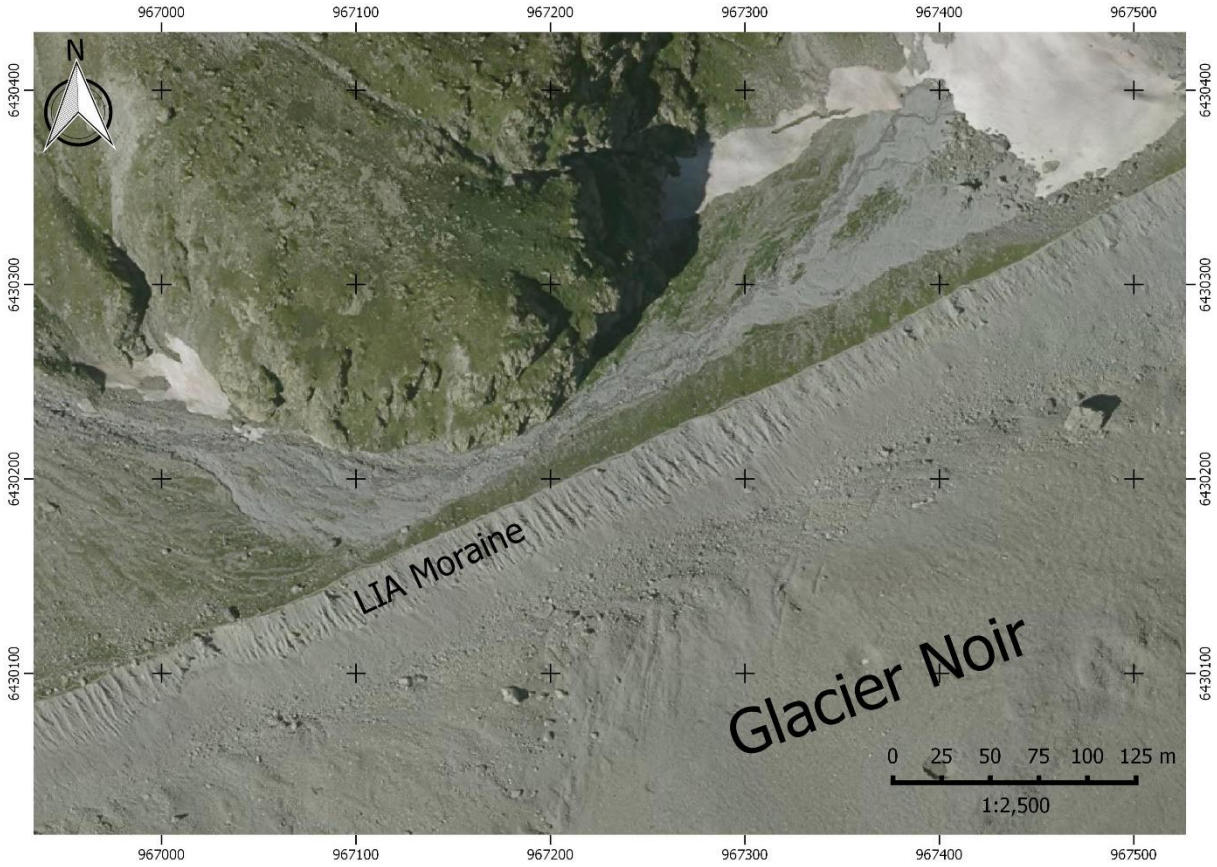

***CH2 - Figure 2: Extract of 2013 orthophotograph illustrating the difficulties in determining the edge of Glacier Noir**, especially in the area between the northern border and the LIA moraine.*

Specific digitising cases

Moraines have been digitised only as moraine ridges. Ridges are the best indicators of the position of a moraine and so help to understand the retreat history of glaciers. The extent of moraines has not been digitised to not overload the map with more polygons. From field observations, crevasses and crevasse traces represent the large majority of the structural features on Glacier Blanc and Glacier Noir. However, due to the ortho-image resolution and the heavily disturbed area in the curve of Glacier Blanc, the recognition of foliations and/or lineations was particularly difficult, and consequently, some might have been digitised as crevasses.

In addition to digitising active and relict meltwater ponds, their areas of topographical influence (see Section 4.3.1) was also mapped as separate features because of their importance in the melting of debris-covered glaciers (Sakai et al., 2000).

Description of the mapped features

The identification - on aerial images and in the field - of the mapped features is a combination of professional experience and comparison to academic descriptions such the ones presented in Singh et al., 2011, Bennett and Glasser, 2009 or Benn and Evans, 1998.

Glaciological features

Glacier outlines

Glaciers were identified using the following definition: “mass of ice presenting active flow pattern” which is a simplified version of the GLIMS definition (Rau et al., 2005). This definition was used as a guide to outline digitization of both glaciers, although defining the lateral and frontal boundaries was easier for Glacier Blanc (i.e., between clean ice and proglacial debris) than for the ablation area of Glacier Noir, where the debris cover makes the identification of the glacier limit (Figure 2) and flow patterns more difficult (Cogley et al., 2011; Paul et al., 2013).

Debris cover

For this map, we defined debris cover as where there is no clean ice visible. The precise limits of debris-covered areas are difficult to define because of the continuous variations in debris concentration that are encountered in the field. In addition, the debris cover must have been persistent, i.e. appearing in images separated by at least one year. By these criteria, no debris cover was mapped on Glacier Blanc because the debris cover areas are temporary and localised, and are rapidly buried by snow in the accumulation area, or removed from the surface through crevasses in the ablation area.

Crevasses

Crevasses form when the extension strain exceeds a critical threshold (Vaughan, 1993) resulting in fields of fractures with distinctive lengths and orientations. Crevasses were identified on aerial images as elongated holes in the surface of the ice and then confirmed visually on the field. This fractured area is particularly visible on the lower section of Glacier Blanc where the glacier changes direction and becomes steeper.

On Glacier Noir, most of the crevasses are filled by debris that leaves only traces of the crevasses visible on the surface. These crevasse traces create only low relief perturbations and are consequently not visible by direct observation in the field.

Nunataks and bare-rock areas

Nunataks are areas of glaciers where the bedrock is exposed (Singh et al., 2011). Nunataks and other bare-rock areas are mainly present on the south-facing side of Glacier Blanc. The locations of these rock exposures vary, as they are dependent on the ice thickness and the ice flow. Consequently, the features mapped are only those present when the aerial images were taken in 2013, as for streams (Section 4.3.2).

Geomorphological features

These features are all related to the former presence of a glacier.

Moraines

Moraines are landforms built by the deposition by glaciers of glacial sediments (Singh et al., 2011). Moraines were identified on aerial images as linear convex features varying in length from a few metres to hundreds of metres positioned in the proglacial area. Moraines can be deposited on older geomorphological features (e.g. other moraines) and also can be crossed by streams. There are many types of moraines (Bennett and Glasser, 2009); around Glacier Noir and Glacier Blanc these are mostly frontal and lateral moraines and were mapped accordingly.

During the LIA, Glacier Noir and Glacier Blanc had a common terminus and produced a large moraine, like many other alpine glaciers. This LIA frontal moraine has been partially washed away by the proglacial stream, and currently, the only large LIA moraine intact is the lateral moraine of Glacier Noir. This moraine is recognisable because of its large size compared to the surrounding moraines (Figure 3).

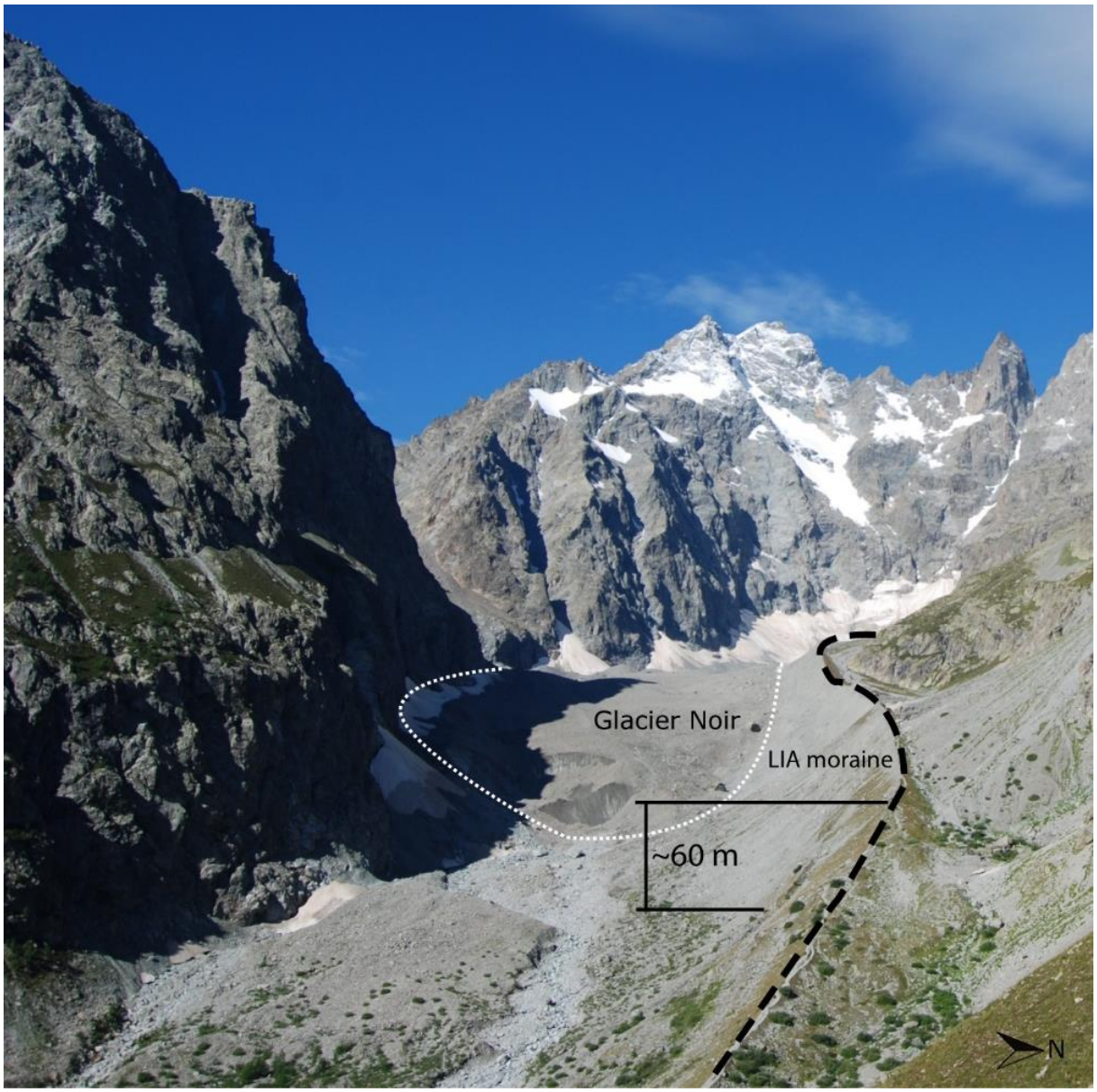

CH2 - Figure 3: Glacier Noir (white dotted line) and its LIA moraine (black dashed line). *The LIA moraine is the largest geomorphological feature in the study site and its ridge is constantly ~50-60 m above the surface of the glacier from the terminus to the headwall.*

Gullies

Gullies are formed in areas of unconsolidated sediment where the runoff from rain and snowmelt creates micro-valleys. Gullies were identified on aerial images as linear depression in unstable terrain and then confirmed visually on the field. In the study site, most of the gullies are on the ice-proximal flank of moraines.

The process of gullying is an active phenomenon (Figure 4) and was observed during heavy rainfall events during the fieldwork period. This process contributes widely to the erosion of moraines.

CH2 - Figure 4: The new gullies (white arrows) created during a heavy rainfall event (26/08/2014) on the southern side of the LIA moraine of Glacier Noir.

Scree areas

According to Singh et al. (2011), scree material (also called debris) is "Unconsolidated sediment, larger than 1 mm, of angular or rounded angular fragments of boulders (clasts), predominantly originating from physical weathering". These characteristics have been visually confirmed in the field. Scree areas are steep zones of scree material. All the active scree areas around Glacier Noir and Glacier Blanc face SW to SE. Scree clast size is variable, ranging from pebble to boulder-size.

Three types of scree areas were mapped:

- Active scree areas where traces of rock falls are visible and where regular rock falls have been observed in the field. They are mainly located around the Glacier Noir catchment.
- Stabilized scree areas without traces of active rock falls located on the eastern side of the terminus of Glacier Blanc and above the outwash plain.
- Vegetated scree areas near the entrance of Haute Vallée de St-Pierre.

Figure 5 presents the geological context for the scree production. Production appears to be independent of lithology (gneiss or granite) and to be primarily driven by the slope orientation (Nagai et al., 2013): 54% of the mapped active scree areas are orientated in the SW-SE quadrant, with almost half of them facing directly South.

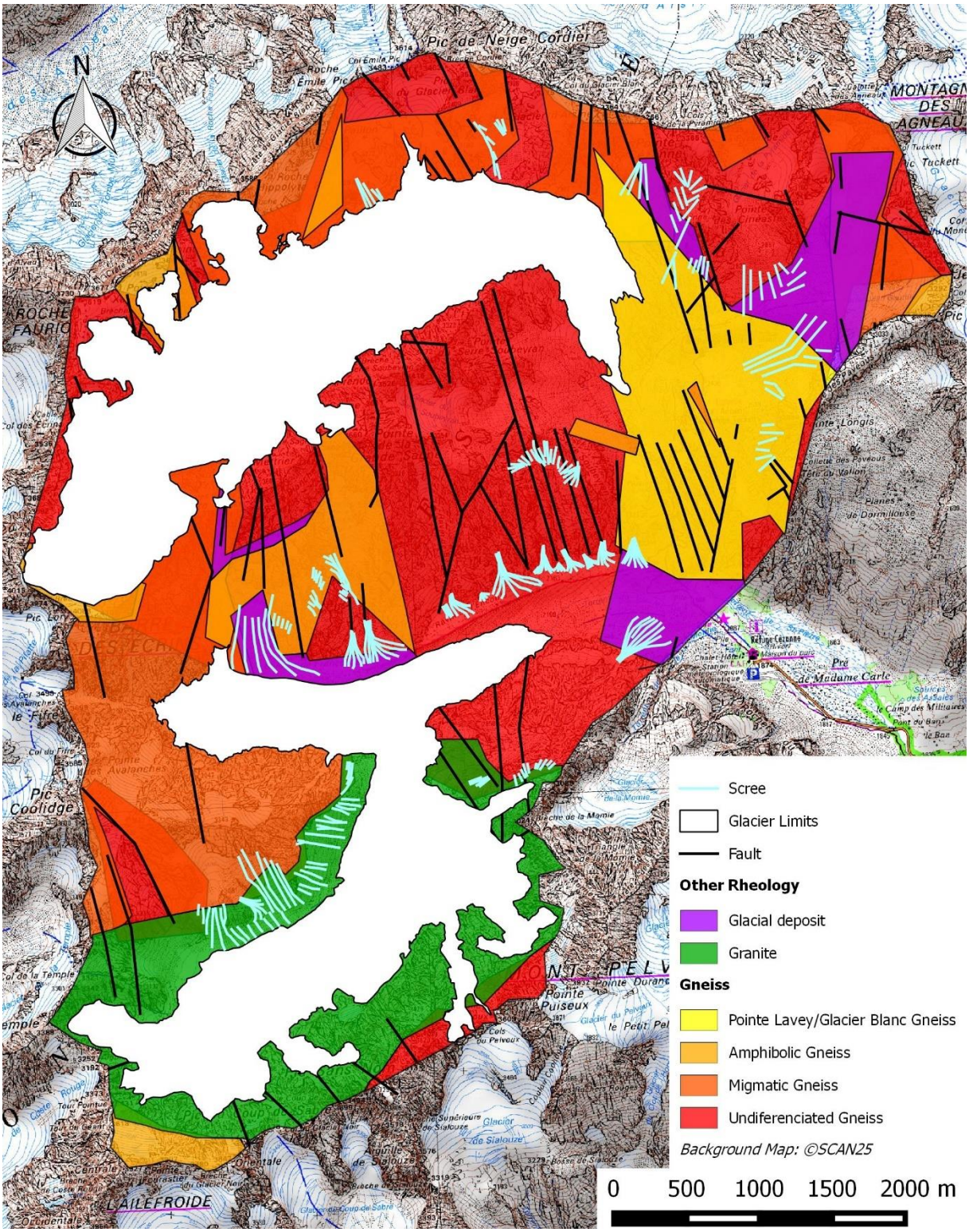

CH2 - Figure 5: Geological map of the study site with superimposed scree areas. *Geological variations (mainly gneiss except for Glacier Noir Sud with granite) in the study area cannot explain the origin of the scree areas. Slope orientation is the main factor in the scree production. Adapted from Bureau de Recherche Géologiques et Minières (BRGM) maps 0822N and 0823N.*

Hummocky terrain

On the map, hummocky terrain (Figure 6) designates an assemblage of debris and glacial sediment pits and mounds including small, possibly ice-cored moraines (Singh et al., 2011). Hummocky terrains were first identified as generic proglacial terrains on aerial images and then visually confirmed as hummocky in the field.

The hummocky terrain is located in the proglacial area of both glaciers and in a former lower accumulation cirque of Glacier Noir Sud. Like gullies, these areas are particularly active and their morphology evolves closely with the variation of the proglacial streams, especially during heavy rainfall events.

CH2 - Figure 6: Hummocky terrain in the proglacial area of Glacier Blanc. *The hummocky moraine (green) are easily eroded by the proglacial stream. The frontal moraine (white) marks the lower limit of this hummocky area.*

Bedrock with incised channels

Large areas of bedrock (gneiss) with incised channels are visible in front of Glacier Blanc, revealed as the glacier receded. In the field, visual inspection of some channels confirms that some have subglacial origins (abrupt beginning, presence of potholes, crossing steep slopes; Bennett and Glasser, 2009) and are possibly Nye channels. Nye channels (or N-Channels) are subglacial channels directly carved into bedrock by meltwater discharge (Nye, 1973). Most of the visible channels are now abandoned except for those occupied by the glacier's main proglacial streams.

Outwash plain

An outwash plain is a large flat area covered with well-sorted glaciofluvial sediment. The outwash plain was identified on aerial images by its position on an almost horizontal flat section of the field site, crossed by multiples braid of a proglacial stream. The well-sorted sediments were recognised as such due to their homogenous texture. Braided rivers often develop widely in outwash plains, for example in Iceland where they are called “sandur” because of the predominance of sand- and gravel-sized sediment across such plains. The proglacial streams of Glacier Noir and Glacier Blanc converge in the upper part of the outwash plain to form a dynamic braided stream system as shown in Figure 7 at two different dates.

CH2 - Figure 7: Outwash plain of Glacier Noir and Glacier Blanc. *As a consequence of the heavy rainfall event of 26th August 2014, the proglacial stream shifted from the northern edge of the outwash plain to the southern edge, illustrating this highly dynamic environment.*

Hydrological features

Meltwater ponds

Meltwater ponds are depressions on the ice surface that are filled with water released by the melt of snow and ice, easily identifiable as such on the glacier surface on aerial images. Numerous, often large, supraglacial meltwater ponds are a common feature on debris-covered glaciers. Indeed, such ponds form the basis of one key classification of the morphological evolution of debris-covered glaciers (Benn et al., 2012).

Meltwater ponds form by differential melting between debris-covered and clean ice areas (Reynolds, 2000). Ablation of the latter is faster than the former, creating a depression – here called the area of topographical influence – where water can be stored. This process involves a positive feedback loop where the edge of the depression becomes steeper and so less debris-covered, inducing further melting and consequently steepening of the side. This feedback loop gradually extends the area of topographic influence of meltwater ponds.

However, these meltwater ponds are eventually drained supraglacially via a channel or englacially via crevasses (Röhl, 2008). The drainage process creates relict/trace ponds (Figure 8) where the difference between the pond itself and the area of topographic influence is still visible.

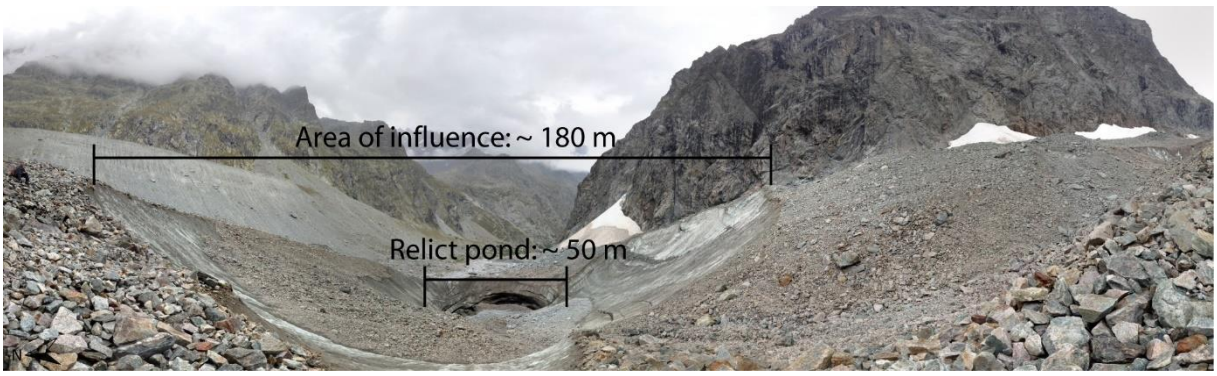

CH2 - Figure 8: Relict meltwater pond and its area of influence at the terminus of Glacier Noir. *The bottom of this pond collapsed in a subglacial channel between 2013 and 2014.*

Streams

Water streams on the study site are produced by the melt of glaciers. Streams were identified on aerial images as linear concave features meandering and/or braiding filled with water. They are found in two different positions: on the surface (supraglacial streams) and in front

(proglacial streams) of both glaciers. Due to the dynamics (water discharge, deposition of sediment) and ephemeral nature of proglacial streams, especially in the outwash plain, only principal active channels were mapped, illustrating the situation at the time the aerial images were acquired.

Supraglacial streams could only be observed on the debris-covered surface of Glacier Noir. Most of the mapped streams were restricted to the ablation area. No visual expression of supraglacial streams was found on aerial images of Glacier Blanc despite their presence in the field (Figure 9). Therefore, supraglacial streams were not mapped on Glacier Blanc.

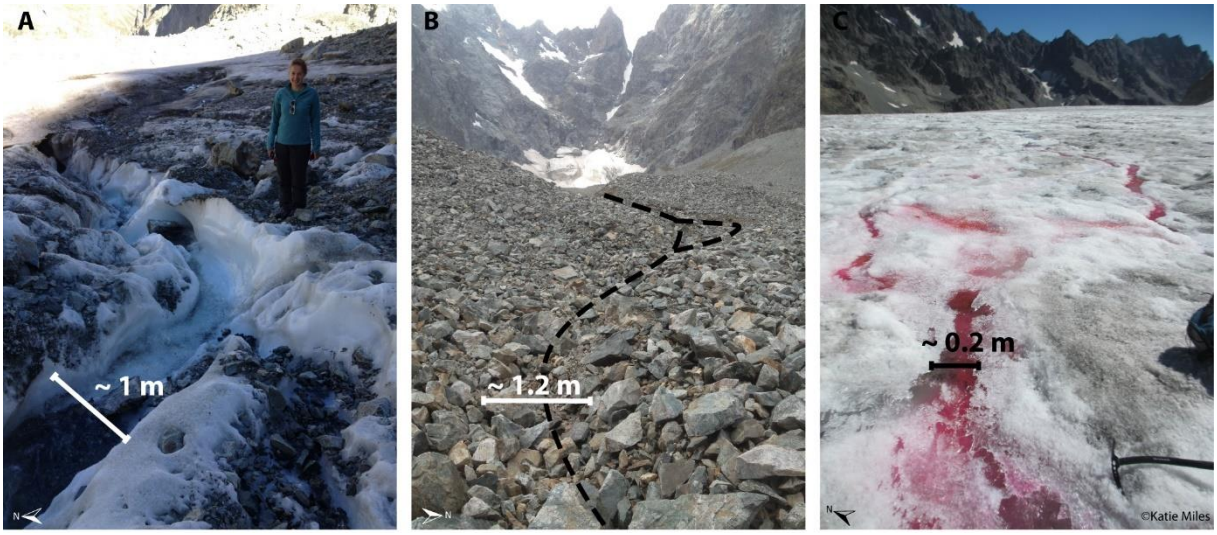

CH2 - Figure 9: Various meltwater channels in the study area. *(A) Active meltwater channel just below the accumulation area of Glacier Noir. (B) Trace of meltwater channels in the ablation area of Glacier Noir. (C) Active meltwater channels on Glacier Blanc highlighted by pink dye. Note the difference in scale between these images.*

Anthropogenic features and elevation data

The Glacier Noir and Glacier Blanc site is a tourist attraction in the "Écrins" National Park and so buildings (three refuges, one visitor centre and public restroom facilities), roads and hiking trails were additionally mapped to provide context.

Contour lines from the IGN 1998 digital elevation model (DEM) were added as background information. To clarify the topographical context of the map, arêtes lines were added on the DEM as well as some altitude points.

Conclusion

We describe here a new glaciological and geomorphological map of Glacier Noir and Glacier Blanc in the French Alps. The mapped features were divided into four different themes (glaciological, geomorphological, hydrological and anthropogenic) to facilitate the understanding of the map and future studies and comparisons. However, these four themes interact closely. Glacier Noir and Glacier Blanc are the main actors of sediment transport and deposition, creating a range of geomorphological features, from sand layers in the proglacial area to LIA moraines. The streams are, on the contrary, the main actors of erosion on the surface of Glacier Noir, acting to transfer sediment of the debris layer from the top of the glacier to the terminus, as well as eroding the proglacial terrain of both glaciers to create an outwash plain further downstream. Meltwater ponds are the perfect example of the interaction of glacial (melting of debris-free ice cliffs), geomorphological (back wasting of debris from the layer) and hydrological (storage and drainage of significant quantities of water) processes. Finally, anthropogenic features such as roads and bridges modify erosional/depositional patterns in a complex way, especially in the outwash plain.

Understanding these processes and their interactions is part of a larger research project on the impact of variations in supraglacial debris cover on glacier evolution and dynamic response to climatic forcing.

Software

Mapping and composing: QGIS 2.2, 2.4, 2.6, and 2.6.1.

Digitizing tools (up to date version): autoSaver plugin, Digitizing Tools plugin, GdalTools plugin, Georeferencer GDAL plugin, GPS Tools plugin, Multipart Split plugin.

Figures on the map: Adobe Illustrator CS2

References

ALLIX, A. 1922. Les glaciers des Alpes françaises en 1921. *Revue de géographie alpine,* 10**,** 325-333.

ALLIX, A. 1929. Observations glaciologiques faites en Dauphiné jusqu'en 1924. *Les Études rhodaniennes,* 5**,** 185-186.

BENN, D. I., BOLCH, T., HANDS, K., GULLEY, J., LUCKMAN, A., NICHOLSON, L. I., QUINCEY, D., THOMPSON, S., TOUMI, R. & WISEMAN, S. 2012. Response of debris-covered glaciers in the Mount Everest region to recent warming, and implications for outburst flood hazards. *Earth-Science Reviews,* 114**,** 156-174.

BENN, D. & EVANS, D. 1998. *Glaciers and Glaciation,* London, Arnold.

BENNETT, M. M. & GLASSER, N. F. 2009. *Glacial geology: ice sheets and landforms*, John Wiley & Sons.

CARRASCO, R. M., PEDRAZA, J., DOMINGUEZ-VILLAR, D., WILLENBRING, J. K. & VILLA, J. 2013. Supraglacial Debris Supply in the Cuerpo de Hombre paleoglacier (Spanish Central System): Reconstruction and Interpretation of a Rock Avalanche Event. *Geografiska Annaler Series a-Physical Geography,* 95**,** 211-226.

COGLEY, J. G., HOCK, R., RASMUSSEN, L. A., ARENDT, A. A., BAUDER, A., BRAITHWAITE, R. J., JANSSON, P., KASER, G., MOLLER, M., NICHOLSON, L. & ZEMP, M. 2011. Glossary of Glacier Mass Balance and Related Terms. *IHP-VII Technical Documents in Hydrology,* 86.

COSSART, E., FORT, M., JOMELLI, V. & GRANCHER, D. 2006. Les variations glaciaires en Haute-Durance (Briançonnais, Hautes-Alpes) depuis la fin du xix e siècle: mise au point d'après les documents d'archives et la lichénométrie. *Quaternaire,* 17**,** 75-92.

DELINE, P. & KIRKBRIDE, M. P. 2009. Rock avalanches on a glacier and morainic complex in Haut Val Ferret (Mont Blanc Massif, Italy). *Geomorphology,* 103**,** 80-92.

ÉCRINS, P. N. D. 2005. Territoire Écrins - Les Cahiers Thematiques du Parc National: Les glaciers. *In:* ÉCRINS, P. N. D. (ed.).

GOODSELL, B., HAMBREY, M. J. & GLASSER, N. F. 2005. Debris transport in a temperate valley glacier: Haut Glacier d'Arolla, Valais, Switzerland. *Journal of Glaciology,* 51**,** 139-146.

HAMBREY, M. J. & EHRMANN, W. 2004. Modification of sediment characteristics during glacial transport in high-alpine catchments: Mount Cook area, New Zealand. *Boreas,* 33**,** 300-318.

HAMBREY, M. J., QUINCEY, D. J., GLASSER, N. F., REYNOLDS, J. M., RICHARDSON, S. J. & CLEMMENS, S. 2008. Sedimentological, geomorphological and dynamic context of debris-mantled glaciers, Mount Everest (Sagarmatha) region, Nepal. *Quaternary Science Reviews,* 27**,** 2361-2389.

HEWITT, K. 2009. Rock avalanches that travel onto glaciers and related developments, Karakoram Himalaya, Inner Asia. *Geomorphology,* 103**,** 66-79.

JACOB, T., WAHR, J., PFEFFER, W. T. & SWENSON, S. 2012. Recent contributions of glaciers and ice caps to sea level rise. *Nature,* 482**,** 514-518.

LETREGUILLY, A. & REYNAUD, L. 1989. Past and forecast fluctuations of glacier Blanc (French Alps). *Annals of Glaciology,* 13**,** 159-163.

MANN, M. E. 2002. Little ice age. *Encyclopedia of global environmental change.* John Wiley & Sons.

MARANGUNIC, C. 1972. Effects of a landslide on Sherman Glacier, Alaska. Institute of Polar Studies.

MOUNT, N. & STOTT, T. 2008. A discrete Bayesian network to investigate suspended sediment concentrations in an Alpine proglacial zone. *Hydrological Processes,* 22**,** 3772-3784.

NAGAI, H., FUJITA, K., NUIMURA, T. & SAKAI, A. 2013. Southwest-facing slopes control the formation of debris-covered glaciers in the Bhutan Himalaya. *Cryosphere,* 7**,** 1303-1314.

NYE, J. F. 1973. Water at the bed of a glacier. *Hydrology of Glaciers.* Cambridge: IASH Publisher.

OTTO, J. C. & SMITH, M. J. 2013. Geomorphological mapping. *Geomorphological Techniques.* British Society for Geomorphology.

PAUL, F., BARRAND, N. E., BAUMANN, S., BERTHIER, E., BOLCH, T., CASEY, K., FREY, H., JOSHI, S. P., KONOVALOV, V., LE BRIS, R., MOLG, N., NOSENKO, G., NUTH, C., POPE, A., RACOVITEANU, A., RASTNER, P., RAUP, B., SCHARRER, K., STEFFEN, S. & WINSVOLD, S. 2013. On the accuracy of glacier outlines derived from remote-sensing data. *Annals of Glaciology,* 54**,** 171-182.

QGIS, D. T. 2014. *QGIS Geographic Information System* [Online]. http://www.qgis.org/: Open Source Geospatial Foundation Project. http://qgis.osgeo.org.

RABATEL, A., DEDIEU, J. P. & REYNAUD, L. 2002. Reconstitution des fluctuations du bilan de masse du Glacier Blanc (Massif des Écrins, France) entre 1985 et 2000, par télédétection optique (imagerie Spot et Landsat). *La Houille Blanche,* 2002**,** 64-71.

RABATEL, A., DEDIEU, J. P., THIBERT, E., LETREGUILLY, A. & VINCENT, C. 2008. 25 years (1981–2005) of equilibrium-line altitude and mass-balance reconstruction on Glacier Blanc, French Alps, using remote-sensing methods and meteorological data. *Journal of Glaciology,* 54**,** 307314.

RABATEL, A., LETREGUILLY, A., DEDIEU, J. P. & ECKERT, N. 2013. Changes in glacier equilibrium-line altitude in the western Alps from 1984 to 2010: evaluation by remote sensing and modeling of the morpho-topographic and climate controls. *Cryosphere,* 7**,** 1455-1471.

RAU, F., MAUZ, F., VOGT, S., KHALSA, S. & RAUP, B. 2005. Illustrated GLIMS Glacier Classification Manual, Version 1.0. *GLIMS Regional Centre,"Antarctic Peninsula", GLIMS (Global Land Ice Measurement from Space), NSIDC.*

REYNAUD, L. & VINCENT, C. 2000. Relevés de fluctuations sur quelques glaciers des Alpes françaises. *La Houille Blanche,* 2000**,** 79-86.

REYNAUD, L. & VINCENT, C. 2002. Histoire des fluctuations des glaciers en remontant le Petit Age de Glace. *La Houille blanche,* 2002**,** 16-19.

REYNOLDS, J. M. On the formation of supraglacial lakes on debris-covered glaciers. Debris-covered Glaciers: Proceedings of an International Workshop Held at the University of Washington in Seattle, Washington, USA, 13-15 September 2000, 2000. IAHS, 153-164.

REZNICHENKO, N., DAVIES, T., SHULMEISTER, J. & MCSAVENEY, M. 2010. Effects of debris on ice-surface melting rates: an experimental study. *Journal of Glaciology,* 56**,** 384-394.

REZNICHENKO, N. V., DAVIES, T. R. H. & ALEXANDER, D. J. 2011. Effects of rock avalanches on glacier behaviour and moraine formation. *Geomorphology,* 132**,** 327-338.

REZNICHENKO, N. V., DAVIES, T. R. H., SHULMEISTER, J. & WINKLER, S. 2012. Influence of rock avalanches upon the formation of moraines and their subsequent palaeoclimatic interpretation: a critical appraisal. *Zeitschrift Fur Geomorphologie,* 56**,** 37-54.

RÖHL, K. 2008. Characteristics and evolution of supraglacial ponds on debris-covered Tasman Glacier, New Zealand. *Journal of Glaciology,* 54**,** 867-880.

SAKAI, A., TAKEUCHI, N., FUJITA, K. & NAKAWO, M. Role of supraglacial ponds in the ablation process of a debris-covered glacier in the Nepal Himalayas. Debris-covered Glaciers: Proceedings of an International Workshop Held at the University of Washington in Seattle, Washington, USA, 13-15 September 2000, 2000. IAHS, 119-132.

SHUGAR, D. H., RABUS, B. T., CLAGUE, J. J. & CAPPS, D. M. 2012. The response of Black Rapids Glacier, Alaska, to the Denali earthquake rock avalanches. *Journal of Geophysical Research-Earth Surface,* 117**,** 14.

SHULMEISTER, J., DAVIES, T. R., EVANS, D. J. A., HYATT, O. M. & TOVAR, D. S. 2009. Catastrophic landslides, glacier behaviour and moraine formation – A view from an active plate margin. *Quaternary Science Reviews,* 28**,** 1085-1096.

SINGH, V. P., SINGH, P. & HARITASHYA, U. K. 2011. *Encyclopedia of snow, ice and glaciers*, Springer.

STOTT, T. & MOUNT, N. 2007. Alpine proglacial suspended sediment dynamics in warm and cool ablation seasons: Implications for global warming. *Journal of Hydrology,* 332**,** 259-270.

THIBERT, E., FAURE, J. & VINCENT, C. 2005. Bilans de masse du Glacier Blanc entre 1952, 1981 et 2002 obtenus par modèles numériques de terrain. *La Houille Blanche,* 2005**,** 72-78.

TOVAR, D. S., SHULMEISTER, J. & DAVIES, T. R. 2008. Evidence for a landslide origin of New Zealand's Waiho Loop moraine. *Nature Geoscience,* 1**,** 524-526.

VACCO, D. A., ALLEY, R. B. & POLLARD, D. 2010. Glacial advance and stagnation caused by rock avalanches. *Earth and Planetary Science Letters,* 294**,** 123130.

VAUGHAN, D. G. 1993. Relating the occurrence of crevasses to surface strain rates. *Journal of Glaciology*.

VIVIAN, R. 1967a. Le glacier Blanc. *Revue de géographie alpine,* 55**,** 729732.

VIVIAN, R. 1967b. Le glacier Noir. *Revue de géographie alpine,* 55**,** 733736.

WGMS & NSIDC 1989, updated 2012. World Glacier Inventory. Compiled and made available by the World Glacier Monitoring Service, Zurich, Switzerland, and the National Snow and Ice Data Center, Boulder CO, U.S.A.

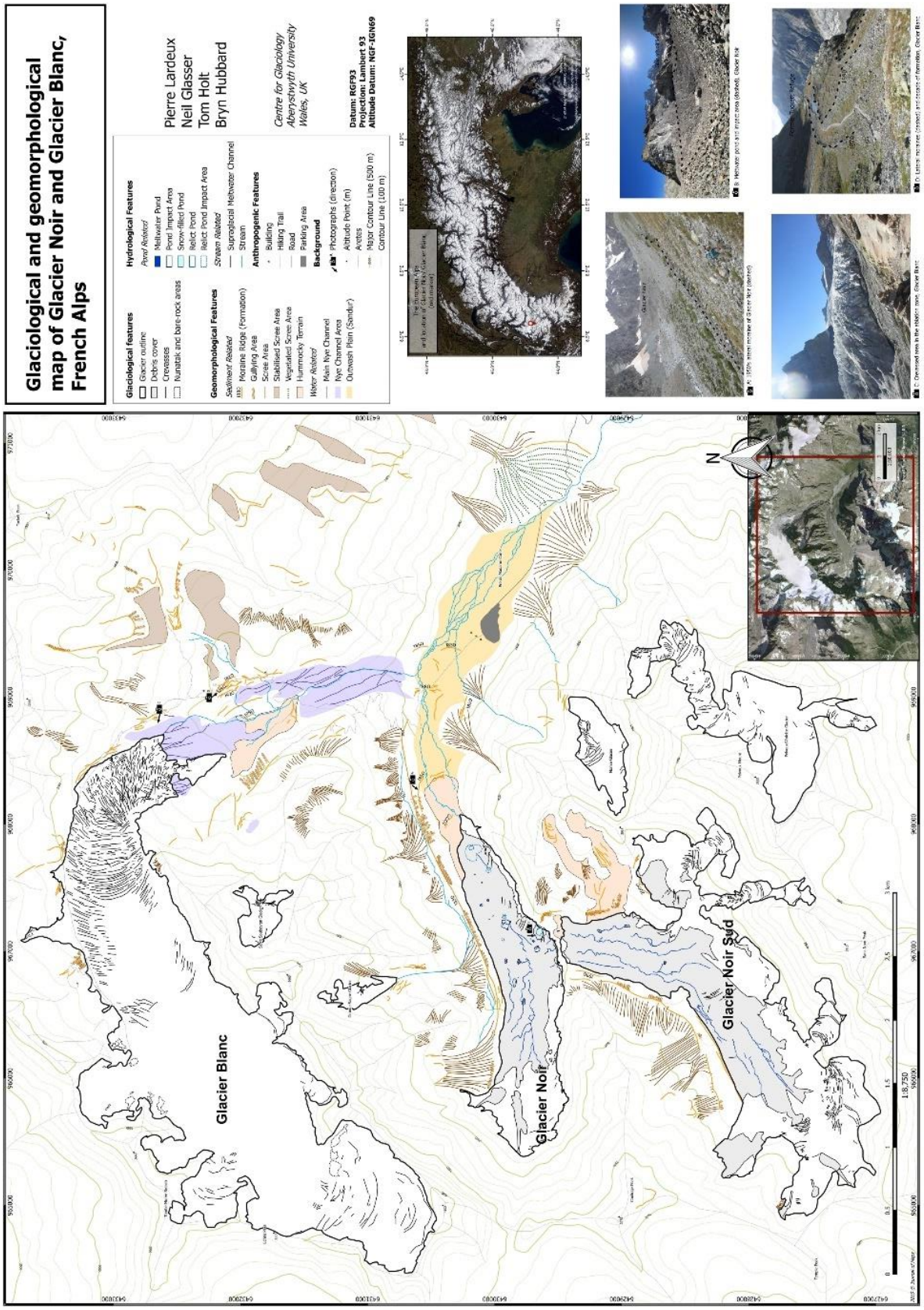

CH2 - Figure 10: Preview of the main map published in Journal of Maps. *Full resolution version is available in Appendix I and also online at https://figshare.com/articles/Glaciological_and_geomorphological_map_of_Glacier_Noir_and_Glacier_Blanc_French_Alps/1451243 (accessed on 26/06/2018) .*

Field site's additional information

Journal of Maps requires that articles accompanying the main map should remain a description of this one only. To complete this description of the map, this section brings additional information concerning the field site itself as well as some interpretation. This section focuses on the following topics: geomorphology, geology and hydrology. Glaciology is not addressed in this section as it is the entire subject of Chapter 4.

Geomorphology

From a geomorphological point of view, the main features of the field site are the moraines. Some frontal moraines of Glacier Noir have been dated through the position of the front of the glacier on historical maps and aerial photographs. However, some other could not be dated as no terminus position matched their location. It remains difficult to date these moraines by remote sensing only, as the terminus of Glacier Noir experienced an advance in the first half of the 20th century (see Chapter 4), probably erasing some former moraines. Additionally, the active (streams and scree) proglacial area also erased some traces. For the same reasons, the age of the frontal moraine of Glacier Blanc remains unknown to us: the terminus of the glacier experienced an advance in the late 1980s – early 1990s. Additionally the steep terrain, where these moraines are, favoured the quick erosion of any geomorphological features. On the contrary, the relatively flat terrain southeast of the terminus of Glacier Blanc allowed the preservation of some lateral moraines dating from the end of the Little Ice Age (LIA) between 1820 and 1890 (Parc National des Écrins, 2005). These moraines are numerous, but remain small in height and extent, reflecting that the side of Glacier Blanc stagnated in this area or that the sediment supply was very low. The LIA moraine of Glacier Noir reflects the opposite: a very large supply of sediment. This moraine stretches all along the ablation area of Glacier Noir, reaching the probable position of junction between Glacier Noir and Glacier Blanc. The ridge of this moraine stands more than 50 m above the surface of Glacier Noir in 2014 (Figure 3). The elevation difference between the glacier surface and the moraine ridge is due to the thinning of the glacier and has multiple consequences. The flank of the LIA moraine is currently unstable, making it the main sediment/debris supply for the surface of Glacier Noir. The vertical extent of this moraine transformed it into a “debris wall”, preventing the surrounding scree area from providing debris to the glacier surface. This LIA moraine is so large that in the 1950s, Glacier Noir built a second lateral moraine on its flank.

Geology

There are two main types of bedrock on the field site (see Figure 5):

- Gneiss around Glacier Blanc and the main branch of Glacier Noir.
- Granite around the south branch of Glacier Noir (Glacier Noir Sud).

Glacier Noir and Glacier Noir Sud are both debris-covered, so it seems that the lithology of the surrounding bedrock does not play a role in providing debris for the glacier surface. This is confirmed by the fact that Glacier Noir and Glacier Blanc are surrounded by the same type of bedrock, but one is debris-covered and the other is not. The higher elevation of the mountain sides around Glacier Blanc is the reason why this glacier is not debris-covered, as the mountain sides are above the freeze-thaw zone (Chapter 1).

The presence of two distinct lithologies around Glacier Noir and Glacier Noir Sud could be found at the terminus of Glacier Noir as debris are transported and deposited there (Figure 11).

CH2 - Figure 11: Different debris lithology at the terminus of Glacier Noir. *Glacier Noir Sud is surrounded by granite. The granite debris is transported by Glacier Noir more or less directly from the junction to the terminus. The scree cone is from the same lithology that is around Glacier Noir (gneiss). The image has been equalized and saturated at 60% to accentuate the difference in colour between the two types of debris, which is clearly visible in the field. Steffan Griffiths for scale.*

Hydrology

The most striking difference between Glacier Blanc and Glacier Noir on a hydrological level is the absence of supraglacial channel on the clean-ice glacier, contrary to the debris-covered one. In the field, the difference is explained by the presence of micro-channels on the surface of Glacier Blanc, which are not visible on aerial photographs, and also by the mostly en- and subglacial hydrology of Glacier Blanc, probably due to the large quantity of crevasses leading the meltwater under the ice. On the other side, Glacier Noir has a very active hydrological system at its surface with active and abandoned channels, moulins and meltwater ponds. These meltwater ponds fill and drain regularly (during summer 2014, we saw a drop of more than 1 m of water level in one of these ponds over 2-3 days) and are created mostly by differential melting. If the ice is exposed in a debris-covered area, it will melt faster than its surroundings creating a depression. However active these meltwater ponds are, they tend to evolve with the ice flow: they will move down glacier preserving their shape if the ice flow is constant and they will close if the ice is disturbed, such as at the junction of Glacier Noir and Glacier Blanc.

Even if Glacier Noir and Glacier Blanc shared a common history in the form of the joined terminus before 1875, they are now displaying very different characteristics in their geomorphology, glaciology and hydrology.

CHAPTER 3: Methods

Overview

Each article, as Chapters in this manuscript, includes its own method section describing the methods and techniques used for each study. The goal of this first section of Chapter 3 is to provide some more details on the Global Navigation Satellite System (GNSS) measurements described in Chapter 4. Additionally, this section describes the fieldwork measurements realised in August-September 2014 on Glacier Noir / Glacier Blanc. These measurements were not directly used to answer the research question of this thesis. However, they were part of individual projects led by a MSc student from Aberystwyth University and two undergraduate students from University of Cambridge. The second section of this Chapter is an article formalising and testing the main method developed for Chapter 4. This method (using Structure-from-Motion on historical aerial images on a landscape scale without fieldwork) is a variation on a method used in glaciology for less than a decade.

During summer 2014 fieldwork, GNSS measurements were conducted to localise ablation stake observations and other experiments such as dye tracing (see below). These GNSS measurements were also used to calculate the surface velocity of both Glacier Noir and Glacier Blanc. The GNSS measurements were realised using a ©Topcon Hiper II receiver and the associated antenna, recording GPS and GLONASS signal at a frequency of 1 Hz. For Glacier Noir, the differential measurement technique was applied, and one base station was set up near the terminus of the glacier on a house-size boulder. This boulder seemed the most stable at the time (in the field) and the station was setup on a field tripod (Figure 0a) for 3 to 7 hours. We used a rover receiver on a surveying tripod for each measurement site for 15 min (Figure 0b). For Glacier Blanc, no good location was found for a base station. Each site was measured with a surveying pole for 3 to 5 min.

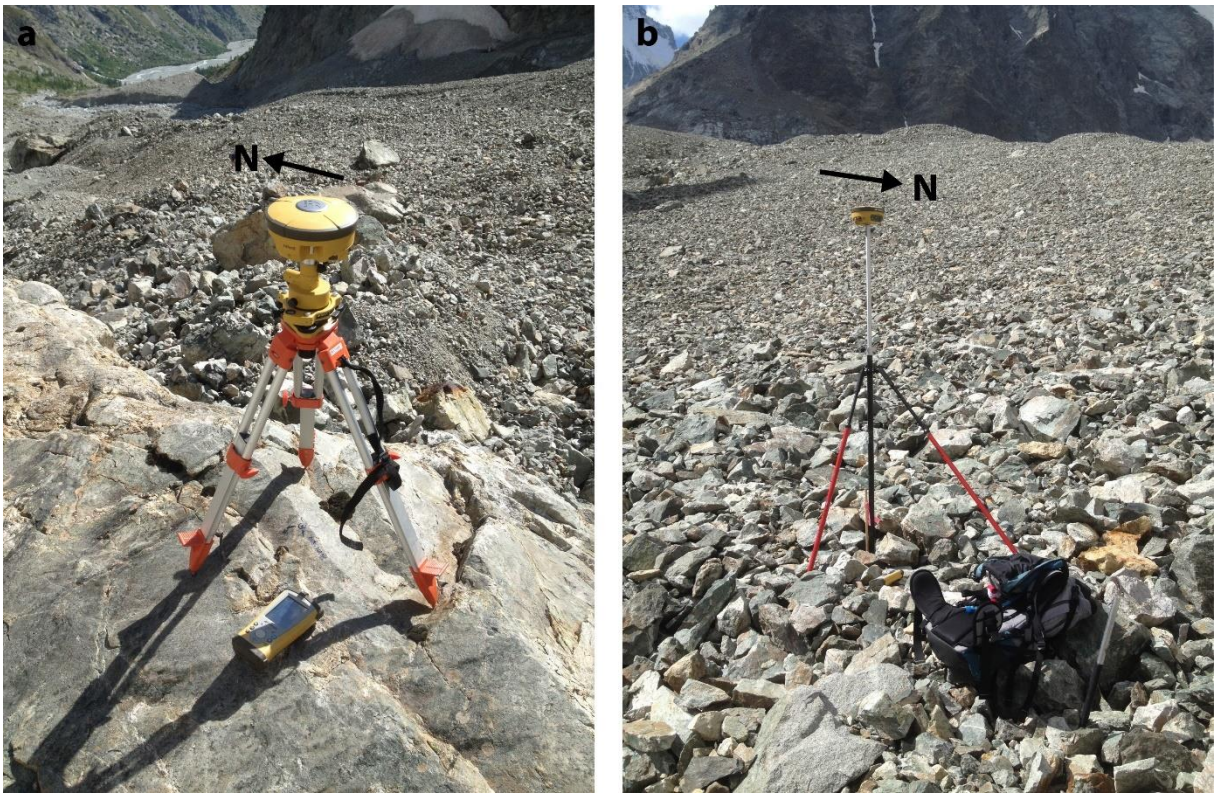

CH3 – Figure 0: GNSS measurements on Glacier Noir. *a) Base station on a house-size boulder. b) Rover station on an ablation stake site.*

The post-processing calculations were conducted with ©Leica GeoOffice 8.3. For Glacier Noir, the base station was calculated using the IGN GNSS permanent network stations of Annecy, Arandon, Barcelonnette, Chambery, Marignier, St Michel l'Observatoire, Modane, Moustiers-Sainte-Marie, Puy Aillaud, La Rosière, Gap and Villard de Lans, depending the availability of each station. Then the rover was calculated using the base station. For Glacier Blanc, each measurement was calculated using the IGN GNSS permanent network stations directly. On this glacier, one set of measurements was also conducted using a hiking GPS Garmin Fenix, which does not allow for any post-processing as it used only the code. Additionally, the raw data of this device are not available. The Garmin Fenix provides only the final position. The limitations of this GPS device explained the larger uncertainty obtained for the surface velocity of Glacier Blanc (Chapter 4).

The other fieldwork measurements are divided in two topics: glaciology and hydrology (Appendix [II]). For the glaciology, we measured the temperature on Glacier Noir at four different levels: at around 2 m from the ground, at 5 cm below the debris surface, at 20 cm below the debris surface and at the debris/ice interface 35 cm below the debris surface. We

also measured the debris thickness at 24 different locations on Glacier Noir. Six ablation stakes were placed on Glacier Noir and measured as often as possible (1-3 day interval). Six other ablation stakes were placed on Glacier Blanc and they were measured twice in addition to three pre-existing stakes placed by the National Park services. After analysis of the Glacier Noir dataset, it appears clearly that the ablation stakes technique needs to be improved for debris-covered glaciers (see Appendix [II] and Chapter 6). The final observation done for the glaciology topic was a time-lapse camera (interval 5 min) placed in front of the terminus of Glacier Noir in order to measure its retreat over the course of 20 days. However, strong luminosity variations and position adjustment did not allow to utilise these 3521 images.

For the hydrology, the goal was to conduct a direct comparison of the glacial streams exiting Glacier Noir and Glacier Blanc. Unfortunately, the loss of the gauging station for Glacier Blanc in a rainstorm on August 26th, 2014 did not allow for this comparison. However, we successfully measured the discharge, the electrical conductivity and the suspended sediment concentration for the stream exiting Glacier Noir.

Only the GNSS and debris thickness measurements were directly use in this PhD project. However, the first analysis of some of these measurements is included in Appendix [II] for information and as a base for future work. Only the analysis conducted by myself is presented in that appendix.

Uncertainties

The following section is about measuring the limitations of, and thus the uncertainties linked to, the main technique during this project: Structure-from-Motion. However, throughout this thesis, uncertainties have been often ascertained separately for each data point and not for an entire technique, method or type of measurement. For example, in Chapter 4, uncertainties on glaciers' length changes have been calculated for each few measurements as the interesting data is the variation and not the absolute length of each glaciers. These intrinsic uncertainties are represented as error bars for each data point on CH4 – Figure 3. The same principles apply for surface area, velocity and surface elevation. In Chapter 5, the uncertainty on the classification is evaluated via the number of undetermined glaciers and the uncertainty of the contribution to runoff is given by the sensitivity tests.

Concerning the significance of the results, as most of them of concern change measurements, the following rule has been used: if the change is larger than the uncertainty linked to this change, the change is considered significant. This rule was necessary because I did not find a statistical index for significance that can cope with different sample sizes (Glacier Noir and Glacier Blanc do not have the same number of measurements), varying time span between samples and correlated data such as length and surface area.

Using Structure-from-Motion on historical aerial images in glaciology

Submitted to Journal of Glaciology on 9th May 2017; Rejected on 6th August 2017.

Currently in revision (June 2018).

Lardeux, P., Holt, T., Glasser, N.F.

Abstract

Producing a fine spatiotemporal-resolution time series for analysing glaciological features, such as terminus position or glacier surface area, is an expensive and time-consuming process, which often demands repeat fieldwork. We present here a variation and formalisation of the method consisting of using Structure-from-Motion on historical aerial images to extend glaciological time series into the past. We implemented some variations compared to previous studies by using only nadir aerial images, general-purpose references to extract control points and requiring no fieldwork. To formalise this variation, we describe experiments quantifying the accuracy and precision of this method, showcasing, in less-than-ideal conditions, the possibilities offered on a technical level (how many images and what kind of sensors can be used), and on a glaciological level (what features can be measured). We also compare it to traditional photogrammetry and to single-image georeferencing. Working in a high-relief mountain environment, it is possible to reach ~5m overall uncertainties on small features such as lateral moraines and larger features such as glacier front position by using any sensor with 9 or more images and 10 or more ground control points. We also explore the major limitations of this method: vertical uncertainties, photograph saturation, and unknown camera lens calibration. Finally, we discuss how this method fits into the landscape of present day glaciological remote sensing techniques.

Introduction

Digital photogrammetry has been used for more than a decade in various domains of geosciences, including geomorphology (Chandler, 1999), archaeology (Chandler & Fryer, 2005) and geohazard monitoring (Walstra and others, 2004).Issued from recent development in computing, the Structure-from-Motion technique (SfM) brought easy access to digital photogrammetry to those domains: e.g. geohazard monitoring (Lucieer and others, 2013) and geomorphology (Fonstad and others, 2013, Prosdocimi and others, 2015); but also to hydrology (Javernick and others, 2014). This technique has been recently taken up in glaciology, including investigations regarding glacial lake outburst floods (Westoby and others, 2014), glacier monitoring (Piermattei and others, 2015), supraglacial hydrology (Rippin and others, 2015), snow studies (Nolan and others, 2015, Harder and others, 2016) and ice surface roughness (Irvine-Fynn and others, 2014). This uptake is due to the many advantages offered

by SfM compared to traditional photogrammetry and field data collection techniques (Micheletti and others, 2015a). SfM is user-friendly, cost effective, accurate, and offers efficient data processing (Westoby and others, 2012). Additionally, the rapid development of unmanned aerial systems (Tonkin and others, 2014, Whitehead & Hugenholtz, 2014a, Whitehead & Hugenholtz, 2014b) has further accelerated the adoption of SfM in glaciology.

Regular glacier monitoring is particularly useful to build continuous glaciological time series (Braun and others, 2011, Huss and others, 2015) and understand glacier evolution. Time-series analysis, which may include glacier terminus position, equilibrium line altitude, transient snow lines, surface area and mass balance, is critical for many glaciological applications, e.g. calibrating and testing models (Moller & Schneider, 2010) and evaluating climate change impacts (Zemp and others, 2009, Roe and others, 2016). However, developing suitable time series remains expensive as it usually requires repeat fieldwork, long-term planning and, therefore, is spatially limited to a few glaciers.

Combining historical images and SfM has already proven successful in at least two recent studies: one in a non-glacial environment in the Alps (Micheletti and others, 2015b) with additional fieldwork, one using oblique aerial images of glaciers in Svalbard (Midgley & Tonkin, 2017), one using terrestrial and oblique aerial images in three different mountain ranges (Mertes and others, 2017) and finally one study (the closest to our main study. See context and data) on one glacier between 1981-2017 in the Southern Alps, New Zealand (Vargo and others, 2017). The three first studies processed only one set of aerial images (thus for only one year) and compared the results to modern datasets from an unmanned aerial vehicle or Lidar. The last one use multiple dataset including modern dedicated imagery and fieldwork-acquired ground control points.

Here, we formalise a variation on the method combining SfM and the use of historical aerial images to build or extend a glaciological time series cost-effectively, quickly and accurately at a landscape scale on any glacier where historical aerial imagery is available and fieldwork not an option. We also summarise the possibilities and limitations of this method and discuss the role of this method in glaciological remote sensing.

Context and data

We developed this variation on the method for a project regarding the long-term comparison (over two centuries) of a debris-covered glacier (Glacier Noir) and a clean-ice glacier (Glacier Blanc) in the French Alps (Figure 1; Letreguilly & Reynaud, 1989, Cossart and others, 2006, Lardeux and others, 2015). There were no pre-existing long-term glaciological time series available for these two glaciers, and with limited financial resources, historical aerial images were freely available from the National Institute of Geographic and Forestry Information (Institut national de l'information géographique et forestière, IGN) in France (see Acknowledgments). This type of data is increasingly available under policies of open data issued by public institutions (e.g., Swisstopo in Switzerland, https://www.swisstopo.admin.ch; Natural Resources Canada, http://www.nrcan.gc.ca).

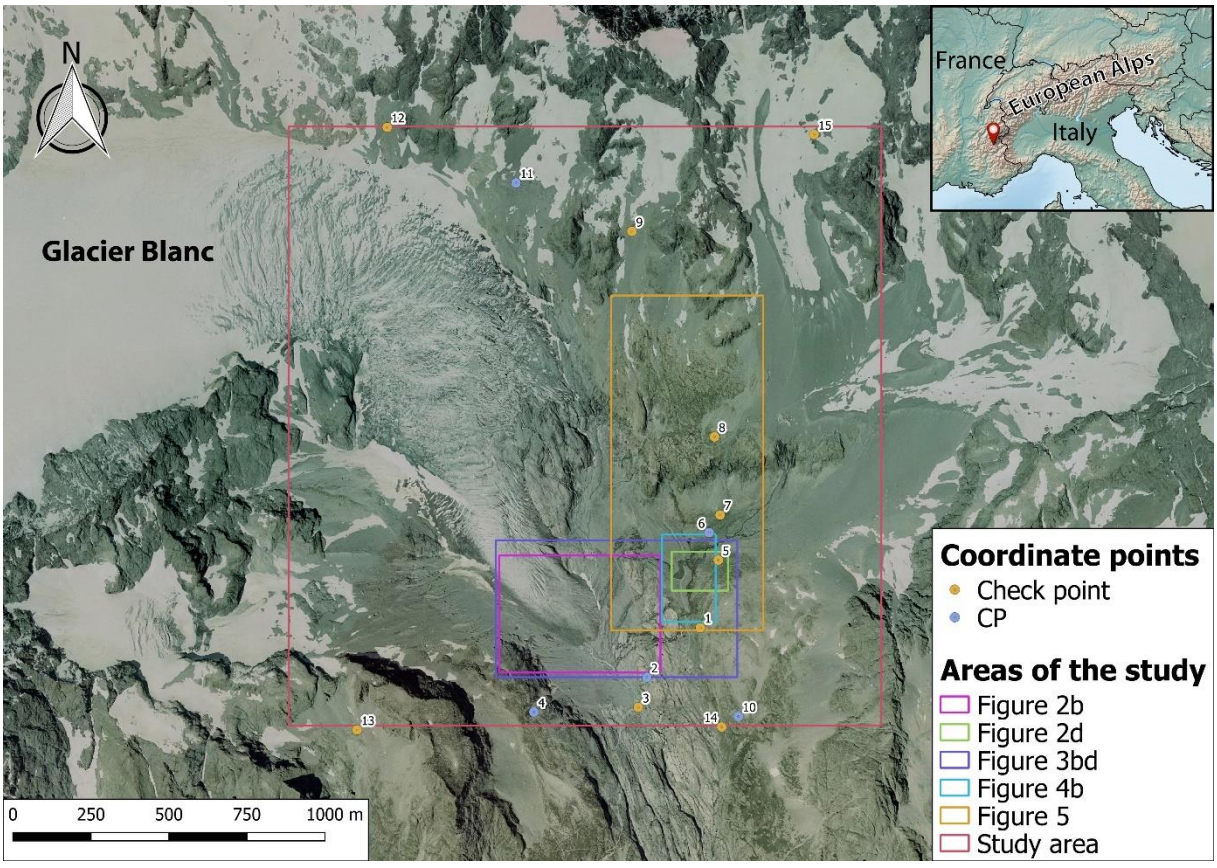

CH3 - Figure 1: Study site location and extent of the figures. *The background image is extracted from ©BDORTHO Historique 1999. CP = control point. Inset map: location map of the study site in the French Alps.*

We used non-georeferenced digital aerial photographs acquired during twenty different years between 1952 and 2013. The resolution of these photographs ranges from less than 0.5 m to

almost 1.5 m and were taken for mapping purposes by manned aircraft, to be processed via traditional photogrammetry. The results of this processing were also available in the form of orthorectified and georeferenced digital tiles with a 0.5 m resolution for 1999, 2003, 2009 and 2013. We used these tiles as references during this processing. The aerial photographs come from the database named "©BDORTHO Historique" and the orthorectified tiles from "©BDORTHO 50cm". The elevation data were retrieved from the "©BDALTI" database in the form of a national digital elevation model (DEM) produced in 1998 (25 m resolution). The 3D uncertainty for "©BDORTHO 50cm" and "©BDALTI" is given to be "métrique" meaning 1-5 m. The results of our processing are twenty time-separated orthoimages and associated DEMs covering a 20 km x 20 km area.

Our method allowed us to produce the following time series for Glacier Noir and Glacier Blanc between 1952 and 2013:

- Terminus position and length variation;
- Surface area and area change;
- Surface elevation; and
- Surface velocity for Glacier Noir (manual tracking approach).

Following these results, we formalised the method and assessed its viability and possible use in different glaciological contexts by applying and testing it in a more control context than a landscape-wide project. The assessment of the possibilities and limitations of this method is based on these different time series and their respective uncertainties. However, it is clear that this process is applicable to other sets of historical and contemporary aerial photographs.

Method

To test and formalise this methodology variation, we used a smaller area (20 km^2, 2-9 images, 5-10 control points) than that used in our main study in order to have better constraints on each element of the processing. The main study covered an area of 200 km^2, requiring 26 to 149 images depending on the year, and 161 control points. The chosen area is representative of the different terrain surrounding most mountain glaciers: the glacier itself, steep-sided

valley walls, proglacial terrain and bedrock. We limited the processing to the years that offered the maximum opportunities for experiments: 1952, 1981, 1994 and 1999.

SfM processing was conducted using ©Agisoft Photoscan (©Agisoft, 2017), which has been used successfully in other studies (Colomina & Molina, 2014, Piermattei and others, 2015). We used software version 1.3 on a workstation with the following configuration: CPU ©Intel i7 8 cores, RAM 8Gb, GPU ©NVidia GTX 680, which met the ©Agisoft recommended configuration. Table 1 summarises the different processing stages and their parameters used in ©Agisoft Photoscan.

CH3 - Table 1: Stages and parameters of processing in ©Agisoft Photoscan.

Stage	Description	Parameters	Values	Comments
1	Picture alignment using a sparse point cloud.	Accuracy	High	Use of full resolution images and not downscaled version
		Pair preselection	Disabled	Images don't follow each other
		Key point limit	100 000[(1)]	Upper limit of feature points on every image
		Tie point limit	100 000[(1)]	Upper limit of matching points for every image
		Constrain features by	No	There is no mask on images
		Adaptative camera model fitting	Yes	Help to prevent divergence of camera calibration parameters
2	Inclusion of GCP	GCP: 10; Check points: 5		
3	Optimization of the camera parameters	Coordinate system	EPSG:2154	RGF93
		Marker accuracy (m)	5[(2)]	Accuracy on the field
		Marker accuracy (pix)	1-2[(2)]	Accuracy on the image
		Other parameters	Default	
4	Creation of a dense point cloud	Quality	High	Use downscaled version (resolution divided by 2)
		Depth filtering	Aggressive	Filtering of the noise in the dense point cloud
5	Creation of a 3D mesh from the dense point cloud	Surface type	Height field	
		Source data	Dense	
		Face count	High	Number of face = number of points / 5
		Interpolation	Enable	Help to fill some hole in the dense cloud
6	Determination of the mesh texture	Mapping mode	Adaptative orthophoto	Different mapping for flat area or steep area
		Blending mode	Mosaic	
		Texture size/count	8192 x 1	
		Enable color correction	No	No adjustement between images to create the texture
		Enable hole filling	Yes	
7	Construction of the selected outputs.	DEM source data	Mesh	
		Orthomosaic surface	DEM	
		Resolution	Default	

(1) Here we used the same point limits as during the main project. We are aware that lower limits could be used, however these numbers were obtained after multiple tests and provided the best results. These high values are probably due to the large extent of the main project site and the lack of lens calibration. The only consequence is a slight increase of the processing time.

(2) The chosen control points (markers) were usually boulders, preventing us of using a better accuracy in the lower resolution images. For consistency, the same parameters have been applied to all processing.

The locations of the control points (CPs) and the check points (points only used to evaluate the results) used during the processing are shown in Figure 1. These points were chosen in stable areas (mostly bedrock) surrounding the terminus of Glacier Blanc in 1999. The coordinates of these points were extracted using the ©BDORTHO Historique 1999 and were used as reference GCPs/check points. We evaluated the results of the processing by calculating the coordinate difference between the reference and these same CPs/check points in the resulting orthoimages. This provides the horizontal residuals for each orthorectified images. The uncertainty on these residuals is given by the standard deviation of the type of point considered (CP or check point or both). Concerning the evaluation of the DEMs, we subtracted the reference DEM from the resulting DEM.

Results of experiments

We present here the results of the different experiments conducted to measure the uncertainty created by combining historical nadir aerial images and the SfM technique with no additional fieldwork and comment on how this method compares to traditional photogrammetry. Concerning the uncertainty on these results, it should be noted that if the processing uncertainty is lower than the reference uncertainty from the image and DEM databases, this one should be considered as prevailing. This is referred in Figure 2 and 3 as "Reference max uncertainty: 5 m". This reference uncertainty is considered as random throughout the different digital products by the data producer (IGN).

Experiments on the number of images

The first aspect to consider regarding the data is how many photographs and how many CPs can be collected and used. Traditional photogrammetry and the principles behind the SfM technique would suggest that the more photographs and more CPs the better (Mikhail and others, 2001). This principle is still valid here, however Figure 2 illustrates some nuances to this assumption.

The results of the experiments on the number of images (2, 4 or 9) are shown by the three different colours in Figure 2a, b and c, and by the multiple lines of each colour in Figure 2d and e. Independently of the number of points (CPs and check points), the use of 9 images gives smaller residuals than only 2 images, only by less than 1 m. This difference has to be relativized

when compared to the ~7-10 m of total residuals. If we consider separately the CPs and the check points (see next section), the influence of the number of images is unclear, as the use of only 2 images gives the best results with the CPs and the use of 4 images gives the best results with the check points. Concerning the influence of the number of images on glaciological measurements, it appears that the terminus position or the delimitation of the proglacial lake remain consistent and that the variations remain within the calculated uncertainty.

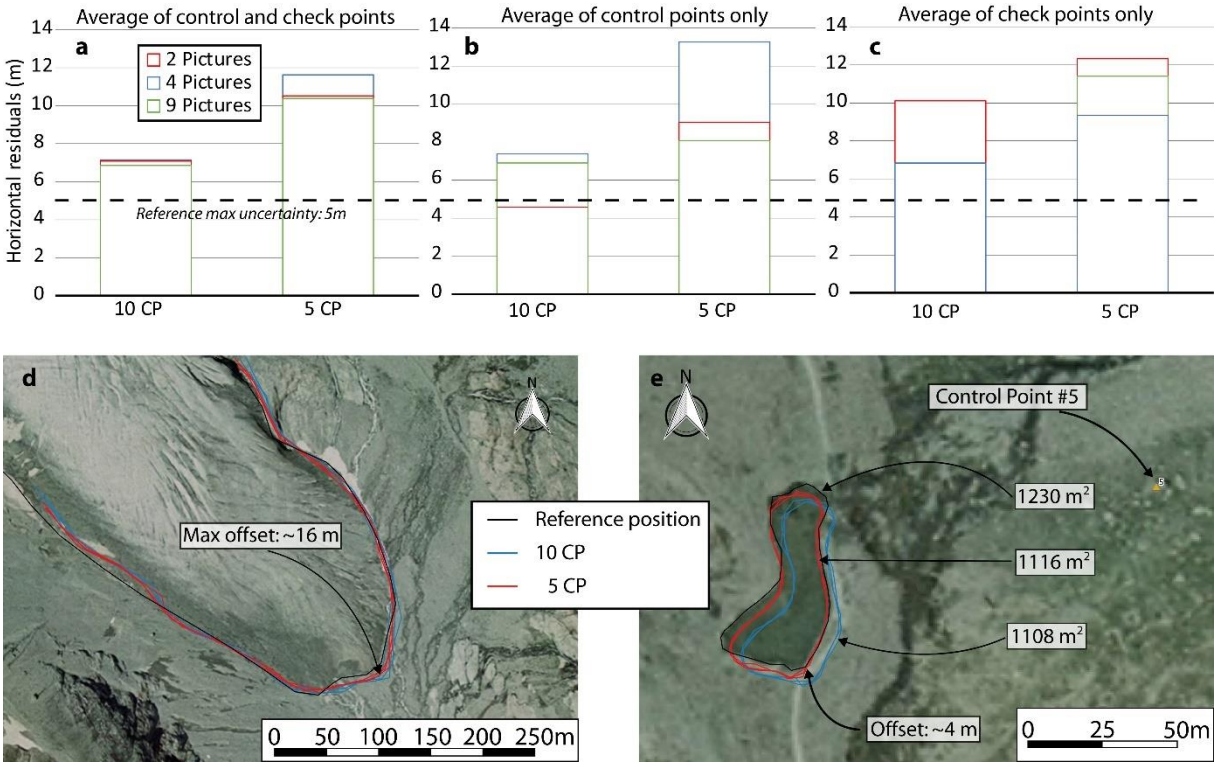

CH3 - Figure 2: Relationship between the number of control points (CP), the number of photographs used and the georeferencing residuals*. The photographs processed were from 1999. a) Average residuals of the CPs and the check points for 10 and 5 CP used in the SfM processing and for 2, 4 and 9 pictures. The "reference max uncertainty" corresponds to the quality of the reference orthoimages given for 1-5m. b) Average residuals of the control points only. c) Average residuals of the check points only. d) Variation in Glacier Blanc terminus positions depending on CP and picture numbers. e) Variation in position and area of a proglacial pond depending on CP and picture numbers. See Figure 1 for location.*

Experiments on the number of CP

The results of the experiment on the number of CPs (5 or 10) are shown by the two different bars in Figure 2a, b and c, and by the two different line colours in Figure 2 d and e. When considering the horizontal residuals, the number of CPs involved in the SfM processing shows a clear influence, independently of which points are used in the calculation with the same

number of images. The average residual is ~7 m for 10 CPs and ~11 m when only 5 CPs are used. This average slightly increases if only the check points are considered (10 CPs: ~8 m; 5 CPs: ~11 m) and decreases if only the CPs are considered (10 CPs: ~6 m; 5 CPs: ~10 m). However, if these raw geometric measurements are compared to actual glaciological measurements such as terminus position and proglacial lake surface area, Figure 2d and e show that the difference between 10 and 5 CPs is mitigated by the number of pictures used during the SfM processing.

Experiments on the camera sensor

Another aspect to consider in the data is the kind of photographs available: panchromatic, Red-Green-Blue (RGB), or Near-Infrared (NIR) scenes. The results of the experiments on the different type of camera sensors are shown by the different bars in Figure 3a and by the different colours in Figure 3b.

To evaluate the impact of the camera sensor on the SfM process, we compared 1981 panchromatic horizontal residuals (and glacier front position) to 1999 RGB residuals and 1981 NIR residuals to 1999 RGB residuals. Then we compared the residuals between panchromatic and NIR on the same year (1981). . The 1981 panchromatic image has very low horizontal residuals (1.6 m ± 1.1) compared to the 1999 RGB image; the 1981 NIR image also has low horizontal residuals (3.3 m ± 2.9; Figure 3a). Compared to the 1999 RGB image, both 1981 residuals are below the reference uncertainty of 5m, demonstrating that this method can give excellent results on non-RGB images. When comparing panchromatic and NIR, the 1981 results (3.6 m ± 2.7) were also below this reference uncertainty, meaning that the results are consistent when looking at glaciological measurements such as terminus position or proglacial lake surface area (Figure 3b).

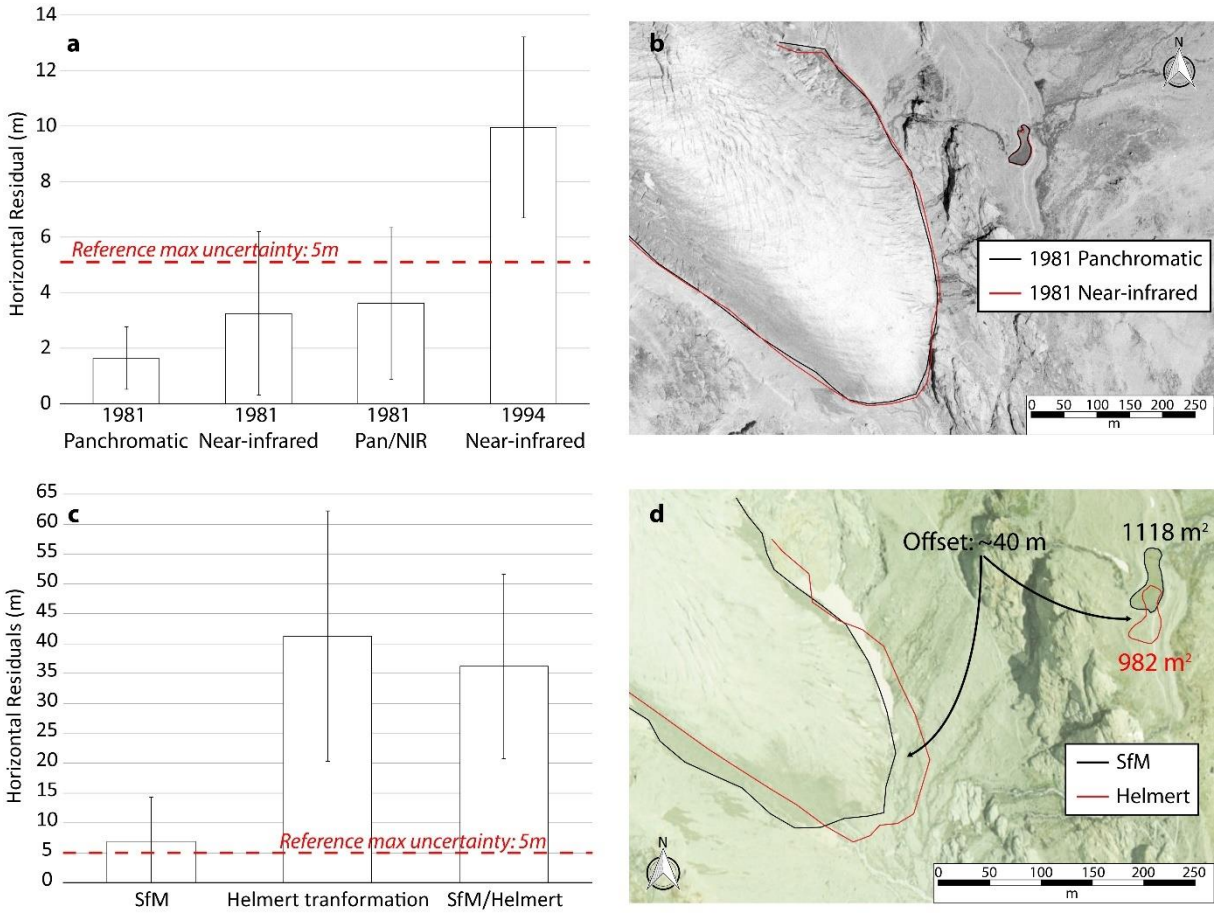

CH3 - Figure 3: Effects of a near-infrared (NIR) sensor in the SfM results and comparison of SfM results and traditional georeferencing process. *a) Residuals of SfM processing for a panchromatic and NIR sensor for 1981 and only a NIR sensor for 1994; the "Pan/NIR" column represents the direct comparison of the two types of sensors. b) Terminus and proglacial pond position in 1981 depending on the sensor used. Background: 1981 Panchromatic orthoimage. c) Residuals of SfM processing and classic georeferencing (planimetric Helmert transformation) for 1999; the "SfM/Helmert" column represents the direct comparison of the two techniques. d) Terminus and proglacial pond positions in 1999 depending on the technique used. See Figure 1 for location. Background: 1999 RGB orthoimage.*

However, these small horizontal residuals partly rely on a good estimation of the camera lens calibration by the software, which may vary depending on the camera and in our case, depending on the year. We processed NIR images from 1994 and compared them to the 1999 RGB reference. We found that the low residuals given by the 1981 NIR sensor are not the rule: 1994 NIR horizontal residuals (9.9 m ± 3.3) are almost double the reference uncertainty. This illustrates one of the limitations of this method.

Comparison to single image georeferencing

One way to separate the glaciological measurements from the estimation of the camera calibration is to use only one photograph displaying the features of interest and to

georeference it, using a Helmert transformation (QGIS, 2017). We conducted this georeferencing for one 1999 image and compared it to the 1999 reference and this 1999 SfM processing. The horizontal residuals are shown in Figure 3c-d. While the SfM results were slightly above the reference uncertainty (6.9 m ± 7.4), the georeferencing results are more than 8-fold above (41.3 m ± 20.9). The georeferencing results are also inconsistent with the SfM processing, as the residuals (compared among themselves) are ~35 m. This offset illustrates the problems created when images with large elevation variations are not orthorectified. Additionally, the difference in surface area of the proglacial lake (Figure 3d) between SfM and georeferencing illustrates scaling problems (the proglacial lake is 12% smaller with the single image georeferencing results).

Results with small features

To demonstrate that our method is applicable for features smaller than a whole glacier terminus, we looked at the elevation of two small moraines on the eastern side of Glacier Blanc (Figure 4).

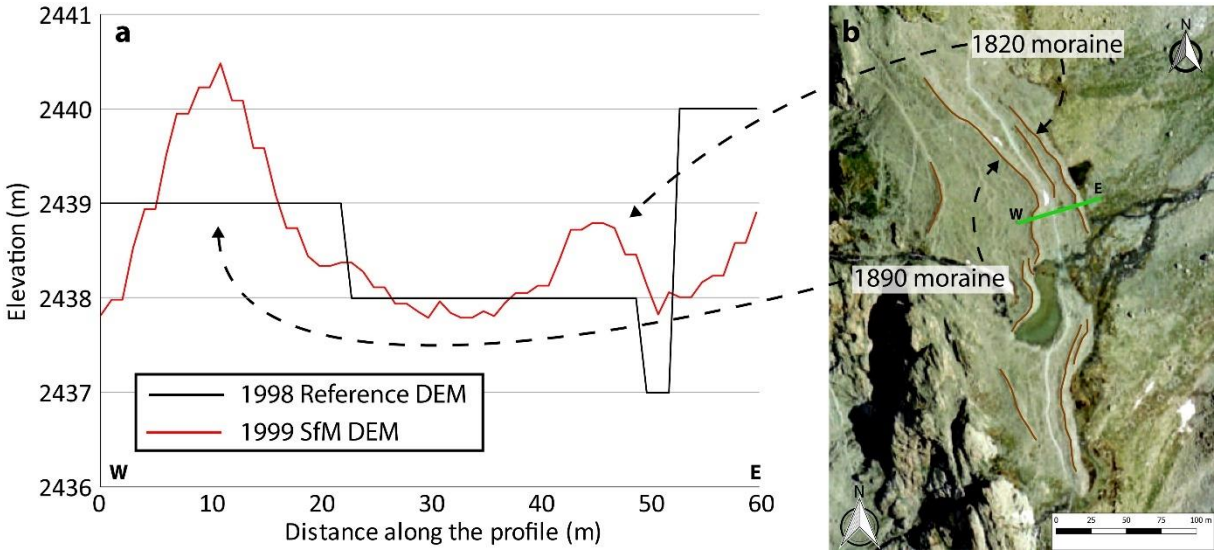

CH3 - Figure 4: Comparison of the 1998 reference DEM and the 1999 SfM DEM. *a) Elevation profiles for two lateral moraines on the eastern side of Glacier Blanc. b) Position of the two moraines (brown lines) and the profile (green line). See Figure 1 for location.*

We sampled the 1999 SfM DEM (resolution 1.5m) along a profile (Figure 4a) crossing the 1820 and the 1890 moraine (Figure 4b). The proglacial pond is surrounded by moraines, which are visible in a transverse profile through the DEM generated via SfM. In the field (September 2014), the 1820 moraine appeared to be ~10 m wide and ~1 m high, which is confirmed by

this transverse profile (Figure 4a) For information, we sampled the 1998 national reference DEM on the same transverse profile. The two moraines are not visible with DEM. However, it must be noted that this DEM resolution is 25 m to fit its purpose as a national DEM, and therefore no direct comparison should be made with the 1999 SfM DEM.

This method that allows the creation of a landscape-wide DEM, also allows the study of the morphology of small features, such as moraines, crevasses or erratic boulders, and not only large features such as sandurs, proglacial lakes or glaciers themselves.

Experiments on elevation determination

Elevation profiles of Figure 4a were not adjusted to have their average elevation match because they are in an area where the reference DEM and the SfM DEM are in good agreement. However, this is not the case everywhere, as shown in Figure 5. When the reference DEM is subtracted from the SfM DEM, stable areas (e.g. bedrock outcrop, proglacial area) should present the same elevation in successive scenes. The resulting difference of DEM (DoD) displays discrepancies ranging from ~-8 m to ~+18 m in a sandur and from ~-28 m to ~+22 m in a steep bedrock zone. In both environments, the shape of these discrepancies is not random. In the sandur, the discrepancy could be approximated to a tilted planar surface and in the bedrock, the discrepancy follows the different thalweg. These phenomena reflect a certain internal consistency of the SfM DEM in each zone.

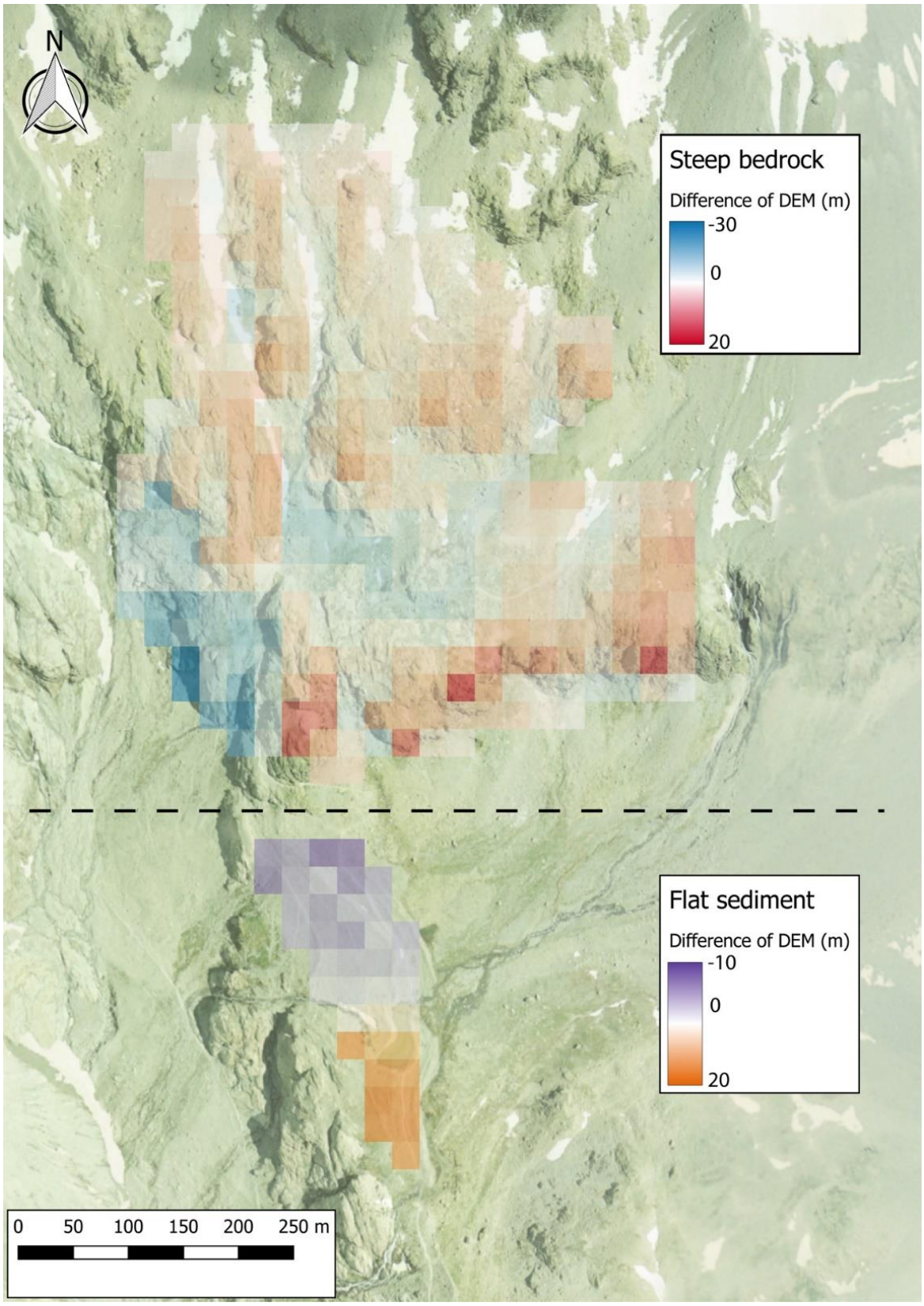

CH3 - Figure 5: Difference of DEM (SfM DEM - reference DEM) for two different zones of the study area illustrating the limitations of this technique regarding vertical resolution*. These two zones – situated on the eastern side of Glacier Blanc – are presumed to be stable and so directly comparable. See Figure 1 for location. The difference in colour intensity between the DEMs and the colour-scale is due to the transparency applied on the DEMs.*

This uncertainty in the elevation, which could be a problem for some applications such as glacial volume calculations, has multiple causes:

1. In steep areas, any horizontal offset between the two DEMs will generate a vertical offset. As low as the horizontal offset can be with this technique, over large areas this phenomenon will become significant. This problem could partially be solved by minimising the horizontal offset, using as many images and GCPs as possible during the SfM process. This is why we did not perform any comparisons between DEM produced with 2, 4 and 9 images, as the results would show a combination of horizontal and vertical offset.

2. The quality of the coordinates (horizontal and vertical) greatly influences the overall georeferencing of the SfM orthoimages and DEMs. In this case, these coordinates have a 5 m uncertainty in all three directions. A simple solution to this problem is using as precise and accurate CPs as possible.

3. The camera lens calibration plays an important role (see below) in the SfM georeferencing. The automatic estimation of this calibration by ©Agisoft Photoscan (or any other SfM software) is a major source of uncertainties in many studies (Wackrow and others, 2007, Micheletti and others, 2015a).

Vertical uncertainty remains one of the major limitations of this method, especially in glaciology where elevation change is important for glacier modelling, energy balance studies, ELA and snowline estimation, meteorology, resolving glacier hypsometry and calculating volume change.

Experiments on image saturation

Another limitation of this method is linked to the glaciological environment: the presence of highly reflective snow. The SfM technique relies on feature detection between different images to reconstruct surfaces. This feature detection does not work on texture-less surfaces such as uniform snowfields or saturated areas of photographs due to the reflection produced by snow.

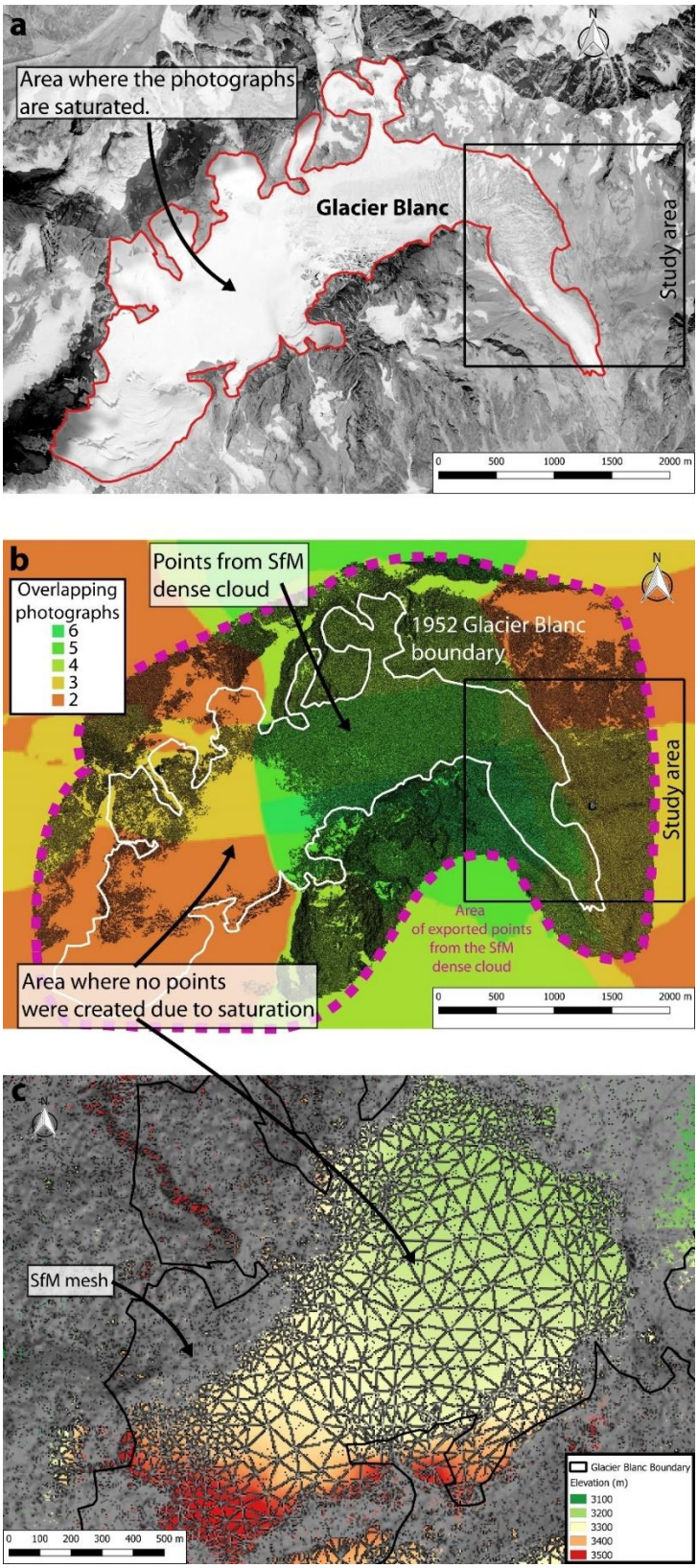

CH3 - Figure 6: Impact of saturated area in images on SfM processing*. a) 1952 orthoimage of Glacier Blanc with the saturated area due to heavy snow cover. b) Dense cloud points produced by SfM processing with number of photographs overlapping for the different zone. In the saturated area, there are no points created. c) Zoom of the saturated zone with the mesh overlaid on the DEM. The mesh created without points of the dense cloud is more relaxed than in the surrounding area. The dense cloud points, the photograph overlap and the mesh have all been produced by ©Agisoft Photoscan directly.*

We illustrate this phenomenon in Figure 6. In 1952, Glacier Blanc was largely snow covered in its upper area, giving an extended bright and saturated zone in the photographs (Figure 6a). For this experiment, we processed the entire Glacier Blanc with 7 photographs and 54 GCPs. The SfM algorithm could not detect any features in this saturated zone and consequently no points were created in the dense point cloud (Figure 6b), even if this zone was visible in 2 to 6 photographs. ©Agisoft Photoscan created a loose mesh in the area lacking points (Figure 6c) and consequently the effective resolution of the DEM in this zone is inferior to the resolution of the surrounding zones.

During the processing of the main study, some features were detected (and so points were created) in other saturated areas. However, the resulting points presented large vertical discrepancies with their surroundings and so were removed from the mesh creation process. At present, we are unaware of solutions to these problems during the image processing stage. A solution, at the post-processing stage like for traditional photogrammetry, is to directly correct the results: e.g. on DEM, it will be possible to manually extract the concerned zones and replace them with interpolated data. It is also possible to apply error detection algorithms (Milan and others, 2011, Lindsay & Creed, 2006) and correct at least the small concerned zones (Lindsay & Creed, 2005). However, in the framework of our main project, these solutions were not viable due the extent of the problematic areas.

Uncertainties due to unknown camera calibration

Using historical aerial images for this method often means that there is no camera lens calibration available and we therefore must rely on the automatic calibration produced by the software. As mentioned earlier, this is a proven a source of uncertainties in other studies and our study is no exception. Figure 7 gives an example of the automatic calibration produced by ©Agisoft Photoscan for 1952 and 1999. In 1952, the residuals on the camera calibration reach 2 pixels (6 in 1999), which translate to 2.6 m (4.6 m in 1999) in the final orthomosaic image. Except for these calibration reports, it remains difficult to evaluate the impact of the automatic calibration without access to the camera itself. However, after excluding or minimising all other sources of uncertainties during processing, we can affirm that until the SfM technique is improved to produce better automatic camera calibration, this will remain a major limitation of this method.

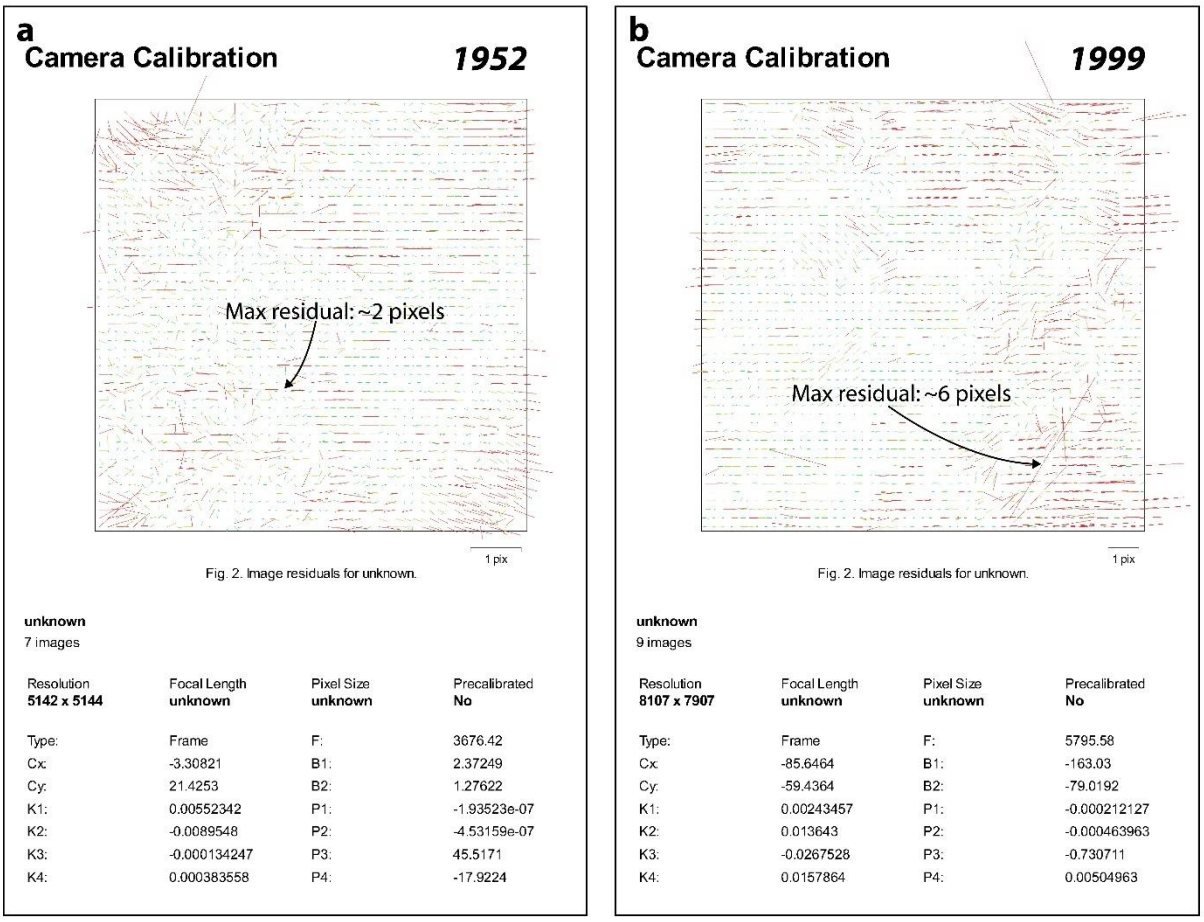

CH3 - Figure 7: Automatic camera calibration report by ©Agisoft Photoscan. *a) Report for 1952 with a maximum internal residual of ~2 pixels. b) Report for 1999 with a maximum internal residual of ~6 pixels.*

Discussion

This method allows the study of glaciers and glacial environments at multiple scales: a large scale (e.g. glacier-wide) to a medium scale (terminus position) to a small scale (lateral moraine). Figure 8 shows where this method fits among the numerous other remote sensing techniques used in glaciology.

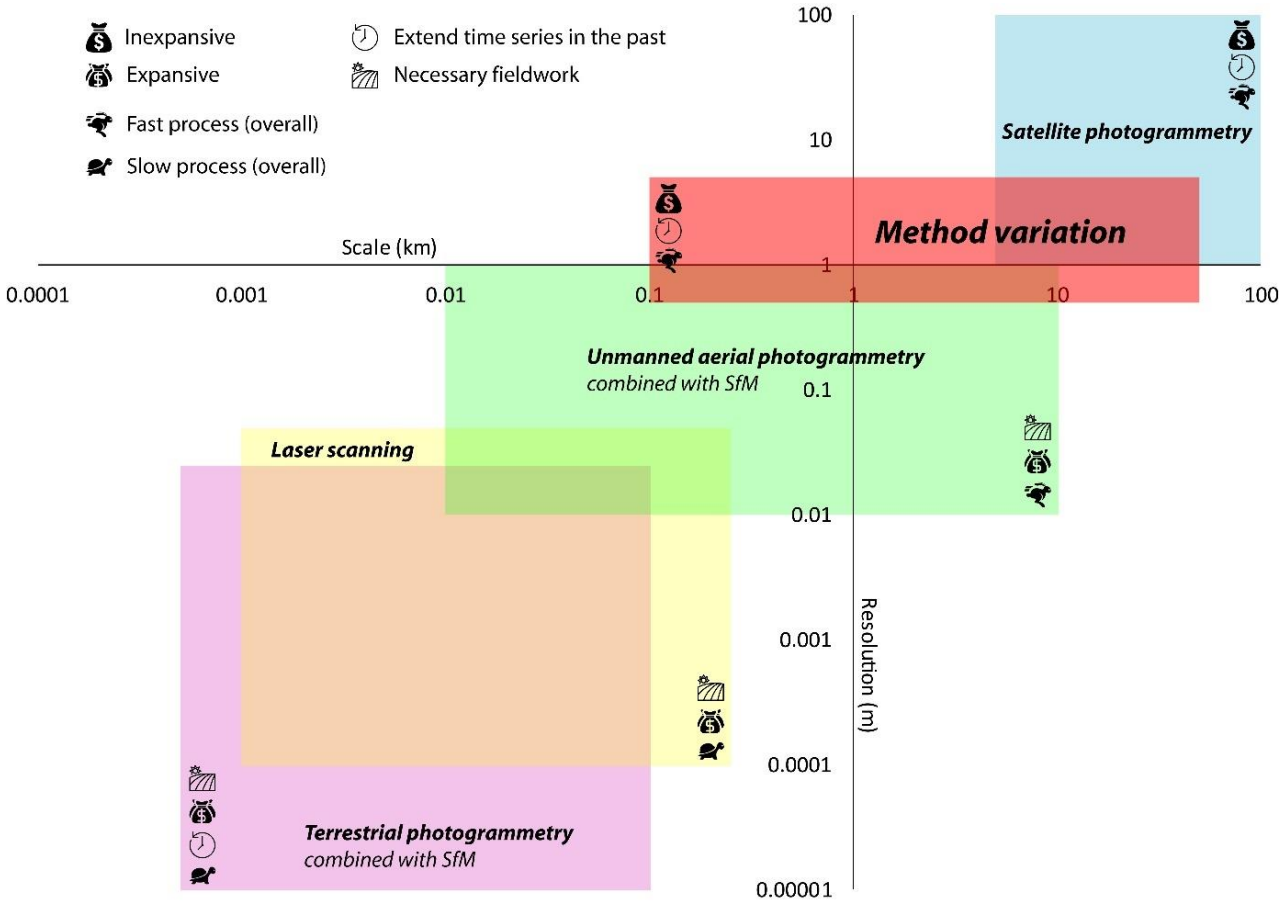

CH3 - Figure 8: Extent in scale and resolution of the various remote sensing techniques used in glaciology and their characteristics*. For the characteristics of "Satellite photogrammetry" and "Method variation", we assume that the images are produced for multiple purposes and the cost resides in purchase the images and not conducting the survey directly. Modified from Figure 1.4 in Luhmann and others (2014).*

In terms of scale and resolution, this method fills the gap between satellite photogrammetry and unmanned aerial photogrammetry. This method still retains the advantage of satellite photogrammetry by being cost effective, fast and giving the possibility of extending a time series in the past without requiring fieldwork.

Despite their costs, unmanned aerial photogrammetry, laser scanning and terrestrial photogrammetry retain as advantages their smaller scales and resolutions, as well as less vertical uncertainties and the glaciology-driven data acquisition.

Thanks to developments in computing and in this age of data mining (Pokrajacl and others, 2003) and big data (Ma and others, 2015), this method could replace traditional photogrammetry for glaciology.

Conclusions

Fine-resolution, orthorectified images and associated DEMs of a glacial environment were produced using SfM with historical aerial imagery, and control points taken from existing referenced datasets. We have shown how glaciological time series analysis can be extended back to the 1930s, providing invaluable datasets concerning glacier terminus position, elevation change and glacier dynamics.

The main advantages of this method over the more traditional approaches are:

- Fast computing time and cost-effectiveness;
- No fieldwork requirement as control points can be obtained with any orthoimage database;
- Only 2 aerial images and 5 control points are necessary to obtain an uncertainty of less than 10 m. Lower uncertainty (2 m) can be reach with more images and CPs;
- Any types of camera sensor can be used (RGB, NIR or panchromatic); and
- Glaciological time series can be extended into the past back to the first aerial photographs in the 1930-1940s.

In this context, the limitations (vertical resolution, image saturation, lens calibration) of this method define the uncertainty of each time series.

Author Contributions

P.L. conducted the study and wrote the paper. T.H. and N.G. supervised the study and co-wrote the paper.

Acknowledgement

The aerial images and geospatial products were provided by the French National Institute of Geographic and Forestry Information under an education and research licence. Information on this licence can be found at the web address http://professionel.ign.fr/enseignement-recherche (accessed online 25/03/2017) and it can be requested at http://professionnels.ign.fr/contact#0 (accessed online 25/03/2017). Some historical aerial

images can be downloaded via the website http://remonterletemps.ign.fr (accessed online 25/03/2017).

References

©Agisoft 2017. Photoscan Professional Edition. http://www.agisoft.com/downloads/installer/, Agisoft LLC.

Braun, M., V.A. Pohjola, R. Pettersson, M. MÖLler, R. Finkelnburg, U. Falk, D. Scherer and C. Schneider 2011. Changes of Glacier Frontal Positions of Vestfonna (Nordaustlandet, Svalbard). Geografiska Annaler: Series A, Physical Geography, 93(4): 301-310.

Chandler, J. 1999. Effective application of automated digital photogrammetry for geomorphological research. Earth Surface Processes and Landforms, 24(1): 51-63.

Chandler, J.H. and J.G. Fryer 2005. Recording aboriginal rock art using cheap digital cameras and digital photogrammetry. Recording aboriginal rock art using cheap digital cameras and digital photogrammetry.

Colomina, I. and P. Molina 2014. Unmanned aerial systems for photogrammetry and remote sensing: A review. ISPRS Journal of Photogrammetry and Remote Sensing, 92: 79-97.

Cossart, E., M. Fort, V. Jomelli and D. Grancher 2006. Les variations glaciaires en Haute-Durance (Briançonnais, Hautes-Alpes) depuis la fin du xix e siècle: mise au point d'après les documents d'archives et la lichénométrie. *Quaternaire*, **17**: 75-92.

Fonstad, M.A., J.T. Dietrich, B.C. Courville, J.L. Jensen and P.E. Carbonneau 2013. Topographic structure from motion: a new development in photogrammetric measurement. Earth Surface Processes and Landforms, 38(4): 421-430.

Harder, P., M. Schirmer, J. Pomeroy and W. Helgason 2016. Accuracy of snow depth estimation in mountain and prairie environments by an unmanned aerial vehicle. The Cryosphere, 10(6): 2559-2571.

Huss, M., L. Dhulst and A. Bauder 2015. New long-term mass-balance series for the Swiss Alps. Journal of Glaciology, 61(227): 551-562.

Irvine-Fynn, T.D.L., E. Sanz-Ablanedo, N. Rutter, M.W. Smith and J.H. Chandler 2014. Measuring glacier surface roughness using plot-scale, close-range digital photogrammetry. Journal of Glaciology, 60(223): 957-969.

Javernick, L., J. Brasington and B. Caruso 2014. Modeling the topography of shallow braided rivers using Structure-from-Motion photogrammetry. Geomorphology, 213: 166-182.

Lardeux, P., N. Glasser, T. Holt and B. Hubbard 2015. Glaciological and geomorphological map of Glacier Noir and Glacier Blanc, French Alps. Journal of Maps, 12(3): 582-596.

Letreguilly, A. and L. Reynaud 1989. Past and forecast fluctuations of glacier Blanc (French Alps). *Annals of Glaciology*, **13**: 159-163.

Lindsay, J.B. and I.F. Creed 2005. Removal of artifact depressions from digital elevation models: towards a minimum impact approach. *Hydrological Processes*, **19**(16): 3113-3126.

Lindsay, J.B. and I.F. Creed 2006. Distinguishing actual and artefact depressions in digital elevation data. *Computers & Geosciences*, **32**(8): 1192-1204.

Lucieer, A., S.M.d. Jong and D. Turner 2013. Mapping landslide displacements using Structure from Motion (SfM) and image correlation of multi-temporal UAV photography. Progress in Physical Geography, 38(1): 97-116.

Luhmann, T., S. Robson, S. Kyle and J. Boehm 2014. Close-Range Photogrammetry and 3D Imaging. De Gruyter.

Ma, Y., H. Wu, L. Wang, B. Huang, R. Ranjan, A. Zomaya and W. Jie 2015. Remote sensing big data computing: Challenges and opportunities. Future Generation Computer Systems, 51: 47-60.

Mertes, J.R., J.D. Gulley, D.I. Benn, S.S. Thompson and L.I. Nicholson 2017. Using structure-from-motion to create glacier DEMs and orthoimagery from historical terrestrial and oblique aerial imagery. *Earth Surface Processes and Landforms*.Micheletti, N., J.H. Chandler and S.N. Lane 2015a. Structure from Motion (SfM) Photogrammetry. Geomorphological Techniques, British Society for Geomorphology, 12.

Micheletti, N., S.N. Lane and J.H. Chandler 2015b. Application of archival aerial photogrammetry to quantify climate forcing of alpine landscapes. Photogrammetric Record, 30(150): 143-165.

Midgley, N.G. and T.N. Tonkin 2017. Reconstruction of former glacier surface topography from archive oblique aerial images. Geomorphology, 282: 18-26.

Mikhail, E.M., J.S. Bethel and J.C. McGlone 2001. Introduction to modern photogrammetry. New York.

Milan, D.J., G.L. Heritage, A.R.G. Large and I.C. Fuller 2011. Filtering spatial error from DEMs: Implications for morphological change estimation. *Geomorphology*, **125**(1): 160-171.

Moller, M. and C. Schneider 2010. Calibration of glacier volume-area relations from surface extent fluctuations and application to future glacier change. Journal of Glaciology, 56(195): 33-40.

Nolan, M., C. Larsen and M. Sturm 2015. Mapping snow depth from manned aircraft on landscape scales at centimeter resolution using structure-from-motion photogrammetry. The Cryosphere, 9(4): 1445-1463.

Piermattei, L., L. Carturan and A. Guarnieri 2015. Use of terrestrial photogrammetry based on structure-from-motion for mass balance estimation of a small glacier in the Italian alps. Earth Surface Processes and Landforms, 40(13): 1791-1802.

Pokrajacl, D., K. Amoakol, H. Patel, J. Brooks, N. Cenat, K. Marcus and S. Darden 2003. Data mining in geosciences. Data mining in geosciences, 534-537.

Prosdocimi, M., S. Calligaro, G. Sofia, G. Dalla Fontana and P. Tarolli 2015. Bank erosion in agricultural drainage networks: new challenges from structure-from-motion photogrammetry for post-event analysis. Earth Surface Processes and Landforms, 40(14): 1891-1906.

QGIS, D.T. 2017. QGIS Geographic Information System. http://www.qgis.org/ , Open Source Geospatial Foundation Project. http://qgis.osgeo.org .

Rippin, D.M., A. Pomfret and N. King 2015. High resolution mapping of supra-glacial drainage pathways reveals link between micro-channel drainage density, surface roughness and surface reflectance. Earth Surface Processes and Landforms, 40(10): 1279-1290.

Roe, Gerard H., Marcia B. Baker and F. Herla 2016. Centennial glacier retreat as categorical evidence of regional climate change. Nature Geoscience, 10(2): 95-99.

Tonkin, T.N., N.G. Midgley, D.J. Graham and J.C. Labadz 2014. The potential of small unmanned aircraft systems and structure-from-motion for topographic surveys: A test of emerging integrated approaches at Cwm Idwal, North Wales. Geomorphology, 226: 35-43.

Vargo, L.J., B.M. Anderson, H.J. Horgan, A.N. Mackintosh, A.M. Lorrey and M. Thoton 2017. Using structure from motion photogrammetry to measure past glacier changes from historic aerial photographs. *Journal of Glaciology*, **63**(242): 1105-1118.

Wackrow, R., J.H. Chandler and P. Bryan 2007. Geometric consistency and stability of consumer-grade digital cameras for accurate spatial measurement. The Photogrammetric Record, 22(118): 121-134.

Walstra, J., J.H. Chandler, N. Dixon and T.A. Dijkstra 2004. Time for change-quantifying landslide evolution using historical aerial photographs and modern photogrammetric methods. *Remote Sensing and Spatial Information Sciences*, **35**(4): 475–480.

Westoby, M.J., J. Brasington, N.F. Glasser, M.J. Hambrey and J.M. Reynolds 2012. 'Structure-from-Motion' photogrammetry: A low-cost, effective tool for geoscience applications. Geomorphology, 179: 300-314.

Westoby, M.J., N.F. Glasser, M.J. Hambrey, J. Brasington, J.M. Reynolds and M.A.A.M. Hassan 2014. Reconstructing historic Glacial Lake Outburst Floods through numerical modelling and geomorphological assessment: Extreme events in the Himalaya. Earth Surface Processes and Landforms, 39(12): n/a-n/a.

Whitehead, K. and C.H. Hugenholtz 2014a. Remote sensing of the environment with small unmanned aircraft systems (UASs), part 1: a review of progress and challenges. Journal of Unmanned Vehicle Systems, 02(03): 69-85.

Whitehead, K. and C.H. Hugenholtz 2014b. Remote sensing of the environment with small unmanned aircraft systems (UASs), part 2: scientific and commercial applications. Journal of Unmanned Vehicle Systems: 86-102.

Zemp, M., M. Hoelzle and W. Haeberli 2009. Six decades of glacier mass-balance observations: a review of the worldwide monitoring network. Annals of Glaciology, 50(50): 101-111.

CHAPTER 4: Evolution of Glacier Noir and Glacier Blanc

Geometric change of adjacent clean-ice and debris-covered glaciers over the past two centuries in the French Alps

Submitted to Journal of Glaciology on 26th April 2017.

Resubmitted on 7th July 2017. Rejected on 18th September 2017.

Currently in revision (June 2018).

Lardeux, P., Glasser, N.F., Holt, T, Hubbard, B.

Abstract

Around 12% of European Alpine glaciers are debris-covered, yet little is known about their long-term geometric evolution or response to climate change. In an effort to estimate the impact of the debris layer over the long-term (~200 years), on a glacier-wide scale, we used historical maps, aerial images with the Structure-from-Motion technique and satellite images to produce a time-series of length and surface area for a debris-covered glacier (Glacier Noir) and an adjacent clean-ice glacier (Glacier Blanc) in the French Alps. We also measured surface elevation variations for both glaciers and established a surface velocity time series for Glacier Noir. Directly comparing these glaciers, we show that since 1815, under the same climatic conditions, Glacier Blanc has retreated 21% more than Glacier Noir. The surface areas of both glaciers overall decreased similarly, but the losses occurred in different zones. The surface elevation of both glaciers has reduced since the 1950s. While Glacier Blanc have thinned by more than 60 m, Glacier Noir have thinned by 30m. Glacier Noir showed a mean surface velocity of 4.7 m a^{-1} between 1952-2016 with three periods of acceleration. These geometric changes have occurred under an increase in temperature of at least +2°C since the 1960s. As debris-covered glaciers are still poorly represented in models, the differences in behaviour and response between Glacier Noir and Glacier Blanc could dramatically change predictions concerning the fate of glaciers in the European Alps under future climate scenarios.

Introduction

Alpine glaciers are known to respond sensitively to climate change (Zemp and others, 2015, Roe and others, 2016). Recession and thinning of glaciers have been accelerating since the end of the Little Ice Age (LIA) across the European Alps (WGMS & NSIDC, 1989, updated 2012), although there is inter-annual and regional variability. Most studies have focused on the response of clean-ice (also called bare-ice or debris-free) glaciers to climate change (Vincent, 2002, Vincent and others, 2004). However, little is documented or known about the influence of climate change on the response of debris-covered glaciers, which represent 12% of all glaciers in the European Alps (Chapter 5).

According to Kirkbride in Singh and others (2011), a debris-covered glacier is “where part of the ablation zone has a continuous cover of supraglacial debris across its full width”. The potential effects of this layer of debris on the surface of a glacier include, but are not limited

to, lower surface melting rate under the debris if the debris thickness is greater than a few centimetres, higher tendency to form supraglacial ponds due to differential melting (Reznichenko and others, 2010), perturbation of hydrological systems (Fyffe, 2012),creation of large “dead ice” masses in proglacial areas (Reznichenko and others, 2011), and formation of large moraines (Lardeux and others, 2015; Santamaria Tovar and others, 2008). Studies have considered combinations of these phenomena, mostly using modelling (Fyffe and others, 2014, Rounce and others, 2015) and mostly in the Himalayas mountain range (Benn and others, 2012, Nicholson & Benn, 2013).

Previous work on the debris-covered Miage glacier in the Italian Alps (Thomson and others, 2000, Reid & Brock, 2010, Collier and others, 2014) indicates that a debris layer has a similar local impact on glaciers in Europe as in the Himalayas. However, the question remains whether on a glacier-wide scale under the same climatic conditions, the evolution of a debris-covered glacier differs from that of a clean-ice glacier. In this study, we reconstruct the geometric changes of a debris-covered glacier and an adjacent clean-ice glacier under the same climatic conditions over the last 200 years, using a range of historical maps (1854-1965), aerial (1952-2013) and satellite imagery (2014-2016). Our main study sites are Glacier Noir (GN) and Glacier Blanc (GB) in “les Ecrins” National Park, French Alps. Our secondary study sites are seven of the surrounding glaciers.

Field site

Glacier Noir (debris-covered) and Glacier Blanc (clean-ice) are located within 1 km of each other in the Haute Vallée de St Pierre in the French Alps (Figure 1). The glaciers’ glaciological and geomorphological context is described by Lardeux and others (2015). Glacier Noir has been debris-covered for over 150 years, as its name (meaning “Black Glacier” in French) appears on a historical map dated from 1854 (Dépôt de la Guerre, 1854). This status as an “established” debris-covered glacier indicates that the effect of the debris layer is likely to be visible over the long-term, i.e. two centuries.

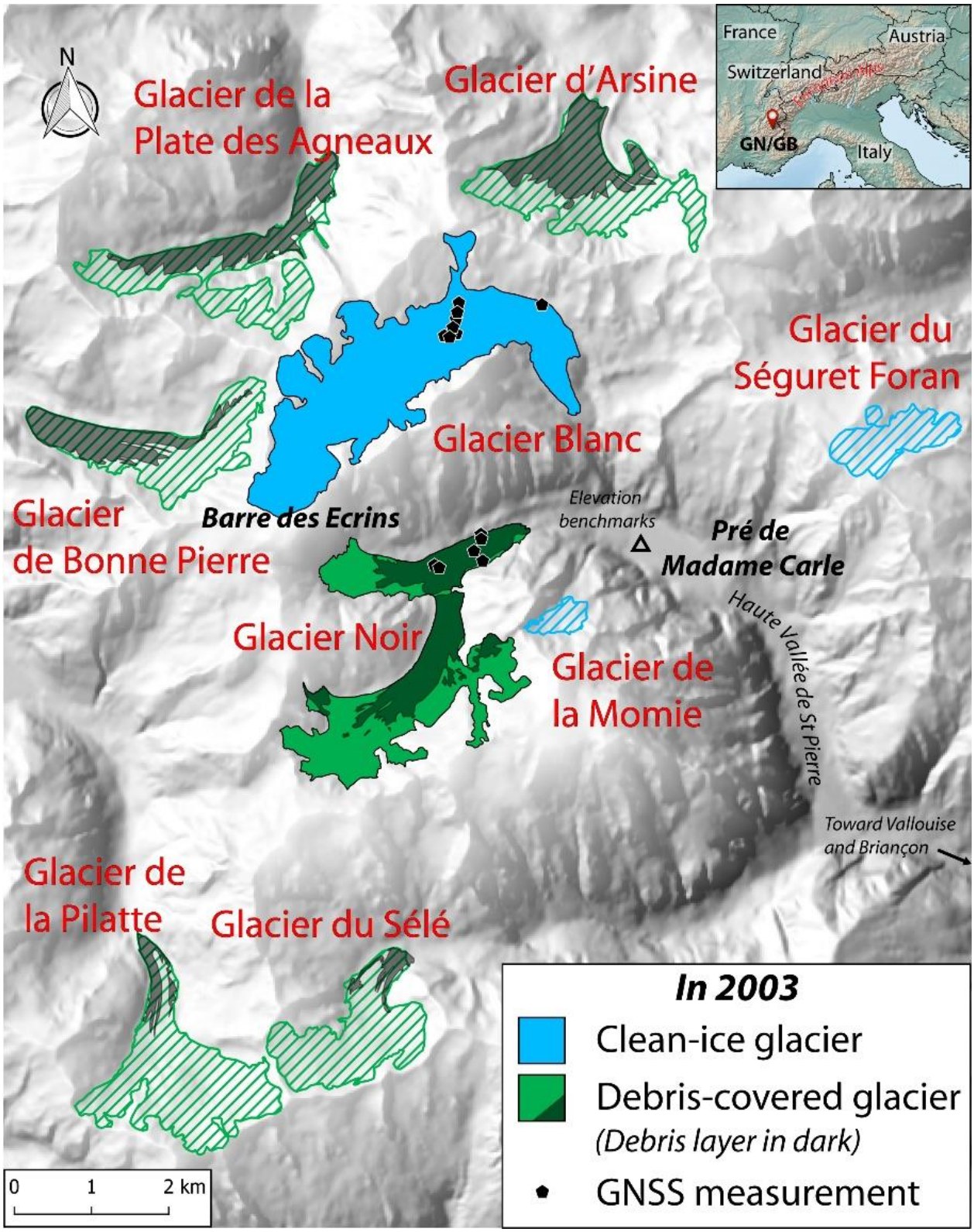

CH4 - Figure 1: Contextual map of Glacier Noir and Glacier Blanc (in 2003*). In solid colour: the main glaciers. In hatch: the secondary glaciers. Inset map: position of the field site in the European Alps. Background: ©BDALTI DEM 25m.*

Until 2009, Glacier Noir was composed of a main branch (~2500 m long in 2016) flowing approximatively west to east and a southern tributary (~3300 m long in 2016) flowing southwest to northeast, whose confluence is ~900 m from its terminus. After 2009, recession and thinning caused the southern tributary to separate from Glacier Noir and was thereafter named Glacier Noir Sud. Given this relatively recent separation, we treat Glacier Noir and Glacier Noir Sud as a single unit. In 2016, Glacier Noir had a surface area of ~3.7 km^2 and an elevation range of 2300-3500 m. During summer 2014, surface debris on the glacier's main trunk was several metres thick near the terminus, and rapidly thinned to 0.3 to 0.4 m up-glacier, reaching a minimum of 0.01 – 0.1 m at ~600 m from the headwall. Although Glacier Noir Sud could not be accessed for survey, the debris layer on Glacier Noir was more than 0.9 m thick at the junction of the two sections, compared to 0.25 m in the surrounding areas (see Methods).

Glacier Blanc (~5000 m long in 2016) predominantly flows southwest to northeast with a southward right-angle turn ~500 m from the terminus in 2016. Its accumulation area is currently composed of one main cirque below the Barre des Ecrins, three smaller glacial cirques on its north side, and two on its south side. Between 2003 and 2009, one of the glaciers on the north side cirques dramatically shrank and after 2014 disappeared. Glacier Blanc has a surface area of ~4.7 km^2 and an elevation range of 2600-3900 m in 2016. Several studies (Rabatel and others, 2002, Rabatel and others, 2008, Rabatel and others, 2013) have evaluated the impact of climate change on Glacier Blanc, particularly on its equilibrium line altitude (ELA) and mass balance. For the period from the 1980s to 2000s, the glacier's ELA rose by ~200 m and its mass balance was negative, losing ~15 m water equivalent during this period. There has been no similar study on Glacier Noir.

Glacier Noir and Glacier Blanc had a common terminus during the LIA, located in the upper section of Pré de Madame Carle in ~1815. The two glaciers started to separate in ~1875. This common history, their proximity and their similarities (orientation, surface area and elevation range) make Glacier Noir and Glacier Blanc a good example of a debris-covered and clean-ice glacier that evolved under the same climatic conditions for at least 200 years.

Datasets

Our datasets cover a period of two centuries, from 1815 to 2016. The 19th century data include historical descriptions of the position of the common terminus in 1815 (around the current position of the National Park buildings in Pré de Madame Carle) and two historical maps, from 1854 and 1874 (Dépôt de la Guerre, 1854, Prudent, 1874).

Additionally, we used almost yearly topographical plans from 1904 to 1965 (Service des Eaux et Forêts, 1921-1965) surveyed by the French national service of "Eaux et Forêts", which detail the position of the terminus of Glacier Noir and Glacier Blanc. After 1952, we also used aerial images that are part of the French national historical collection called "©BDORTHO Historique", consisting of ungeoreferenced aerial images produced for mapping until 2013. We also used orthoimages from the database "©BDORTHO 50cm" consisting of georeferenced orthorectified tiles with a resolution of 50 cm for 1999, 2003 and 2013. These two databases are produced by the National Institute of Geographic and Forestry Information (Institut national de l'information géographique et forestière, IGN). For 2014-2016, we used ©SPOT 6 orthoimages, also distributed by IGN. For altimetry data, we used the French national digital elevation model (DEM) with a 25 m resolution contained in the IGN database "©BDALTI 25m" from 1998. In addition to these remotely sensed data, we also collected global navigation satellite system (GNSS) velocity measurements in August-September 2014. The data type used for each year is detailed in supplementary Table S1 and S2. Given the large quantity of data available, we preferentially used datasets that allowed uncertainties to be minimized.

To evaluate the amplitude of climate change on the field site, we accessed meteorological data from the Météo France national weather service at the Pelvoux station (located ~10 km from Glacier Noir/Glacier Blanc, supplementary Figure S4). This station provides monthly temperature data since the 1960s and precipitation data since 1950s to the present day. These datasets have been adjusted by Météo France for equipment changes. Unfortunately, for unknown reasons, both datasets are incomplete. To compensate for the difference in elevation between the weather station (1270 m) and higher area of Pré de Madame Carle (2000 m), we used a lapse rate of -0.6 °C per 100 m (Rolland, 2003).

Methods

Maps, plans and image processing

Historical maps are typically in the form of ungeoreferenced digital documents. Consequently, we georeferenced them using a Helmert transformation (7 parameters for scaling, translations and rotations) with the official 1/25,000 topographical map of Glacier Noir/Glacier Blanc area as a reference. Topographical plans were original paper documents. We digitized them using a SLR camera (10 mega-pixels) and then rectified them to remove distortions. Following the same process as the historical maps, we georeferenced the topographical plans using a Helmert transformation with a working document of IRSTEA (Institut national de recherche en sciences et technologies pour l'environnement et l'agriculture) in collaboration with “les Ecrins” National Park describing historical ground control points (GCPs) with their modern coordinates as a reference. ©SPOT 6 satellite orthoimages are distributed by IGN as georeferenced digital tiles. They were directly incorporated in our geographic information system (GIS).

Finally, aerial images were supplied as digital scans of original photographs without geographic information. To obtain orthorectified and georeferenced images, and associated DEMs, we processed these digital scans with the Structure-from-Motion (SfM) technique using ©Agisoft Photoscan (©Agisoft, 2017) (Figure 2). SfM is currently a widely-used technique in geosciences (Westoby and others, 2012), which uses multiple 2-dimensional (2D) digital images of an object at different angles to reconstruct a 3-dimensional (3D) surface. SfM is usually performed with pictures from a camera on the ground or mounted on an unmanned aerial system (UAS). However, as long as pictures present enough texture for the SfM algorithms to recognise the same features in multiple images, this technique can be used with any pictures, including historical aerial images (Midgley & Tonkin, 2017). The SfM process requires GCPs. 161 GCPs were chosen to be off-glacier and visible on as many aerial images as possible (supplementary Figure S1). The final georeferencing results are detailed in supplementary Table S2.

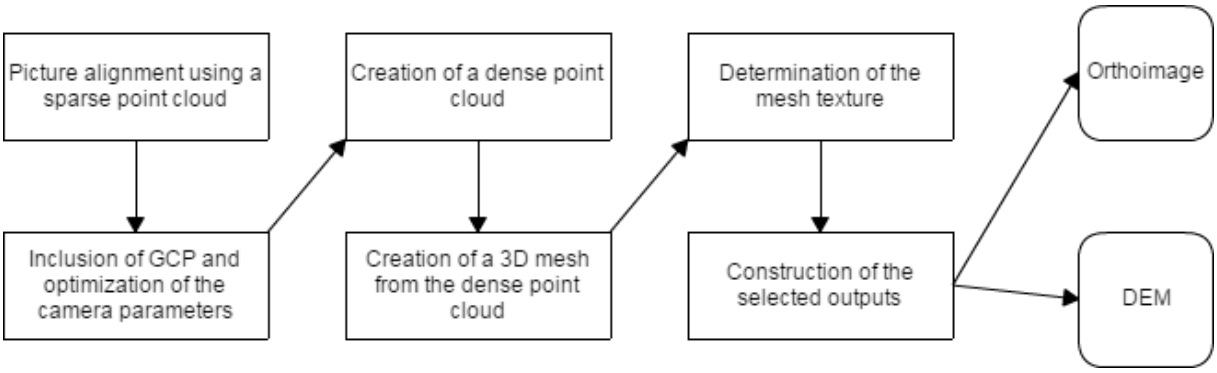

CH4 - Figure 2: Processing steps used for the SfM technique with ©Agisoft Photoscan.

In our case, the outputs were orthorectified and georeferenced images as well as georeferenced DEMs. Due to camera lens distortion, some of these images required a secondary orientation and scaling based on "©BDORTHO 50cm" images of 2013. The GCPs used in the SfM process are also based on "©BDORTHO 50cm" images of 2013 in combination with elevation data of "©BDALTI 25m". For the aerial images of 1999, 2003 and 2009, the GCPs were based on the respective "©BDORTHO 50cm" images of 1999, 2003 and 2009.

Length and area measurements

We used our georeferenced dataset to delineate the terminus position of Glacier Noir and Glacier Blanc at all time periods where the data allowed for such measurements. Based on the different options to measure the terminus position proposed by Lea and others (2014), we chose to use a modified version of the centreline method to accommodate the past variation in the direction of both termini and the past common terminus. The 2013 centreline of each glacier was extended via straight segments to the position of the common terminus in 1815 (Figure 3). These extended centrelines have a common segment and follow the middle of both glaciers as drawn on the 1854 map. We opted for this technique instead of the box method (which smooths the length variation due to change in the terminus shape), as it has known to be more reliable in situations where there is a relatively narrow (compared to the width of the glacier) tongue (Lea and others, 2014).

While terminus positions on maps and plans were digitised only once, terminus positions on orthoimages were digitised three times by a single operator to estimate uncertainty, adapting the method of Paul and others (2013). The operator followed the rules below:

1. The first digitisation is the most "plausible". Following the operator's glaciological experience and the geomorphological context, each glacier is digitised in as much detail as possible.

2. The second digitisation is "positive". If the operator encounters an area of the glacier where the outline position is not certain, the operator includes this area into the glacier (or the digitised feature, e.g. debris layer).

3. The third digitisation is "negative". If the operator encounters an area of the glacier where the outline position is not certain, the operator excludes this area from the glacier or the digitised feature.

We then calculated the coordinates of the point of intersection of the extended centreline and these three terminus positions. The final position of the terminus for a given year is considered to be the average of the coordinates of the three intersections; the uncertainty is the standard deviation of the coordinates. For the maps and plans, we considered the georeferencing residuals to be the uncertainty. In total, we calculated the position of each glacier terminus at 47 time points between 1854 and 2016. Using the final coordinates, we calculated the distance between these terminus positions and different reference points along the centreline (to take into account that the centreline is not a straight line) to arrive at the distance between the terminus at a certain date and the known position of the common front in 1815.

Following the same set of rules, one operator digitized three times the whole glacier outlines, the outlines of the nunataks present in both glaciers, and the debris layer outlines for Glacier Noir (Figure 3). The final surface area of a glacier for a given year is the average of glacier surface area minus nunataks surface area. Uncertainty in the final surface area is the standard deviation of that calculated by the three digitisations. The same methods were used on seven surrounding glaciers, however only for the years 1952 and 2003.

Surface velocity measurements

In August-September 2014, we conducted differential GNSS (code and phase) measurements and global positioning system (GPS) code measurements of six markers on Glacier Noir and eight markers on Glacier Blanc. Measurements were collected on three different dates (24 August, 8-13 September 2014) for Glacier Noir and on two different dates (3-12 September 2014) for Glacier Blanc. Subtracting the coordinates for the different markers and different dates, we calculated the surface velocity of both glaciers over a period of 9 (GB) and 20 (GN) days. The surface velocity for each glacier is calculated by averaging the velocity of all markers.

To extend velocity time-series before 2014 we used manual feature-tracking, since automated feature tracking using ©Cosi-Corr (Leprince and others, 2007) or ©ImGRAFT (Messerli & Grinsted, 2015) was not possible because of the substantial changes in the glaciers' surface appearance between orthoimages. Textureless snow cover and the high surface velocity of Glacier Blanc relative to Glacier Noir meant that it was not possible to track features (such as crevasses) manually on Glacier Blanc. In contrast, feature tracking was possible for Glacier Noir due to its lower velocity and the presence of large identifiable boulders on its surface. One operator manually digitised the position of 895 boulders visible on 18 orthoimages of Glacier Noir from 1952 to 2016. We then compiled the coordinates of these boulders for successive years (17 time slices) and calculated a velocity applied at the mean geometric position of each boulder. Using the kriging method (Zhang, 2009) implemented in ©Golden Software Surfer 8 (Golden Software, 2002), we interpolated a velocity field for each available year, with the boundary condition that the velocity is null at the glacier's margins. We then sampled these different velocity fields at the same location as the field-based GNSS measurements for comparison (Figure 4).

Surface elevation measurements

We used the DEM constructed via the SfM technique to measure the surface elevations of Glacier Noir and Glacier Blanc. Like some orthoimages, due to camera lens distortion, some DEMs required a second georeferencing process. Each DEM was then vertically translated to best fit to actual IGN elevation benchmarks located in Pré de Madame Carle (Supplementary Figure S2).

The lack of accurate GCPs and the fact that certain, particularly older (e.g., 1952) aerial images were 'saturated' due the presence of snow (especially on Glacier Blanc) yielded large data gaps and prevented direct comparison of DEMs for both glaciers. These data gaps (both holes in the data and data artefacts) created inconsistencies between DEMs of stable areas ranging from tens to hundreds of metres vertically. The data gaps and some distortions created by the absence of photogrammetric camera calibration prevented the calculation of DEMs of difference, and consequently the calculation of geodetic mass balance.

However, by using corrected two-dimensional profiles with minimum data gaps, we were able to give an estimation of the surface elevation change between 1952 and 2013 for both glaciers at two different locations on each glacier. These profiles have been chosen to be the longest possible with no or very few artefacts/distortion problems across the fifteen time slices.

Two transverse profiles and one longitudinal profile were selected on each glacier (Figure 5). Each profile starts and ends at a bedrock location, assumed to be stationary through the 61-year period. This allowed us to correct each pair of profiles to these tie points. Every profile has been adjusted to fit the 1952 tie points as a reference year.

After correction, the elevation was sampled every 50 m for each profile. The sampling point closest to the centreline was chosen to calculate the surface elevation changes by subtracting the elevation from one period from the previous (e.g. Z_{1960}-Z_{1952}). Uncertainty for each time slice corresponds to the correction applied on the sampling point to fit each profile with 1952.

Debris thickness

The debris layer thickness presented in the field site section was measured manually at in 24 different locations on Glacier Noir. At each location, the debris was excavated down to the ice surface. Then, using a measuring tape placed vertically along an ice axe, the debris thickness was measured against a horizontal marker laid on the debris surface in three different directions. The results were directly averaged to the closest centimetre.

Results

Changes in glacier length

We examined the distance from the 1904 terminus of Glacier Noir and Glacier Blanc to the respective terminus positions – therefore the change in length – for 47 different years (Figure 3). Glacier Noir and Glacier Blanc display two distinct behaviours in their retreat pattern. The Glacier Noir terminus retreated 536 m between 1904 and 2016 (~5 m a^{-1}). In the same period, Glacier Blanc retreated 1376 m (~11 m a^{-1}). These recession rates vary depending on the time period considered. To facilitate the direct comparison of Glacier Noir and Glacier Blanc, we divided the time series into periods characterised by specific behaviour of one or the other glacier (grey areas in Figure 3) and summarised the different recession rates in Table 1.

CH4 - Table 1: Length variation rate for Glacier Noir and Glacier Blanc. *The length variation rate in metres per year (m a^{-1}) was calculated using linear regression over the period. Grey rows correspond to grey areas in Figure 3.*

	Length variation rate (m a^{-1})	
Period	**Glacier Noir**	**Glacier Blanc**
1815-2016	-7.4 ± 0.1	-10.5 ± 0.1
1904-2016	-4.9 ± 0.2	-10.8 ± 0.2
1815-1904	-14.9 ± 0.3	-12.4 ± 0.4
1904-1945	3.5 ± 0.5	-4.7 ± 0.5
1945-1974	-6.5 ± 1.1	-16.6 ± 0.6
1974-1988	-6.3 ± 1.6	11 ± 1.2
1988-2009	-4.3 ± 0.6	-22.5 ± 0.7
2009-2016	-34.2 ± 6.2	-64.3 ± 13.5

Overall, during the well-documented period 1904 to 2016, the recession rate of Glacier Blanc was 2.2 times faster than Glacier Noir, bringing its terminus 2.6 times further from its 1904 position than Glacier Noir.

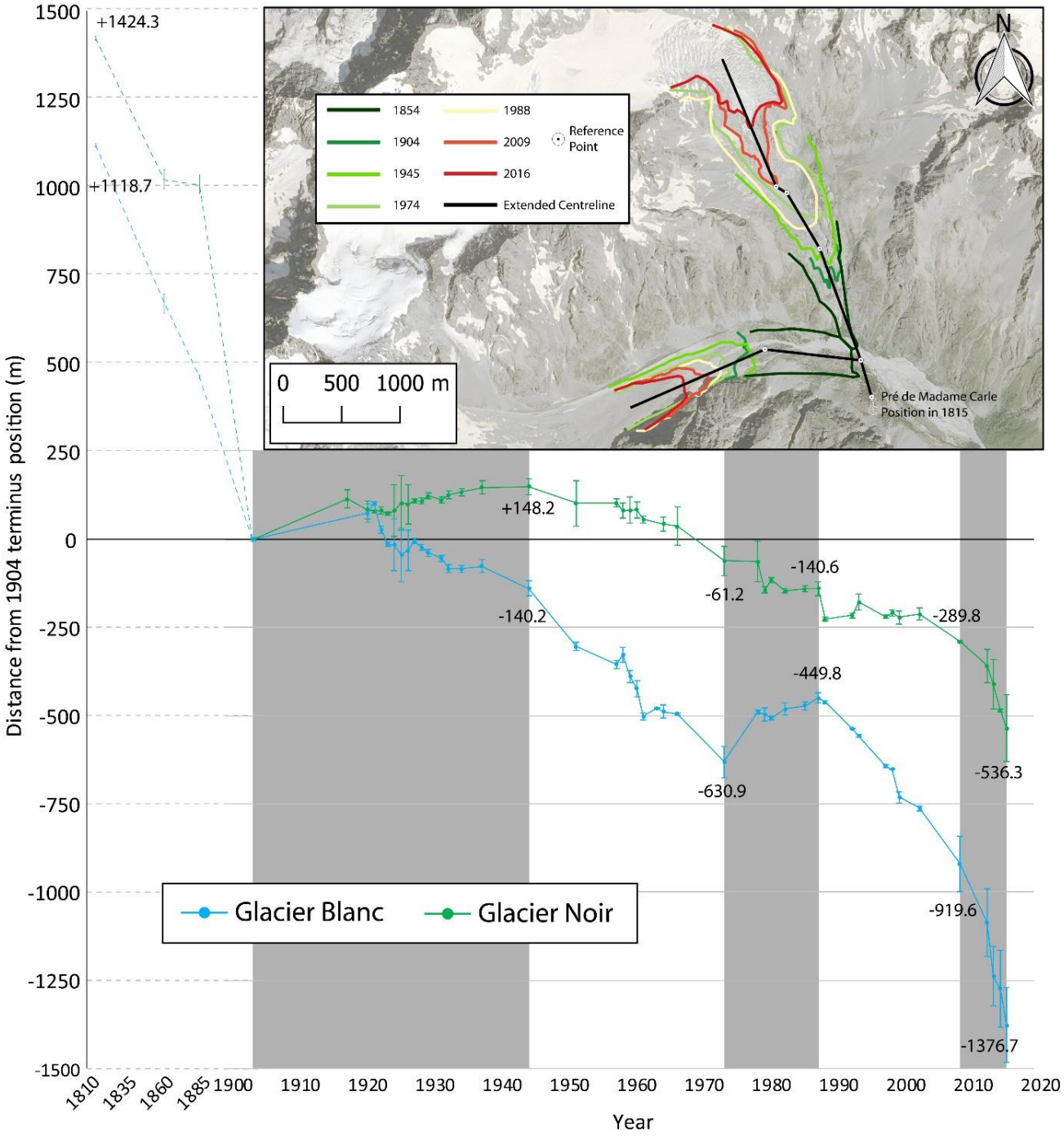

CH4 - Figure 3: Length variations of Glacier Noir and Glacier Blanc between 1815 and 2016. *For readability, the time scale is different for the 1810-1900 period. The sign of the distance indicates the direction of change: positive indicates an advance, negative indicates a recession. The grey areas are referenced and described in the text. The numbers at the boundaries of each grey areas correspond to the distance of the terminus at that time. The inset map shows the position of the termini for the years of the grey areas on the chart. The thick black line represents that along which the length variations were measured. The reference points are fixed and used to link the different parts of the measuring line.*

Changes in glacier surface area

We calculated the surface area changes of Glacier Noir and Glacier Blanc between 1854 and 2016 (21 different years), as well as the percentage debris cover of Glacier Noir for 1952-2016 (19 different years; Figure 4). Contrary to the changes in length, the two glaciers have similar behaviour in terms of changes in their surface areas. The surface area of Glacier Noir decreased from ~7 km^2 in 1854 to less than 4 km^2 in 2016. During the same period, the surface area of Glacier Blanc decreased from ~8 km^2 to less than 5 km^2, a loss of 3 km^2.

Where possible, we separated the comparison times into the same periods (or as close as possible depending on the available data) as those used for the length (grey areas in Figure 4). Similarly to the length variation, we summarised the surface area variation rates in Table 2 for Glacier Noir and the its debris cover, and Glacier Blanc.

***CH4 - Table 2: Surface area variation rate for Glacier Noir and Glacier Blanc**. The surface area variation rate is in kilometre squared per year (km^2 yr^{-1}) and was calculated using linear regression over the period. Grey rows fit grey areas in Figure 4.*

	Area variation rate (km^2 yr^{-1})		
Period	**Glacier Noir**	**Glacier Blanc**	**Debris cover**
1854-2016	-0.019 ± 0.001	-0.022 ± 0.002	-
1952-2016	-0.012 ± 0.002	-0.019 ± 0.003	0.005 ± 0.004
1854-1952	-0.026 ± 0.003	-0.026 ± 0.008	-
1952-1979	-0.016 ± 0.005	-0.008 ± 0.011	-0.015 ± 0.007
1979-1988	0.018 ± 0.02	-0.005 ± 0.027	0.004 ± 0.037
1988-2009	-0.015 ± 0.006	-0.035 ± 0.007	0.022 ± 0.009
2009-2016	-0.027 ± 0.022	-0.026 ± 0.017	-0.038 ± 0.026

The inset map of Figure 4 shows that Glacier Noir and Glacier Blanc lost surface area at different elevations. Glacier Blanc lost surface area mostly in the terminus zone and via the disappearance of one of its feeding glaciers. Glacier Noir lost less area in the terminus zone, but more at higher elevation in the South branch and, since 2009, at the junction of Glacier Noir and Glacier Noir Sud.

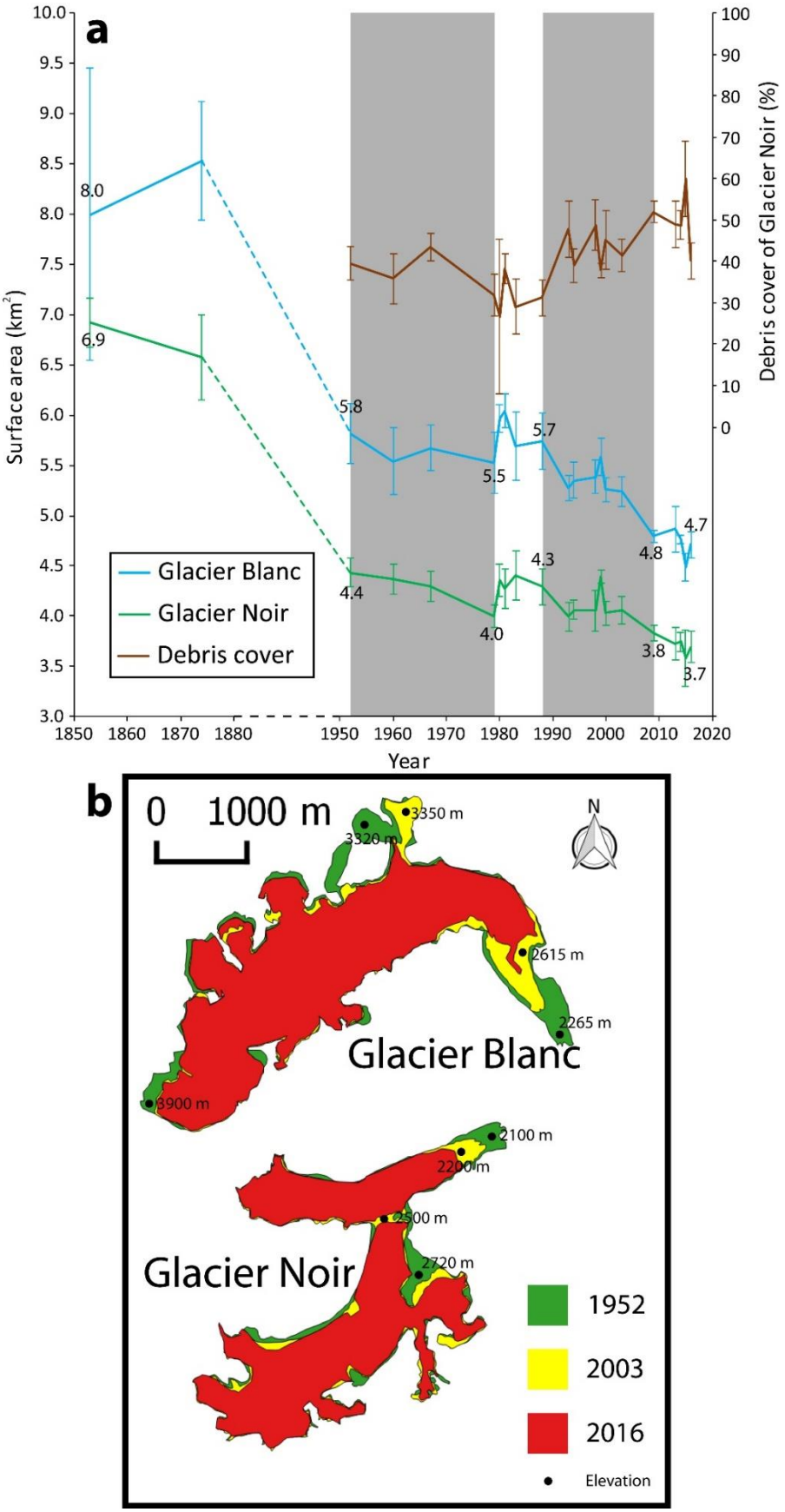

CH4 - Figure 4: Surface area of Glacier Noir and Glacier Blanc*. a) Variations of surface area of Glacier Noir and Glacier Blanc and debris cover of Glacier Noir. For readability, the time scale is different for the 1850-1950 period. The grey areas are described more fully in the text. b) Map showing the extent of both glaciers for three different years and the different elevation where changes happened.*

Overall, Glacier Noir lost almost 50% of its surface since 1854 and Glacier Blanc 40%. Concerning the debris-covered area on Glacier Noir, Glacier Noir was covered on average 41% for 1952-2016 (Figure 4). The debris cover variations present no significant trend and the variability probably does not represent any real change in the quantity of debris on the surface of Glacier Noir (see Interpretation and discussion).

Changes in glacier surface velocity

The GNSS measurements show a clear difference in surface velocity between Glacier Noir and Glacier Blanc. At the end of summer 2014, Glacier Noir had a surface velocity of 0.008 m d^{-1} ± 0.003, while Glacier Blanc is 181-fold faster, with a surface velocity of 1.5 m d^{-1} ± 1.0.

We calculated the surface velocity of Glacier Noir for 17 time slices between 1952 and 2016 using manual feature tracking. During the entire period, the mean surface velocity was 4.7 m a^{-1} ± 2.7, giving a total displacement of ~300 m. The time series can be split into 5 different periods: two acceleration events and three "stable" periods. The two acceleration events occurred between 1980-1983 and 1993-2000 with surface velocity ranging from ~12 to ~16 m a^{-1}. The second and longest event (1993-2000) presents two maxima at ~6 and ~12 m a^{-1}. Between these events, during the "stable" periods, Glacier Noir showed surface velocity ranging from 1.5 to 3.9 m a^{-1} with a mean velocity of 2.4 m a^{-1} ± 1.1. The uncertainty of measurement during those acceleration events is up to 9 times larger than during the "stable" periods, requiring caution in the interpretation.

The inset map of Figure 5 gives the velocity field for 2013-2014, which reveals that the highest surface velocity (~21 m a^{-1}) is found in the upper part of Glacier Noir Sud. Here surface velocities are 10 times faster than the lower/middle part (~2.1 m a^{-1}) of the main branch.

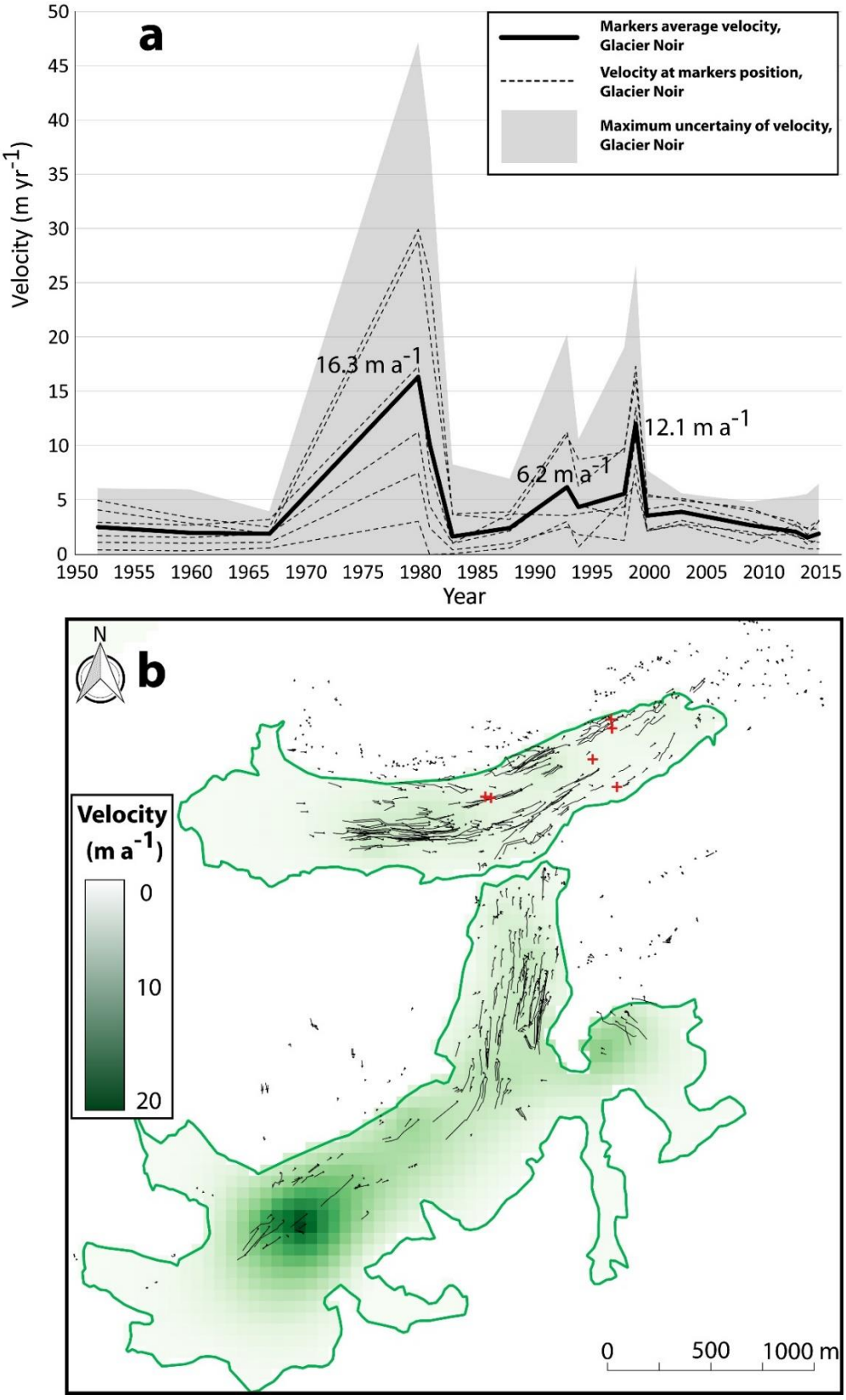

CH4 - Figure 5: Surface velocity of Glacier Noir. *a) Surface velocity variations and GNSS velocity of summer 2014 for Glacier Noir and Glacier Blanc. b) Surface velocity field (background green gradient) of Glacier Noir for 2013-2014 as well as the trajectories (black thin lines) of every tracked boulder between 1952 and 2016. The red crosses are the location of the GNSS measurements and are the sampling points for each velocity field generated. The green line represents the boundaries of Glacier Noir in 2014.*

Changes in glacier surface elevation

Figure 6 summarizes surface elevation changes for Glacier Noir, Glacier Noir Sud and Glacier Blanc between 1952 and 2013. Although the uncertainties remain large for some data points preventing detailed conclusions, some general observations are possible by the length of the time series. The relative surface elevation variations of the six transverse profiles (Figure 6b) can be grouped as follows:

The Glacier Noir and Glacier Blanc lower profiles show similar behaviour with a lowering trend in 2013 with relative variations around -20 m (GB) and -40 m (GN).

The Glacier Noir higher profile and both Glacier Noir Sud profiles show a gain in elevation until 2000 and then a lowering starting in 2013 with relative variations around -10 m (GNS) and -20 m (GN).

Finally, the Glacier Blanc higher profile shows high variability during this 61-year period probably due to the presence of snow with, in 2013, a relative variation of ±100 m. This large elevation decrease is visible in the field when observing the access points between the glacier and the mountain side: in the lower part of the glacier, the access points remain on stable terrain on the mountain side, contrary to the higher part where the access points are in freshly exposed and unstable terrain.

Due to the uncertainties in the amplitude of the elevation changes, no inferences could be made about the timing of these changes.

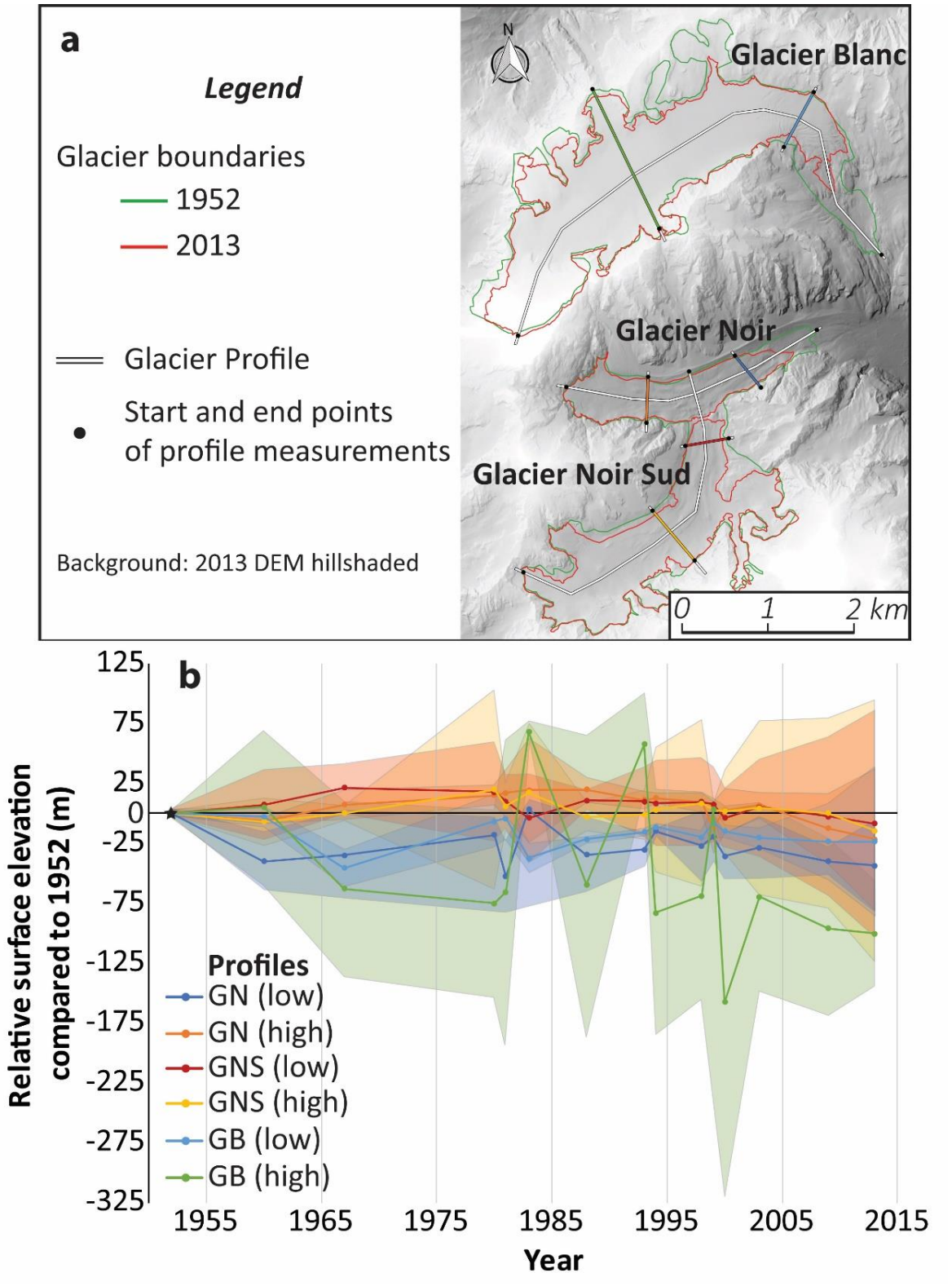

CH4 - Figure 6: Surface elevation changes of Glacier Noir and Glacier Blanc*. a) Map showing the 1952 and 2013 boundaries of Glacier Noir and Glacier Blanc as well as the location of the sampling profiles. b) Time series of surface elevation changes for Glacier Noir and Glacier Blanc. Elevation zero has been setup in 1952. GN = Glacier Noir, GNS = Glacier Noir Sud, GB = Glacier Blanc.*

Figure 7 visually expresses the difference between the various profiles and reflects the analysis of the variations. Figure 7b and f show that little change happened in the highest section (accumulation area) of Glacier Noir and Glacier Blanc. Figure 7d shows that the surface of Glacier Noir Sud lowered almost uniformly between 1952 and 2013.

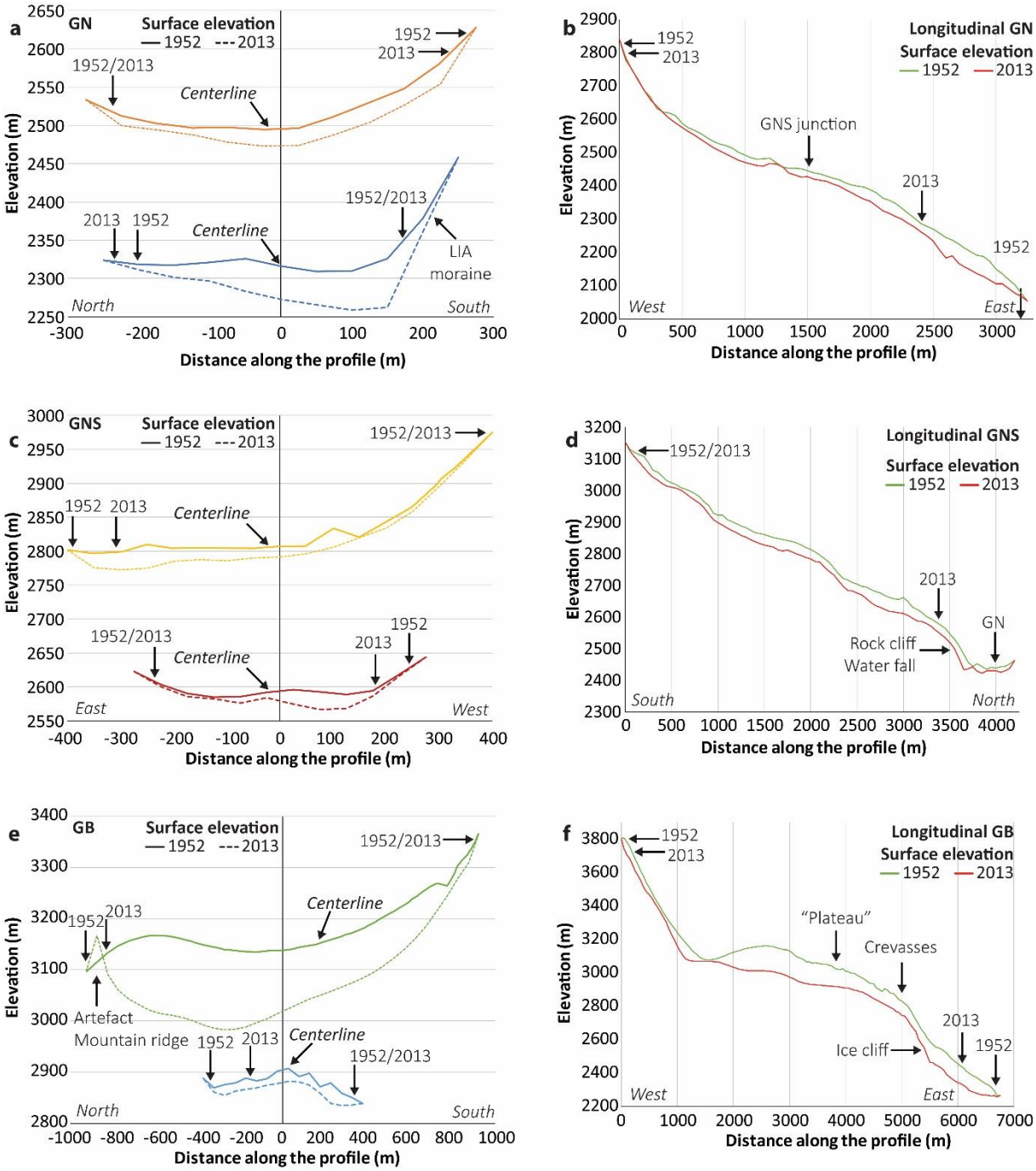

CH4 – Figure 7: Corrected profiles on Glacier Noir, Glacier Noir Sud and Glacier Blanc for 1952 and 2013. *a), c) and e) are transverse profiles (see Figure 6). They are colour-coded the same as Figure 6. b), d) and f) and longitudinal profiles. The 1952 and 2013 arrows represent the location of the glacier headwall and terminus during these years. GN = Glacier Noir, GNS = Glacier Noir Sud, GB = Glacier Blanc.*

Changes in surrounding glaciers

The length and area losses between 1952 and 2003 of Glacier Noir, Glacier Blanc and seven smaller surrounding glaciers (see Figure 1 for locations) are shown in Figure 7. The 1952-2003 losses are expressed as percentage of the 1952 length/area and as a function of the 2003 length and area of each glacier. Glacier Noir and Glacier Blanc stand out as longer and larger glaciers, with relatively small losses of length and area compared to the smaller surrounding glaciers. The smaller glaciers lost between ~4 and ~30% of their length and/or area.

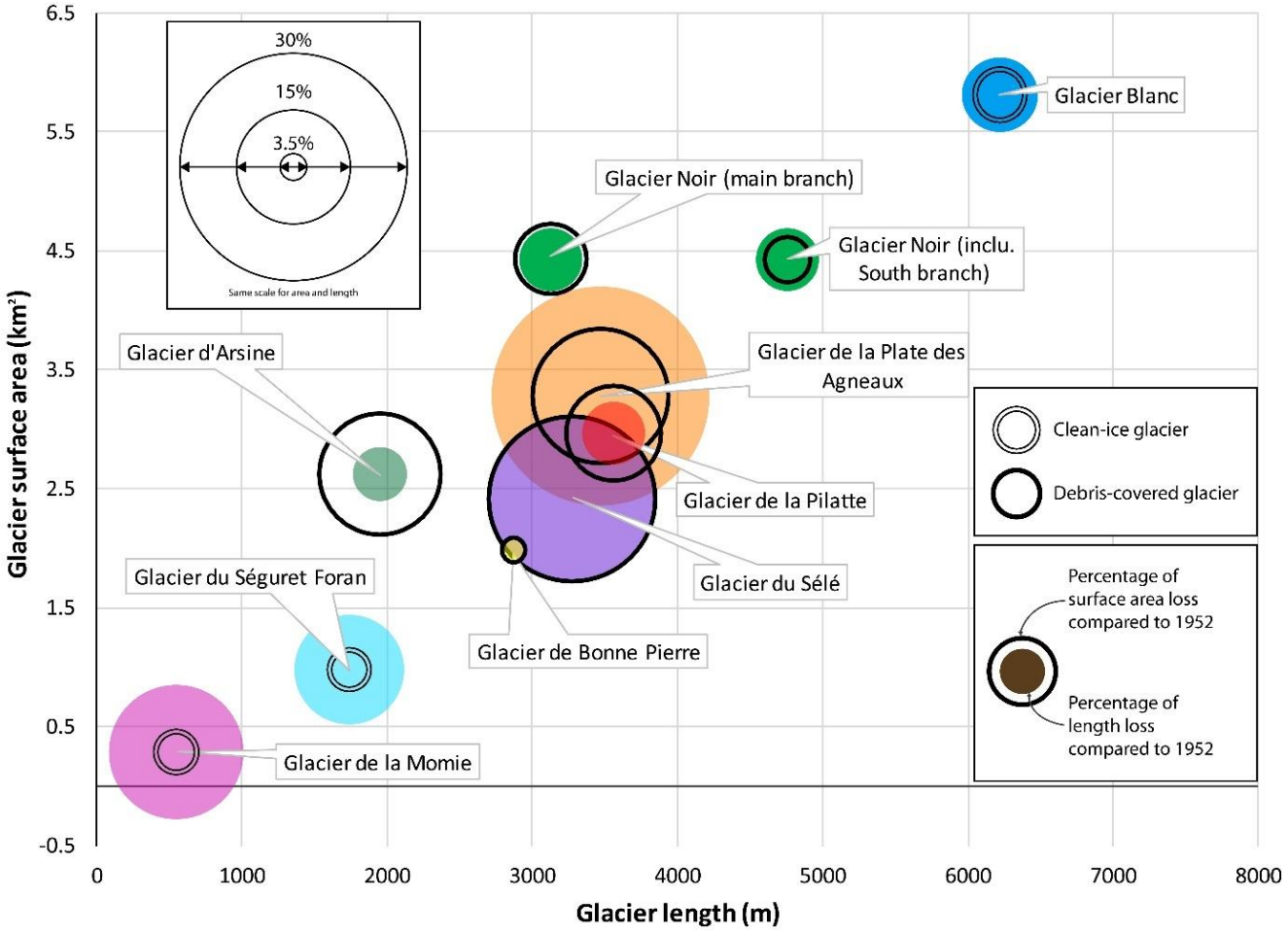

***CH4 - Figure 8: Glacier Noir and Glacier Blanc in their regional context**. Glacier surface area as a function of glacier length for seven surrounding glaciers. The diameter of the bubble represents the percentage of loss in area (filled) and length (empty). The two bubbles for Glacier Noir represent the length measurement from the terminus to the headwall of the main branch and to the headwall of the South branch.*

Climate change

We conducted only a basic analysis of the meteorological data, as our goal was solely to evaluate which factor (temperature or precipitation) was most strongly influenced by climate change and also to evaluate the amplitude of climate change locally.

In the study area, the average annual temperature for the 1961-2015 period (39 data points) was 3.3°C ± 0.8. We represented the deviation of annual mean temperature from this average. For 1961-2015, the study area experienced an increase in mean annual temperature of 1.9°C (Figure 8). This increase reflects both warmer summers (+1.1°C for the average temperature of June, July, August and September) and warmer winters (+2.9°C for the average temperature of November, December, January, February and March). The precipitation data extend from 1950 to 2015 (62 data points) and during this period, the average annual cumulative precipitation is 985 mm (water equivalent) ± 192. During the same period, the average winter cumulative precipitation is 458 mm ± 154 and the average summer cumulative precipitation is 248 mm ± 94. In the same manner as temperature, Figure 8 shows the deviation of annual cumulative precipitation from this average. From 2005-2015, the study area experienced a decrease of 132 mm. However, over the entire period (1950-2015), this decreasing trend is not statistically significant ($R^2 = 0.05$). Seasonally, the 2005-2015 decrease is translated as drier summers (-70 mm) and slightly wetter winters (+55 mm).

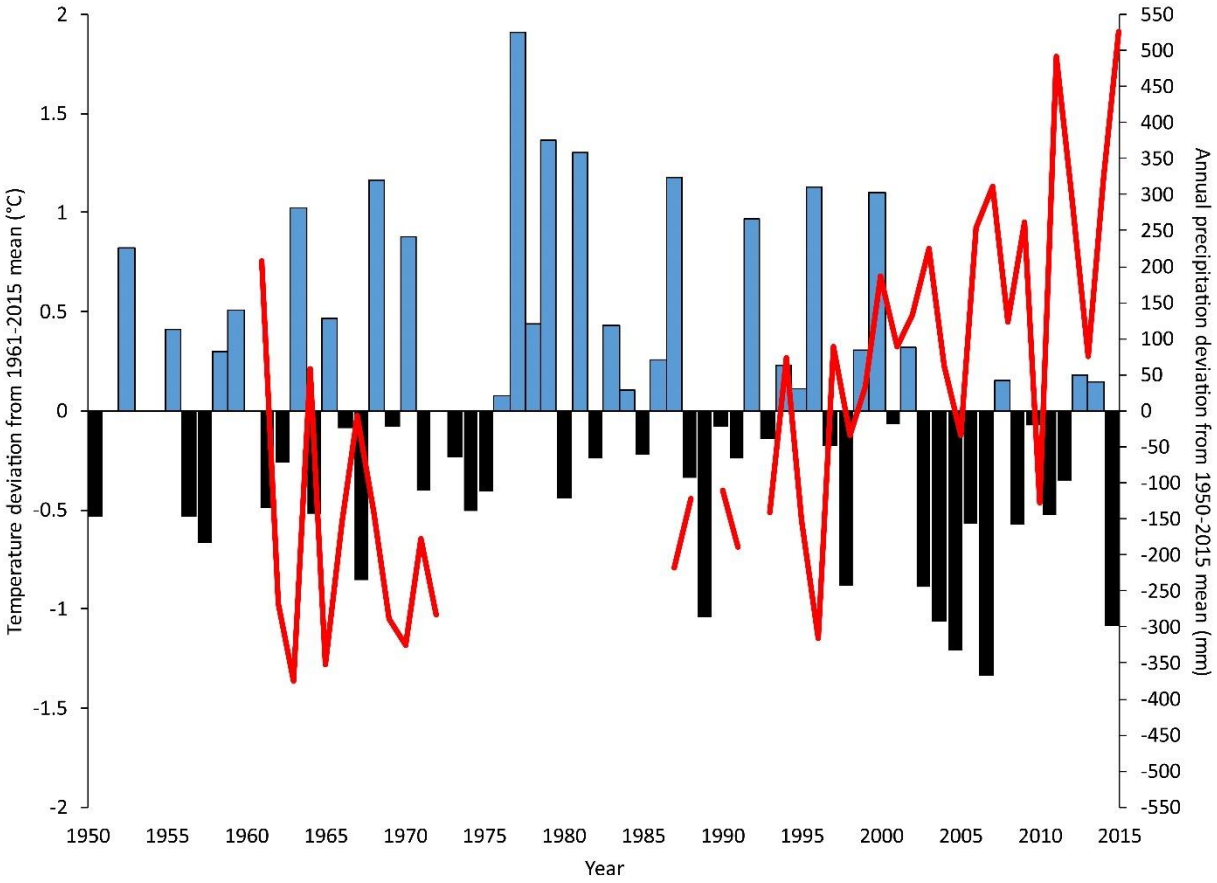

CH4 - Figure 9: Temperature and precipitation deviations in the Glacier Noir/Glacier Blanc area*. The temperature deviation (green line) is calculated using the mean temperature for the 1961-2015 period. The precipitation deviation (blue bar for positive, red bar for negative) is calculated using the mean cumulative precipitation for the 1950-2015 period.*

Interpretation and discussion

Here we interpret the behaviours of Glacier Noir and Glacier Blanc through each of six characteristic time periods displayed in Figure 3 (1815-1904, 1904-1945, 1945-1974, 1974-1988, 1988-2009, 2009-2016) or through periods as close as possible depending on the available data. The comparison and interpretation of both glaciers' length variations, as well as the other parameters (surface area and elevation variations) are used to evaluate the impact of the debris layer on changes in Glacier Noir. It should be noted that variations in length, surface area and elevation are influenced by dynamic effects, response time and by local glacier-specific conditions summarized in Table 3. This sensitivity to local conditions is partially tempered by the long-term perspective (200-year time-series).

CH4 - Table 3: Summary of the local conditions controlling the evolution of Glacier Noir and Glacier Blanc.

Control	Glacier Noir	Glacier Blanc	Influence
Debris cover	Covered	Non-covered	Debris cover decreases melting
Solar radiation*	82% (60% for GNS)	79%	More shadow decreases melting
Bedrock topography	Flat terminus	Steep terminus	Flat topography slows retreat
Basal Conditions	Unknown		Influence the ice flow
Micro-climate	Unknown		Influence melting

** Percentage of the glacier surface area exposed to direct solar radiation (sun exposure), calculated on August 1st, 2013 at noon local time, using the DEM produced via SfM.*

It is assumed that the overall evolution of Glacier Noir and Glacier Blanc is the result of a combination of all the local conditions. In the following discussion, every time it was possible, we strived to explain the possible impact of the debris and the local conditions to explain the differences between the two glaciers. However, it should be assumed that the dominant factor is the mass balance.

Two different recession behaviours

During the first period (1815-1904), both glaciers experienced a recession consistent with the end of the LIA in the European Alps (Luthi, 2014). However, the scarcity of front position data for this period prevents us from giving further interpretation. The lack of data before 1904 makes it difficult to explain the advance of Glacier Noir during the second period (1904-1945). However, Glacier Noir may have been reacting to an isolated climatic (lower temperature and/or higher precipitation) event that happened before 1904, as Glacier Blanc also showed an advance until 1923 and only then retreated. The difference between Glacier Noir and Glacier Blanc could be explained by a longer response time for GN (around 40 years) than GB (around 20 years). Another possibility is that the advance of Glacier Noir was due to a large rock avalanche increasing the supraglacial debris cover and triggering an advance (Marangunic, 1972, Shugar and others, 2012). However, this option does not explain the advance of Glacier Blanc.

During the third period (1945-1974), Glacier Noir showed a much lower recession rate than Glacier Blanc, potentially explained by the insulation effect of the debris cover. The fourth period (1974-1988) corresponds to the advance of many glaciers in the Alps (WGMS & NSIDC, 1989, updated 2012) and Glacier Blanc shows the same behaviour. The climatic reasons for this advance are still unclear (Letreguilly & Reynaud, 1989, Hoelzle and others, 2003). If the advance is due an isolated climatic event, Glacier Noir was not affected, as its recession rate remains the same as in the previous period. However, during the fifth period (1988-2009), Glacier Noir showed a lower recession rate, which could be interpreted as a response to the isolated climatic event of the 1980-1990s. This delayed response of Glacier Noir is probably due to the insulation effect produced by the debris cover. During this fifth period, Glacier Blanc showed a large acceleration of its retreat, reflecting the sharp rise in temperature (Figure 8).

Finally, during the last period (2009-2016), both glaciers showed an accelerated retreat, possibly reflecting the impact of the warmer climatic conditions on their behaviour. Even through this accelerated retreat, the recession rate of Glacier Noir is two time lower than the rate of Glacier Blanc. Part of the acceleration of recession of Glacier Noir might be due to the separation of Glacier Noir Sud. However, the mass balance of both glaciers would be necessary to quantify the impact of this separation.

Considering that both glaciers evolved under similar climatic conditions, and that Glacier Blanc is overall at a higher elevation and has a larger surface area than Glacier Noir, all else being equal, Glacier Blanc would be expected to retreat slower and less than Glacier Noir. However, it is the contrary. Therefore, overall, the difference in length change between Glacier Noir and Glacier Blanc could possibly be explained by the presence of debris on the surface of Glacier Noir. Another possible factor explaining the difference in retreat pattern could be the slope of the bedrock in the terminus area of both glacier: the Glacier Blanc terminus area is steeper than the that of Glacier Noir, making the terminus position more sensitive to mass losses. However, modelling and precise bedrock topography would be necessary to evaluate the impact of the local slope in this context.

Circumstantial similarities in shrinking behaviours

Changes in surface area (Figure 4) are very similar for Glacier Noir and Glacier Blanc ($R > 0.95$ for 1854-2016). These very similar graphs could be explained by two unrelated phenomena. First, the area loss by both glaciers is not in the same part of each glacier (terminus for Glacier Blanc, higher elevation zone for Glacier Noir). It seems coincidental that these losses happened at the same time. Second, the similarities of the surface area change may be partly due to the measured surface areas varying with the presence or absence of snow on both glaciers. This phenomenon is included in the error bars in Figure 4.

Concerning the Glacier Noir Sud glacial area loss, it should be noted that the debris cover in this area appeared less thick than at lower elevation (i.e. at Glacier Noir terminus). This lighter debris cover had probably a reduced insulation effect or even increased melting if the debris layer is very thin (Reznichenko and others, 2010).

Concerning the change in the debris area, it is very likely that it did not vary significantly during this period even with a constant low delivery of fresh debris to the surface. The slight increase in the percentage of coverage is likely due to the shrinking of the glacier itself. This explanation is supported by the fact that the debris area is moderately negatively correlated ($R = -0.5$) with the total surface area of Glacier Noir. This negative correlation may suggest that the years of high melting are the years when the debris delivery slightly increases.

Overall, the similarities in changes of glacier total surface area for Glacier Noir and Glacier Blanc seems coincidental, and mostly reflect the effects of local topography. However, if those effects are excluded, we can see that the surface area losses mostly happened in the terminus zone of both glaciers. Coherently with the length changes, Glacier Noir lost less surface area in the zone with a thick debris layer.

Slow flowing Glacier Noir

Our two GNSS velocity measurements indicate that Glacier Blanc is more dynamic than Glacier Noir. These GNSS measurements should not be directly compared to the longer dataset available for Glacier Noir as the velocities we measured are seasonal (end of summer) and

span only a short period. For information, as of summer 2014, Glacier Noir surface velocity seems consistent with a “stable” period with a velocity around 8 mm ± 3 per day.

The larger surface velocity dataset available for Glacier Noir allows us to refine our description of this glacier. During its “stable” period, Glacier Noir could be considered an almost stagnant glacier in its lower half, at least for the European Alps. However, the acceleration events that Glacier Noir has experienced since 1952 show that the glacier still remains active. The reasons for these events is unknown as none could be linked to a length, surface area or elevation variation. However, fieldwork observations suggest that these acceleration events could be linked to changes in the hydrological system (opening or closing of subglacial channels) of the glacier, as it seems that Glacier Noir during the summer 2014 presented only one main drainage channel. Limitations to our velocity field calculations are given by the boulder trajectories:

- Velocity fields are valid only where boulders are present;
- Local topography of the glacier (supra- and sub-glacial) can influence boulder movements, especially at the boundaries of the glacier where they may fall off-glacier and are re-deposited.

Finally, the boulder trajectories are informative for the overall nature and stability of the terrain surrounding Glacier Noir. For example, some off-glacier boulders on moraines are still moving years after being deposited (up to ~1 m a^{-1}), probably due to the presence of melting ice underneath.

As a first approach, tracking ice-surface boulder movements as a proxy for glacier surface velocity is a useful technique. However, further work is needed to fully understand the specific dynamics of these boulders and how it influences the interpretation of this proxy.

Glacier surface elevation changes

Over the course of 61 years, the surface of Glacier Blanc has lowered by a total of 24 m in its lower part and 100 m higher up. At the same time, Glacier Noir’s lower part has lowered by 44 m and its higher part 22 m. If considered separately, Glacier Noir Sud’s surface has lowered

by 8 and 14 m. If we generalize these thinning trends, we can say that Glacier Noir's surface became steeper when Glacier Blanc and Glacier Noir Sud's surfaces became flatter.

Even with the large uncertainties remaining on the surface elevation variations, Figure 6c-h show a general thinning of both glaciers. Field observations confirm the thinning tendency: the surface elevation lowering of Glacier Noir is expressed by a progressively larger extent of the LIA lateral moraine being exposed (Lardeux and others, 2015);for Glacier Blanc, the thinning is expressed by increased exposure of high-elevation nunataks (Figure S3) and by more difficult access to the glacier surface due to recently exposed unstable terrain.

Without mass balance and flow modelling, the interpretation of the surface elevation changes remains difficult as the uncertainties present in the time series prevent any detailed analysis of potential signals. However, for Glacier Noir, combining the slow surface velocity and the lowering, we can infer that thinning is dominated by surface lowering and not dynamically.

Regional changes

The nine glaciers located in the study area and on which we were able to collect data can be split into three groups. Glacier Noir and Glacier Blanc are in a large (> 4 km^2) and long (> 4 km) glacier group, the debris-covered glaciers (excluding Glacier Noir) form a medium size glaciers group (2-3 km^2, 2-3.5 km), and the two remaining clean-ice glaciers forms a small size glaciers group (< 1 km^2, < 2 km).

Both small glaciers (Glacier du Séguret Foran and Glacier de la Momie) present the same characteristics as Glacier Blanc, with greater relative loss of length than surface area. This could be explained in the same manner as Glacier Blanc, with the majority of surface area occurring in the terminus area, and a consequent reduction in length.

In a similar manner, the medium size glaciers group (Glacier de Bonne Pierre, du Sélé, de la Pilatte, d'Arsine and de la Plate des Agneaux) presents the same characteristics as Glacier Noir: higher or similar loss of surface area than length. This could be explained by a loss of surface area in every zone of the glacier and not only in the terminus. One exception is Glacier de la Plate des Agneaux, which presents the highest percentage of length loss (~19%). This large length loss may be due to the low elevation and relative flatness of the tongue of the glacier, its complex topography and the erosion created by a stream on the North side of the glacier.

With their larger size and length, Glacier Noir and Glacier Blanc do not directly represent the glaciers surrounding them. However, the changes they underwent between 1952 and 2003 are representative of their type (debris-cover, clean-ice), confirming that Glacier Noir and Glacier Blanc evolution can be related to regional phenomena such as climate.

A warmer and drier climate

Similarly to the rest of the French Alps (Durand and others, 2009), the climate of our study area overall has become warmer and drier since the 1950s. Although the precipitation trend remains unclear, it seems likely that the accelerated retreat of Glacier Noir and Glacier Blanc since 2009 is due to the combination of warmer and drier summers and warmer and wetter winters. In summer, the warmer temperatures increase glacial melt directly for Glacier Blanc and through the debris layer for Glacier Noir. Although the increase in temperature is probably enough to partly counteract the insulation effect of the debris layer (Reznichenko and others, 2010). Surface melting could be reduced by lower precipitation and consequently less melting due to rain. In winter, the warmer temperatures lead to less accumulation because of greater winter snowmelt. Even though precipitation increases, due to higher temperature, it may be liquid (rain) and not solid (snow), which also leads to less accumulation and could increase the heat transfer to the glacier surface even through a debris layer (Reznichenko and others, 2010).

Overall, the almost 2°C temperature increase since the 1960s is a clear sign of climate change and could be considered as a main control on the behaviour of Glacier Noir and Glacier Blanc, independently of their surface characteristics (debris-cover or clean-ice).

Conclusion

Overall Glacier Noir has slowed its recession by more than 2-fold (-536 m since 1904) in comparison with the adjacent clean-ice Glacier Blanc (-1376 m), but both glaciers lost ~3 km^2 since 1854. Additionally, Glacier Noir has steepened contrary to Glacier Blanc and Glacier Noir Sud, which have flattened. The influence of the debris layer on all the geometric changes (length, area, velocity, elevation) is nuanced: the presence of debris on the surface of Glacier Noir alone cannot entirely explain differences in variation with Glacier Blanc. Other factors such as local topography, hydrological system and mass balance, are also important and

should be considered in current and paleo-interpretation associated with debris-covered glaciers. Accurate and exhaustive modelling would help differentiate each control and their influence.

Climate change in our study area is clear (almost +3°C in the winter since 1961) and impacts not only Glacier Noir and Glacier Blanc but also the surrounding glaciers. Glacier Noir and Glacier Blanc are representative of those other glaciers. Our study highlights the need to include the surface debris layer in studies of glacier response to climate, especially in mountain range-scale modelling.

In conclusion, we showed here on a long time-scale (over two centuries) and on a glacier-wide scale that a debris-covered glacier and a clean-ice glacier can evolve in significantly different (difference larger than uncertainty) manners despite being under the same climatic conditions. The supraglacial debris layer can potentially influence the behaviour of the debris-covered glacier, modify its response to climate change and thus partially explain the difference.

Acknowledgement

We would like to thank all the personnel of “Ecrins” National Park, who facilitated work in the field and access to the historical documentation. We also would like to thank Emmanuel Thibert from IRSTEA for his help in the field and for all the information he provided. We would like to thank the LGGE for equipment. Finally, we thank Steffan Griffiths, Katie Miles and Helena Pomfret for their help in the field.

All fieldwork was conducted under the activity authorisation 060/2014 of “Ecrins” National Park and was funded by the British Society for Geomorphology under the Postgraduate Research Grant programme and by the Department of Geography and Earth Sciences of Aberystwyth University under the Postgraduate Discretionary Research Fund programme.

The aerial images and geospatial products were provided by the French National Institute of Geographic and Forestry Information under an education and research licence.

The meteorological data have been provided by Météo France under the education and research licence reference MF_FO_GESFI.

References

©Agisoft 2017. Photoscan Professional Edition. http://www.agisoft.com/downloads/installer/, Agisoft LLC.

Benn, D.I., T. Bolch, K. Hands, J. Gulley, A. Luckman, L.I. Nicholson, D. Quincey, S. Thompson, R. Toumi and S. Wiseman 2012. Response of debris-covered glaciers in the Mount Everest region to recent warming, and implications for outburst flood hazards. *Earth-Science Reviews*, **114**(1-2): 156-174.

Cogley, J.G., R. Hock, L.A. Rasmussen, A.A. Arendt, A. Bauder, R.J. Braithwaite, P. Jansson, G. Kaser, M. Moller, L. Nicholson and M. Zemp 2011. Glossary of Glacier Mass Balance and Related Terms. *IHP-VII Technical Documents in Hydrology*, **86**.

Collier, E., L. Nicholson, B.W. Brock, F. Maussion, R. Essery and A. Bush 2014. Representing moisture fluxes and phase changes in glacier debris cover using a reservoir approach. *The Cryosphere*, **8**(4): 1429-1444.

Cuffey, K.M. and W.S.B. Paterson 2010. The physics of glaciers. *The physics of glaciers*.

Dépôt de la Guerre, D.d.l. 1854. Feuille de Briançon. *Carte d'Etat-Major*, Institut national de l'information géographique et forestière.

Durand, Y., M. Laternser, G. Giraud, P. Etchevers, B. Lesaffre and L. Merindol 2009. Reanalysis of 44 Yr of Climate in the French Alps (1958-2002): Methodology, Model Validation, Climatology, and Trends for Air Temperature and Precipitation. *Journal of Applied Meteorology and Climatology*, **48**(3): 429-449.

Fyffe, C.L. 2012. The hydrology of debris-covered glaciers. (PhD University of Dundee.)

Fyffe, C.L., T.D. Reid, B.W. Brock, M.P. Kirkbride, G. Diolaiuti, C. Smiraglia and F. Diotri 2014. A distributed energy-balance melt model of an alpine debris-covered glacier. *Journal of Glaciology*, **60**(221): 587-602.

Golden Software. 2002. Surfer 8. Golden, Colorado 80401, USA, Golden Software, LLC.

Hoelzle, M., W. Haeberli, M. Dischl and W. Peschke 2003. Secular glacier mass balances derived from cumulative glacier length changes. *Global and Planetary Change*, **36**(4): 295-306.

Lardeux, P., N. Glasser, T. Holt and B. Hubbard 2015. Glaciological and geomorphological map of Glacier Noir and Glacier Blanc, French Alps. *Journal of Maps*: 1-15.

Lea, J.M., D.W.F. Mair and B.R. Rea 2014. Evaluation of existing and new methods of tracking glacier terminus change. *Journal of Glaciology*, **60**(220): 323-332.

Leprince, S., S. Barbot, F. Ayoub and J.P. Avouac 2007. Automatic and precise orthorectification, coregistration, and subpixel correlation of satellite images, application to ground deformation measurements. *Ieee Transactions on Geoscience and Remote Sensing*, **45**(6): 1529-1558.

Letreguilly, A. and L. Reynaud 1989. Past and forecast fluctuations of glacier Blanc (French Alps). *Annals of Glaciology*, **13**: 159-163.

Luthi, M.P. 2014. Little Ice Age climate reconstruction from ensemble reanalysis of Alpine glacier fluctuations. *Cryosphere*, **8**(2): 639-650.

Marangunic, C. 1972. Effects of a landslide on Sherman Glacier, Alaska. Institute of Polar Studies.

Messerli, A. and A. Grinsted 2015. Image georectification and feature tracking toolbox: ImGRAFT. *Geoscientific Instrumentation Methods and Data Systems*, **4**(1): 23-34.

Midgley, N.G. and T.N. Tonkin 2017. Reconstruction of former glacier surface topography from archive oblique aerial images. *Geomorphology*, **282**: 18-26.

Nicholson, L. and D. Benn 2013. Properties of natural supraglacial debris in relation to modelling sub-debris ice ablation. *Earth Surface Processes and Landforms*, **38**(5): 490-501.

Oerlemans, J. 2010. The microclimate of valley glaciers. *The microclimate of valley glaciers*.

Paul, F., N.E. Barrand, S. Baumann, E. Berthier, T. Bolch, K. Casey, H. Frey, S.P. Joshi, V. Konovalov, R. Le Bris, N. Molg, G. Nosenko, C. Nuth, A. Pope, A. Racoviteanu, P. Rastner, B. Raup, K. Scharrer, S. Steffen and S. Winsvold 2013. On the accuracy of glacier outlines derived from remote-sensing data. *Annals of Glaciology*, **54**(63): 171-182.

Prudent, C. 1874. Carte topographique du massif du Mont-Pelvoux. Club Alpin Français.

Rabatel, A., J.P. Dedieu and L. Reynaud 2002. Reconstitution des fluctuations du bilan de masse du Glacier Blanc (Massif des Ecrins, France) entre 1985 et 2000, par télédétection optique (imagerie Spot et Landsat). *La Houille Blanche*, **2002**(6-7): 64-71.

Rabatel, A., J.P. Dedieu, E. Thibert, A. Letreguilly and C. Vincent 2008. 25 years (1981-2005) of equilibrium-line altitude and mass-balance reconstruction on Glacier Blanc, French Alps, using remote-sensing methods and meteorological data. *Journal of Glaciology*, **54**(185): 307-314.

Rabatel, A., A. Letreguilly, J.P. Dedieu and N. Eckert 2013. Changes in glacier equilibrium-line altitude in the western Alps from 1984 to 2010: evaluation by remote sensing and modeling of the morpho-topographic and climate controls. *The Cryosphere*, **7**(5): 1455-1471.

Reid, T.D. and B.W. Brock 2010. An energy-balance model for debris-covered glaciers including heat conduction through the debris layer. *Journal of Glaciology*, **56**(199): 903-916.

Reznichenko, N., T. Davies, J. Shulmeister and M. McSaveney 2010. Effects of debris on ice-surface melting rates: an experimental study. *Journal of Glaciology*, **56**(197): 384-394.

Reznichenko, N.V., T.R.H. Davies and D.J. Alexander 2011. Effects of rock avalanches on glacier behaviour and moraine formation. *Geomorphology*, **132**(3-4): 327-338.

Roe, Gerard H., Marcia B. Baker and F. Herla 2016. Centennial glacier retreat as categorical evidence of regional climate change. *Nature Geoscience*.

Rolland, C. 2003. Spatial and Seasonal Variations of Air Temperature Lapse Rates in Alpine Regions. *Journal of Climate*, **16**(7): 1032-1046.

Rounce, D.R., D.J. Quincey and D.C. McKinney 2015. Debris-covered glacier energy balance model for Imja-Lhotse Shar Glacier in the Everest region of Nepal. *Cryosphere*, **9**(6): 2295-2310.

Santamaria Tovar, D., J. Shulmeister and T.R. Davies 2008. Evidence for a landslide origin of New Zealand's Waiho Loop moraine. Nature Geoscience, 1(8): 524-526.

Service des Eaux et Forêts. 1921-1965. Plan du Glacier Blanc et du Glacier Noir. In Forêts, S.d.E.e., *ed. Observations Glaciologiques*, Service des Eaux et Forêts.

Shugar, D.H., B.T. Rabus, J.J. Clague and D.M. Capps 2012. The response of Black Rapids Glacier, Alaska, to the Denali earthquake rock avalanches. *Journal of Geophysical Research-Earth Surface*, **117**(F01006): 14.

Singh, V.P., P. Singh and U.K. Haritashya 2011. *Encyclopedia of snow, ice and glaciers.* Dordrecht, Springer.

Thomson, M., M. Kirkbride and B. Brock 2000. Twentieth century surface elevation change of the Miage Glacier, Italian Alps. Debris-covered Glaciers: Proceedings of an International Workshop Held at the University of Washington in Seattle, Washington, USA, 13-15 September 2000, IAHS, 219-226. (264).

Vincent, C. 2002. Influence of climate change over the 20th Century on four French glacier mass balances. *Journal of Geophysical Research-Atmospheres*, **107**(D19).

Vincent, C., G. Kappenberger, F. Valla, A. Bauder, M. Funk and E. Le Meur 2004. Ice ablation as evidence of climate change in the Alps over the 20th century. *Journal of Geophysical Research-Atmospheres*, **109**(D10).

Westoby, M.J., J. Brasington, N.F. Glasser, M.J. Hambrey and J.M. Reynolds 2012. 'Structure-from-Motion' photogrammetry: A low-cost, effective tool for geoscience applications. *Geomorphology*, **179**: 300-314.

WGMS and NSIDC 1989, updated 2012. World Glacier Inventory. Compiled and made available by the World Glacier Monitoring Service, Zurich, Switzerland, and the National Snow and Ice Data Center, Boulder CO, U.S.A.

Zemp, M., H. Frey, I. Gärtner-Roer, S.U. Nussbaumer, M. Hoelzle, F. Paul, W. Haeberli, F. Denzinger, A.P. Ahlstrøm, B. Anderson, S. Bajracharya, C. Baroni, L.N. Braun, B.E. Cáceres, G. Casassa, G. Cobos, L.R. Dávila, H. Delgado Granados, M.N. Demuth, L. Espizua, A. Fischer, K. Fujita, B. Gadek, A. Ghazanfar, J.O. Hagen, P. Holmlund, N. Karimi, Z. Li, M. Pelto, P. Pitte, V.V. Popovnin, C.A. Portocarrero, R. Prinz, C.V. Sangewar, I. Severskiy, O. Sigurðsson, A. Soruco, R. Usubaliev and C. Vincent 2015. Historically unprecedented global glacier decline in the early 21st century. *Journal of Glaciology*, **61**(228): 745-762.

Zhang, Y. 2009. Introduction to Geostatistics—Course Notes. *Laramie*.

Supplementary material for Geometric change of adjacent clean-ice and debris-covered glaciers over the past two centuries in the French Alps

Data type and usage

CH4 - Table S1: Data type for every year of the study and measurements conducted.

Year	Historical Map	Topographical Plan	Aerial image (number used)	Orthoimage	Spot 6 image	Terminus position	Surface area	Elevation	Glacier Noir velocity	Georeferencement
1815	Local traditional knowledge - Reference for terminus position									
1853	x					x	x			
1874	x					x	x			
1904		x				x				
1918		x				x				
1921		x				x (GN only)				
1922		x				x				
1923		x				x				
1924		x				x				
1925		x				x				
1926		x				x				
1927		x				x				
1928		x				x				
1929		x				x				
1930		x				x				
1932		x				x				
1933		x				x				
1935		x				x				
1938		x				x				
1945		x				x				
1952			26			x	x	x	X	
1958		x				x				
1959		x				x				
1960		x	32			x	x	x	X	
1961		x				x				
1962		x				x				
1964			7			x (GB only)				
1965		x				x				
1967			43			x	x	x	X	
1974			1			x				

1979			5			x	x			
1980			38			x	x	x	X	
1981			56			x	x	x	X	
1983			30			x	x	x	X	
1986			13			x				
1988			25			x	x	x	X	
1989			1			x				
1993			86			x	x	x	X	
1994			43			x	x	x	X	
1998			17			x	x	x	X	
1999			54	x		x	x	x	X	x
2000			56			x	x	x	X	
2003			149	x		x	x	x	X	x
2009			19	x		x	x	x	X	x
2013			50	x		x	x	x	X	x
2014					x	x	x		X	
2015					x	x	x		X	
2016					x	x	x			

CH4 - Table S2: List of the images used. *RGB = Red, Green, Blue. Pan = Panchromatic. NIR = Near Infrared.*

Name	Date	Sensor	Size (MB)	Type
IGNF_PVA_1-0__1952-08-01__C3435-0081_1952_F3435-3438_0108.jp2	01 Aug 1952	Pan	5.6	JPEG 2000 Image
IGNF_PVA_1-0__1952-08-01__C3435-0081_1952_F3435-3438_0109.jp2	01 Aug 1952	Pan	5.6	JPEG 2000 Image
IGNF_PVA_1-0__1952-08-01__C3435-0081_1952_F3435-3438_0110.jp2	01 Aug 1952	Pan	5.6	JPEG 2000 Image
IGNF_PVA_1-0__1952-08-01__C3435-0081_1952_F3435-3438_0111.jp2	01 Aug 1952	Pan	5.6	JPEG 2000 Image
IGNF_PVA_1-0__1952-08-01__C3435-0081_1952_F3435-3438_0112.jp2	01 Aug 1952	Pan	5.6	JPEG 2000 Image
IGNF_PVA_1-0__1952-08-01__C3435-0081_1952_F3435-3438_0113.jp2	01 Aug 1952	Pan	5.6	JPEG 2000 Image
IGNF_PVA_1-0__1952-08-01__C3435-0081_1952_F3435-3438_0129.jp2	01 Aug 1952	Pan	5.6	JPEG 2000 Image
IGNF_PVA_1-0__1952-08-01__C3435-0081_1952_F3435-3438_0130.jp2	01 Aug 1952	Pan	5.6	JPEG 2000 Image
IGNF_PVA_1-0__1952-08-01__C3435-0081_1952_F3435-3438_0131.jp2	01 Aug 1952	Pan	5.6	JPEG 2000 Image
IGNF_PVA_1-0__1952-08-01__C3435-0081_1952_F3435-3438_0132.jp2	01 Aug 1952	Pan	5.6	JPEG 2000 Image
IGNF_PVA_1-0__1952-08-01__C3435-0081_1952_F3435-3438_0133.jp2	01 Aug 1952	Pan	5.6	JPEG 2000 Image
IGNF_PVA_1-0__1952-08-01__C3435-0081_1952_F3435-3438_0134.jp2	01 Aug 1952	Pan	5.6	JPEG 2000 Image
IGNF_PVA_1-0__1952-08-01__C3435-0081_1952_F3435-3438_0135.jp2	01 Aug 1952	Pan	5.6	JPEG 2000 Image
IGNF_PVA_1-0__1952-08-01__C3435-0081_1952_F3435-3438_0153.jp2	01 Aug 1952	Pan	5.6	JPEG 2000 Image
IGNF_PVA_1-0__1952-08-01__C3435-0081_1952_F3435-3438_0155.jp2	01 Aug 1952	Pan	5.6	JPEG 2000 Image
IGNF_PVA_1-0__1952-08-01__C3435-0081_1952_F3435-3438_0156.jp2	01 Aug 1952	Pan	5.6	JPEG 2000 Image

IGNF_PVA_1-0__1952-08-01__C3435-0081_1952_F3435-3438_0157.jp2	01 Aug 1952	Pan	5.6	JPEG 2000 Image
IGNF_PVA_1-0__1952-08-01__C3435-0081_1952_F3435-3438_0158.jp2	01 Aug 1952	Pan	5.6	JPEG 2000 Image
IGNF_PVA_1-0__1952-08-01__C3435-0081_1952_F3435-3438_0159.jp2	01 Aug 1952	Pan	5.6	JPEG 2000 Image
IGNF_PVA_1-0__1952-08-01__C3435-0081_1952_F3435-3438_0160.jp2	01 Aug 1952	Pan	5.6	JPEG 2000 Image
IGNF_PVA_1-0__1952-08-01__C3435-0081_1952_F3435-3438_0167.jp2	01 Aug 1952	Pan	5.6	JPEG 2000 Image
IGNF_PVA_1-0__1952-08-01__C3435-0081_1952_F3435-3438_0168.jp2	01 Aug 1952	Pan	5.6	JPEG 2000 Image
IGNF_PVA_1-0__1952-08-01__C3435-0081_1952_F3435-3438_0169.jp2	01 Aug 1952	Pan	5.6	JPEG 2000 Image
IGNF_PVA_1-0__1952-08-01__C3435-0081_1952_F3435-3438_0170.jp2	01 Aug 1952	Pan	5.6	JPEG 2000 Image
IGNF_PVA_1-0__1952-08-01__C3435-0081_1952_F3435-3438_0171.jp2	01 Aug 1952	Pan	5.6	JPEG 2000 Image
IGNF_PVA_1-0__1952-08-01__C3435-0081_1952_F3435-3438_0173.jp2	01 Aug 1952	Pan	5.6	JPEG 2000 Image
IGNF_PVA_1-0__1960-08-22__C94PHQ3091_1960_F3336-3436_0008.jp2	22 Aug 1960	Pan	5.5	JPEG 2000 Image
IGNF_PVA_1-0__1960-08-22__C94PHQ3091_1960_F3336-3436_0009.jp2	22 Aug 1960	Pan	5.5	JPEG 2000 Image
IGNF_PVA_1-0__1960-08-22__C94PHQ3091_1960_F3336-3436_0010.jp2	22 Aug 1960	Pan	5.5	JPEG 2000 Image
IGNF_PVA_1-0__1960-08-22__C94PHQ3091_1960_F3336-3436_0011.jp2	22 Aug 1960	Pan	5.5	JPEG 2000 Image
IGNF_PVA_1-0__1960-08-22__C94PHQ3091_1960_F3336-3436_0012.jp2	22 Aug 1960	Pan	5.5	JPEG 2000 Image
IGNF_PVA_1-0__1960-08-22__C94PHQ3091_1960_F3336-3436_0013.jp2	22 Aug 1960	Pan	5.5	JPEG 2000 Image
IGNF_PVA_1-0__1960-08-22__C94PHQ3091_1960_F3336-3436_0016.jp2	22 Aug 1960	Pan	5.5	JPEG 2000 Image
IGNF_PVA_1-0__1960-08-22__C94PHQ3091_1960_F3336-3436_0017.jp2	22 Aug 1960	Pan	5.5	JPEG 2000 Image
IGNF_PVA_1-0__1960-08-22__C94PHQ3091_1960_F3336-3436_0018.jp2	22 Aug 1960	Pan	5.5	JPEG 2000 Image
IGNF_PVA_1-0__1960-08-22__C94PHQ3091_1960_F3336-3436_0019.jp2	22 Aug 1960	Pan	5.5	JPEG 2000 Image
IGNF_PVA_1-0__1960-08-22__C94PHQ3091_1960_F3336-3436_0020.jp2	22 Aug 1960	Pan	5.5	JPEG 2000 Image
IGNF_PVA_1-0__1960-08-22__C94PHQ3091_1960_F3336-3436_0021.jp2	22 Aug 1960	Pan	5.5	JPEG 2000 Image
IGNF_PVA_1-0__1960-08-22__C94PHQ3091_1960_F3336-3436_0022.jp2	22 Aug 1960	Pan	5.5	JPEG 2000 Image
IGNF_PVA_1-0__1960-08-22__C94PHQ3091_1960_F3336-3436_0046.jp2	22 Aug 1960	Pan	5.5	JPEG 2000 Image
IGNF_PVA_1-0__1960-08-22__C94PHQ3091_1960_F3336-3436_0047.jp2	22 Aug 1960	Pan	5.5	JPEG 2000 Image
IGNF_PVA_1-0__1960-08-22__C94PHQ3091_1960_F3336-3436_0049.jp2	22 Aug 1960	Pan	5.5	JPEG 2000 Image
IGNF_PVA_1-0__1960-08-22__C94PHQ3091_1960_F3336-3436_0050.jp2	22 Aug 1960	Pan	5.5	JPEG 2000 Image
IGNF_PVA_1-0__1960-08-22__C94PHQ3091_1960_F3336-3436_0051.jp2	22 Aug 1960	Pan	5.5	JPEG 2000 Image
IGNF_PVA_1-0__1960-08-22__C94PHQ3091_1960_F3336-3436_0052.jp2	22 Aug 1960	Pan	5.5	JPEG 2000 Image
IGNF_PVA_1-0__1960-08-22__C94PHQ3091_1960_F3336-3436_0055.jp2	22 Aug 1960	Pan	5.5	JPEG 2000 Image
IGNF_PVA_1-0__1960-08-22__C94PHQ3091_1960_F3336-3436_0056.jp2	22 Aug 1960	Pan	5.5	JPEG 2000 Image
IGNF_PVA_1-0__1960-08-22__C94PHQ3091_1960_F3336-3436_0057.jp2	22 Aug 1960	Pan	5.5	JPEG 2000 Image
IGNF_PVA_1-0__1960-08-22__C94PHQ3091_1960_F3336-3436_0058.jp2	22 Aug 1960	Pan	5.5	JPEG 2000 Image
IGNF_PVA_1-0__1960-08-22__C94PHQ3091_1960_F3336-3436_0059.jp2	22 Aug 1960	Pan	5.5	JPEG 2000 Image
IGNF_PVA_1-0__1960-08-22__C94PHQ3091_1960_F3336-3436_0060.jp2	22 Aug 1960	Pan	5.5	JPEG 2000 Image
IGNF_PVA_1-0__1960-08-22__C94PHQ3091_1960_F3336-3436_0061.jp2	22 Aug 1960	Pan	5.5	JPEG 2000 Image
IGNF_PVA_1-0__1960-08-22__C94PHQ3091_1960_F3336-3436_0084.jp2	22 Aug 1960	Pan	5.5	JPEG 2000 Image
IGNF_PVA_1-0__1960-08-22__C94PHQ3091_1960_F3336-3436_0085.jp2	22 Aug 1960	Pan	5.5	JPEG 2000 Image
IGNF_PVA_1-0__1960-08-22__C94PHQ3091_1960_F3336-3436_0086.jp2	22 Aug 1960	Pan	5.5	JPEG 2000 Image
IGNF_PVA_1-0__1960-08-22__C94PHQ3091_1960_F3336-3436_0087.jp2	22 Aug 1960	Pan	5.5	JPEG 2000 Image

IGNF_PVA_1-0__1960-08-22__C94PHQ3091_1960_F3336-3436_0088.jp2	22 Aug 1960	Pan	5.5	JPEG 2000 Image
IGNF_PVA_1-0__1960-08-22__C94PHQ3091_1960_F3336-3436_0089.jp2	22 Aug 1960	Pan	5.5	JPEG 2000 Image
IGNF_PVA_1-0__1964-01-03__C3537-0141_1964_CDP3917_4265.jp2	03 Jan 1964	Pan	25.6	JPEG 2000 Image
IGNF_PVA_1-0__1964-01-03__C3537-0141_1964_CDP3917_4267.jp2	03 Jan 1964	Pan	25.6	JPEG 2000 Image
IGNF_PVA_1-0__1964-01-03__C3537-0141_1964_CDP3917_4268.jp2	03 Jan 1964	Pan	25.6	JPEG 2000 Image
IGNF_PVA_1-0__1964-01-03__C3537-0141_1964_CDP3917_4269.jp2	03 Jan 1964	Pan	25.6	JPEG 2000 Image
IGNF_PVA_1-0__1964-01-03__C3537-0141_1964_CDP3917_4270.jp2	03 Jan 1964	Pan	25.6	JPEG 2000 Image
IGNF_PVA_1-0__1964-01-03__C3537-0141_1964_CDP3917_4271.jp2	03 Jan 1964	Pan	25.6	JPEG 2000 Image
IGNF_PVA_1-0__1964-01-03__C3537-0141_1964_CDP3917_4266.jp2	03 Jan 1964	Pan	25.6	JPEG 2000 Image
IGNF_PVA_1-0__1967-09-27__C3436-0011_1967_F3436_0003.jp2	27 Sep 1967	Pan	5.5	JPEG 2000 Image
IGNF_PVA_1-0__1967-09-27__C3436-0011_1967_F3436_0004.jp2	27 Sep 1967	Pan	5.5	JPEG 2000 Image
IGNF_PVA_1-0__1967-09-27__C3436-0011_1967_F3436_0005.jp2	27 Sep 1967	Pan	5.5	JPEG 2000 Image
IGNF_PVA_1-0__1967-09-27__C3436-0011_1967_F3436_0006.jp2	27 Sep 1967	Pan	5.5	JPEG 2000 Image
IGNF_PVA_1-0__1967-09-27__C3436-0011_1967_F3436_0007.jp2	27 Sep 1967	Pan	5.5	JPEG 2000 Image
IGNF_PVA_1-0__1967-09-27__C3436-0011_1967_F3436_0008.jp2	27 Sep 1967	Pan	5.5	JPEG 2000 Image
IGNF_PVA_1-0__1967-09-27__C3436-0011_1967_F3436_0009.jp2	27 Sep 1967	Pan	5.5	JPEG 2000 Image
IGNF_PVA_1-0__1967-09-27__C3436-0011_1967_F3436_0010.jp2	27 Sep 1967	Pan	5.5	JPEG 2000 Image
IGNF_PVA_1-0__1967-09-27__C3436-0011_1967_F3436_0011.jp2	27 Sep 1967	Pan	5.5	JPEG 2000 Image
IGNF_PVA_1-0__1967-09-27__C3436-0011_1967_F3436_0033.jp2	27 Sep 1967	Pan	5.5	JPEG 2000 Image
IGNF_PVA_1-0__1967-09-27__C3436-0011_1967_F3436_0034.jp2	27 Sep 1967	Pan	5.5	JPEG 2000 Image
IGNF_PVA_1-0__1967-09-27__C3436-0011_1967_F3436_0035.jp2	27 Sep 1967	Pan	5.5	JPEG 2000 Image
IGNF_PVA_1-0__1967-09-27__C3436-0011_1967_F3436_0036.jp2	27 Sep 1967	Pan	5.5	JPEG 2000 Image
IGNF_PVA_1-0__1967-09-27__C3436-0011_1967_F3436_0037.jp2	27 Sep 1967	Pan	5.5	JPEG 2000 Image
IGNF_PVA_1-0__1967-09-27__C3436-0011_1967_F3436_0038.jp2	27 Sep 1967	Pan	5.5	JPEG 2000 Image
IGNF_PVA_1-0__1967-09-27__C3436-0011_1967_F3436_0039.jp2	27 Sep 1967	Pan	5.5	JPEG 2000 Image
IGNF_PVA_1-0__1967-09-27__C3436-0011_1967_F3436_0040.jp2	27 Sep 1967	Pan	5.5	JPEG 2000 Image
IGNF_PVA_1-0__1967-09-27__C3436-0011_1967_F3436_0043.jp2	27 Sep 1967	Pan	5.5	JPEG 2000 Image
IGNF_PVA_1-0__1967-09-27__C3436-0011_1967_F3436_0044.jp2	27 Sep 1967	Pan	5.5	JPEG 2000 Image
IGNF_PVA_1-0__1967-09-27__C3436-0011_1967_F3436_0045.jp2	27 Sep 1967	Pan	5.5	JPEG 2000 Image
IGNF_PVA_1-0__1967-09-27__C3436-0011_1967_F3436_0046.jp2	27 Sep 1967	Pan	5.5	JPEG 2000 Image
IGNF_PVA_1-0__1967-09-27__C3436-0011_1967_F3436_0047.jp2	27 Sep 1967	Pan	5.5	JPEG 2000 Image
IGNF_PVA_1-0__1967-09-27__C3436-0011_1967_F3436_0048.jp2	27 Sep 1967	Pan	5.5	JPEG 2000 Image
IGNF_PVA_1-0__1967-09-27__C3436-0011_1967_F3436_0049.jp2	27 Sep 1967	Pan	5.5	JPEG 2000 Image
IGNF_PVA_1-0__1967-09-27__C3436-0011_1967_F3436_0050.jp2	27 Sep 1967	Pan	5.5	JPEG 2000 Image
IGNF_PVA_1-0__1967-09-27__C3436-0011_1967_F3436_0051.jp2	27 Sep 1967	Pan	5.5	JPEG 2000 Image
IGNF_PVA_1-0__1967-09-27__C3436-0011_1967_F3436_0052.jp2	27 Sep 1967	Pan	5.5	JPEG 2000 Image
IGNF_PVA_1-0__1967-09-27__C3436-0011_1967_F3436_0073.jp2	27 Sep 1967	Pan	5.5	JPEG 2000 Image
IGNF_PVA_1-0__1967-09-27__C3436-0011_1967_F3436_0074.jp2	27 Sep 1967	Pan	5.5	JPEG 2000 Image
IGNF_PVA_1-0__1967-09-27__C3436-0011_1967_F3436_0075.jp2	27 Sep 1967	Pan	5.5	JPEG 2000 Image
IGNF_PVA_1-0__1967-09-27__C3436-0011_1967_F3436_0077.jp2	27 Sep 1967	Pan	5.5	JPEG 2000 Image

IGNF_PVA_1-0__1967-09-27__C3436-0011_1967_F3436_0078.jp2	27 Sep 1967	Pan	5.5	JPEG 2000 Image
IGNF_PVA_1-0__1967-09-27__C3436-0011_1967_F3436_0079.jp2	27 Sep 1967	Pan	5.5	JPEG 2000 Image
IGNF_PVA_1-0__1967-09-27__C3436-0011_1967_F3436_0080.jp2	27 Sep 1967	Pan	5.5	JPEG 2000 Image
IGNF_PVA_1-0__1967-09-27__C3436-0011_1967_F3436_0081.jp2	27 Sep 1967	Pan	5.5	JPEG 2000 Image
IGNF_PVA_1-0__1967-09-27__C3436-0011_1967_F3436_0082.jp2	27 Sep 1967	Pan	5.5	JPEG 2000 Image
IGNF_PVA_1-0__1967-09-27__C3436-0011_1967_F3436_0084.jp2	27 Sep 1967	Pan	5.5	JPEG 2000 Image
IGNF_PVA_1-0__1967-09-27__C3436-0011_1967_F3436_0085.jp2	27 Sep 1967	Pan	5.5	JPEG 2000 Image
IGNF_PVA_1-0__1967-09-27__C3436-0011_1967_F3436_0086.jp2	27 Sep 1967	Pan	5.5	JPEG 2000 Image
IGNF_PVA_1-0__1967-09-27__C3436-0011_1967_F3436_0087.jp2	27 Sep 1967	Pan	5.5	JPEG 2000 Image
IGNF_PVA_1-0__1967-09-27__C3436-0011_1967_F3436_0088.jp2	27 Sep 1967	Pan	5.5	JPEG 2000 Image
IGNF_PVA_1-0__1967-09-27__C3436-0011_1967_F3436_0089.jp2	27 Sep 1967	Pan	5.5	JPEG 2000 Image
IGNF_PVA_1-0__1967-09-27__C3436-0011_1967_F3436_0090.jp2	27 Sep 1967	Pan	5.5	JPEG 2000 Image
IGNF_PVA_1-0__1974-08-12__C1200-0061_1974_FR2620_0118.jp2	12 Aug 1974	Pan	25.9	JPEG 2000 Image
IGNF_PVA_1-0__1979-07-25__C0600-0291_1979_FR7029_0006.jp2	25 Jul 1979	Pan	25.7	JPEG 2000 Image
IGNF_PVA_1-0__1979-07-25__C0600-0291_1979_FR7029_0007.jp2	25 Jul 1979	Pan	25.7	JPEG 2000 Image
IGNF_PVA_1-0__1979-07-25__C0600-0291_1979_FR7029_0008.jp2	25 Jul 1979	Pan	25.7	JPEG 2000 Image
IGNF_PVA_1-0__1979-07-25__C0600-0291_1979_FR7029_0009.jp2	25 Jul 1979	Pan	25.7	JPEG 2000 Image
IGNF_PVA_1-0__1979-07-25__C0600-0291_1979_FR7029_0010.jp2	25 Jul 1979	Pan	25.7	JPEG 2000 Image
IGNF_PVA_1-0__1979-07-25__C0600-0291_1979_FR7029_0006.jp2	25 Jul 1979	Pan	25.7	JPEG 2000 Image
IGNF_PVA_1-0__1979-07-25__C0600-0291_1979_FR7029_0007.jp2	25 Jul 1979	Pan	25.7	JPEG 2000 Image
IGNF_PVA_1-0__1979-07-25__C0600-0291_1979_FR7029_0008.jp2	25 Jul 1979	Pan	25.7	JPEG 2000 Image
IGNF_PVA_1-0__1979-07-25__C0600-0291_1979_FR7029_0009.jp2	25 Jul 1979	Pan	25.7	JPEG 2000 Image
IGNF_PVA_1-0__1979-07-25__C0600-0291_1979_FR7029_0010.jp2	25 Jul 1979	Pan	25.7	JPEG 2000 Image
IGNF_PVA_1-0__1980-09-15__C3336-0021_1980_F3336-3636_0138.jp2	15 Sep 1980	Pan	25.9	JPEG 2000 Image
IGNF_PVA_1-0__1980-09-15__C3336-0021_1980_F3336-3636_0139.jp2	15 Sep 1980	Pan	25.9	JPEG 2000 Image
IGNF_PVA_1-0__1980-09-15__C3336-0021_1980_F3336-3636_0140.jp2	15 Sep 1980	Pan	25.9	JPEG 2000 Image
IGNF_PVA_1-0__1980-09-15__C3336-0021_1980_F3336-3636_0141.jp2	15 Sep 1980	Pan	25.9	JPEG 2000 Image
IGNF_PVA_1-0__1980-09-15__C3336-0021_1980_F3336-3636_0142.jp2	15 Sep 1980	Pan	25.9	JPEG 2000 Image
IGNF_PVA_1-0__1980-09-15__C3336-0021_1980_F3336-3636_0143.jp2	15 Sep 1980	Pan	25.9	JPEG 2000 Image
IGNF_PVA_1-0__1980-09-15__C3336-0021_1980_F3336-3636_0180.jp2	15 Sep 1980	Pan	25.9	JPEG 2000 Image
IGNF_PVA_1-0__1980-09-15__C3336-0021_1980_F3336-3636_0181.jp2	15 Sep 1980	Pan	25.9	JPEG 2000 Image
IGNF_PVA_1-0__1980-09-15__C3336-0021_1980_F3336-3636_0182.jp2	15 Sep 1980	Pan	25.9	JPEG 2000 Image
IGNF_PVA_1-0__1980-09-15__C3336-0021_1980_F3336-3636_0183.jp2	15 Sep 1980	Pan	25.9	JPEG 2000 Image
IGNF_PVA_1-0__1980-09-15__C3336-0021_1980_F3336-3636_0185.jp2	15 Sep 1980	Pan	25.9	JPEG 2000 Image
IGNF_PVA_1-0__1980-09-15__C3336-0021_1980_F3336-3636_0186.jp2	15 Sep 1980	Pan	25.9	JPEG 2000 Image
IGNF_PVA_1-0__1980-09-15__C3336-0021_1980_F3336-3636_0137.jp2	15 Sep 1980	Pan	25.9	JPEG 2000 Image
IGNF_PVA_1-0__1980-09-15__C3336-0021_1980_F3336-3636_0144.jp2	15 Sep 1980	Pan	25.9	JPEG 2000 Image
IGNF_PVA_1-0__1980-09-15__C3336-0021_1980_F3336-3636_0178.jp2	15 Sep 1980	Pan	25.9	JPEG 2000 Image
IGNF_PVA_1-0__1980-09-15__C3336-0021_1980_F3336-3636_0179.jp2	15 Sep 1980	Pan	25.9	JPEG 2000 Image
IGNF_PVA_1-0__1980-09-15__C3336-0021_1980_F3336-3636_0184.jp2	15 Sep 1980	Pan	25.9	JPEG 2000 Image

IGNF_PVA_1-0__1980-08-14__C0600-0291_1979_FR7029_0198.jp2	14 Aug 1980	Pan	25.7	JPEG 2000 Image
IGNF_PVA_1-0__1980-08-14__C0600-0291_1979_FR7029_0199.jp2	14 Aug 1980	Pan	25.7	JPEG 2000 Image
IGNF_PVA_1-0__1980-08-14__C0600-0291_1979_FR7029_0200.jp2	14 Aug 1980	Pan	25.7	JPEG 2000 Image
IGNF_PVA_1-0__1980-08-14__C0600-0291_1979_FR7029_0233.jp2	14 Aug 1980	Pan	25.7	JPEG 2000 Image
IGNF_PVA_1-0__1980-08-14__C0600-0291_1979_FR7029_0235.jp2	14 Aug 1980	Pan	25.7	JPEG 2000 Image
IGNF_PVA_1-0__1980-08-14__C0600-0291_1979_FR7029_0215.jp2	14 Aug 1980	Pan	25.7	JPEG 2000 Image
IGNF_PVA_1-0__1980-08-14__C0600-0291_1979_FR7029_0216.jp2	14 Aug 1980	Pan	25.7	JPEG 2000 Image
IGNF_PVA_1-0__1980-08-14__C0600-0291_1979_FR7029_0217.jp2	14 Aug 1980	Pan	25.7	JPEG 2000 Image
IGNF_PVA_1-0__1980-08-14__C0600-0291_1979_FR7029_0218.jp2	14 Aug 1980	Pan	25.7	JPEG 2000 Image
IGNF_PVA_1-0__1980-08-14__C0600-0291_1979_FR7029_0219.jp2	14 Aug 1980	Pan	25.7	JPEG 2000 Image
IGNF_PVA_1-0__1980-08-14__C0600-0291_1979_FR7029_0230.jp2	14 Aug 1980	Pan	25.7	JPEG 2000 Image
IGNF_PVA_1-0__1980-08-14__C0600-0291_1979_FR7029_0231.jp2	14 Aug 1980	Pan	25.7	JPEG 2000 Image
IGNF_PVA_1-0__1980-08-14__C0600-0291_1979_FR7029_0232.jp2	14 Aug 1980	Pan	25.7	JPEG 2000 Image
IGNF_PVA_1-0__1980-08-14__C0600-0291_1979_FR7029_0234.jp2	14 Aug 1980	Pan	25.7	JPEG 2000 Image
IGNF_PVA_1-0__1980-08-21__C3336-0021_1980_F3336-3636_0011.jp2	21 Aug 1980	Pan	25.9	JPEG 2000 Image
IGNF_PVA_1-0__1980-08-21__C3336-0021_1980_F3336-3636_0012.jp2	21 Aug 1980	Pan	25.9	JPEG 2000 Image
IGNF_PVA_1-0__1980-08-21__C3336-0021_1980_F3336-3636_0010.jp2	21 Aug 1980	Pan	25.9	JPEG 2000 Image
IGNF_PVA_1-0__1980-08-21__C3336-0021_1980_F3336-3636_0013.jp2	21 Aug 1980	Pan	25.9	JPEG 2000 Image
IGNF_PVA_1-0__1980-08-21__C3336-0021_1980_F3336-3636_0014.jp2	21 Aug 1980	Pan	25.9	JPEG 2000 Image
IGNF_PVA_1-0__1980-08-21__C3336-0021_1980_F3336-3636_0015.jp2	21 Aug 1980	Pan	25.9	JPEG 2000 Image
IGNF_PVA_1-0__1980-08-21__C3336-0021_1980_F3336-3636_0016.jp2	21 Aug 1980	Pan	25.9	JPEG 2000 Image
IGNF_PVA_1-0__1981-08-27__C3435-0021_1981_IFN05P_1509.jp2	27 Aug 1981	Pan	26.4	JPEG 2000 Image
IGNF_PVA_1-0__1981-08-27__C3435-0021_1981_IFN05P_1510.jp2	27 Aug 1981	Pan	26.4	JPEG 2000 Image
IGNF_PVA_1-0__1981-08-27__C3435-0021_1981_IFN05P_1511.jp2	27 Aug 1981	Pan	26.4	JPEG 2000 Image
IGNF_PVA_1-0__1981-08-27__C3435-0021_1981_IFN05P_1506.jp2	27 Aug 1981	Pan	26.4	JPEG 2000 Image
IGNF_PVA_1-0__1981-08-27__C3435-0021_1981_IFN05P_1507.jp2	27 Aug 1981	Pan	26.4	JPEG 2000 Image
IGNF_PVA_1-0__1981-08-27__C3435-0021_1981_IFN05P_1508.jp2	27 Aug 1981	Pan	26.4	JPEG 2000 Image
IGNF_PVA_1-0__1981-07-29__C3435-0021_1981_IFN05P_0385.jp2	29 Jul 1981	Pan	26.4	JPEG 2000 Image
IGNF_PVA_1-0__1981-07-29__C3435-0021_1981_IFN05P_0386.jp2	29 Jul 1981	Pan	26.4	JPEG 2000 Image
IGNF_PVA_1-0__1981-07-29__C3435-0021_1981_IFN05P_0387.jp2	29 Jul 1981	Pan	26.4	JPEG 2000 Image
IGNF_PVA_1-0__1981-07-29__C3435-0021_1981_IFN05P_0388.jp2	29 Jul 1981	Pan	26.4	JPEG 2000 Image
IGNF_PVA_1-0__1981-07-29__C3435-0021_1981_IFN05P_0389.jp2	29 Jul 1981	Pan	26.4	JPEG 2000 Image
IGNF_PVA_1-0__1981-07-29__C3435-0021_1981_IFN05P_0390.jp2	29 Jul 1981	Pan	26.4	JPEG 2000 Image
IGNF_PVA_1-0__1981-07-29__C3435-0021_1981_IFN05P_0391.jp2	29 Jul 1981	Pan	26.4	JPEG 2000 Image
IGNF_PVA_1-0__1981-07-29__C3435-0021_1981_IFN05P_0398.jp2	29 Jul 1981	Pan	26.4	JPEG 2000 Image
IGNF_PVA_1-0__1981-07-29__C3435-0021_1981_IFN05P_0399.jp2	29 Jul 1981	Pan	26.4	JPEG 2000 Image
IGNF_PVA_1-0__1981-07-29__C3435-0021_1981_IFN05P_0400.jp2	29 Jul 1981	Pan	26.4	JPEG 2000 Image
IGNF_PVA_1-0__1981-07-29__C3435-0021_1981_IFN05P_0401.jp2	29 Jul 1981	Pan	26.4	JPEG 2000 Image
IGNF_PVA_1-0__1981-07-29__C3435-0021_1981_IFN05P_0402.jp2	29 Jul 1981	Pan	26.4	JPEG 2000 Image
IGNF_PVA_1-0__1981-07-29__C3435-0021_1981_IFN05P_0403.jp2	29 Jul 1981	Pan	26.4	JPEG 2000 Image

IGNF_PVA_1-0__1981-07-29__C3435-0021_1981_IFN05P_0404.jp2	29 Jul 1981	Pan	26.4	JPEG 2000 Image
IGNF_PVA_1-0__1981-07-29__C3435-0021_1981_IFN05P_0405.jp2	29 Jul 1981	Pan	26.4	JPEG 2000 Image
IGNF_PVA_1-0__1981-07-29__C3435-0021_1981_IFN05P_0407.jp2	29 Jul 1981	Pan	26.4	JPEG 2000 Image
IGNF_PVA_1-0__1981-07-29__C3435-0021_1981_IFN05P_0408.jp2	29 Jul 1981	Pan	26.4	JPEG 2000 Image
IGNF_PVA_1-0__1981-07-29__C3435-0021_1981_IFN05P_0409.jp2	29 Jul 1981	Pan	26.4	JPEG 2000 Image
IGNF_PVA_1-0__1981-07-29__C3435-0021_1981_IFN05P_0410.jp2	29 Jul 1981	Pan	26.4	JPEG 2000 Image
IGNF_PVA_1-0__1981-07-29__C3435-0021_1981_IFN05P_0411.jp2	29 Jul 1981	Pan	26.4	JPEG 2000 Image
IGNF_PVA_1-0__1981-07-29__C3435-0021_1981_IFN05P_0412.jp2	29 Jul 1981	Pan	26.4	JPEG 2000 Image
IGNF_PVA_1-0__1981-07-29__C3435-0021_1981_IFN05P_0413.jp2	29 Jul 1981	Pan	26.4	JPEG 2000 Image
IGNF_PVA_1-0__1981-07-29__C3435-0021_1981_IFN05P_0414.jp2	29 Jul 1981	Pan	26.4	JPEG 2000 Image
IGNF_PVA_1-0__1981-07-29__C3435-0021_1981_IFN05P_0415.jp2	29 Jul 1981	Pan	26.4	JPEG 2000 Image
IGNF_PVA_1-0__1981-07-29__C3435-0021_1981_IFN05P_0416.jp2	29 Jul 1981	Pan	26.4	JPEG 2000 Image
IGNF_PVA_1-0__1981-07-29__C3435-0021_1981_IFN05P_0417.jp2	29 Jul 1981	Pan	26.4	JPEG 2000 Image
IGNF_PVA_1-0__1981-07-29__C3435-0021_1981_IFN05P_0422.jp2	29 Jul 1981	Pan	26.4	JPEG 2000 Image
IGNF_PVA_1-0__1981-07-29__C3435-0021_1981_IFN05P_0423.jp2	29 Jul 1981	Pan	26.4	JPEG 2000 Image
IGNF_PVA_1-0__1981-07-29__C3435-0021_1981_IFN05P_0424.jp2	29 Jul 1981	Pan	26.4	JPEG 2000 Image
IGNF_PVA_1-0__1981-07-29__C3435-0021_1981_IFN05P_0438.jp2	29 Jul 1981	Pan	26.4	JPEG 2000 Image
IGNF_PVA_1-0__1981-07-29__C3435-0021_1981_IFN05P_0439.jp2	29 Jul 1981	Pan	26.4	JPEG 2000 Image
IGNF_PVA_1-0__1981-07-29__C3435-0021_1981_IFN05P_0440.jp2	29 Jul 1981	Pan	26.4	JPEG 2000 Image
IGNF_PVA_1-0__1981-07-29__C3435-0021_1981_IFN05P_0441.jp2	29 Jul 1981	Pan	26.4	JPEG 2000 Image
IGNF_PVA_1-0__1981-07-29__C3435-0021_1981_IFN05P_0442.jp2	29 Jul 1981	Pan	26.4	JPEG 2000 Image
IGNF_PVA_1-0__1981-07-29__C3435-0021_1981_IFN05P_0443.jp2	29 Jul 1981	Pan	26.4	JPEG 2000 Image
IGNF_PVA_1-0__1981-07-29__C3435-0021_1981_IFN05P_0444.jp2	29 Jul 1981	Pan	26.4	JPEG 2000 Image
IGNF_PVA_1-0__1981-07-29__C3435-0021_1981_IFN05P_0445.jp2	29 Jul 1981	Pan	26.4	JPEG 2000 Image
IGNF_PVA_1-0__1981-07-29__C3435-0021_1981_IFN05P_0446.jp2	29 Jul 1981	Pan	26.4	JPEG 2000 Image
IGNF_PVA_1-0__1981-07-29__C3435-0021_1981_IFN05P_0447.jp2	29 Jul 1981	Pan	26.4	JPEG 2000 Image
IGNF_PVA_1-0__1981-07-29__C3435-0021_1981_IFN05P_0448.jp2	29 Jul 1981	Pan	26.4	JPEG 2000 Image
IGNF_PVA_1-0__1981-07-29__C3435-0021_1981_IFN05P_0449.jp2	29 Jul 1981	Pan	26.4	JPEG 2000 Image
IGNF_PVA_1-0__1981-07-29__C3435-0021_1981_IFN05P_0511.jp2	29 Jul 1981	Pan	26.4	JPEG 2000 Image
IGNF_PVA_1-0__1981-07-29__C3435-0021_1981_IFN05P_0512.jp2	29 Jul 1981	Pan	26.4	JPEG 2000 Image
IGNF_PVA_1-0__1981-07-29__C3435-0021_1981_IFN05P_0513.jp2	29 Jul 1981	Pan	26.4	JPEG 2000 Image
IGNF_PVA_1-0__1981-07-29__C3435-0021_1981_IFN05P_0590.jp2	29 Jul 1981	Pan	26.4	JPEG 2000 Image
IGNF_PVA_1-0__1981-07-29__C3435-0021_1981_IFN05P_0591.jp2	29 Jul 1981	Pan	26.4	JPEG 2000 Image
IGNF_PVA_1-0__1981-07-29__C3435-0021_1981_IFN05P_0592.jp2	29 Jul 1981	Pan	26.4	JPEG 2000 Image
IGNF_PVA_1-0__1981-07-29__C3435-0021_1981_IFN05P_0593.jp2	29 Jul 1981	Pan	26.4	JPEG 2000 Image
IGNF_PVA_1-0__1981-07-29__C3435-0021_1981_IFN05P_0594.jp2	29 Jul 1981	Pan	26.4	JPEG 2000 Image
IGNF_PVA_1-0__1981-07-29__C3435-0021_1981_IFN05P_0595.jp2	29 Jul 1981	Pan	26.4	JPEG 2000 Image
IGNF_PVA_1-0__1983-07-13__C3336-0011_1983_F3336-3436_0089.jp2	13 Jul 1983	Pan	25.9	JPEG 2000 Image
IGNF_PVA_1-0__1983-07-13__C3336-0011_1983_F3336-3436_0091.jp2	13 Jul 1983	Pan	25.9	JPEG 2000 Image
IGNF_PVA_1-0__1983-07-13__C3336-0011_1983_F3336-3436_0014.jp2	13 Jul 1983	Pan	25.9	JPEG 2000 Image

IGNF_PVA_1-0__1983-07-13__C3336-0011_1983_F3336-3436_0015.jp2	13 Jul 1983	Pan	25.9	JPEG 2000 Image
IGNF_PVA_1-0__1983-07-13__C3336-0011_1983_F3336-3436_0016.jp2	13 Jul 1983	Pan	25.9	JPEG 2000 Image
IGNF_PVA_1-0__1983-07-13__C3336-0011_1983_F3336-3436_0021.jp2	13 Jul 1983	Pan	25.9	JPEG 2000 Image
IGNF_PVA_1-0__1983-07-13__C3336-0011_1983_F3336-3436_0022.jp2	13 Jul 1983	Pan	25.9	JPEG 2000 Image
IGNF_PVA_1-0__1983-07-13__C3336-0011_1983_F3336-3436_0023.jp2	13 Jul 1983	Pan	25.9	JPEG 2000 Image
IGNF_PVA_1-0__1983-07-13__C3336-0011_1983_F3336-3436_0024.jp2	13 Jul 1983	Pan	25.9	JPEG 2000 Image
IGNF_PVA_1-0__1983-07-13__C3336-0011_1983_F3336-3436_0025.jp2	13 Jul 1983	Pan	25.9	JPEG 2000 Image
IGNF_PVA_1-0__1983-07-13__C3336-0011_1983_F3336-3436_0026.jp2	13 Jul 1983	Pan	25.9	JPEG 2000 Image
IGNF_PVA_1-0__1983-07-13__C3336-0011_1983_F3336-3436_0052.jp2	13 Jul 1983	Pan	25.9	JPEG 2000 Image
IGNF_PVA_1-0__1983-07-13__C3336-0011_1983_F3336-3436_0053.jp2	13 Jul 1983	Pan	25.9	JPEG 2000 Image
IGNF_PVA_1-0__1983-07-13__C3336-0011_1983_F3336-3436_0054.jp2	13 Jul 1983	Pan	25.9	JPEG 2000 Image
IGNF_PVA_1-0__1983-07-13__C3336-0011_1983_F3336-3436_0055.jp2	13 Jul 1983	Pan	25.9	JPEG 2000 Image
IGNF_PVA_1-0__1983-07-13__C3336-0011_1983_F3336-3436_0056.jp2	13 Jul 1983	Pan	25.9	JPEG 2000 Image
IGNF_PVA_1-0__1983-07-13__C3336-0011_1983_F3336-3436_0057.jp2	13 Jul 1983	Pan	25.9	JPEG 2000 Image
IGNF_PVA_1-0__1983-07-13__C3336-0011_1983_F3336-3436_0058.jp2	13 Jul 1983	Pan	25.9	JPEG 2000 Image
IGNF_PVA_1-0__1983-07-13__C3336-0011_1983_F3336-3436_0059.jp2	13 Jul 1983	Pan	25.9	JPEG 2000 Image
IGNF_PVA_1-0__1983-07-13__C3336-0011_1983_F3336-3436_0079.jp2	13 Jul 1983	Pan	25.9	JPEG 2000 Image
IGNF_PVA_1-0__1983-07-13__C3336-0011_1983_F3336-3436_0080.jp2	13 Jul 1983	Pan	25.9	JPEG 2000 Image
IGNF_PVA_1-0__1983-07-13__C3336-0011_1983_F3336-3436_0081.jp2	13 Jul 1983	Pan	25.9	JPEG 2000 Image
IGNF_PVA_1-0__1983-07-13__C3336-0011_1983_F3336-3436_0082.jp2	13 Jul 1983	Pan	25.9	JPEG 2000 Image
IGNF_PVA_1-0__1983-07-13__C3336-0011_1983_F3336-3436_0083.jp2	13 Jul 1983	Pan	25.9	JPEG 2000 Image
IGNF_PVA_1-0__1983-07-13__C3336-0011_1983_F3336-3436_0084.jp2	13 Jul 1983	Pan	25.9	JPEG 2000 Image
IGNF_PVA_1-0__1983-07-13__C3336-0011_1983_F3336-3436_0085.jp2	13 Jul 1983	Pan	25.9	JPEG 2000 Image
IGNF_PVA_1-0__1983-07-13__C3336-0011_1983_F3336-3436_0086.jp2	13 Jul 1983	Pan	25.9	JPEG 2000 Image
IGNF_PVA_1-0__1983-07-13__C3336-0011_1983_F3336-3436_0087.jp2	13 Jul 1983	Pan	25.9	JPEG 2000 Image
IGNF_PVA_1-0__1983-07-13__C3336-0011_1983_F3336-3436_0088.jp2	13 Jul 1983	Pan	25.9	JPEG 2000 Image
IGNF_PVA_1-0__1983-07-13__C3336-0011_1983_F3336-3436_0090.jp2	13 Jul 1983	Pan	25.9	JPEG 2000 Image
IGNF_PVA_1-0__1986-09-05__C3536-0041_1986_F3536-3636_0030.jp2	05 Sep 1986	Pan	25.6	JPEG 2000 Image
IGNF_PVA_1-0__1986-09-05__C3536-0041_1986_F3536-3636_0032.jp2	05 Sep 1986	Pan	25.6	JPEG 2000 Image
IGNF_PVA_1-0__1986-09-05__C3536-0041_1986_F3536-3636_0034.jp2	05 Sep 1986	Pan	25.6	JPEG 2000 Image
IGNF_PVA_1-0__1986-09-05__C3536-0041_1986_F3536-3636_0086.jp2	05 Sep 1986	Pan	25.6	JPEG 2000 Image
IGNF_PVA_1-0__1986-09-05__C3536-0041_1986_F3536-3636_0088.jp2	05 Sep 1986	Pan	25.6	JPEG 2000 Image
IGNF_PVA_1-0__1986-09-05__C3536-0041_1986_F3536-3636_0090.jp2	05 Sep 1986	Pan	25.6	JPEG 2000 Image
IGNF_PVA_1-0__1986-09-05__C3536-0041_1986_F3536-3636_0092.jp2	05 Sep 1986	Pan	25.6	JPEG 2000 Image
IGNF_PVA_1-0__1986-09-06__C3536-0041_1986_F3536-3636_0168.jp2	06 Sep 1986	Pan	25.6	JPEG 2000 Image
IGNF_PVA_1-0__1986-09-06__C3536-0041_1986_F3536-3636_0170.jp2	06 Sep 1986	Pan	25.6	JPEG 2000 Image
IGNF_PVA_1-0__1986-09-06__C3536-0041_1986_F3536-3636_0172.jp2	06 Sep 1986	Pan	25.6	JPEG 2000 Image
IGNF_PVA_1-0__1986-09-06__C3536-0041_1986_F3536-3636_0174.jp2	06 Sep 1986	Pan	25.6	JPEG 2000 Image
IGNF_PVA_1-0__1986-09-06__C3536-0041_1986_F3536-3636_0176.jp2	06 Sep 1986	Pan	25.6	JPEG 2000 Image
IGNF_PVA_1-0__1986-09-06__C3536-0041_1986_F3536-3636_0178.jp2	06 Sep 1986	Pan	25.6	JPEG 2000 Image

IGNF_PVA_1-0__1988-07-10__C2205-0571_1988_F3336-3436_0151.jp2	10 Jul 1988	Pan	25.6	JPEG 2000 Image
IGNF_PVA_1-0__1988-07-10__C2205-0571_1988_F3336-3436_0152.jp2	10 Jul 1988	Pan	25.6	JPEG 2000 Image
IGNF_PVA_1-0__1988-07-10__C2205-0571_1988_F3336-3436_0121.jp2	10 Jul 1988	Pan	25.6	JPEG 2000 Image
IGNF_PVA_1-0__1988-07-10__C2205-0571_1988_F3336-3436_0122.jp2	10 Jul 1988	Pan	25.6	JPEG 2000 Image
IGNF_PVA_1-0__1988-07-10__C2205-0571_1988_F3336-3436_0123.jp2	10 Jul 1988	Pan	25.6	JPEG 2000 Image
IGNF_PVA_1-0__1988-07-10__C2205-0571_1988_F3336-3436_0124.jp2	10 Jul 1988	Pan	25.6	JPEG 2000 Image
IGNF_PVA_1-0__1988-07-10__C2205-0571_1988_F3336-3436_0125.jp2	10 Jul 1988	Pan	25.6	JPEG 2000 Image
IGNF_PVA_1-0__1988-07-10__C2205-0571_1988_F3336-3436_0126.jp2	10 Jul 1988	Pan	25.6	JPEG 2000 Image
IGNF_PVA_1-0__1988-07-10__C2205-0571_1988_F3336-3436_0127.jp2	10 Jul 1988	Pan	25.6	JPEG 2000 Image
IGNF_PVA_1-0__1988-07-10__C2205-0571_1988_F3336-3436_0128.jp2	10 Jul 1988	Pan	25.6	JPEG 2000 Image
IGNF_PVA_1-0__1988-07-10__C2205-0571_1988_F3336-3436_0145.jp2	10 Jul 1988	Pan	25.6	JPEG 2000 Image
IGNF_PVA_1-0__1988-07-10__C2205-0571_1988_F3336-3436_0146.jp2	10 Jul 1988	Pan	25.6	JPEG 2000 Image
IGNF_PVA_1-0__1988-07-10__C2205-0571_1988_F3336-3436_0147.jp2	10 Jul 1988	Pan	25.6	JPEG 2000 Image
IGNF_PVA_1-0__1988-07-10__C2205-0571_1988_F3336-3436_0148.jp2	10 Jul 1988	Pan	25.6	JPEG 2000 Image
IGNF_PVA_1-0__1988-07-10__C2205-0571_1988_F3336-3436_0149.jp2	10 Jul 1988	Pan	25.6	JPEG 2000 Image
IGNF_PVA_1-0__1988-07-10__C2205-0571_1988_F3336-3436_0150.jp2	10 Jul 1988	Pan	25.6	JPEG 2000 Image
IGNF_PVA_1-0__1988-07-10__C2205-0571_1988_F3336-3436_0153.jp2	10 Jul 1988	Pan	25.6	JPEG 2000 Image
IGNF_PVA_1-0__1988-07-11__C2205-0571_1988_F3336-3436_0177.jp2	11 Jul 1988	Pan	25.6	JPEG 2000 Image
IGNF_PVA_1-0__1988-07-11__C2205-0571_1988_F3336-3436_0178.jp2	11 Jul 1988	Pan	25.6	JPEG 2000 Image
IGNF_PVA_1-0__1988-07-11__C2205-0571_1988_F3336-3436_0179.jp2	11 Jul 1988	Pan	25.6	JPEG 2000 Image
IGNF_PVA_1-0__1988-07-11__C2205-0571_1988_F3336-3436_0180.jp2	11 Jul 1988	Pan	25.6	JPEG 2000 Image
IGNF_PVA_1-0__1988-07-11__C2205-0571_1988_F3336-3436_0181.jp2	11 Jul 1988	Pan	25.6	JPEG 2000 Image
IGNF_PVA_1-0__1988-07-11__C2205-0571_1988_F3336-3436_0182.jp2	11 Jul 1988	Pan	25.6	JPEG 2000 Image
IGNF_PVA_1-0__1988-07-11__C2205-0571_1988_F3336-3436_0183.jp2	11 Jul 1988	Pan	25.6	JPEG 2000 Image
IGNF_PVA_1-0__1988-07-11__C2205-0571_1988_F3336-3436_0184.jp2	11 Jul 1988	Pan	25.6	JPEG 2000 Image
IGNF_PVA_1-0__1989-10-27__C2205-0551_1989_F3536-3636_0028.jp2	27 Oct 1989	Pan	25.7	JPEG 2000 Image
IGNF_PVA_1-0__1993-08-11__C93SAA0981_1993_FD38_2283.jp2	11 Aug 1993	Pan	29.8	JPEG 2000 Image
IGNF_PVA_1-0__1993-08-11__C93SAA0981_1993_FD38_2284.jp2	11 Aug 1993	Pan	29.8	JPEG 2000 Image
IGNF_PVA_1-0__1993-08-11__C93SAA0981_1993_FD38_2280.jp2	11 Aug 1993	Pan	29.8	JPEG 2000 Image
IGNF_PVA_1-0__1993-08-11__C93SAA0981_1993_FD38_2281.jp2	11 Aug 1993	Pan	29.8	JPEG 2000 Image
IGNF_PVA_1-0__1993-08-11__C93SAA0981_1993_FD38_2282.jp2	11 Aug 1993	Pan	29.8	JPEG 2000 Image
IGNF_PVA_1-0__1993-08-11__C93SAA1351_1993_FD05_2277.jp2	11 Aug 1993	Pan	26.6	JPEG 2000 Image
IGNF_PVA_1-0__1993-08-11__C93SAA1351_1993_FD05_2278.jp2	11 Aug 1993	Pan	26.6	JPEG 2000 Image
IGNF_PVA_1-0__1993-08-11__C93SAA1351_1993_FD05_2298.jp2	11 Aug 1993	Pan	26.6	JPEG 2000 Image
IGNF_PVA_1-0__1993-08-11__C93SAA1351_1993_FD05_2300.jp2	11 Aug 1993	Pan	26.6	JPEG 2000 Image
IGNF_PVA_1-0__1993-08-11__C93SAA1351_1993_FD05_2301.jp2	11 Aug 1993	Pan	26.6	JPEG 2000 Image
IGNF_PVA_1-0__1993-08-11__C93SAA1351_1993_FD05_2306.jp2	11 Aug 1993	Pan	26.6	JPEG 2000 Image
IGNF_PVA_1-0__1993-08-11__C93SAA1351_1993_FD05_2336.jp2	11 Aug 1993	Pan	26.6	JPEG 2000 Image
IGNF_PVA_1-0__1993-08-11__C93SAA1351_1993_FD05_2279.jp2	11 Aug 1993	Pan	26.6	JPEG 2000 Image
IGNF_PVA_1-0__1993-08-11__C93SAA1351_1993_FD05_2299.jp2	11 Aug 1993	Pan	26.6	JPEG 2000 Image

IGNF_PVA_1-0__1993-08-11__C93SAA1351_1993_FD05_2302.jp2	11 Aug 1993	Pan	26.6	JPEG 2000 Image
IGNF_PVA_1-0__1993-08-11__C93SAA1351_1993_FD05_2303.jp2	11 Aug 1993	Pan	26.6	JPEG 2000 Image
IGNF_PVA_1-0__1993-08-11__C93SAA1351_1993_FD05_2304.jp2	11 Aug 1993	Pan	26.6	JPEG 2000 Image
IGNF_PVA_1-0__1993-08-11__C93SAA1351_1993_FD05_2312.jp2	11 Aug 1993	Pan	26.6	JPEG 2000 Image
IGNF_PVA_1-0__1993-08-11__C93SAA1351_1993_FD05_2313.jp2	11 Aug 1993	Pan	26.6	JPEG 2000 Image
IGNF_PVA_1-0__1993-08-11__C93SAA1351_1993_FD05_2314.jp2	11 Aug 1993	Pan	26.6	JPEG 2000 Image
IGNF_PVA_1-0__1993-08-11__C93SAA1351_1993_FD05_2315.jp2	11 Aug 1993	Pan	26.6	JPEG 2000 Image
IGNF_PVA_1-0__1993-08-11__C93SAA1351_1993_FD05_2316.jp2	11 Aug 1993	Pan	26.6	JPEG 2000 Image
IGNF_PVA_1-0__1993-08-11__C93SAA1351_1993_FD05_2317.jp2	11 Aug 1993	Pan	26.6	JPEG 2000 Image
IGNF_PVA_1-0__1993-08-11__C93SAA1351_1993_FD05_2318.jp2	11 Aug 1993	Pan	26.6	JPEG 2000 Image
IGNF_PVA_1-0__1993-08-11__C93SAA1351_1993_FD05_2319.jp2	11 Aug 1993	Pan	26.6	JPEG 2000 Image
IGNF_PVA_1-0__1993-08-11__C93SAA1351_1993_FD05_2332.jp2	11 Aug 1993	Pan	26.6	JPEG 2000 Image
IGNF_PVA_1-0__1993-08-11__C93SAA1351_1993_FD05_2333.jp2	11 Aug 1993	Pan	26.6	JPEG 2000 Image
IGNF_PVA_1-0__1993-08-11__C93SAA1351_1993_FD05_2334.jp2	11 Aug 1993	Pan	26.6	JPEG 2000 Image
IGNF_PVA_1-0__1993-08-11__C93SAA1351_1993_FD05_2335.jp2	11 Aug 1993	Pan	26.6	JPEG 2000 Image
IGNF_PVA_1-0__1993-08-11__C93SAA1351_1993_FD05_2337.jp2	11 Aug 1993	Pan	26.6	JPEG 2000 Image
IGNF_PVA_1-0__1993-08-11__C93SAA1351_1993_FD05_2338.jp2	11 Aug 1993	Pan	26.6	JPEG 2000 Image
IGNF_PVA_1-0__1993-08-11__C93SAA1351_1993_FD05_2353.jp2	11 Aug 1993	Pan	26.6	JPEG 2000 Image
IGNF_PVA_1-0__1993-08-11__C93SAA1351_1993_FD05_2354.jp2	11 Aug 1993	Pan	26.6	JPEG 2000 Image
IGNF_PVA_1-0__1993-08-11__C93SAA1351_1993_FD05_2355.jp2	11 Aug 1993	Pan	26.6	JPEG 2000 Image
IGNF_PVA_1-0__1994-08-03__CN93000024_1993_IFN05_IRC_1118.jp2	03 Aug 1994	NIR	39.4	JPEG 2000 Image
IGNF_PVA_1-0__1994-08-03__CN93000024_1993_IFN05_IRC_1119.jp2	03 Aug 1994	NIR	39.4	JPEG 2000 Image
IGNF_PVA_1-0__1994-08-03__CN93000024_1993_IFN05_IRC_1120.jp2	03 Aug 1994	NIR	39.4	JPEG 2000 Image
IGNF_PVA_1-0__1994-08-03__CN93000024_1993_IFN05_IRC_1121.jp2	03 Aug 1994	NIR	39.4	JPEG 2000 Image
IGNF_PVA_1-0__1994-08-03__CN93000024_1993_IFN05_IRC_1122.jp2	03 Aug 1994	NIR	39.4	JPEG 2000 Image
IGNF_PVA_1-0__1994-08-03__CN93000024_1993_IFN05_IRC_1123.jp2	03 Aug 1994	NIR	39.4	JPEG 2000 Image
IGNF_PVA_1-0__1994-08-03__CN93000024_1993_IFN05_IRC_1140.jp2	03 Aug 1994	NIR	39.4	JPEG 2000 Image
IGNF_PVA_1-0__1994-08-03__CN93000024_1993_IFN05_IRC_1141.jp2	03 Aug 1994	NIR	39.4	JPEG 2000 Image
IGNF_PVA_1-0__1994-08-03__CN93000024_1993_IFN05_IRC_1142.jp2	03 Aug 1994	NIR	39.4	JPEG 2000 Image
IGNF_PVA_1-0__1994-08-03__CN93000024_1993_IFN05_IRC_1143.jp2	03 Aug 1994	NIR	39.4	JPEG 2000 Image
IGNF_PVA_1-0__1994-08-03__CN93000024_1993_IFN05_IRC_1144.jp2	03 Aug 1994	NIR	39.4	JPEG 2000 Image
IGNF_PVA_1-0__1994-08-03__CN93000024_1993_IFN05_IRC_1145.jp2	03 Aug 1994	NIR	39.4	JPEG 2000 Image
IGNF_PVA_1-0__1994-08-03__CN93000024_1993_IFN05_IRC_1146.jp2	03 Aug 1994	NIR	39.4	JPEG 2000 Image
IGNF_PVA_1-0__1994-08-03__CN93000024_1993_IFN05_IRC_1147.jp2	03 Aug 1994	NIR	39.4	JPEG 2000 Image
IGNF_PVA_1-0__1994-08-03__CN93000024_1993_IFN05_IRC_1169.jp2	03 Aug 1994	NIR	39.4	JPEG 2000 Image
IGNF_PVA_1-0__1994-08-03__CN93000024_1993_IFN05_IRC_1170.jp2	03 Aug 1994	NIR	39.4	JPEG 2000 Image
IGNF_PVA_1-0__1994-08-03__CN93000024_1993_IFN05_IRC_1171.jp2	03 Aug 1994	NIR	39.4	JPEG 2000 Image
IGNF_PVA_1-0__1994-08-03__CN93000024_1993_IFN05_IRC_1172.jp2	03 Aug 1994	NIR	39.4	JPEG 2000 Image
IGNF_PVA_1-0__1994-08-03__CN93000024_1993_IFN05_IRC_1173.jp2	03 Aug 1994	NIR	39.4	JPEG 2000 Image
IGNF_PVA_1-0__1994-08-03__CN93000024_1993_IFN05_IRC_1174.jp2	03 Aug 1994	NIR	39.4	JPEG 2000 Image

IGNF_PVA_1-0__1994-08-03__CN93000024_1993_IFN05_IRC_1175.jp2	03 Aug 1994	NIR	39.4	JPEG 2000 Image
IGNF_PVA_1-0__1994-08-03__CN93000024_1993_IFN05_IRC_1176.jp2	03 Aug 1994	NIR	39.4	JPEG 2000 Image
IGNF_PVA_1-0__1994-08-03__CN93000024_1993_IFN05_IRC_1177.jp2	03 Aug 1994	NIR	39.4	JPEG 2000 Image
IGNF_PVA_1-0__1994-08-03__CN93000024_1993_IFN05_IRC_1196.jp2	03 Aug 1994	NIR	39.4	JPEG 2000 Image
IGNF_PVA_1-0__1994-08-03__CN93000024_1993_IFN05_IRC_1197.jp2	03 Aug 1994	NIR	39.4	JPEG 2000 Image
IGNF_PVA_1-0__1994-08-03__CN93000024_1993_IFN05_IRC_1198.jp2	03 Aug 1994	NIR	39.4	JPEG 2000 Image
IGNF_PVA_1-0__1994-08-03__CN93000024_1993_IFN05_IRC_1199.jp2	03 Aug 1994	NIR	39.4	JPEG 2000 Image
IGNF_PVA_1-0__1994-08-03__CN93000024_1993_IFN05_IRC_1200.jp2	03 Aug 1994	NIR	39.4	JPEG 2000 Image
IGNF_PVA_1-0__1994-08-03__CN93000024_1993_IFN05_IRC_1201.jp2	03 Aug 1994	NIR	39.4	JPEG 2000 Image
IGNF_PVA_1-0__1994-08-03__CN93000024_1993_IFN05_IRC_1202.jp2	03 Aug 1994	NIR	39.4	JPEG 2000 Image
IGNF_PVA_1-0__1994-08-03__CN93000024_1993_IFN05_IRC_1203.jp2	03 Aug 1994	NIR	39.4	JPEG 2000 Image
IGNF_PVA_1-0__1994-08-03__CN93000024_1993_IFN05_IRC_1204.jp2	03 Aug 1994	NIR	39.4	JPEG 2000 Image
IGNF_PVA_1-0__1994-08-03__CN93000024_1993_IFN05_IRC_1242.jp2	03 Aug 1994	NIR	39.4	JPEG 2000 Image
IGNF_PVA_1-0__1994-08-03__CN93000024_1993_IFN05_IRC_1243.jp2	03 Aug 1994	NIR	39.4	JPEG 2000 Image
IGNF_PVA_1-0__1994-08-03__CN93000024_1993_IFN05_IRC_1244.jp2	03 Aug 1994	NIR	39.4	JPEG 2000 Image
IGNF_PVA_1-0__1994-08-03__CN93000024_1993_IFN05_IRC_1245.jp2	03 Aug 1994	NIR	39.4	JPEG 2000 Image
IGNF_PVA_1-0__1994-08-15__CN93000024_1993_IFN05_IRC_1153.jp2	15 Aug 1994	NIR	39.4	JPEG 2000 Image
IGNF_PVA_1-0__1994-08-15__CN93000024_1993_IFN05_IRC_1154.jp2	15 Aug 1994	NIR	39.4	JPEG 2000 Image
IGNF_PVA_1-0__1994-08-15__CN93000024_1993_IFN05_IRC_1181.jp2	15 Aug 1994	NIR	39.4	JPEG 2000 Image
IGNF_PVA_1-0__1994-08-15__CN93000024_1993_IFN05_IRC_1182.jp2	15 Aug 1994	NIR	39.4	JPEG 2000 Image
IGNF_PVA_1-0__1994-08-15__CN93000024_1993_IFN05_IRC_1251.jp2	15 Aug 1994	NIR	39.4	JPEG 2000 Image
IGNF_PVA_1-0__1994-08-15__CN93000024_1993_IFN05_IRC_1252.jp2	15 Aug 1994	NIR	39.4	JPEG 2000 Image
IGNF_PVA_1-0__1994-08-15__CN93000024_1993_IFN05_IRC_1253.jp2	15 Aug 1994	NIR	39.4	JPEG 2000 Image
IGNF_PVA_1-0__1998-07-24__CA98S01232_1998_FD38_0009.jp2	24 Jul 1998	RGB	22.7	JPEG 2000 Image
IGNF_PVA_1-0__1998-07-24__CA98S01232_1998_FD38_0025.jp2	24 Jul 1998	RGB	22.7	JPEG 2000 Image
IGNF_PVA_1-0__1998-07-24__CA98S01232_1998_FD38_0026.jp2	24 Jul 1998	RGB	22.7	JPEG 2000 Image
IGNF_PVA_1-0__1998-07-24__CA98S01232_1998_FD38_0027.jp2	24 Jul 1998	RGB	22.7	JPEG 2000 Image
IGNF_PVA_1-0__1998-07-24__CA98S01232_1998_FD38_0028.jp2	24 Jul 1998	RGB	22.7	JPEG 2000 Image
IGNF_PVA_1-0__1998-07-24__CA98S01232_1998_FD38_0029.jp2	24 Jul 1998	RGB	22.7	JPEG 2000 Image
IGNF_PVA_1-0__1998-07-24__CA98S01232_1998_FD38_0030.jp2	24 Jul 1998	RGB	22.7	JPEG 2000 Image
IGNF_PVA_1-0__1998-07-24__CA98S01232_1998_FD38_0031.jp2	24 Jul 1998	RGB	22.7	JPEG 2000 Image
IGNF_PVA_1-0__1998-07-24__CA98S01232_1998_FD38_0032.jp2	24 Jul 1998	RGB	22.7	JPEG 2000 Image
IGNF_PVA_1-0__1998-07-24__CA98S01232_1998_FD38_0033.jp2	24 Jul 1998	RGB	22.7	JPEG 2000 Image
IGNF_PVA_1-0__1998-07-24__CA98S01232_1998_FD38_0034.jp2	24 Jul 1998	RGB	22.7	JPEG 2000 Image
IGNF_PVA_1-0__1998-07-24__CA98S01232_1998_FD38_0035.jp2	24 Jul 1998	RGB	22.7	JPEG 2000 Image
IGNF_PVA_1-0__1998-07-24__CA98S01232_1998_FD38_0050.jp2	24 Jul 1998	RGB	22.7	JPEG 2000 Image
IGNF_PVA_1-0__1998-07-24__CA98S01232_1998_FD38_0051.jp2	24 Jul 1998	RGB	22.7	JPEG 2000 Image
IGNF_PVA_1-0__1998-07-24__CA98S01232_1998_FD38_0052.jp2	24 Jul 1998	RGB	22.7	JPEG 2000 Image
IGNF_PVA_1-0__1998-07-24__CA98S01232_1998_FD38_0053.jp2	24 Jul 1998	RGB	22.7	JPEG 2000 Image
IGNF_PVA_1-0__1998-07-24__CA98S01232_1998_FD38_0054.jp2	24 Jul 1998	RGB	22.7	JPEG 2000 Image

IGNF_PVA_1-0__1999-07-01__CA99S00532_1999_FD05_1705.jp2	01 Jul 1999	RGB	23.2	JPEG 2000 Image
IGNF_PVA_1-0__1999-07-01__CA99S00532_1999_FD05_1706.jp2	01 Jul 1999	RGB	23.2	JPEG 2000 Image
IGNF_PVA_1-0__1999-07-01__CA99S00532_1999_FD05_1707.jp2	01 Jul 1999	RGB	23.2	JPEG 2000 Image
IGNF_PVA_1-0__1999-07-01__CA99S00532_1999_FD05_1708.jp2	01 Jul 1999	RGB	23.2	JPEG 2000 Image
IGNF_PVA_1-0__1999-07-01__CA99S00532_1999_FD05_1709.jp2	01 Jul 1999	RGB	23.2	JPEG 2000 Image
IGNF_PVA_1-0__1999-07-01__CA99S00532_1999_FD05_1710.jp2	01 Jul 1999	RGB	23.2	JPEG 2000 Image
IGNF_PVA_1-0__1999-07-01__CA99S00532_1999_FD05_1711.jp2	01 Jul 1999	RGB	23.2	JPEG 2000 Image
IGNF_PVA_1-0__1999-07-01__CA99S00532_1999_FD05_1747.jp2	01 Jul 1999	RGB	23.2	JPEG 2000 Image
IGNF_PVA_1-0__1999-07-01__CA99S00532_1999_FD05_1748.jp2	01 Jul 1999	RGB	23.2	JPEG 2000 Image
IGNF_PVA_1-0__1999-07-01__CA99S00532_1999_FD05_1749.jp2	01 Jul 1999	RGB	23.2	JPEG 2000 Image
IGNF_PVA_1-0__1999-07-01__CA99S00532_1999_FD05_1750.jp2	01 Jul 1999	RGB	23.2	JPEG 2000 Image
IGNF_PVA_1-0__1999-07-01__CA99S00532_1999_FD05_1751.jp2	01 Jul 1999	RGB	23.2	JPEG 2000 Image
IGNF_PVA_1-0__1999-07-01__CA99S00532_1999_FD05_1753.jp2	01 Jul 1999	RGB	23.2	JPEG 2000 Image
IGNF_PVA_1-0__1999-07-01__CA99S00532_1999_FD05_1754.jp2	01 Jul 1999	RGB	23.2	JPEG 2000 Image
IGNF_PVA_1-0__1999-07-01__CA99S00532_1999_FD05_1755.jp2	01 Jul 1999	RGB	23.2	JPEG 2000 Image
IGNF_PVA_1-0__1999-07-01__CA99S00532_1999_FD05_1756.jp2	01 Jul 1999	RGB	23.2	JPEG 2000 Image
IGNF_PVA_1-0__1999-07-01__CA99S00532_1999_FD05_1757.jp2	01 Jul 1999	RGB	23.2	JPEG 2000 Image
IGNF_PVA_1-0__1999-07-01__CA99S00532_1999_FD05_1758.jp2	01 Jul 1999	RGB	23.2	JPEG 2000 Image
IGNF_PVA_1-0__1999-07-01__CA99S00532_1999_FD05_1759.jp2	01 Jul 1999	RGB	23.2	JPEG 2000 Image
IGNF_PVA_1-0__1999-07-01__CA99S00532_1999_FD05_1760.jp2	01 Jul 1999	RGB	23.2	JPEG 2000 Image
IGNF_PVA_1-0__1999-07-01__CA99S00532_1999_FD05_1762.jp2	01 Jul 1999	RGB	23.2	JPEG 2000 Image
IGNF_PVA_1-0__1999-07-01__CA99S00532_1999_FD05_1763.jp2	01 Jul 1999	RGB	23.2	JPEG 2000 Image
IGNF_PVA_1-0__1999-07-01__CA99S00532_1999_FD05_1764.jp2	01 Jul 1999	RGB	23.2	JPEG 2000 Image
IGNF_PVA_1-0__1999-07-01__CA99S00532_1999_FD05_1765.jp2	01 Jul 1999	RGB	23.2	JPEG 2000 Image
IGNF_PVA_1-0__1999-07-01__CA99S00532_1999_FD05_1767.jp2	01 Jul 1999	RGB	23.2	JPEG 2000 Image
IGNF_PVA_1-0__1999-07-01__CA99S00532_1999_FD05_1768.jp2	01 Jul 1999	RGB	23.2	JPEG 2000 Image
IGNF_PVA_1-0__1999-07-01__CA99S00532_1999_FD05_1769.jp2	01 Jul 1999	RGB	23.2	JPEG 2000 Image
IGNF_PVA_1-0__1999-07-02__CA99S00532_1999_FD05_1794.jp2	02 Jul 1999	RGB	23.2	JPEG 2000 Image
IGNF_PVA_1-0__1999-07-02__CA99S00532_1999_FD05_1795.jp2	02 Jul 1999	RGB	23.2	JPEG 2000 Image
IGNF_PVA_1-0__1999-07-02__CA99S00532_1999_FD05_1796.jp2	02 Jul 1999	RGB	23.2	JPEG 2000 Image
IGNF_PVA_1-0__1999-07-02__CA99S00532_1999_FD05_1797.jp2	02 Jul 1999	RGB	23.2	JPEG 2000 Image
IGNF_PVA_1-0__1999-07-02__CA99S00532_1999_FD05_1798.jp2	02 Jul 1999	RGB	23.2	JPEG 2000 Image
IGNF_PVA_1-0__1999-07-02__CA99S00532_1999_FD05_1799.jp2	02 Jul 1999	RGB	23.2	JPEG 2000 Image
IGNF_PVA_1-0__1999-07-02__CA99S00532_1999_FD05_1800.jp2	02 Jul 1999	RGB	23.2	JPEG 2000 Image
IGNF_PVA_1-0__1999-07-02__CA99S00532_1999_FD05_1801.jp2	02 Jul 1999	RGB	23.2	JPEG 2000 Image
IGNF_PVA_1-0__1999-07-02__CA99S00532_1999_FD05_1802.jp2	02 Jul 1999	RGB	23.2	JPEG 2000 Image
IGNF_PVA_1-0__1999-06-20__CA99S00532_1999_FD05_0778.jp2	20 Jun 1999	RGB	23.2	JPEG 2000 Image
IGNF_PVA_1-0__1999-06-20__CA99S00532_1999_FD05_0779.jp2	20 Jun 1999	RGB	23.2	JPEG 2000 Image
IGNF_PVA_1-0__1999-06-20__CA99S00532_1999_FD05_0780.jp2	20 Jun 1999	RGB	23.2	JPEG 2000 Image
IGNF_PVA_1-0__1999-06-20__CA99S00532_1999_FD05_0781.jp2	20 Jun 1999	RGB	23.2	JPEG 2000 Image

IGNF_PVA_1-0__1999-06-20__CA99S00532_1999_FD05_0782.jp2	20 Jun 1999	RGB	23.2	JPEG 2000 Image
IGNF_PVA_1-0__1999-06-20__CA99S00532_1999_FD05_0783.jp2	20 Jun 1999	RGB	23.2	JPEG 2000 Image
IGNF_PVA_1-0__1999-06-20__CA99S00532_1999_FD05_0815.jp2	20 Jun 1999	RGB	23.2	JPEG 2000 Image
IGNF_PVA_1-0__1999-06-20__CA99S00532_1999_FD05_0816.jp2	20 Jun 1999	RGB	23.2	JPEG 2000 Image
IGNF_PVA_1-0__1999-06-20__CA99S00532_1999_FD05_0817.jp2	20 Jun 1999	RGB	23.2	JPEG 2000 Image
IGNF_PVA_1-0__1999-06-20__CA99S00532_1999_FD05_0818.jp2	20 Jun 1999	RGB	23.2	JPEG 2000 Image
IGNF_PVA_1-0__1999-06-20__CA99S00532_1999_FD05_0819.jp2	20 Jun 1999	RGB	23.2	JPEG 2000 Image
IGNF_PVA_1-0__1999-06-20__CA99S00532_1999_FD05_0820.jp2	20 Jun 1999	RGB	23.2	JPEG 2000 Image
IGNF_PVA_1-0__1999-06-20__CA99S00532_1999_FD05_0821.jp2	20 Jun 1999	RGB	23.2	JPEG 2000 Image
IGNF_PVA_1-0__1999-06-20__CA99S00532_1999_FD05_0822.jp2	20 Jun 1999	RGB	23.2	JPEG 2000 Image
IGNF_PVA_1-0__1999-06-20__CA99S00532_1999_FD05_0938.jp2	20 Jun 1999	RGB	23.2	JPEG 2000 Image
IGNF_PVA_1-0__1999-06-20__CA99S00532_1999_FD05_0966.jp2	20 Jun 1999	RGB	23.2	JPEG 2000 Image
IGNF_PVA_1-0__1999-06-20__CA99S00532_1999_FD05_0967.jp2	20 Jun 1999	RGB	23.2	JPEG 2000 Image
IGNF_PVA_1-0__1999-06-20__CA99S00532_1999_FD05_0968.jp2	20 Jun 1999	RGB	23.2	JPEG 2000 Image
IGNF_PVA_1-0__2000-07-19__CA00S01041_2000_F3335-3536_0036.jp2	19 Jul 2000	Pan	26.3	JPEG 2000 Image
IGNF_PVA_1-0__2000-07-19__CA00S01041_2000_F3335-3536_0037.jp2	19 Jul 2000	Pan	26.3	JPEG 2000 Image
IGNF_PVA_1-0__2000-07-19__CA00S01041_2000_F3335-3536_0038.jp2	19 Jul 2000	Pan	26.3	JPEG 2000 Image
IGNF_PVA_1-0__2000-07-19__CA00S01041_2000_F3335-3536_0039.jp2	19 Jul 2000	Pan	26.3	JPEG 2000 Image
IGNF_PVA_1-0__2000-07-19__CA00S01041_2000_F3335-3536_0040.jp2	19 Jul 2000	Pan	26.3	JPEG 2000 Image
IGNF_PVA_1-0__2000-07-19__CA00S01041_2000_F3335-3536_0041.jp2	19 Jul 2000	Pan	26.3	JPEG 2000 Image
IGNF_PVA_1-0__2000-07-19__CA00S01041_2000_F3335-3536_0043.jp2	19 Jul 2000	Pan	26.3	JPEG 2000 Image
IGNF_PVA_1-0__2000-07-19__CA00S01041_2000_F3335-3536_0044.jp2	19 Jul 2000	Pan	26.3	JPEG 2000 Image
IGNF_PVA_1-0__2000-07-19__CA00S01041_2000_F3335-3536_0045.jp2	19 Jul 2000	Pan	26.3	JPEG 2000 Image
IGNF_PVA_1-0__2000-07-19__CA00S01041_2000_F3335-3536_0075.jp2	19 Jul 2000	Pan	26.3	JPEG 2000 Image
IGNF_PVA_1-0__2000-07-19__CA00S01041_2000_F3335-3536_0076.jp2	19 Jul 2000	Pan	26.3	JPEG 2000 Image
IGNF_PVA_1-0__2000-07-19__CA00S01041_2000_F3335-3536_0077.jp2	19 Jul 2000	Pan	26.3	JPEG 2000 Image
IGNF_PVA_1-0__2000-07-19__CA00S01041_2000_F3335-3536_0078.jp2	19 Jul 2000	Pan	26.3	JPEG 2000 Image
IGNF_PVA_1-0__2000-07-19__CA00S01041_2000_F3335-3536_0079.jp2	19 Jul 2000	Pan	26.3	JPEG 2000 Image
IGNF_PVA_1-0__2000-07-19__CA00S01041_2000_F3335-3536_0080.jp2	19 Jul 2000	Pan	26.3	JPEG 2000 Image
IGNF_PVA_1-0__2000-07-19__CA00S01041_2000_F3335-3536_0111.jp2	19 Jul 2000	Pan	26.3	JPEG 2000 Image
IGNF_PVA_1-0__2000-07-19__CA00S01041_2000_F3335-3536_0112.jp2	19 Jul 2000	Pan	26.3	JPEG 2000 Image
IGNF_PVA_1-0__2000-07-19__CA00S01041_2000_F3335-3536_0113.jp2	19 Jul 2000	Pan	26.3	JPEG 2000 Image
IGNF_PVA_1-0__2000-07-19__CA00S01041_2000_F3335-3536_0114.jp2	19 Jul 2000	Pan	26.3	JPEG 2000 Image
IGNF_PVA_1-0__2000-07-19__CA00S01041_2000_F3335-3536_0115.jp2	19 Jul 2000	Pan	26.3	JPEG 2000 Image
IGNF_PVA_1-0__2000-07-19__CA00S01041_2000_F3335-3536_0116.jp2	19 Jul 2000	Pan	26.3	JPEG 2000 Image
IGNF_PVA_1-0__2000-07-19__CA00S01041_2000_F3335-3536_0146.jp2	19 Jul 2000	Pan	26.3	JPEG 2000 Image
IGNF_PVA_1-0__2000-07-19__CA00S01041_2000_F3335-3536_0147.jp2	19 Jul 2000	Pan	26.3	JPEG 2000 Image
IGNF_PVA_1-0__2000-07-19__CA00S01041_2000_F3335-3536_0148.jp2	19 Jul 2000	Pan	26.3	JPEG 2000 Image
IGNF_PVA_1-0__2000-07-19__CA00S01041_2000_F3335-3536_0149.jp2	19 Jul 2000	Pan	26.3	JPEG 2000 Image
IGNF_PVA_1-0__2000-07-19__CA00S01041_2000_F3335-3536_0081.jp2	19 Jul 2000	Pan	26.3	JPEG 2000 Image

IGNF_PVA_1-0__2000-07-22__CA00S01041_2000_F3335-3536_0253.jp2	22 Jul 2000	Pan	26.3	JPEG 2000 Image
IGNF_PVA_1-0__2000-07-22__CA00S01041_2000_F3335-3536_0254.jp2	22 Jul 2000	Pan	26.3	JPEG 2000 Image
IGNF_PVA_1-0__2000-07-22__CA00S01041_2000_F3335-3536_0255.jp2	22 Jul 2000	Pan	26.3	JPEG 2000 Image
IGNF_PVA_1-0__2000-07-22__CA00S01041_2000_F3335-3536_0256.jp2	22 Jul 2000	Pan	26.3	JPEG 2000 Image
IGNF_PVA_1-0__2000-07-22__CA00S01041_2000_F3335-3536_0267.jp2	22 Jul 2000	Pan	26.3	JPEG 2000 Image
IGNF_PVA_1-0__2000-07-22__CA00S01041_2000_F3335-3536_0268.jp2	22 Jul 2000	Pan	26.3	JPEG 2000 Image
IGNF_PVA_1-0__2000-07-22__CA00S01041_2000_F3335-3536_0269.jp2	22 Jul 2000	Pan	26.3	JPEG 2000 Image
IGNF_PVA_1-0__2000-07-22__CA00S01041_2000_F3335-3536_0289.jp2	22 Jul 2000	Pan	26.3	JPEG 2000 Image
IGNF_PVA_1-0__2000-07-22__CA00S01041_2000_F3335-3536_0290.jp2	22 Jul 2000	Pan	26.3	JPEG 2000 Image
IGNF_PVA_1-0__2000-07-22__CA00S01041_2000_F3335-3536_0291.jp2	22 Jul 2000	Pan	26.3	JPEG 2000 Image
IGNF_PVA_1-0__2000-07-22__CA00S01041_2000_F3335-3536_0292.jp2	22 Jul 2000	Pan	26.3	JPEG 2000 Image
IGNF_PVA_1-0__2000-07-22__CA00S01041_2000_F3335-3536_0307.jp2	22 Jul 2000	Pan	26.3	JPEG 2000 Image
IGNF_PVA_1-0__2000-07-22__CA00S01041_2000_F3335-3536_0308.jp2	22 Jul 2000	Pan	26.3	JPEG 2000 Image
IGNF_PVA_1-0__2000-07-22__CA00S01041_2000_F3335-3536_0309.jp2	22 Jul 2000	Pan	26.3	JPEG 2000 Image
IGNF_PVA_1-0__2000-07-22__CA00S01041_2000_F3335-3536_0310.jp2	22 Jul 2000	Pan	26.3	JPEG 2000 Image
IGNF_PVA_1-0__2000-07-22__CA00S01041_2000_F3335-3536_0311.jp2	22 Jul 2000	Pan	26.3	JPEG 2000 Image
IGNF_PVA_1-0__2000-07-22__CA00S01041_2000_F3335-3536_0320.jp2	22 Jul 2000	Pan	26.3	JPEG 2000 Image
IGNF_PVA_1-0__2000-07-22__CA00S01041_2000_F3335-3536_0321.jp2	22 Jul 2000	Pan	26.3	JPEG 2000 Image
IGNF_PVA_1-0__2000-07-22__CA00S01041_2000_F3335-3536_0322.jp2	22 Jul 2000	Pan	26.3	JPEG 2000 Image
IGNF_PVA_1-0__2000-07-22__CA00S01041_2000_F3335-3536_0323.jp2	22 Jul 2000	Pan	26.3	JPEG 2000 Image
IGNF_PVA_1-0__2000-07-22__CA00S01041_2000_F3335-3536_0324.jp2	22 Jul 2000	Pan	26.3	JPEG 2000 Image
IGNF_PVA_1-0__2000-07-22__CA00S01041_2000_F3335-3536_0325.jp2	22 Jul 2000	Pan	26.3	JPEG 2000 Image
IGNF_PVA_1-0__2000-07-22__CA00S01041_2000_F3335-3536_0326.jp2	22 Jul 2000	Pan	26.3	JPEG 2000 Image
IGNF_PVA_1-0__2000-07-22__CA00S01041_2000_F3335-3536_0327.jp2	22 Jul 2000	Pan	26.3	JPEG 2000 Image
IGNF_PVA_1-0__2000-07-22__CA00S01041_2000_F3335-3536_0328.jp2	22 Jul 2000	Pan	26.3	JPEG 2000 Image
IGNF_PVA_1-0__2000-07-22__CA00S01041_2000_F3335-3536_0329.jp2	22 Jul 2000	Pan	26.3	JPEG 2000 Image
IGNF_PVA_1-0__2000-07-22__CA00S01041_2000_F3335-3536_0330.jp2	22 Jul 2000	Pan	26.3	JPEG 2000 Image
IGNF_PVA_1-0__2000-07-22__CA00S01041_2000_F3335-3536_0331.jp2	22 Jul 2000	Pan	26.3	JPEG 2000 Image
IGNF_PVA_1-0__2000-07-22__CA00S01041_2000_F3335-3536_0332.jp2	22 Jul 2000	Pan	26.3	JPEG 2000 Image
IGNF_PVA_1-0__2000-07-31__CA00S01041_2000_F3335-3536_0444.jp2	31 Jul 2000	Pan	26.3	JPEG 2000 Image
IGNF_PVA_1-0__2003-08-01__CP03000082_2003_fd0038_250_c_1101.jp2	01 Aug 2003	RGB	21.9	JPEG 2000 Image
IGNF_PVA_1-0__2003-08-01__CP03000082_2003_fd0038_250_c_1102.jp2	01 Aug 2003	RGB	21.9	JPEG 2000 Image
IGNF_PVA_1-0__2003-07-05__CP03000092_2003_fd0005_250_c_0022.jp2	05 Jul 2003	RGB	21.9	JPEG 2000 Image
IGNF_PVA_1-0__2003-07-05__CP03000092_2003_fd0005_250_c_0023.jp2	05 Jul 2003	RGB	21.9	JPEG 2000 Image
IGNF_PVA_1-0__2003-07-05__CP03000092_2003_fd0005_250_c_0024.jp2	05 Jul 2003	RGB	21.9	JPEG 2000 Image
IGNF_PVA_1-0__2003-07-05__CP03000092_2003_fd0005_250_c_0025.jp2	05 Jul 2003	RGB	21.9	JPEG 2000 Image
IGNF_PVA_1-0__2003-07-05__CP03000092_2003_fd0005_250_c_0026.jp2	05 Jul 2003	RGB	21.9	JPEG 2000 Image
IGNF_PVA_1-0__2003-07-05__CP03000092_2003_fd0005_250_c_0027.jp2	05 Jul 2003	RGB	21.9	JPEG 2000 Image
IGNF_PVA_1-0__2003-07-05__CP03000092_2003_fd0005_250_c_0031.jp2	05 Jul 2003	RGB	21.9	JPEG 2000 Image
IGNF_PVA_1-0__2003-07-05__CP03000092_2003_fd0005_250_c_0032.jp2	05 Jul 2003	RGB	21.9	JPEG 2000 Image

IGNF_PVA_1-0__2003-07-05__CP03000092_2003_fd0005_250_c_0033.jp2	05 Jul 2003	RGB	21.9	JPEG 2000 Image
IGNF_PVA_1-0__2003-07-05__CP03000092_2003_fd0005_250_c_0034.jp2	05 Jul 2003	RGB	21.9	JPEG 2000 Image
IGNF_PVA_1-0__2003-07-05__CP03000092_2003_fd0005_250_c_0035.jp2	05 Jul 2003	RGB	21.9	JPEG 2000 Image
IGNF_PVA_1-0__2003-07-05__CP03000092_2003_fd0005_250_c_0036.jp2	05 Jul 2003	RGB	21.9	JPEG 2000 Image
IGNF_PVA_1-0__2003-07-05__CP03000092_2003_fd0005_250_c_0051.jp2	05 Jul 2003	RGB	21.9	JPEG 2000 Image
IGNF_PVA_1-0__2003-07-05__CP03000092_2003_fd0005_250_c_0052.jp2	05 Jul 2003	RGB	21.9	JPEG 2000 Image
IGNF_PVA_1-0__2003-07-05__CP03000092_2003_fd0005_250_c_0053.jp2	05 Jul 2003	RGB	21.9	JPEG 2000 Image
IGNF_PVA_1-0__2003-07-05__CP03000092_2003_fd0005_250_c_0054.jp2	05 Jul 2003	RGB	21.9	JPEG 2000 Image
IGNF_PVA_1-0__2003-07-05__CP03000092_2003_fd0005_250_c_0071.jp2	05 Jul 2003	RGB	21.9	JPEG 2000 Image
IGNF_PVA_1-0__2003-07-05__CP03000092_2003_fd0005_250_c_0072.jp2	05 Jul 2003	RGB	21.9	JPEG 2000 Image
IGNF_PVA_1-0__2003-07-05__CP03000092_2003_fd0005_250_c_0073.jp2	05 Jul 2003	RGB	21.9	JPEG 2000 Image
IGNF_PVA_1-0__2003-07-05__CP03000092_2003_fd0005_250_c_0074.jp2	05 Jul 2003	RGB	21.9	JPEG 2000 Image
IGNF_PVA_1-0__2003-07-05__CP03000092_2003_fd0005_250_c_0075.jp2	05 Jul 2003	RGB	21.9	JPEG 2000 Image
IGNF_PVA_1-0__2003-07-05__CP03000092_2003_fd0005_250_c_0169.jp2	05 Jul 2003	RGB	21.9	JPEG 2000 Image
IGNF_PVA_1-0__2003-07-05__CP03000092_2003_fd0005_250_c_0170.jp2	05 Jul 2003	RGB	21.9	JPEG 2000 Image
IGNF_PVA_1-0__2003-07-05__CP03000092_2003_fd0005_250_c_0171.jp2	05 Jul 2003	RGB	21.9	JPEG 2000 Image
IGNF_PVA_1-0__2003-07-05__CP03000092_2003_fd0005_250_c_0172.jp2	05 Jul 2003	RGB	21.9	JPEG 2000 Image
IGNF_PVA_1-0__2003-07-05__CP03000092_2003_fd0005_250_c_0183.jp2	05 Jul 2003	RGB	21.9	JPEG 2000 Image
IGNF_PVA_1-0__2003-07-05__CP03000092_2003_fd0005_250_c_0185.jp2	05 Jul 2003	RGB	21.9	JPEG 2000 Image
IGNF_PVA_1-0__2003-07-05__CP03000092_2003_fd0005_250_c_0187.jp2	05 Jul 2003	RGB	21.9	JPEG 2000 Image
IGNF_PVA_1-0__2003-07-05__CP03000092_2003_fd0005_250_c_0188.jp2	05 Jul 2003	RGB	21.9	JPEG 2000 Image
IGNF_PVA_1-0__2003-07-05__CP03000092_2003_fd0005_250_c_0189.jp2	05 Jul 2003	RGB	21.9	JPEG 2000 Image
IGNF_PVA_1-0__2003-07-05__CP03000092_2003_fd0005_250_c_0190.jp2	05 Jul 2003	RGB	21.9	JPEG 2000 Image
IGNF_PVA_1-0__2003-07-05__CP03000092_2003_fd0005_250_c_0223.jp2	05 Jul 2003	RGB	21.9	JPEG 2000 Image
IGNF_PVA_1-0__2003-07-05__CP03000092_2003_fd0005_250_c_0224.jp2	05 Jul 2003	RGB	21.9	JPEG 2000 Image
IGNF_PVA_1-0__2003-07-05__CP03000092_2003_fd0005_250_c_0225.jp2	05 Jul 2003	RGB	21.9	JPEG 2000 Image
IGNF_PVA_1-0__2003-07-05__CP03000092_2003_fd0005_250_c_0226.jp2	05 Jul 2003	RGB	21.9	JPEG 2000 Image
IGNF_PVA_1-0__2003-07-05__CP03000092_2003_fd0005_250_c_0227.jp2	05 Jul 2003	RGB	21.9	JPEG 2000 Image
IGNF_PVA_1-0__2003-07-05__CP03000092_2003_fd0005_250_c_0228.jp2	05 Jul 2003	RGB	21.9	JPEG 2000 Image
IGNF_PVA_1-0__2003-07-05__CP03000092_2003_fd0005_250_c_0252.jp2	05 Jul 2003	RGB	21.9	JPEG 2000 Image
IGNF_PVA_1-0__2003-07-05__CP03000092_2003_fd0005_250_c_0253.jp2	05 Jul 2003	RGB	21.9	JPEG 2000 Image
IGNF_PVA_1-0__2003-07-05__CP03000092_2003_fd0005_250_c_0254.jp2	05 Jul 2003	RGB	21.9	JPEG 2000 Image
IGNF_PVA_1-0__2003-07-05__CP03000092_2003_fd0005_250_c_0255.jp2	05 Jul 2003	RGB	21.9	JPEG 2000 Image
IGNF_PVA_1-0__2003-07-05__CP03000092_2003_fd0005_250_c_0379.jp2	05 Jul 2003	RGB	21.9	JPEG 2000 Image
IGNF_PVA_1-0__2003-07-05__CP03000092_2003_fd0005_250_c_0380.jp2	05 Jul 2003	RGB	21.9	JPEG 2000 Image
IGNF_PVA_1-0__2003-07-05__CP03000092_2003_fd0005_250_c_0381.jp2	05 Jul 2003	RGB	21.9	JPEG 2000 Image
IGNF_PVA_1-0__2003-07-05__CP03000092_2003_fd0005_250_c_0382.jp2	05 Jul 2003	RGB	21.9	JPEG 2000 Image
IGNF_PVA_1-0__2003-07-05__CP03000092_2003_fd0005_250_c_0383.jp2	05 Jul 2003	RGB	21.9	JPEG 2000 Image
IGNF_PVA_1-0__2003-07-05__CP03000092_2003_fd0005_250_c_0384.jp2	05 Jul 2003	RGB	21.9	JPEG 2000 Image
IGNF_PVA_1-0__2003-07-05__CP03000092_2003_fd0005_250_c_0385.jp2	05 Jul 2003	RGB	21.9	JPEG 2000 Image

IGNF_PVA_1-0__2003-07-05__CP03000092_2003_fd0005_250_c_0386.jp2	05 Jul 2003	RGB	21.9	JPEG 2000 Image
IGNF_PVA_1-0__2003-07-05__CP03000092_2003_fd0005_250_c_0387.jp2	05 Jul 2003	RGB	21.9	JPEG 2000 Image
IGNF_PVA_1-0__2003-07-05__CP03000092_2003_fd0005_250_c_0403.jp2	05 Jul 2003	RGB	21.9	JPEG 2000 Image
IGNF_PVA_1-0__2003-07-05__CP03000092_2003_fd0005_250_c_0405.jp2	05 Jul 2003	RGB	21.9	JPEG 2000 Image
IGNF_PVA_1-0__2003-07-05__CP03000092_2003_fd0005_250_c_0406.jp2	05 Jul 2003	RGB	21.9	JPEG 2000 Image
IGNF_PVA_1-0__2003-07-05__CP03000092_2003_fd0005_250_c_0407.jp2	05 Jul 2003	RGB	21.9	JPEG 2000 Image
IGNF_PVA_1-0__2003-07-05__CP03000092_2003_fd0005_250_c_0408.jp2	05 Jul 2003	RGB	21.9	JPEG 2000 Image
IGNF_PVA_1-0__2003-07-05__CP03000092_2003_fd0005_250_c_0409.jp2	05 Jul 2003	RGB	21.9	JPEG 2000 Image
IGNF_PVA_1-0__2003-07-05__CP03000092_2003_fd0005_250_c_0410.jp2	05 Jul 2003	RGB	21.9	JPEG 2000 Image
IGNF_PVA_1-0__2003-07-05__CP03000092_2003_fd0005_250_c_0411.jp2	05 Jul 2003	RGB	21.9	JPEG 2000 Image
IGNF_PVA_1-0__2003-07-05__CP03000092_2003_fd0005_250_c_0412.jp2	05 Jul 2003	RGB	21.9	JPEG 2000 Image
IGNF_PVA_1-0__2003-07-05__CP03000092_2003_fd0005_250_c_0413.jp2	05 Jul 2003	RGB	21.9	JPEG 2000 Image
IGNF_PVA_1-0__2003-07-05__CP03000092_2003_fd0005_250_c_0463.jp2	05 Jul 2003	RGB	21.9	JPEG 2000 Image
IGNF_PVA_1-0__2003-07-05__CP03000092_2003_fd0005_250_c_0464.jp2	05 Jul 2003	RGB	21.9	JPEG 2000 Image
IGNF_PVA_1-0__2003-07-05__CP03000092_2003_fd0005_250_c_0168.jp2	05 Jul 2003	RGB	21.9	JPEG 2000 Image
IGNF_PVA_1-0__2003-07-05__CP03000092_2003_fd0005_250_c_0465.jp2	05 Jul 2003	RGB	21.9	JPEG 2000 Image
IGNF_PVA_1-0__2003-07-05__CP03000092_2003_fd0005_250_c_0466.jp2	05 Jul 2003	RGB	21.9	JPEG 2000 Image
IGNF_PVA_1-0__2003-08-06__CP03000082_2003_fd0038_250_c_2602.jp2	06 Aug 2003	RGB	21.9	JPEG 2000 Image
IGNF_PVA_1-0__2003-08-06__CP03000082_2003_fd0038_250_c_2603.jp2	06 Aug 2003	RGB	21.9	JPEG 2000 Image
IGNF_PVA_1-0__2003-08-06__CP03000082_2003_fd0038_250_c_2604.jp2	06 Aug 2003	RGB	21.9	JPEG 2000 Image
IGNF_PVA_1-0__2003-08-06__CP03000082_2003_fd0038_250_c_2605.jp2	06 Aug 2003	RGB	21.9	JPEG 2000 Image
IGNF_PVA_1-0__2003-08-06__CP03000082_2003_fd0038_250_c_2606.jp2	06 Aug 2003	RGB	21.9	JPEG 2000 Image
IGNF_PVA_1-0__2003-08-06__CP03000082_2003_fd0038_250_c_2607.jp2	06 Aug 2003	RGB	21.9	JPEG 2000 Image
IGNF_PVA_1-0__2003-08-06__CP03000082_2003_fd0038_250_c_2608.jp2	06 Aug 2003	RGB	21.9	JPEG 2000 Image
IGNF_PVA_1-0__2003-07-08__CP03000092_2003_fd0005_250_c_1546.jp2	08 Jul 2003	RGB	21.9	JPEG 2000 Image
IGNF_PVA_1-0__2003-07-08__CP03000092_2003_fd0005_250_c_1547.jp2	08 Jul 2003	RGB	21.9	JPEG 2000 Image
IGNF_PVA_1-0__2003-07-08__CP03000092_2003_fd0005_250_c_1548.jp2	08 Jul 2003	RGB	21.9	JPEG 2000 Image
IGNF_PVA_1-0__2003-07-08__CP03000092_2003_fd0005_250_c_1571.jp2	08 Jul 2003	RGB	21.9	JPEG 2000 Image
IGNF_PVA_1-0__2003-07-08__CP03000092_2003_fd0005_250_c_1572.jp2	08 Jul 2003	RGB	21.9	JPEG 2000 Image
IGNF_PVA_1-0__2003-07-08__CP03000092_2003_fd0005_250_c_1573.jp2	08 Jul 2003	RGB	21.9	JPEG 2000 Image
IGNF_PVA_1-0__2003-07-08__CP03000092_2003_fd0005_250_c_1574.jp2	08 Jul 2003	RGB	21.9	JPEG 2000 Image
IGNF_PVA_1-0__2003-07-08__CP03000092_2003_fd0005_250_c_1575.jp2	08 Jul 2003	RGB	21.9	JPEG 2000 Image
IGNF_PVA_1-0__2003-07-08__CP03000092_2003_fd0005_250_c_1576.jp2	08 Jul 2003	RGB	21.9	JPEG 2000 Image
IGNF_PVA_1-0__2003-07-08__CP03000092_2003_fd0005_250_c_1577.jp2	08 Jul 2003	RGB	21.9	JPEG 2000 Image
IGNF_PVA_1-0__2003-07-08__CP03000092_2003_fd0005_250_c_1578.jp2	08 Jul 2003	RGB	21.9	JPEG 2000 Image
IGNF_PVA_1-0__2003-07-08__CP03000092_2003_fd0005_250_c_1579.jp2	08 Jul 2003	RGB	21.9	JPEG 2000 Image
IGNF_PVA_1-0__2003-07-08__CP03000092_2003_fd0005_250_c_1608.jp2	08 Jul 2003	RGB	21.9	JPEG 2000 Image
IGNF_PVA_1-0__2003-07-08__CP03000092_2003_fd0005_250_c_1609.jp2	08 Jul 2003	RGB	21.9	JPEG 2000 Image
IGNF_PVA_1-0__2003-07-08__CP03000092_2003_fd0005_250_c_1610.jp2	08 Jul 2003	RGB	21.9	JPEG 2000 Image
IGNF_PVA_1-0__2003-07-08__CP03000092_2003_fd0005_250_c_1613.jp2	08 Jul 2003	RGB	21.9	JPEG 2000 Image

IGNF_PVA_1-0__2003-07-08__CP03000092_2003_fd0005_250_c_1614.jp2	08 Jul 2003	RGB	21.9	JPEG 2000 Image
IGNF_PVA_1-0__2003-07-08__CP03000092_2003_fd0005_250_c_1615.jp2	08 Jul 2003	RGB	21.9	JPEG 2000 Image
IGNF_PVA_1-0__2003-07-08__CP03000092_2003_fd0005_250_c_1544.jp2	08 Jul 2003	RGB	21.9	JPEG 2000 Image
IGNF_PVA_1-0__2003-07-08__CP03000092_2003_fd0005_250_c_1545.jp2	08 Jul 2003	RGB	21.9	JPEG 2000 Image
IGNF_PVA_1-0__2003-07-08__CP03000092_2003_fd0005_250_c_1611.jp2	08 Jul 2003	RGB	21.9	JPEG 2000 Image
IGNF_PVA_1-0__2003-07-08__CP03000092_2003_fd0005_250_c_1612.jp2	08 Jul 2003	RGB	21.9	JPEG 2000 Image
IGNF_PVA_1-0__2003-07-08__CP03000082_2003_fd0038_250_c_0226.jp2	08 Jul 2003	RGB	21.9	JPEG 2000 Image
IGNF_PVA_1-0__2003-07-08__CP03000082_2003_fd0038_250_c_0227.jp2	08 Jul 2003	RGB	21.9	JPEG 2000 Image
IGNF_PVA_1-0__2003-07-08__CP03000082_2003_fd0038_250_c_0228.jp2	08 Jul 2003	RGB	21.9	JPEG 2000 Image
IGNF_PVA_1-0__2003-07-08__CP03000082_2003_fd0038_250_c_0229.jp2	08 Jul 2003	RGB	21.9	JPEG 2000 Image
IGNF_PVA_1-0__2003-07-08__CP03000082_2003_fd0038_250_c_0293.jp2	08 Jul 2003	RGB	21.9	JPEG 2000 Image
IGNF_PVA_1-0__2003-07-08__CP03000082_2003_fd0038_250_c_0294.jp2	08 Jul 2003	RGB	21.9	JPEG 2000 Image
IGNF_PVA_1-0__2003-07-08__CP03000082_2003_fd0038_250_c_0295.jp2	08 Jul 2003	RGB	21.9	JPEG 2000 Image
IGNF_PVA_1-0__2003-07-08__CP03000082_2003_fd0038_250_c_0296.jp2	08 Jul 2003	RGB	21.9	JPEG 2000 Image
IGNF_PVA_1-0__2003-07-08__CP03000082_2003_fd0038_250_c_0297.jp2	08 Jul 2003	RGB	21.9	JPEG 2000 Image
IGNF_PVA_1-0__2003-07-08__CP03000082_2003_fd0038_250_c_0298.jp2	08 Jul 2003	RGB	21.9	JPEG 2000 Image
IGNF_PVA_1-0__2003-07-08__CP03000082_2003_fd0038_250_c_0299.jp2	08 Jul 2003	RGB	21.9	JPEG 2000 Image
IGNF_PVA_1-0__2003-07-08__CP03000082_2003_fd0038_250_c_0300.jp2	08 Jul 2003	RGB	21.9	JPEG 2000 Image
IGNF_PVA_1-0__2003-07-08__CP03000082_2003_fd0038_250_c_0301.jp2	08 Jul 2003	RGB	21.9	JPEG 2000 Image
IGNF_PVA_1-0__2003-07-08__CP03000082_2003_fd0038_250_c_0302.jp2	08 Jul 2003	RGB	21.9	JPEG 2000 Image
IGNF_PVA_1-0__2003-07-08__CP03000082_2003_fd0038_250_c_0303.jp2	08 Jul 2003	RGB	21.9	JPEG 2000 Image
IGNF_PVA_1-0__2003-07-08__CP03000082_2003_fd0038_250_c_0331.jp2	08 Jul 2003	RGB	21.9	JPEG 2000 Image
IGNF_PVA_1-0__2003-07-08__CP03000082_2003_fd0038_250_c_0332.jp2	08 Jul 2003	RGB	21.9	JPEG 2000 Image
IGNF_PVA_1-0__2003-07-08__CP03000082_2003_fd0038_250_c_0333.jp2	08 Jul 2003	RGB	21.9	JPEG 2000 Image
IGNF_PVA_1-0__2003-07-08__CP03000082_2003_fd0038_250_c_0335.jp2	08 Jul 2003	RGB	21.9	JPEG 2000 Image
IGNF_PVA_1-0__2003-07-08__CP03000082_2003_fd0038_250_c_0336.jp2	08 Jul 2003	RGB	21.9	JPEG 2000 Image
IGNF_PVA_1-0__2003-07-08__CP03000082_2003_fd0038_250_c_0337.jp2	08 Jul 2003	RGB	21.9	JPEG 2000 Image
IGNF_PVA_1-0__2003-07-08__CP03000082_2003_fd0038_250_c_0338.jp2	08 Jul 2003	RGB	21.9	JPEG 2000 Image
IGNF_PVA_1-0__2003-07-11__CP03000082_2003_fd0038_250_c_0361.jp2	11 Jul 2003	RGB	21.9	JPEG 2000 Image
IGNF_PVA_1-0__2003-07-11__CP03000082_2003_fd0038_250_c_0362.jp2	11 Jul 2003	RGB	21.9	JPEG 2000 Image
IGNF_PVA_1-0__2003-07-11__CP03000082_2003_fd0038_250_c_0363.jp2	11 Jul 2003	RGB	21.9	JPEG 2000 Image
IGNF_PVA_1-0__2003-07-11__CP03000082_2003_fd0038_250_c_0364.jp2	11 Jul 2003	RGB	21.9	JPEG 2000 Image
IGNF_PVA_1-0__2003-07-11__CP03000082_2003_fd0038_250_c_0365.jp2	11 Jul 2003	RGB	21.9	JPEG 2000 Image
IGNF_PVA_1-0__2003-07-11__CP03000082_2003_fd0038_250_c_0366.jp2	11 Jul 2003	RGB	21.9	JPEG 2000 Image
IGNF_PVA_1-0__2003-07-11__CP03000082_2003_fd0038_250_c_0367.jp2	11 Jul 2003	RGB	21.9	JPEG 2000 Image
IGNF_PVA_1-0__2003-07-11__CP03000082_2003_fd0038_250_c_0368.jp2	11 Jul 2003	RGB	21.9	JPEG 2000 Image
IGNF_PVA_1-0__2003-07-11__CP03000082_2003_fd0038_250_c_0369.jp2	11 Jul 2003	RGB	21.9	JPEG 2000 Image
IGNF_PVA_1-0__2003-07-11__CP03000082_2003_fd0038_250_c_0379.jp2	11 Jul 2003	RGB	21.9	JPEG 2000 Image
IGNF_PVA_1-0__2003-07-11__CP03000082_2003_fd0038_250_c_0380.jp2	11 Jul 2003	RGB	21.9	JPEG 2000 Image
IGNF_PVA_1-0__2003-07-11__CP03000082_2003_fd0038_250_c_0381.jp2	11 Jul 2003	RGB	21.9	JPEG 2000 Image

IGNF_PVA_1-0__2003-07-11__CP03000082_2003_fd0038_250_c_0382.jp2	11 Jul 2003	RGB	21.9	JPEG 2000 Image
IGNF_PVA_1-0__2003-07-11__CP03000082_2003_fd0038_250_c_0383.jp2	11 Jul 2003	RGB	21.9	JPEG 2000 Image
IGNF_PVA_1-0__2003-07-11__CP03000082_2003_fd0038_250_c_0384.jp2	11 Jul 2003	RGB	21.9	JPEG 2000 Image
IGNF_PVA_1-0__2003-07-11__CP03000082_2003_fd0038_250_c_0385.jp2	11 Jul 2003	RGB	21.9	JPEG 2000 Image
IGNF_PVA_1-0__2003-07-11__CP03000082_2003_fd0038_250_c_0386.jp2	11 Jul 2003	RGB	21.9	JPEG 2000 Image
IGNF_PVA_1-0__2003-07-19__CP03000092_2003_fd0005_250_c_2834.jp2	19 Jul 2003	RGB	21.9	JPEG 2000 Image
IGNF_PVA_1-0__2003-07-19__CP03000092_2003_fd0005_250_c_2839.jp2	19 Jul 2003	RGB	21.9	JPEG 2000 Image
IGNF_PVA_1-0__2003-07-19__CP03000082_2003_fd0038_250_c_0832.jp2	19 Jul 2003	RGB	21.9	JPEG 2000 Image
IGNF_PVA_1-0__2003-07-19__CP03000082_2003_fd0038_250_c_0833.jp2	19 Jul 2003	RGB	21.9	JPEG 2000 Image
IGNF_PVA_1-0__2003-07-19__CP03000082_2003_fd0038_250_c_0834.jp2	19 Jul 2003	RGB	21.9	JPEG 2000 Image
IGNF_PVA_1-0__2003-07-19__CP03000082_2003_fd0038_250_c_0877.jp2	19 Jul 2003	RGB	21.9	JPEG 2000 Image
IGNF_PVA_1-0__2003-07-19__CP03000082_2003_fd0038_250_c_0878.jp2	19 Jul 2003	RGB	21.9	JPEG 2000 Image
IGNF_PVA_1-0__2003-07-19__CP03000082_2003_fd0038_250_c_0879.jp2	19 Jul 2003	RGB	21.9	JPEG 2000 Image
IGNF_PVA_1-0__2003-07-20__CP03000082_2003_fd0038_250_c_1008.jp2	20 Jul 2003	RGB	21.9	JPEG 2000 Image
IGNF_PVA_1-0__2003-07-20__CP03000082_2003_fd0038_250_c_1009.jp2	20 Jul 2003	RGB	21.9	JPEG 2000 Image
IGNF_PVA_1-0__2003-07-20__CP03000082_2003_fd0038_250_c_1010.jp2	20 Jul 2003	RGB	21.9	JPEG 2000 Image
IGNF_PVA_1-0__2003-07-20__CP03000082_2003_fd0038_250_c_1011.jp2	20 Jul 2003	RGB	21.9	JPEG 2000 Image
IGNF_PVA_1-0__2003-07-20__CP03000082_2003_fd0038_250_c_1012.jp2	20 Jul 2003	RGB	21.9	JPEG 2000 Image
IGNF_PVA_1-0__2003-07-20__CP03000082_2003_fd0038_250_c_1013.jp2	20 Jul 2003	RGB	21.9	JPEG 2000 Image
FD05x037_02094.jp2	2009	RGB	56.3	JPEG 2000 Image
FD05x037_02095.jp2	2009	RGB	56.3	JPEG 2000 Image
FD05x037_02096.jp2	2009	RGB	56.3	JPEG 2000 Image
FD05x037_02097.jp2	2009	RGB	56.3	JPEG 2000 Image
FD05x037_02098.jp2	2009	RGB	56.3	JPEG 2000 Image
FD05x037_02099.jp2	2009	RGB	56.3	JPEG 2000 Image
FD05x037_02100.jp2	2009	RGB	56.3	JPEG 2000 Image
FD05x037_02101.jp2	2009	RGB	56.3	JPEG 2000 Image
FD05x037_02102.jp2	2009	RGB	56.3	JPEG 2000 Image
FD05x037_02103.jp2	2009	RGB	56.3	JPEG 2000 Image
FD05x039_02048.jp2	2009	RGB	56.3	JPEG 2000 Image
FD05x039_02049.jp2	2009	RGB	56.3	JPEG 2000 Image
FD05x039_02050.jp2	2009	RGB	56.3	JPEG 2000 Image
FD05x039_02051.jp2	2009	RGB	56.3	JPEG 2000 Image
FD05x039_02054.jp2	2009	RGB	56.3	JPEG 2000 Image
FD05x039_02055.jp2	2009	RGB	56.3	JPEG 2000 Image
FD05x039_02056.jp2	2009	RGB	56.3	JPEG 2000 Image
FD05x039_02052.jp2	2009	RGB	56.3	JPEG 2000 Image
FD05x039_02053.jp2	2009	RGB	56.3	JPEG 2000 Image
13FD0535x00013_02857.jp2	2013	RGB	44.5	JPEG 2000 Image
13FD0535x00013_02858.jp2	2013	RGB	44.5	JPEG 2000 Image

13FD0535x00012_02734.jp2	2013	RGB	44.5	JPEG 2000 Image
13FD0535x00012_02735.jp2	2013	RGB	44.5	JPEG 2000 Image
13FD0535x00012_02736.jp2	2013	RGB	44.5	JPEG 2000 Image
13FD0535x00012_02737.jp2	2013	RGB	44.5	JPEG 2000 Image
13FD0535x00012_02739.jp2	2013	RGB	44.5	JPEG 2000 Image
13FD0535x00012_02740.jp2	2013	RGB	44.5	JPEG 2000 Image
13FD0535x00013_02854.jp2	2013	RGB	44.5	JPEG 2000 Image
13FD0535x00013_02855.jp2	2013	RGB	44.5	JPEG 2000 Image
13FD0535x00013_02856.jp2	2013	RGB	44.5	JPEG 2000 Image
13FD0535x00013_02859.jp2	2013	RGB	44.5	JPEG 2000 Image
13FD0535x00013_02860.jp2	2013	RGB	44.5	JPEG 2000 Image
13FD0535x00012_02732.jp2	2013	RGB	44.5	JPEG 2000 Image
13FD0535x00012_02733.jp2	2013	RGB	44.5	JPEG 2000 Image
13FD0535x00012_02738.jp2	2013	RGB	44.5	JPEG 2000 Image
13FD0535x00012_02741.jp2	2013	RGB	44.5	JPEG 2000 Image
13FD0535x00012_02742.jp2	2013	RGB	44.5	JPEG 2000 Image
13FD0535x00013_02853.jp2	2013	RGB	44.5	JPEG 2000 Image
13FD0535x00011_01762.jp2	2013	RGB	44.4	JPEG 2000 Image
13FD0535x00009_01860.jp2	2013	RGB	44.4	JPEG 2000 Image
13FD0535x00009_01861.jp2	2013	RGB	44.4	JPEG 2000 Image
13FD0535x00009_01862.jp2	2013	RGB	44.4	JPEG 2000 Image
13FD0535x00009_01863.jp2	2013	RGB	44.4	JPEG 2000 Image
13FD0535x00009_01864.jp2	2013	RGB	44.4	JPEG 2000 Image
13FD0535x00009_01868.jp2	2013	RGB	44.4	JPEG 2000 Image
13FD0535x00010_01782.jp2	2013	RGB	44.4	JPEG 2000 Image
13FD0535x00010_01783.jp2	2013	RGB	44.4	JPEG 2000 Image
13FD0535x00010_01784.jp2	2013	RGB	44.4	JPEG 2000 Image
13FD0535x00010_01785.jp2	2013	RGB	44.4	JPEG 2000 Image
13FD0535x00010_01786.jp2	2013	RGB	44.4	JPEG 2000 Image
13FD0535x00010_01787.jp2	2013	RGB	44.4	JPEG 2000 Image
13FD0535x00010_01788.jp2	2013	RGB	44.4	JPEG 2000 Image
13FD0535x00010_01789.jp2	2013	RGB	44.4	JPEG 2000 Image
13FD0535x00010_01790.jp2	2013	RGB	44.4	JPEG 2000 Image
13FD0535x00010_01791.jp2	2013	RGB	44.4	JPEG 2000 Image
13FD0535x00010_01792.jp2	2013	RGB	44.4	JPEG 2000 Image
13FD0535x00011_01757.jp2	2013	RGB	44.4	JPEG 2000 Image
13FD0535x00011_01758.jp2	2013	RGB	44.4	JPEG 2000 Image
13FD0535x00011_01759.jp2	2013	RGB	44.4	JPEG 2000 Image
13FD0535x00011_01760.jp2	2013	RGB	44.4	JPEG 2000 Image
13FD0535x00011_01761.jp2	2013	RGB	44.4	JPEG 2000 Image

13FD0535x00011_01763.jp2	2013	RGB	44.4	JPEG 2000 Image
13FD0535x00011_01764.jp2	2013	RGB	44.4	JPEG 2000 Image
13FD0535x00009_01865.jp2	2013	RGB	44.4	JPEG 2000 Image
13FD0535x00009_01866.jp2	2013	RGB	44.4	JPEG 2000 Image
13FD0535x00009_01867.jp2	2013	RGB	44.4	JPEG 2000 Image
13FD0535x00011_01754.jp2	2013	RGB	44.4	JPEG 2000 Image
13FD0535x00011_01755.jp2	2013	RGB	44.4	JPEG 2000 Image
13FD0535x00011_01756.jp2	2013	RGB	44.4	JPEG 2000 Image
666-2015-0963-6429-L93.tif	2014	Spot 6	57.9	TIF Image
666-2015-0963-6432-L93.tif	2014	Spot 6	57.9	TIF Image
666-2015-0963-6435-L93.tif	2014	Spot 6	57.9	TIF Image
666-2015-0966-6429-L93.tif	2014	Spot 6	57.9	TIF Image
666-2015-0966-6432-L93.tif	2014	Spot 6	57.9	TIF Image
666-2015-0966-6435-L93.tif	2014	Spot 6	57.9	TIF Image
666-2015-0969-6429-L93.tif	2014	Spot 6	57.9	TIF Image
666-2015-0969-6432-L93.tif	2014	Spot 6	57.9	TIF Image
666-2015-0969-6435-L93.tif	2014	Spot 6	57.9	TIF Image
666-2016-0969-6429-L93.jp2	2015	Spot 6	16.9	JPEG 2000 Image
666-2016-0969-6438-L93.jp2	2015	Spot 6	16.5	JPEG 2000 Image
666-2016-0960-6432-L93.jp2	2015	Spot 6	16.5	JPEG 2000 Image
666-2016-0969-6432-L93.jp2	2015	Spot 6	16.2	JPEG 2000 Image
666-2016-0972-6435-L93.jp2	2015	Spot 6	16.0	JPEG 2000 Image
666-2016-0972-6432-L93.jp2	2015	Spot 6	15.7	JPEG 2000 Image
666-2016-0963-6426-L93.jp2	2015	Spot 6	15.7	JPEG 2000 Image
666-2016-0960-6426-L93.jp2	2015	Spot 6	15.4	JPEG 2000 Image
666-2016-0963-6438-L93.jp2	2015	Spot 6	15.4	JPEG 2000 Image
666-2016-0966-6438-L93.jp2	2015	Spot 6	15.2	JPEG 2000 Image
666-2016-0960-6435-L93.jp2	2015	Spot 6	15.1	JPEG 2000 Image
666-2016-0969-6435-L93.jp2	2015	Spot 6	14.9	JPEG 2000 Image
666-2016-0966-6432-L93.jp2	2015	Spot 6	14.9	JPEG 2000 Image
666-2016-0963-6429-L93.jp2	2015	Spot 6	14.9	JPEG 2000 Image
666-2016-0963-6435-L93.jp2	2015	Spot 6	14.5	JPEG 2000 Image
666-2016-0966-6435-L93.jp2	2015	Spot 6	14.3	JPEG 2000 Image
666-2016-0966-6429-L93.jp2	2015	Spot 6	13.8	JPEG 2000 Image
666-2016-0963-6432-L93.jp2	2015	Spot 6	13.5	JPEG 2000 Image
666-2016-0969-6432-L93.jp2	2016	Spot 6	14.4	JPEG 2000 Image
666-2016-0963-6429-L93.jp2	2016	Spot 6	13.4	JPEG 2000 Image
666-2016-0966-6429-L93.jp2	2016	Spot 6	12.7	JPEG 2000 Image
666-2016-0966-6432-L93.jp2	2016	Spot 6	12.5	JPEG 2000 Image
666-2016-0963-6435-L93.jp2	2016	Spot 6	12.5	JPEG 2000 Image

666-2016-0969-6435-L93.jp2	2016	Spot 6	12.3	JPEG 2000 Image
666-2016-0966-6435-L93.jp2	2016	Spot 6	11.4	JPEG 2000 Image
666-2016-0963-6432-L93.jp2	2016	Spot 6	11.1	JPEG 2000 Image
666-2016-0966-6429-L93.jp2	2016	Spot 6	12.7	JPEG 2000 Image
666-2016-0966-6432-L93.jp2	2016	Spot 6	12.5	JPEG 2000 Image
666-2016-0963-6435-L93.jp2	2016	Spot 6	12.5	JPEG 2000 Image
666-2016-0969-6435-L93.jp2	2016	Spot 6	12.3	JPEG 2000 Image
666-2016-0966-6435-L93.jp2	2016	Spot 6	11.4	JPEG 2000 Image
666-2016-0963-6432-L93.jp2	2016	Spot 6	11.1	JPEG 2000 Image
Number of images	**745**			
Total size (GB)			**18.5**	

Georeferencing data

CH4 - Table S3: Georeferencing residuals

Year	Average residuals compared to BDORTHO 50cm 2013 (m)	Standard deviation of residuals (m)	Number of check points
1952	6.9	5.5	21
1960	5.6	3.4	19
1964	2.6	1.0	9
1967	20.8	14.5	21
1974	144.3	48.1	11
1979	63.1	37.9	14
1980	5.8	5.2	21
1981	16.2	14.6	20
1983	18.7	15.0	17
1986	20.8	11.1	16
1988	12.1	9.0	20
1989	65.9	22.9	14
1993	10.3	8.5	20
1994	2.2	1.7	21
1998	6.3	4.3	21
1999	6.6	21.1	21
2000	6.4	4.8	21

2003	1.7	1.1	21
2009	2.0	1.9	21
2013	BDORTHO 50cm - 2013 - Published uncertainty: 1-5 m		
2014	2.0	1.5	20
2015	2.3	1.4	21
2016	2.4	1.5	19

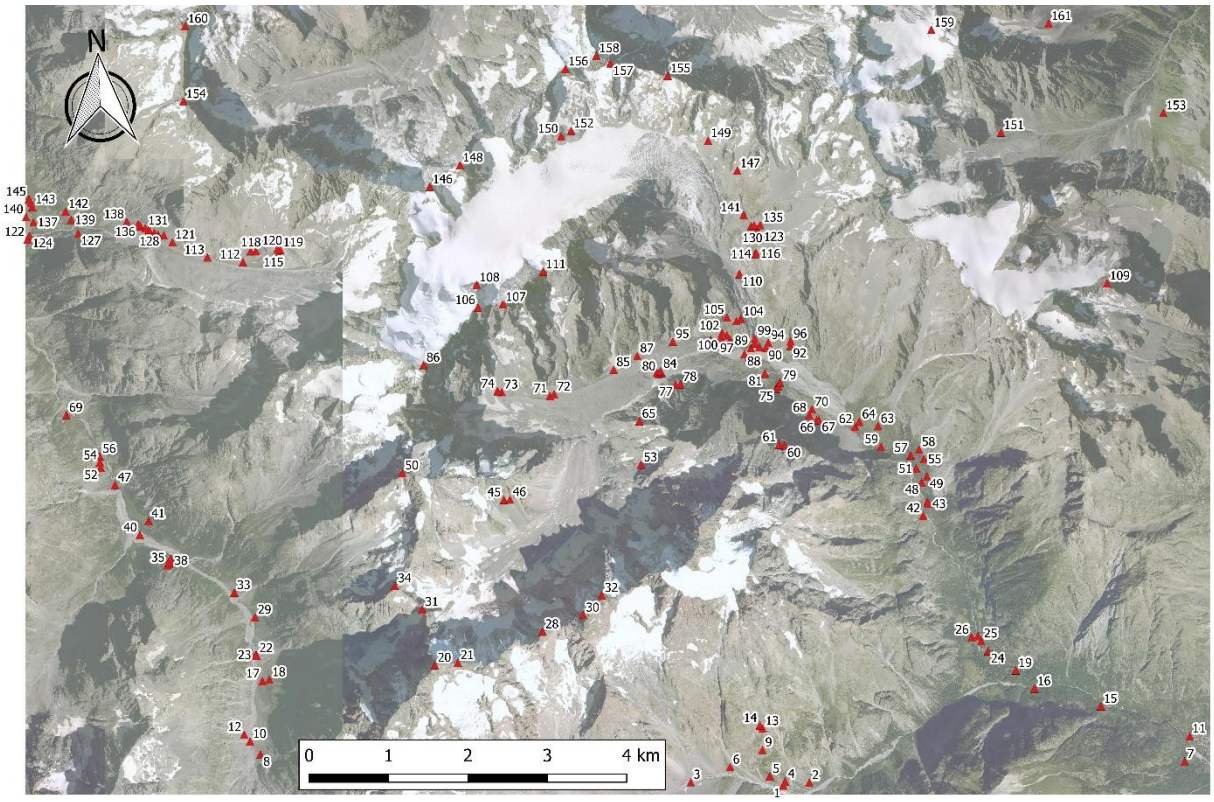

CH4 - Figure S1: Location map of the ground control points (red triangles) used during the SfM process. *Background: ©BDORTHO 50cm 2013.*

Elevation benchmarks description

IGN *Nivellement Général de la France*

Repère de nivellement

Matricule : **X'.C.R3 - 146**

Système d'altitude : NGF-IGN 1969

1 874,135 m

ALTITUDE NORMALE

Année de dernière détermination : 1982

Repère vu en place en 2002

Type : **M REPERE CYLINDRIQUE DU NIVELLEMENT GENERAL**

Complément :

Système : RGF93 - Ellipsoide : IAG GRS 1980 - Méridien origine : GREENWICH

Longitude (dms) : **6° 24' 56" E** *Latitude (dms) :* **44° 55' 04" N**

Système : RGF93 - Projection : LAMBERT-93

E (km) : **969.46** *N (km) :* **6430.12**

Département : **HAUTES-ALPES** *Numéro INSEE :* **05101** *Commune :* **PELVOUX**

Voie suivie : **CHEMIN**

de : **AILEFROIDE** *à :* **LE CHALET-HOTEL CEZANNE**

Coté : **Gauche** *PK :* **-** *Distance :* **1,15** *km du repère* **X'.C.R3 - 145**

Localisation : **AU LIEU-DIT "PRE DE MADAME CARLE"**

Support : **CHALET-HOTEL "CEZANNE"**

Partie support : **MUR DE FACADE NORD-EST, FACE ROUTE**

Repèrements : **A 0.59 M DE L'EXTREMITE SUD-EST**
A 0.50 M AU-DESSUS DU SOL

Remarques : **Inexploitable par GPS**

Le repère est au centre de la photo

Carte : 3436 SAINT-CHRISTOPHE-EN-OISANS

Avertissement

Compte-tenu des risques de déplacement des repères, il est indispensable de rattacher vos opérations de nivellement à plusieurs repères proches, ceci afin de contrôler leur stabilité.
La responsabilité de l'IGN ne saurait être engagée en l'absence d'un tel contrôle. En savoir plus sur les mouvements verticaux.
Toute remarque concernant la destruction, la disparition ou le mauvais état des repères doit être signalée au Service de la Géodésie et du Nivellement : sgn@ign.fr

IGN/SGN *06/02/2015* *Page 1/1*

IGN *Nivellement Général de la France*

Repère de nivellement

Matricule : **X'.C.R3 - 147**

Système d'altitude : NGF-IGN 1969

1 874,614 m

ALTITUDE NORMALE

Année de dernière détermination : 1982

Repère vu en place en 2002

Type : **M REPERE CYLINDRIQUE DU NIVELLEMENT GENERAL**

Complément :

Système : RGF93 - Ellipsoïde : IAG GRS 1980 - Méridien origine : GREENWICH

Longitude (dms) : **6° 24' 57" E** *Latitude (dms) :* **44° 55' 04" N**

Système : RGF93 - Projection : LAMBERT-93

E (km) : **969.47** *N (km) :* **6430.11**

Département : **HAUTES-ALPES** *Numéro INSEE :* **05101** *Commune :* **PELVOUX**

Voie suivie : **CHEMIN**

de : **PRE DE MADAME CARLE** *à :* **LE REFUGE DU GLACIER BLANC**

Coté : **Gauche** *PK :* **-** *Distance :* **0,01** *km du repère* **X'.C.R3 - 146**

Localisation : **AU LIEU-DIT "PRE DE MADAME CARLE"**

Support : **REFUGE "CEZANNE" DU CLUB ALPIN FRANCAIS**

Partie support : **MUR DE FACADE LATERAL SUD-EST**

Repèrements : **A 0.48 M DE L'EXTREMITE NORD-EST**
A 0.43 M AU-DESSUS DU SOL

Remarques : **Inexploitable par GPS**

Le repère est au centre de la photo

Carte : 3436 SAINT-CHRISTOPHE-EN-OISANS

Avertissement

Compte-tenu des risques de déplacement des repères, il est indispensable de rattacher vos opérations de nivellement à plusieurs repères proches, ceci afin de contrôler leur stabilité.
La responsabilité de l'IGN ne saurait être engagée en l'absence d'un tel contrôle. En savoir plus sur les mouvements verticaux.
Toute remarque concernant la destruction, la disparition ou le mauvais état des repères doit être signalée au Service de la Géodésie et du Nivellement : sgn@ign.fr

IGN/SGN *06/02/2015* *Page 1/1*

CH4 - Figure S2: Official IGN description of elevation benchmarks present in Pré de Madame Carle. *Downloaded on 06/02/2015 from http://geodesie.ign.fr/fiches/.*

Nunataks and thinning

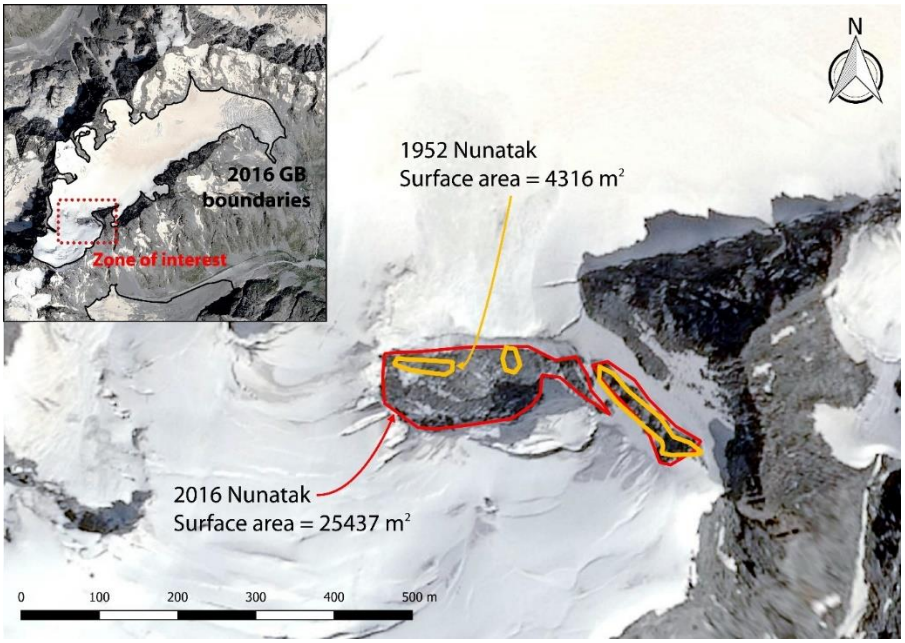

CH4 - Figure S3: Difference in nunataks at high elevation on Glacier Blanc. *These nunataks are located in the accumulation area of GB.*

Weather station location

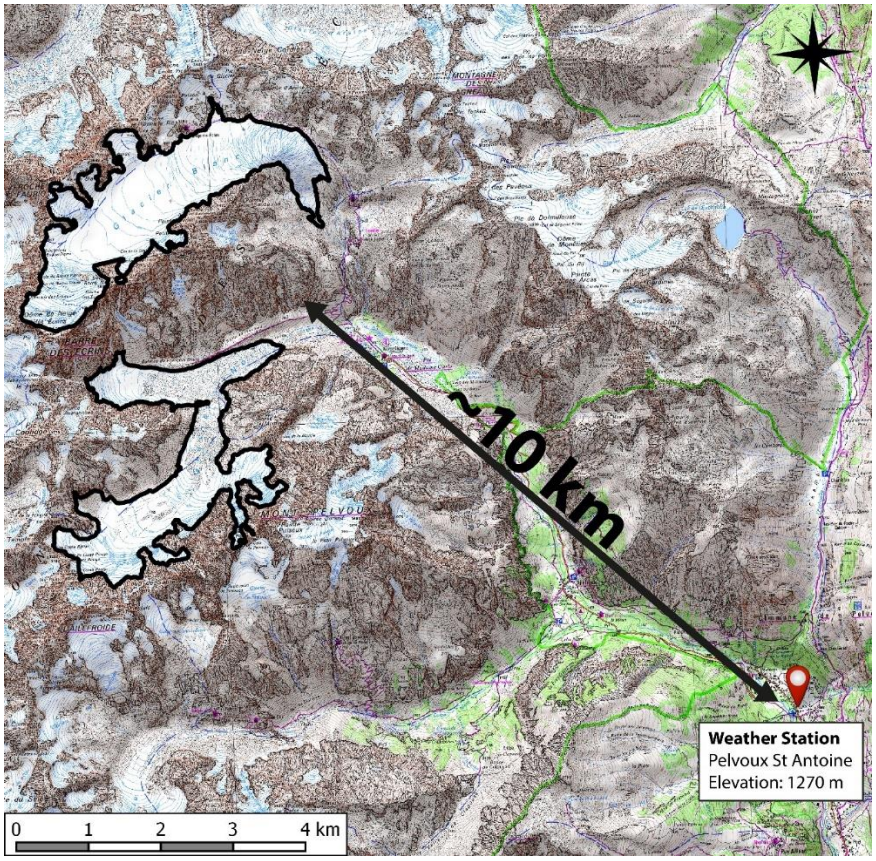

CH4 - Figure S4: Location of the Pelvoux weather station.

Hypsometry of Glacier Noir and Glacier Blanc

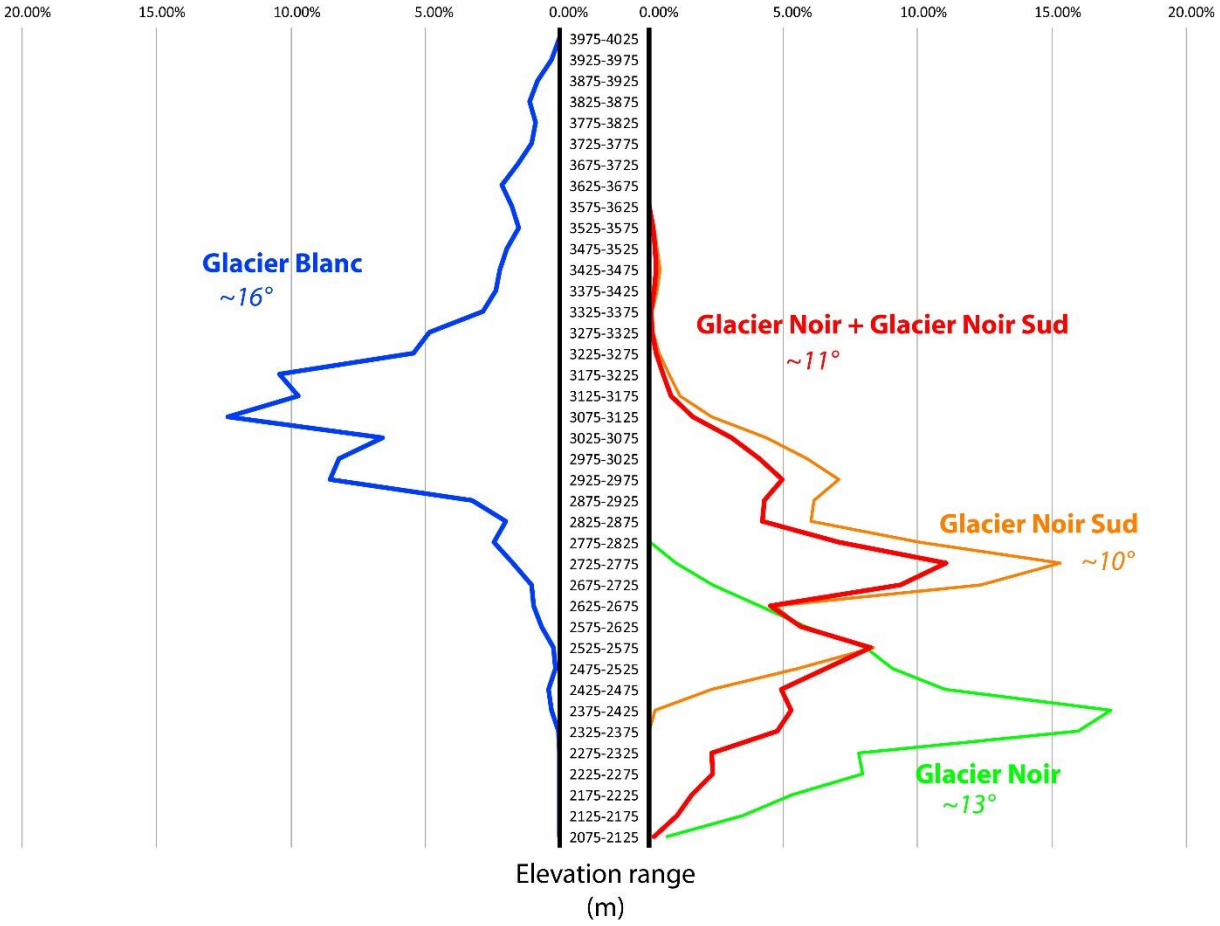

CH4 - Figure S5: Hypsometry and slope of Glacier Noir, Glacier Noir Sud and Glacier Blanc in 2013. *Glacier Noir + Glacier Noir Sud present an elevation distribution a little more "rectangular" than Glacier Blanc.*

CHAPTER 5: At the European Alps scale

Impact of debris cover on glacier runoff and future water resources in the European Alps

Submitted to Nature Geoscience on 25th November 2016.

Resubmitted on 7th July 2017. Rejected on 31st October 2017.

Currently in revision (June 2018).

Lardeux, P., Glasser, N.F., Holt, T, Hubbard, B.

In the Himalayas, some debris-covered glaciers are known to be the main source of fresh water for human usage for entire valleys, making that type of glacier a major component of the hydrological cycle of these areas. In the European Alps, the present and future contributions of debris-covered glaciers to water supplies remain unknown due to the lack of inventorial data. Debris-covered glaciers behave differently to clean-ice glaciers as the insulation effect of the debris layer on the glacier surface strongly influences their response to climate change. In this study, we show that debris-covered glaciers represent 59% of Alpine ice volume, strongly influencing the Alpine water supply upon which more than 145 million people rely. Debris-covered glaciers will provide around 25% of the glacial runoff originating from the Alps by the middle of the 21st century and this, combined with a slower release of the glacial meltwater, will prolong the Alpine water supply in the face of climate change.

Five watersheds originate from the European Alps: the Danube, Rhine, Rhone, Po and Adige. These watersheds extend across 1.1x10^6 km^2, representing 11% of the European landmass[1]; they intersect 23 countries and accommodate 30% of Europe's population[2]. The largest four watersheds (Danube, Rhine, Rhone and Po) account for 95% of the total discharge of the five watersheds. A substantial proportion of this water originates from approximately 3500 glaciers located in the Alps[3,4]. Worldwide, it is difficult to evaluate how glacial hydrology will be influenced by climate change as most glacierized mountain ranges, including the Alps, currently lack comprehensive glacier classifications. To our knowledge, debris-covered glaciers are only explicitly included as a glacier type in inventories for the Andes[5], South America, the Torngat Mountains[6], Canada, the Caucasus Mountains[7] and the Buthan Himalaya[8]. The influence of the likely recession and possible disappearance of debris-covered glaciers is particularly unclear. Beyond a certain thickness of supraglacial rock debris, the melting rate significantly decreases[9]. In addition to this slowdown in melting, the greater roughness and lower albedo of the glacier surface introduce important effects on the dynamics and mass balance of this type of glacier and mass loss becomes dominated by surface lowering rather than frontal recession. The dynamic and geometrical response of debris-covered glaciers to anticipated climate change remains uncertain. However, it is highly likely that the number of debris-covered glaciers will increase as climate change renders

mountain slopes increasingly unstable[10], favouring debris deposition on adjacent glacier surfaces via rockfalls and avalanches.

At the same time as they are increasing in number, debris-covered glaciers have a marked impact on water supplies globally, including in the Andes and Himalayas[11]. In the Himalayas, it is estimated that debris-covered glaciers represent more than 20% of the total number of glaciers[12,13] and thus are a major water source for the region's population.

Debris-covered glaciers are a major component of the European Alpine cryosphere

Using the Randolph Glacier Inventory[4], we identified 3530 glaciers located in the European Alps, covering approximately 2070 km^2 with a total volume of around 100 km^3 (supplementary section 1). This ice coverage makes the Alps the most glacierised mountain range in Europe. The Rhone watershed contains 32% (n = 1133) of the total number of Alpine glaciers and the Danube, Rhine and Po have respectively 22% (n = 780), 20% (n = 705) and 19% (n = 676). The Adige watershed has less than 7% (n = 236) of the total number of glaciers. As the third largest Alpine watershed[1], the Rhone is the most glacierized (0.9% of the surface area of the watershed is glacier-covered), accounting for 43% (892 km^2) of the Alpine glacier surface area and 46-54% (46-61 km^3) of its ice volume (see Methods). This basin is therefore highly likely to be the most sensitive to changes in glacial meltwater delivery. The Danube, Rhine and Po retain 21% (423 km^2), 16% (334 km^2) and 15% (313 km^2) of the glacier surface area respectively, with 16-19% (18-19 km^3), 14-17% (16-17 km^3) and 12-14% (14 km^3) of the ice volume. Although the smallest of the Alpine watersheds, the Adige watershed is the second most glacierized (0.7%); however, it only retains 5% (104 km^2) of the total Alpine glacial surface area and 3-4% (4 km^3) of its ice volume. In summary, individual watersheds show very different glacial characteristics, and the Rhone watershed is the most significant to the Alpine cryosphere. It contains more glaciers, more ice surface, and more ice volume than any other.

We classified each glacier into one of four categories (supplementary section 3). These categories are based on the established definition of debris-covered glaciers[14], which states that a debris-covered glacier is a "glacier where part of the ablation zone has a continuous cover of supraglacial debris across its full width". However, some glaciers have a substantial debris layer that nevertheless does not cover the full width of the glacier: herein we refer to

these glaciers as 'debris-influenced'. These two categories (debris-covered and debris-influenced) constitute the 'debris-type' glacier class. In some cases, the imagery used to conduct the classification (see Methods) does not allow a clear determination (e.g. due to snow coverage, low resolution or heavily shaded/clouded areas). Glaciers in this case were categorized as 'undetermined-type' glaciers. All other glaciers were considered to belong to the 'clean-ice' glacier category, although they likely have some small proportion of their surface covered by light debris. The distribution of glaciers by category is represented in Figure 1.

This classification is sometimes difficult to strictly apply, and one example of a borderline case is Grosser Aletschgletscher situated in the Rhone watershed, which alone represents 4% (82 km^2) of the total glacier surface area and 3-11% (3-13 km^3) of the Alpine ice volume. Grosser Aletschgletscher fits the definition of a debris-covered glacier (see below). However, due to its large proportions, small debris coverage (~5%) and general behaviour, it is often recognised as a clean-ice glacier (e.g. in Jouvet et al. (2011)[15]). The proportions of Grosser Aletschgletscher should be kept in mind during the analysis of the inventory statistics (supplementary section 2).

Debris-type glaciers are spread across the Alps (supplementary section 4) and individually tend to present a larger surface area than clean-ice glaciers. As a first approach to study the impact of debris-type glaciers, we examined the volume of ice per watershed per glacier type (Figure 1b). Across the entire Alps, debris-type glaciers represent 50-59% of the ice volume (see Methods) and clean-ice glaciers represent 37-46%. Of the five Alpine watersheds, the Rhone watershed has the largest volume of ice (45.78-61.35 km^3) and shows the highest proportion by volume of debris-type glaciers (55-69%), while the Po watershed (with 13.71-14.13 km^3 of ice in debris-covered glaciers) displays the lowest proportion by volume (37-39%).

As a second approach, we considered only the volume of ice under a layer of debris (supplementary section 1b). Over the entire Alps, the debris layer covers 6% of the total glacial surface (each debris-type glacier is covered on average across 32% of its surface area, with a range of 0.6-97%). The ice under the debris layer represents 6% of the total Alpine ice volume, which is 12% of the debris-type ice volume and, therefore, is highly likely to represent an important factor in the response of these glaciers to mass balance change. The Rhine watershed has the largest proportion of ice volume (10%) directly covered by debris in the

Alps. The Rhone and Rhine watersheds are therefore likely to be those showing the largest amplitude in change in response to any variation in the area of supraglacial debris.

The two other indicators of the sensitivity of a watershed to the proportion of debris-covered glaciers within it are the equilibrium-line altitude (ELA) and hypsometry of each type of glacier (Figure 1c). Debris-type glaciers extend to lower elevations due to the insulation effect, and their ELA is correspondingly lower (supplementary section 5). The hypsometry shows, in contrast, an unusual behaviour. Instead of displaying a 'bulge (large proportion of surface area) at lower altitude, the hypsometry of debris-type glaciers is 'flattened', with a more equal distribution of surface area at every elevation. This phenomenon is particularly visible in the Po watershed, where debris-covered glaciers (red line) have 2-4% of their area distributed at each elevation range between 2500 m a.s.l. and 4000 m a.s.l.

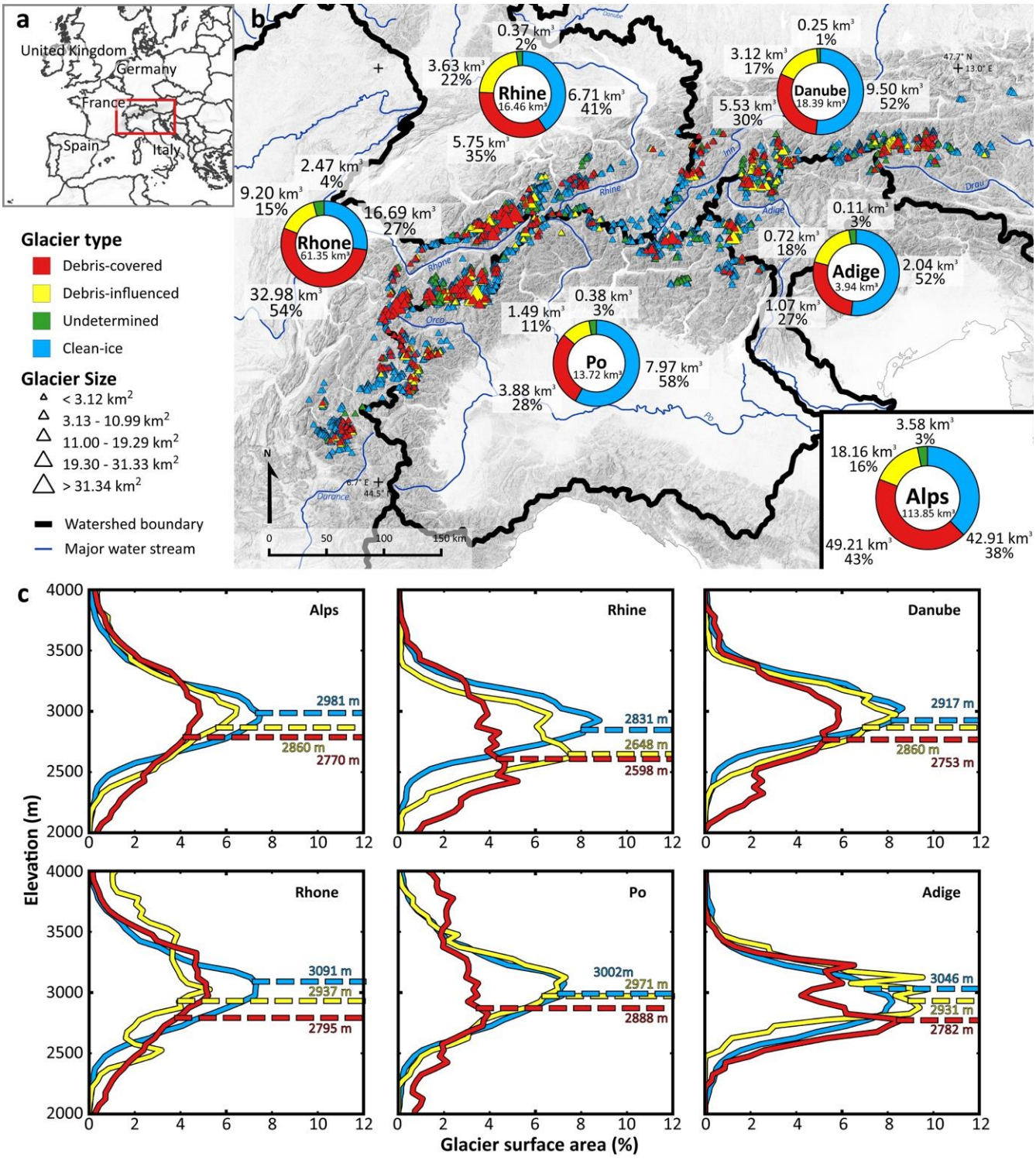

CH5 - Figure 1| Distribution of the different types of glaciers in the European Alps. *a, Map showing the location of the Alps in Europe. b, Location map of the glaciers by category (colour) and by surface area (triangle size). Each pie represents the volume of ice in cubic kilometres produced by the "Volume/Area scaling" method (km³, top number) in each watershed and their percentage (bottom number) within this watershed. The bottom right pie represents the total volume of ice for the Alps. Detailed numbers are given in supplementary section 1. The background is the ASTER GDEM-SRTM hillshaded. c, Hypsometry curve for each category of glacier (colour-coded the same as the map) by watershed. Undetermined glaciers are not included here for readability. The dashed lines represent the altitude of the equilibrium line (ELA) for clean-ice, debris-covered and debris-influenced glaciers.*

Contribution of debris-covered glaciers to European Alpine water supply

We next evaluated the contribution of debris-type glaciers to total Alpine runoff. All glacial meltwater from a debris-type glacier is potentially influenced by the debris layer on the top of the ice; debris creates spatial variation in snowmelt due to rough surfaces, blocks preferential runoff routes with boulders and it reduces ice melt rate as a result of insulation. Of these, the insulation effect is the most critical because surface ablation is proportional to the surface area of the debris layer[16].

Using a simple mathematical model of melt for the different types of glaciers to calculate their runoff (see Methods) and combined with published data from Huss (2011)[17], we evaluated the extent to which debris influences the total supraglacial meltwater production of debris-type glaciers in the Alps for the period 1908-2008, for the month of August (end of the ablation season). The Huss data are the contributions of all glaciers' runoff to the major Alpine river discharge calculated using a distributed glacier model, which was adjusted to fit the volume changes of 50 Swiss glaciers and then scaled-up to the European Alps.

The Huss dataset covers only four out the five Alpine watersheds (Danube, Rhine, Rhone and Po) excluding the Adige watershed. These four watersheds represent 95% of the Alpine runoff. At the time of the study, it was not possible for us to access data and calculations concerning glacier contribution to Adige runoff.

Given the dominance of surface melting at alpine glaciers relative to en- and sub- glacial melting, herein we focus exclusively on surface melting. In Huss (2011)[17], the global storage change in August is always negative, corresponding to a mass loss and thus is equivalent to glacial runoff. For the considered 'bare ice' component, this is equivalent to supraglacial melt.

The debris layer, by changing the albedo and the roughness of the surface of the glacier, changes the snowmelt pattern depending on local conditions, for example, enhancing snowmelt due to lower albedo of the surrounding areas, or decreasing the snowmelt due to shading. Additionally, the debris layer disturbs the hydrology of debris-type glaciers[16] by modifying meltwater pathways and consequently the transit time of meltwater in the glacier. These small-scale phenomena are not specifically considered and evaluated in the Huss model. As such, the global storage change does not represent the best proxy to measure the

debris-type glacier output. However, the Huss model calculated the fraction of global storage change accounted for by 'bare ice', i.e. storage change coming from the ice only (whether covered by debris or not). In our study, we only considered this 'bare ice' fraction, which corresponds to the supraglacial melt only.

In the Alps, in August, for the 1908-2008 period, the supraglacial melt runoff from debris-type glaciers represents 1.1% of total runoff (Figure 2a), compared to the 3.5% contribution of all glaciers (supplementary section 1c). Considering total glacial runoff, the supraglacial melt of debris-type glaciers contributes 13.6% (Figure 2b), which corresponds to almost a third of the total supraglacial runoff (Figure 2c). Concerning the different watersheds, the contribution of the supraglacial melt of debris-type glaciers to their respective total runoff varies from 4.8% for the Rhone to 0.2% for the Danube. These percentages are linearly proportional (R^2=0.99) to the glacierization of each watershed. Regarding the contribution to total glacial runoff, the Rhone watershed retains the highest percentage (19.3%) and the Danube has the lowest (8.8%). All these values demonstrate that supraglacial melt of debris-type glaciers is a major component of the glacial runoff. It is also important to the total runoff, though to a smaller extent.

Focusing on total supraglacial runoff, the melt contribution from debris-type glaciers rises from 24.2% for the Po to 35.5% for the Rhone. These values of around 25% or greater demonstrate that, in all watersheds, supraglacial debris layer variations will likely have major impacts on the supraglacial components of the glacial runoff.

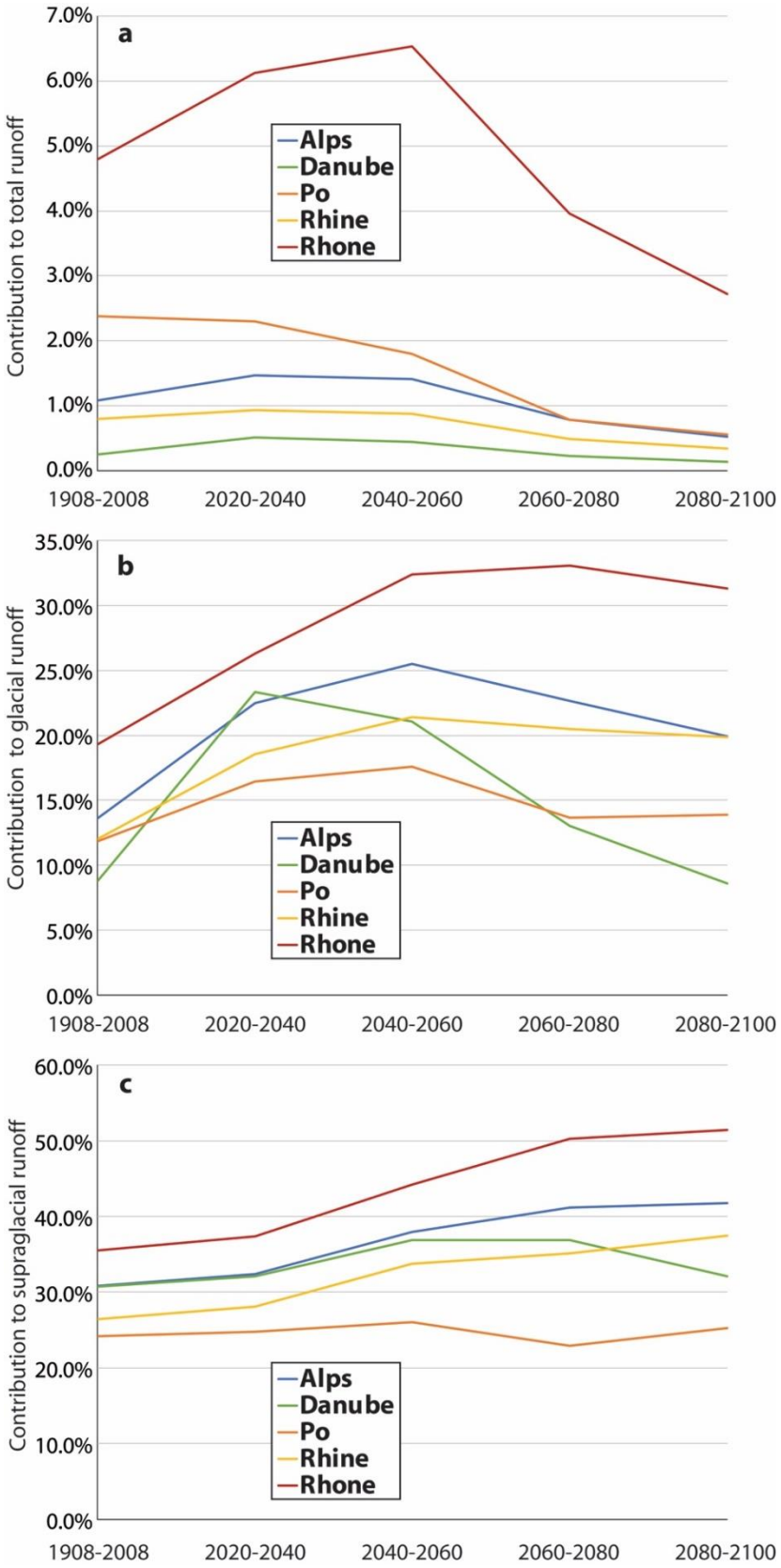

CH5 - Figure 2| Contribution of supraglacial melt from debris-type glaciers to the August Alpine runoff. *a, Contribution of supraglacial melt from debris-type glaciers to the total runoff. It includes the current period (1908-2008) and the forecast contributions for the 2020-2100 period per 20 year sub-periods. b, Contribution of supraglacial melt from debris-type glaciers to total glacial runoff. c, Contribution of supraglacial melt from debris-type glaciers to total supraglacial runoff.*

Future water supply in the European Alps

Large uncertainties remain concerning the impact of climate change on the water supply provided by glacierized watersheds[18]. A first approximation of this impact was modelled by Huss (2011)[16] for the four main Alpine watersheds, which we extend over the entire Alps (Figure 2a). The forecast contributions of glaciers to total runoff in the Alps are based on the median climate scenario (+4.2°C between 1990-2100 and -7% in precipitation for the same period) of the PRUDENCE project[19], and there was assumed to be no change in the discharge of the four rivers compared to 2008. Between 2008 and 2100, the "all" glacier total contribution to total runoff in the Alps is projected to decrease from 8% to less than 3% (supplementary section 1c). During the same period, the contribution of supraglacial melt to total runoff follows a convex curve from 3.5% to 1.3%, peaking at 4.4% in 2020-2040. Every Alpine watershed follows a similar pattern and shows proportionally similar decreases.

The Danube and the Rhine watersheds experience an increase of the contribution of debris-type supraglacial melt to their respective total runoff until the 2020-2040 period, then a decrease to levels lower than 2008. The increase lasts until the 2040-2060 period for the Rhone, while the Po experiences a continued decreased from 2008 to 2080-2100. These different trends combined for the Alps give a slight increase for 2020-2040 and then a decrease until the end of the century. By that time, all contributions have been halved compared to 2008. Translating these trends to the total glacial runoff (Figure 2b) results in different responses depending on the watershed: continuous decrease (23.3 to 8.6%) for the Danube, relative stability for the Po and increase for the Rhine (by almost 100%) and the Rhone (by 50%). These differences between watersheds reflect feedback to which debris-type glaciers are subject.

Detailed analysis of the Alpine supraglacial runoff forecast to 2100 reveals a shift in the origin of the meltwater from clean-ice to debris-covered glaciers (Figure 2c). The predicted contribution of supraglacial melt from debris-type glaciers to total supraglacial runoff increases for the Alps (from 30.9% in 2020 to 41.8% in 2100). This contribution increases also overall for the Rhone (from 37.4 to 51.4%) and the Rhine (from 28.1 to 37.5%). The Po and the Danube show relative stability with a contribution around 25% and 30%. These two different trends partially reflect how supraglacial melt is affected by the interaction of two phenomena: the variation of surface area subject to ablation (modifying the quantity of

meltwater that can be produced by a glacier) and variation in the surface area covered by debris (modifying the melt rate of a glacier surface). The amplitude and timing of these two phenomena are local and specific to each glacier. Additionally, ablation area variations reflect both terminus change (i.e. retreat or advance) and ELA change. At the same time, the area of ice under surface debris will increase or remain constant. All these interactions and movements lead to complex trends in the contribution of debris-type supraglacial melt to total supraglacial runoff.

Independently of the precise trajectory followed by each watershed, the source of the supraglacial meltwater shows a clear long-term trend for all basins. By 2100, a quarter to a half of the supraglacial runoff will come from debris-type glaciers depending on the watershed.

Debris-type glaciers and future water supply in the European Alps

Although the forecast contribution of glaciers in the Alps to total supraglacial runoff presents large uncertainties – namely the choice of the Huss median climate change scenario and the assumption of no discharge variation[17], and our simple parametrization of the icemelt rate under a debris layer (supplementary section 6) – this work demonstrates the importance of debris-covered and debris-influenced glaciers to the Alpine water supply. Debris-type glaciers' distinct behaviour will temper the rapid disappearance of the clean-ice glaciers in the Alps by releasing a lower but also less variable flux of meltwater until – assuming these trends continue – they become the main source of glacial meltwater around 2120 (supplementary section 1c).

Debris-covered glaciers currently represent approximately half of the total ice volume in the Alps. We show here that the contribution of these debris-type glaciers to supraglacial runoff will increase during the 21st century, as debris cover increases with climate change. Thus, in the face of climate change, debris-covered glaciers will extend the lifespan of the water supply in the European Alps.

Methods

This study required two different stages: first, the classification and measurement of all glaciers in the European Alps, and second, the modelling of the contribution of the different glacier types to runoff.

Following the definitions of our categories (see main text), the Randolph Glacier Inventory (RGI)[20] version 5.0 was overlaid on Google Earth imagery[21]. After sorting the RGI dataset (see supplementary section 3), each glacier was visually checked and categorized. The presence of supraglacial debris perturbed the RGI outlines determination[4], and consequently, the sizes of debris-covered and debris-influenced glaciers are often underestimated. To compensate, we re-digitized the debris-type glaciers where this underestimation occurred. Additionally, we digitized the debris layer of each debris-type glacier which made it possible to calculate the volume of ice under debris.

The volume of ice was calculated via two methods to obtain an upper and lower estimation (yielding the range in volume specified in the main text). We first used the volume/area scaling method[22] for each group of glaciers (combination of type and watershed) with equation (1):

$$(1)\quad V_{group} = \sum c \times {A_g}^{\gamma}$$

$$\begin{cases} c = 0.03 \\ \gamma = 1.375 \end{cases}$$

where V_{group} is the volume of ice (m^3) in a group of glaciers, A_g is the surface area of one glacier (m^2) in that group.

The value for *c* is the most accepted in the literature[23] and the value of *γ* is fixed by the theory (see supplementary section 7). This method is known to overestimate the glacier volume; it is therefore our upper boundary for the volume. We then used the ice thickness data of Huss & Farinotti (2012)[24]. The spatial integration of this updated dataset yielded the lower boundary for the ice volume as it does not include our re-digitized outline for debris-type glaciers. This ice thickness dataset gave us the lower boundary for the volume of ice present under a debris layer.

The hypsometry of clean-ice and undetermined glaciers is that provided with the RGI. For the debris-type glaciers and their new outline, we used the same Shuttle Radar Topography Mission (SRTM) digital elevation model (DEM)[25] as the RGI.

The ELA of each glacier was calculated as the mean of two methods: the area × altitude (AA) method[26] and the accumulation area ratio (AAR) method[27]. These two methods were combined for simplicity, reproducibility, and to balance the advantages of both. Additionally,

given the large number of glaciers but little data on each, it was necessary to keep the overall method reasonable in terms of processing time. The AA method offers a reliable ELA estimation for various glacier shapes and sizes, not only the standard Alpine valley glacier. However it relies largely on an accurate determination of the hypsometry, which unfortunately presents some uncertainties (DEM and glacier outline accuracy). In an attempt to reduce the uncertainty linked to the AA method, we decided to combine its results with those obtained by the AAR method. To apply a realistic ratio for each glacier in the Alps, and not the 'generic' ratio established in 1982 for the Colorado Front Range glaciers[28], we established a relationship between the glacier surface area and the accumulation area ratio (independently calculated in Kern & Laszlo, 2010)[27] (see supplementary section 8).

The second process was the calculation of the contribution of debris-type glaciers to total Alpine runoff. To do this, we used the following assumptions:

- Any debris cover is entirely in the glacier ablation area.
- All glaciers are located in the European Alps, hence melting during the summer.
- Calculations are valid for the end of the melt season in August. We therefore considered that the melting is restricted to the ablation area, which is considered snow-free.
- Meltwater is produced solely by supraglacial melt, whether the surface is debris covered or not.
- The melt rate beneath debris is set to be 50% of the melting outside the debris cover for the entire debris layer. Thus, the melting rate under debris remains independent from the actual thickness of the debris layer, which controls the strength of the insulation effect. As such, the melt rate under the debris value has to be a compromise between a debris layer preventing any melt (0%) and a debris layer with no insulation effect (100%) or even increasing the melt (>100%). It is currently impossible to calculate a mean melt rate under the debris for one entire glacier without debris thickness assessment, and consequently it is not possible to calculate one for an entire mountain range.

The calculation is based on two datasets: percentage of supraglacial meltwater in the four main watersheds of the Alps, following Huss (2011)[17], and the runoff volume from each watershed from the Global Runoff Data Centre[3]. The calculation relies on the following parametrisation (equations (2), (3) and (4)) of the total volume of runoff:

$$(2)\quad Q = \frac{m_{CIG} \times A_{CIG} + m_{CIG} \times (1-\alpha) \times A_{DG} + m_{DG} \times \alpha \times A_{DG}}{c} \times d_{ice}$$

$$(3)\quad m_{DG} = \beta \times m_{CIG}$$

$$(4)\quad d_{ice} = \frac{\rho_{ice}}{\rho_{water}}$$

where Q is the total volume of runoff for a watershed (m^3 of water), m_{CIG} is the equivalent thickness of ice melted on clean-ice glaciers (m) to accommodate the global storage change, A_{CIG} is the area of the ablation zone of clean-ice glaciers (m^2), α is the percentage of the ablation zone covered with debris for debris-type glaciers, A_{DG} is the area of the ablation zone of debris-type glaciers (m^2), c is the contribution of glacier to the total runoff for a watershed (%), ρ_{ice} is the density of ice (910 kg m^{-3}), ρ_{water} is the density of water (1000 kg m^{-3}), m_{DG} is the equivalent thickness of ice melted under the debris layer for debris-type glaciers (m) to accommodate the global storage change, β is the parameter representing how much less melt is happening under the debris layer (%).

To make this parametrisation valid, we assumed that the 'bare ice' component of the global storage change of a glacier, as defined by Huss (2011)[17], can be translated into a thickness of ice melted in the ablation area of that same glacier. The results obtained for alternative melt rates are presented in supplementary section 6. By inverting equation (2), we obtained the volume of water contributed by debris-type glaciers to the total runoff for each watershed.

Using the same parametrisation and the following assumptions, we calculated the forecasted contributions:

- The total runoff stays the same than as the period 1908-2008
- The size of each glacier follows the curve in Figure 7 of Huss (2011)[17] depending on their size classes. The glacier's type is not taken into account for the calculation of size variation.
- The surface area of debris is constant, except if the size of the ablation area becomes smaller than the size of the debris layer, in which case their sizes become the same, generating a completely debris-covered ablation area.

Regarding Grosser Aletschgletscher's runoff, we used an iterative process, alternatively excluding and including its parameters in equation (2) and (3), to calculate its contribution. During the 1908-2008 period, Grosser Aletschgletscher's surface area was equivalent to that of all undetermined-type glaciers combined. For the future periods, the undetermined-type glacier surface area becomes smaller than Grosser Aletschgletscher, as smaller glaciers shrink faster than larger ones. Taking into account the previous assumptions, the available data, and that undetermined-type glaciers are present across the entire Alps, we were not able to estimate an uncertainty range for the runoff contribution values.

References

1 Lehner, B., Verdin, K. & Jarvis, A. New global hydrography derived from spaceborne elevation data. *Eos* **89**, 93-95, doi:10.1029/eost2008EO10 (2008).

2 Eurostat. Population Census. (2011). Available online at http://ec.europa.eu/eurostat/web/gisco/geodata/reference-data . Accessed 18/08/2016.

3 GRDC. Long-Term Mean Monthly Discharges and Annual Characteristics of GRDC Stations. (2015).

4 Pfeffer, W. T. *et al.* The Randolph Glacier Inventory: a globally complete inventory of glaciers. *Journal of Glaciology* **60**, 537-552, doi:10.3189/2014JoG13J176 (2014).

5 Janke, J. R., Bellisario, A. C. & Ferrando, F. A. Classification of debris-covered glaciers and rock glaciers in the Andes of central Chile. *Geomorphology* **241**, 98-121, doi:10.1016/j.geomorph.2015.03.034 (2015).

6 Way, R. G., Bell, T. & Barrand, N. E. An inventory and topographic analysis of glaciers in the Torngat Mountains, northern Labrador, Canada. *Journal of Glaciology* **60**, 945-956, doi:10.3189/2014JoG13J195 (2014).

7 Tielidze, L. G. & Wheate, R. D. The Greater Caucasus Glacier Inventory (Russia/Georgia/Azerbaijan). *The Cryosphere Discussions*, 1-27, doi:10.5194/tc-2017-48 (2017).

8 Nagai, H., Fujita, K., Sakai, A., Nuimura, T. & Tadono, T. Comparison of multiple glacier inventories with a new inventory derived from high-resolution ALOS imagery in the Bhutan Himalaya. *The Cryosphere* **10**, 65-85, doi:10.5194/tc-10-65-2016 (2016).

9 Reznichenko, N., Davies, T., Shulmeister, J. & McSaveney, M. Effects of debris on ice-surface melting rates: an experimental study. *Journal of Glaciology* **56**, 384-394, doi:10.3189/002214310792447725 (2010).

10 Nagai, H., Fujita, K., Nuimura, T. & Sakai, A. Southwest-facing slopes control the formation of debris-covered glaciers in the Bhutan Himalaya. *The Cryosphere* **7**, 1303-1314, doi:10.5194/tc-7-1303-2013 (2013).

11 Pritchard, H. D. Asia's glaciers are a regionally important buffer against drought. *Nature* **545**, 169-174, doi:10.1038/nature22062 (2017).

12 Immerzeel, W. W., Pellicciotti, F. & Bierkens, M. F. P. Rising river flows throughout the twenty-first century in two Himalayan glacierized watersheds. *Nature Geoscience* **6**, 742-745, doi:10.1038/ngeo1896 (2013).

13 Scherler, D., Bookhagen, B. & Strecker, M. R. Spatially variable response of Himalayan glaciers to climate change affected by debris cover. *Nature Geoscience* **4**, 156-159, doi:10.1038/ngeo1068 (2011).

14 Singh, V. P., Singh, P. & Haritashya, U. K. *Encyclopedia of snow, ice and glaciers*. (Springer, 2011).

15 Jouvet, G., Huss, M., Funk, M. & Blatter, H. Modelling the retreat of Grosser Aletschgletscher, Switzerland, in a changing climate. Journal of Glaciology 57, 1033-1045, doi:10.3189/002214311798843359 (2017).

16 Fyffe, C. L. *The hydrology of debris-covered glaciers* PhD thesis, University of Dundee, (2012).

17 Huss, M. Present and future contribution of glacier storage change to runoff from macroscale drainage basins in Europe. *Water Resources Research* **47**, 14, doi:10.1029/2010wr010299 (2011).

18 Huss, M., Zemp, M., Joerg, P. C. & Salzmann, N. High uncertainty in 21st century runoff projections from glacierized basins. *Journal of Hydrology* **510**, 35-48, doi:10.1016/j.jhydrol.2013.12.017 (2014).

19 Christensen, J. H. & Christensen, O. B. A summary of the PRUDENCE model projections of changes in European climate by the end of this century. *Climatic Change* **81**, 7-30, doi:10.1007/s10584-006-9210-7 (2007).

20 Arendt, A. *et al.* Randolph Glacier Inventory – A Dataset of Global Glacier Outlines: Version 5.0. (2015).

21 ©Google. Google Earth Imagery. Software available online at https://www.google.com/earth/ . Data accessed 07/09/2015 – 15/09/2015.

22 Bahr, D. B., Meier, M. F. & Peckham, S. D. The physical basis of glacier volume-area scaling. *Journal of Geophysical Research: Solid Earth* **102**, 20355-20362, doi:10.1029/97jb01696 (1997).

23 Bahr, D. B., Pfeffer, W. T. & Kaser, G. A review of volume-area scaling of glaciers. *Reviews of Geophysics* **53**, 95-140, doi:Doi 10.1002/2014rg000470 (2015).

24 Huss, M. & Farinotti, D. Distributed ice thickness and volume of all glaciers around the globe. *Journal of Geophysical Research: Earth Surface* **117**, n/a-n/a, doi:10.1029/2012jf002523 (2012).

25 Frey, H. & Paul, F. On the suitability of the SRTM DEM and ASTER GDEM for the compilation of topographic parameters in glacier inventories. *International Journal of Applied Earth Observation and Geoinformation* **18**, 480-490, doi:10.1016/j.jag.2011.09.020 (2012).

26 Osmaston, H. Estimates of glacier equilibrium line altitudes by the Area×Altitude, the Area×Altitude Balance Ratio and the Area×Altitude Balance Index methods and their validation. *Quaternary International* **138-139**, 22-31, doi:10.1016/j.quaint.2005.02.004 (2005).

27 Kern, Z. & László, P. Size specific steady-state accumulation-area ratio: an improvement for equilibrium-line estimation of small palaeoglaciers. *Quaternary Science Reviews* **29**, 2781-2787, doi:10.1016/j.quascirev.2010.06.033 (2010).

28 Meierding, T. C. Late Pleistocene Glacial Equilibrium-Line Altitudes in the Colorado Front Range - a Comparison of Methods. *Quaternary Research* **18**, 289-310, doi:Doi 10.1016/0033-5894(82)90076-X (1982).

Supplementary material for Impact of debris cover on glacier runoff and future water resources in the European Alps

Detailed Statistics

Statistics per basin

***CH5 - Table S1.1 | Number of glaciers**. CIG = Clean-ice glacier, DCG = Debris-covered glacier, DIG = Debris-influenced glacier.*

	CIG	DCG	DIG	Undetermined	Total
Adige	191	20	6	19	236
Danube	607	68	46	59	780
Po	544	57	26	49	676
Rhine	607	49	26	23	705
Rhone	964	91	28	50	1133
Total	2913	285	132	200	3530

***CH5 - Table S1.2 | Percentage per category of number of glaciers**. 0.1% corresponds to 0.1-3.5 glaciers depending the type of glacier.*

	CIG	DCG	DIG	Undetermined	Total
Adige	6.6%	7.0%	4.5%	9.5%	6.7%
Danube	20.8%	23.9%	34.8%	29.5%	22.1%
Po	18.7%	20.1%	19.7%	24.5%	19.2%
Rhine	20.8%	17.3%	19.7%	11.5%	20.0%
Rhone	33.1%	31.9%	21.2%	25.0%	32.1%
Total	100.0%	100.0%	100.0%	100.0%	100.0%

***CH5 - Table S1.3 | Percentage per basin of number of glaciers.** 0.1% corresponds to 0.2-3.5 glaciers depending the watershed.*

	CIG	DCG	DIG	Undetermined	Total
Adige	80.9%	8.5%	2.5%	8.1%	100.0%
Danube	77.8%	8.7%	5.9%	7.6%	100.0%
Po	80.5%	8.4%	3.8%	7.2%	100.0%
Rhine	86.1%	7.0%	3.7%	3.3%	100.0%
Rhone	85.1%	8.0%	2.5%	4.4%	100.0%
Total	82.5%	8.0%	3.7%	5.7%	100.0%

CH5 - Table S1.4 | Glaciers surface area in kilometre squared. *CIG = Clean-ice glacier, DCG = Debris-covered glacier, DIG = Debris-influenced glacier.*

km²	CIG	DCG	DIG	Undetermined	Total
Adige	64.28	22.87	13.07	3.85	104.07
Danube	244.60	96.06	72.01	10.35	423.02
Po	196.60	74.98	29.47	12.42	313.47
Rhine	183.23	85.51	56.05	9.52	334.31
Rhone	403.41	353.05	90.15	45.12	891.73
Total	1092.11	632.47	260.75	81.27	2066.60

CH5 - Table S1.5 | Percentage per category of glaciers surface area in kilometre squared. *0.1% corresponds to 0.1-2.0 km² (0.1-3.3 time the size of the average Alpine glacier) depending the type of glacier.***.**

	CIG	DCG	DIG	Undetermined	Total
Adige	5.9%	3.6%	5.0%	4.7%	5.0%
Danube	22.4%	15.2%	27.6%	12.7%	20.5%
Po	18.0%	11.9%	11.3%	15.3%	15.2%
Rhine	16.8%	13.5%	21.5%	11.7%	16.2%
Rhone	36.9%	55.8%	34.6%	55.5%	43.1%
Total	100.0%	100.0%	100.0%	100.0%	100.0%

CH5 - Table S1.6 | Percentage per basin of glaciers surface area in kilometre squared*. 0.1% corresponds to 0.2-2.2 km² (0.2-3.3 time the size of the average Alpine glacier) depending the watershed.*

	CIG	DCG	DIG	Undetermined	Total
Adige	61.8%	22.0%	12.6%	3.7%	100.0%
Danube	57.8%	22.7%	17.0%	2.4%	100.0%
Po	62.7%	23.9%	9.4%	4.0%	100.0%
Rhine	54.8%	25.6%	16.8%	2.8%	100.0%
Rhone	45.2%	39.6%	10.1%	5.1%	100.0%
Total	52.8%	30.6%	12.6%	3.9%	100.0%

CH5 - Table S1.7 | Glaciers volume in kilometre cubed, using Volume/Area scaling method*. CIG = Clean-ice glacier, DCG = Debris-covered glacier, DIG = Debris-influenced glacier.*

km^3	CIG	DCG	DIG	Undetermined	Total
Adige	2.043	1.066	0.722	0.107	3.939
Danube	9.496	5.526	3.122	0.250	18.395
Po	7.967	3.882	1.490	0.376	13.715
Rhine	6.713	5.748	3.627	0.373	16.460
Rhone	16.691	32.983	9.201	2.469	61.345
Total	42.910	49.205	18.162	3.576	113.853

CH5 - Table S1.8 | Percentage per category of glaciers volume in kilometre cubed, using Volume/Area scaling method. *0.1% corresponds to 0.0035-0.11 km^3 (0.1-3.4 time the volume of the average Alpine glacier) depending the type of glacier.*

	CIG	DCG	DIG	Undetermined	Total
Adige	4.8%	2.2%	4.0%	3.0%	3.5%
Danube	22.1%	11.2%	17.2%	7.0%	16.2%
Po	18.6%	7.9%	8.2%	10.5%	12.0%
Rhine	15.6%	11.7%	20.0%	10.4%	14.5%
Rhone	38.9%	67.0%	50.7%	69.0%	53.9%
Total	100.0%	100.0%	100.0%	100.0%	100.0%

CH5 - Table S1.9 | Percentage per basin of glaciers volume in kilometre cubed, using Volume/Area scaling method. *0.1% corresponds to 0.0039-0.11 km^3 (0.1-3.4 time the volume of the average Alpine glacier) depending the watershed.*

	CIG	DCG	DIG	Undetermined	Total
Adige	51.9%	27.1%	18.3%	2.7%	100.0%
Danube	51.6%	30.0%	17.0%	1.4%	100.0%
Po	58.1%	28.3%	10.9%	2.7%	100.0%
Rhine	40.8%	34.9%	22.0%	2.3%	100.0%
Rhone	27.2%	53.8%	15.0%	4.0%	100.0%
Total	37.7%	43.2%	16.0%	3.1%	100.0%

CH5 - Table S1.10 | Glaciers volume in kilometre cubed, using dataset from Huss & Farinotti (2012)[1]. *CIG = Clean-ice glacier, DCG = Debris-covered glacier, DIG = Debris-influenced glacier.*

km^3	CIG	DCG	DIG	Undetermined	Total
Adige	2.283	1.108	0.737	0.117	4.244
Danube	10.429	5.554	3.140	0.282	19.405
Po	8.531	3.870	1.304	0.432	14.137
Rhine	7.496	5.734	3.410	0.332	16.973
Rhone	17.539	22.096	3.137	3.010	45.781
Total	46.277	38.362	11.727	4.173	100.540

CH5 - Table S1.11 | Percentage per category of glaciers volume in kilometre cubed, using dataset from Huss & Farinotti (2012)[1]. *0.1% corresponds to 0.0042-0.1 km^3 (0.2-3.6 time the volume of the average Alpine glacier) depending the type of glacier.*

	CIG	DCG	DIG	Undetermined	Total
Adige	4.9%	2.9%	6.3%	2.8%	4.2%
Danube	22.5%	14.5%	26.8%	6.8%	19.3%
Po	18.4%	10.1%	11.1%	10.4%	14.1%
Rhine	16.2%	14.9%	29.1%	8.0%	16.9%
Rhone	37.9%	57.6%	26.7%	72.1%	45.5%
Total	100.0%	100.0%	100.0%	100.0%	100.0%

CH5 - Table S1.12 | Percentage per basin of glaciers volume in kilometre cubed, using dataset from Huss & Farinotti (2012)[1]. *0.1% corresponds to 0.0042-0.1 km^3 (0.2-3.6 time the volume of the average Alpine glacier) depending the watershed.*

	CIG	DCG	DIG	Undetermined	Total
Adige	53.8%	26.1%	17.4%	2.7%	100.0%
Danube	53.7%	28.6%	16.2%	1.5%	100.0%
Po	60.3%	27.4%	9.2%	3.1%	100.0%
Rhine	44.2%	33.8%	20.1%	2.0%	100.0%
Rhone	38.3%	48.3%	6.9%	6.6%	100.0%
Total	46.0%	38.2%	11.7%	4.2%	100.0%

CH5 - Table S1.13 | Average of glacier surface area in kilometre squared. *CIG = Clean-ice glacier, DCG = Debris-covered glacier, DIG = Debris-influenced glacier.*

km^2	CIG	DCG	DIG	Undetermined	Total
Adige	0.34	1.14	2.18	0.20	0.44
Danube	0.40	1.41	1.57	0.18	0.54
Po	0.36	1.32	1.13	0.25	0.46
Rhine	0.30	1.75	2.16	0.41	0.47
Rhone	0.42	3.88	3.22	0.90	0.79
Total	0.37	2.22	1.98	0.41	0.59

CH5 - Table S1.14 | Average of glacier volume (Volume/Area scaling method) in kilometre cubed.

km^3	CIG	DCG	DIG	Undetermined	Total
Adige	0.011	0.053	0.120	0.006	0.017
Danube	0.016	0.081	0.068	0.004	0.024
Po	0.015	0.068	0.057	0.008	0.020
Rhine	0.011	0.117	0.139	0.016	0.023
Rhone	0.017	0.362	0.329	0.049	0.054
Total	0.015	0.173	0.138	0.018	0.032

CH5 - Table S1.15 | Average of glacier volume (Dataset from Huss & Farinotti (2012)[1]) in kilometre cubed.

km^3	CIG	DCG	DIG	Undetermined	Total
Adige	0.012	0.055	0.123	0.006	0.018
Danube	0.017	0.082	0.068	0.005	0.025
Po	0.016	0.068	0.050	0.009	0.021
Rhine	0.012	0.117	0.131	0.014	0.024
Rhone	0.018	0.243	0.112	0.060	0.040
Total	0.016	0.135	0.089	0.021	0.028

CH5 - Table S1.16 | Average glacier length in metres. *CIG = Clean-ice glacier, DCG = Debris-covered glacier, DIG = Debris-influenced glacier.*

m	CIG	DCG	DIG	Undetermined	Total
Adige	683	1439	2023	553	772
Danube	675	1390	1663	456	777
Po	604	1462	1160	632	700
Rhine	589	1694	1848	707	717
Rhone	701	2683	2190	1228	920
Total	653	1876	1725	728	796

CH5 - Table S1.17 | Average glacier mean thickness in metres.

m	CIG	DCG	DIG	Undetermined	Total
Adige	18	28	34	15	19
Danube	19	25	30	15	20
Po	16	25	25	16	17
Rhine	17	26	30	17	18
Rhone	18	33	34	23	20
Total	17	28	30	17	19

CH5 - Table S1.18 | Average glacier slope in degrees.

°	CIG	DCG	DIG	Undetermined	Total
Adige	26	24	24	25	26
Danube	25	25	22	26	25
Po	27	26	26	27	27
Rhine	28	25	23	25	28
Rhone	30	27	24	26	29
Total	28	26	23	26	27

CH5 - Table S1.19 | Statistics relative to watersheds.

	Surface area (km²)	Percentage of the total	Glacierization
Adige	14495.41	1.27%	0.72%
Danube	791059.19	69.42%	0.05%
Po	73458.34	6.45%	0.43%
Rhine	163550.74	14.35%	0.20%
Rhone	96913.81	8.51%	0.92%
Total	1139477.49	100.00%	0.18%

Debris statistics

***CH5 - Table S1.20 | Surface area of debris layers in kilometre squared**. DCG = Debris-covered glacier, DIG = Debris-influenced glacier.*

km²	DCG	DIG	Total
Adige	4.74	0.64	5.38
Danube	15.00	5.58	20.58
Po	16.33	2.48	18.81
Rhine	20.30	4.89	25.19
Rhone	37.22	5.80	43.02
Total	93.58	19.39	112.98

CH5 - Table S1.21 | Percentage per category of surface area of debris layers.

	DCG	DIG	Total
Adige	5.1%	3.3%	4.8%
Danube	16.0%	28.8%	18.2%
Po	17.4%	12.8%	16.7%
Rhine	21.7%	25.2%	22.3%
Rhone	39.8%	29.9%	38.1%
Total	100.0%	100.0%	100.0%

CH5 - Table S1.22 | Percentage per basin of surface area of debris layers.

	DCG	DIG	Total
Adige	88.1%	11.9%	100.0%
Danube	72.9%	27.1%	100.0%
Po	86.8%	13.2%	100.0%
Rhine	80.6%	19.4%	100.0%
Rhone	86.5%	13.5%	100.0%
Total	82.8%	17.2%	100.0%

CH5 - Table S1.23 | Percentage of glacier surface area (DCG/DIG only) covered by debris layers.

	DCG	DIG	Total
Adige	20.7%	4.9%	5.2%
Danube	15.6%	7.8%	4.9%
Po	21.8%	8.4%	6.0%
Rhine	23.7%	8.7%	7.5%
Rhone	10.5%	6.4%	4.8%
Total	14.8%	7.4%	5.5%

CH5 - Table S1.24 | Volume of ice under debris in kilometre cubed. *DCG = Debris-covered glacier, DIG = Debris-influenced glacier.*

km^3	DCG	DIG	Total
Adige	0.060	0.014	0.074
Danube	0.629	0.121	0.750
Po	0.850	0.052	0.902
Rhine	1.381	0.248	1.630
Rhone	2.268	0.162	2.430
Total	5.189	0.597	5.786

CH5 - Table S1.25 | Percentage per category of volume of ice under debris.

	DCG	DIG	Total
Adige	1.2%	2.3%	1.3%
Danube	12.1%	20.2%	13.0%
Po	16.4%	8.8%	15.6%
Rhine	26.6%	41.6%	28.2%
Rhone	43.7%	27.1%	42.0%
Total	100.0%	100.0%	100.0%

CH5 - Table S1.26 | Percentage per basin of volume of ice under debris.

	DCG	DIG	Total
Adige	81.2%	18.8%	100.0%
Danube	83.9%	16.1%	100.0%
Po	94.2%	5.8%	100.0%
Rhine	84.8%	15.2%	100.0%
Rhone	93.3%	6.7%	100.0%
Total	89.7%	10.3%	100.0%

CH5 - Table S1.27 | | Percentage of glacier (DCG/DIG only) ice volume under debris.

	DCG	DIG	Total
Adige	5.4%	1.9%	1.7%
Danube	11.3%	3.8%	3.9%
Po	22.0%	4.0%	6.4%
Rhine	24.1%	7.3%	9.6%
Rhone	10.3%	5.2%	5.3%
Total	5.2%	0.6%	5.8%

Change in glacial water source

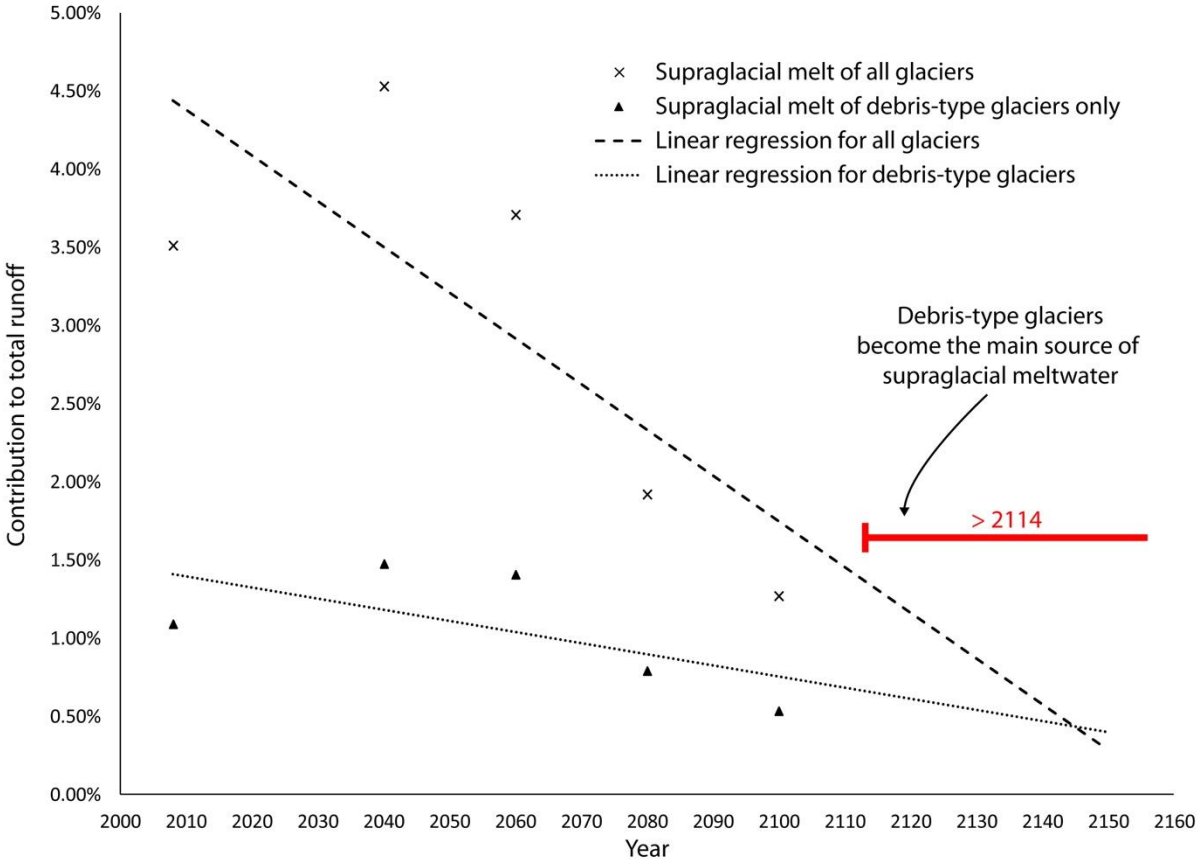

CH5 - Figure S1 | Forecast contribution of supraglacial melt from all glaciers and debris-type glaciers to total runoff after 2100, assuming trends continue. *In 2114, the debris-type contribution becomes half of the contribution of all glaciers, meaning that debris-type glaciers become the main source of supraglacial meltwater in the European Alps.*

The case of Grosser Aletschgletscher

CH5 - Figure S2 | Grosser Aletschgletscher by the numbers. *The inset image is a zoom in of the terminus area of the glacier. This part is covered by debris across its entire width, defining Grosser Aletschgletscher as a debris-covered glacier.*

CH5 - Table S2.1 | Statistics relative to the geometry of Grosser Aletschgletscher.

Statistic	**Value**
Surface area (km^2)	82.05
Percentage of the glacial surface area of the Alps	3.97%
Debris layer surface area (km^2)	3.83
Percentage of the surface area covered	4.66%
Volume - Volume / Area scaling method (km^3)	12.886
Percentage of ice volume of the Alps (VAs)	11.32%
Volume - Huss & Farinotti (2012) dataset (km^3)	3.166
Percentage of ice volume of the Alps (H&F2012)	3.15%

CH5 - Table S2.2 | Statistics relative to the runoff of Grosser Aletschgletscher. *For comparison, the supraglacial melt of one debris-type glacier contributes 0.003% to Alps total runoff.*

Contribution of supraglacial melt to	**1908-2008**	**2020-2040**	**2040-2060**	**2060-2080**	**2080-2100**
Rhone total runoff	1.0%	1.3%	1.5%	1.0%	0.7%
Alps total runoff	0.11%	0.16%	0.17%	0.13%	0.08%
Rhone total glacial runoff	4.2%	5.7%	7.2%	8.1%	7.5%
Alps total glacial runoff	1.4%	2.4%	3.1%	3.6%	3.2%
Rhone total supraglacial runoff	7.6%	8.1%	9.8%	12.3%	12.3%
Alps total supraglacial runoff	3.2%	3.5%	4.6%	6.6%	6.7%

Details of the classification process

RGI and Google Earth imagery assessment

Before using the RGI v5.0[2] and Google Earth imagery[3] for an exhaustive classification of glaciers in the European Alps, we assessed how the combination of these two datasets would work together for a classification. We present below some statistics and examples of this assessment.

CH5 - Table S3 | Statistics relative to the RGI v5.0 Central Europe (zone 11) dataset.

Statistic	Value
Total number of glaciers	3980
Number of excluded glaciers*	168
Percentage of excluded glaciers relative to the total number of glaciers	4.2%
Number of selected glaciers	3530
Surface area of selected glaciers (km^2)	2036.33
Number of "Error" glaciers**	282
Surface area of "Error" glaciers (km^2)	15.64
Percentage of "Error" glaciers relative to non-excluded glaciers***	7.4%
Percentage of surface area of "Error" glaciers relative to non-excluded glaciers	0.8%

***** *Excluded glacier: glacier that is not in the Alps or only present in the RGI under its nominal form (Figure S1.1).*

*** "Error" glacier: glacier in the RGI that was detected as a glacier but was actually a snow patch (Figure S1.2), one glacier detected as multiple glaciers (Figure S1.3), or a glacier created due to a problem in the DEM (Figure S1.4).*

**** non-excluded glacier: selected glacier + "error" glacier.*

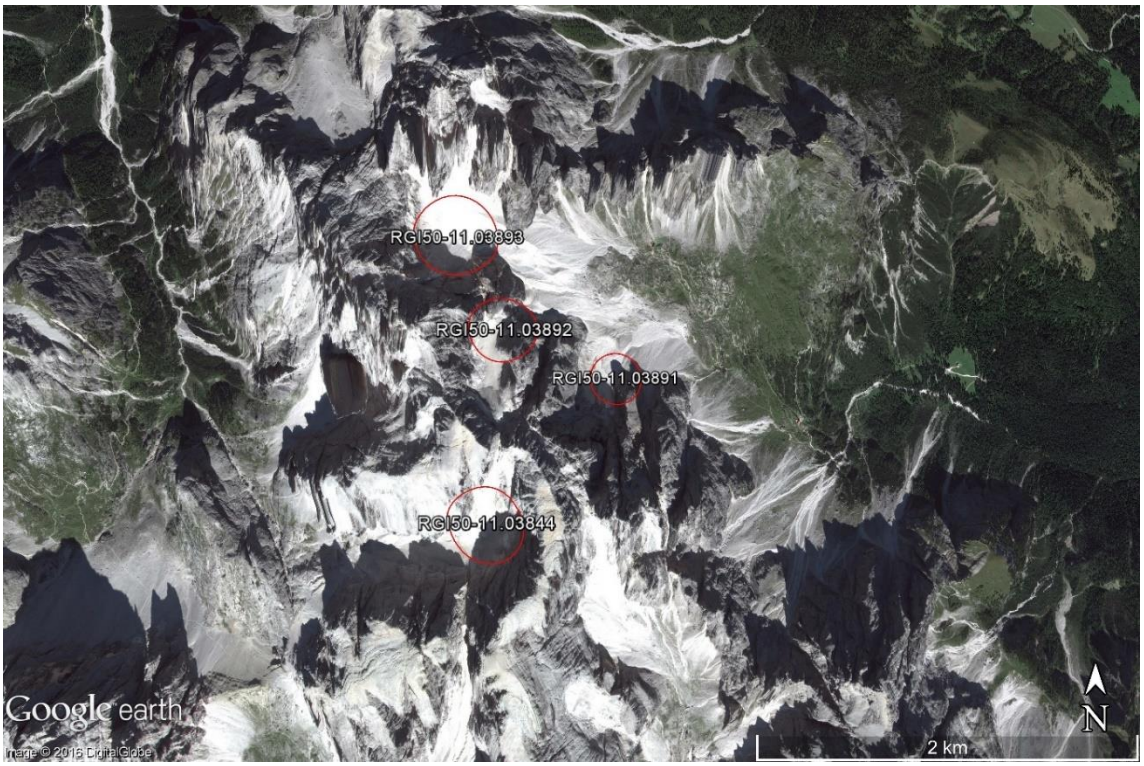

CH5 - Figure S3.1 | Nominal form of Alpine glaciers in the RGI*. As these circles are only placeholders, these glaciers have been excluded from the classification. Google Earth imagery from 30/08/2015 accessed on 02/09/2016.*

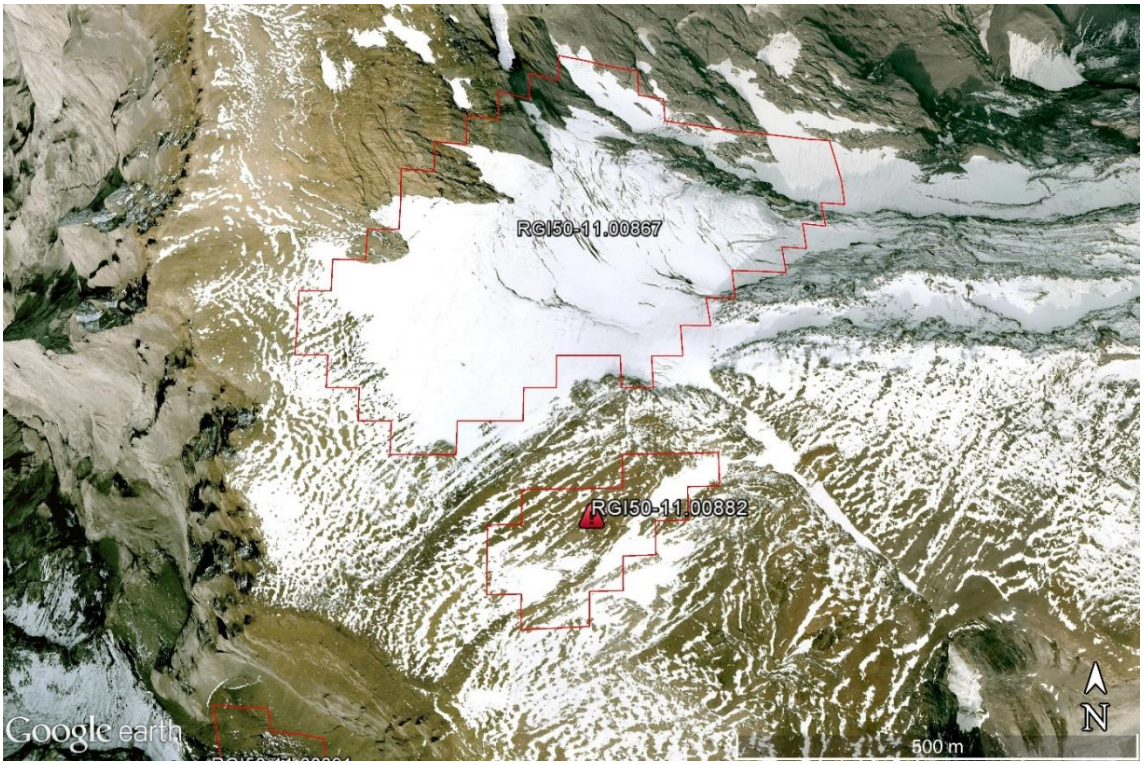

CH5 - Figure S3.2 | Snow patch considered as a glacier in the RGI. *The glacier RGI50-11_00882 appears to be a snow patch situated on the opposite side of ridge of the glacier RGI50-11_00867. Consequently, this glacier has been considered as an "error" glacier. Google Earth imagery from 30/10/2009 accessed on 02/09/2016.*

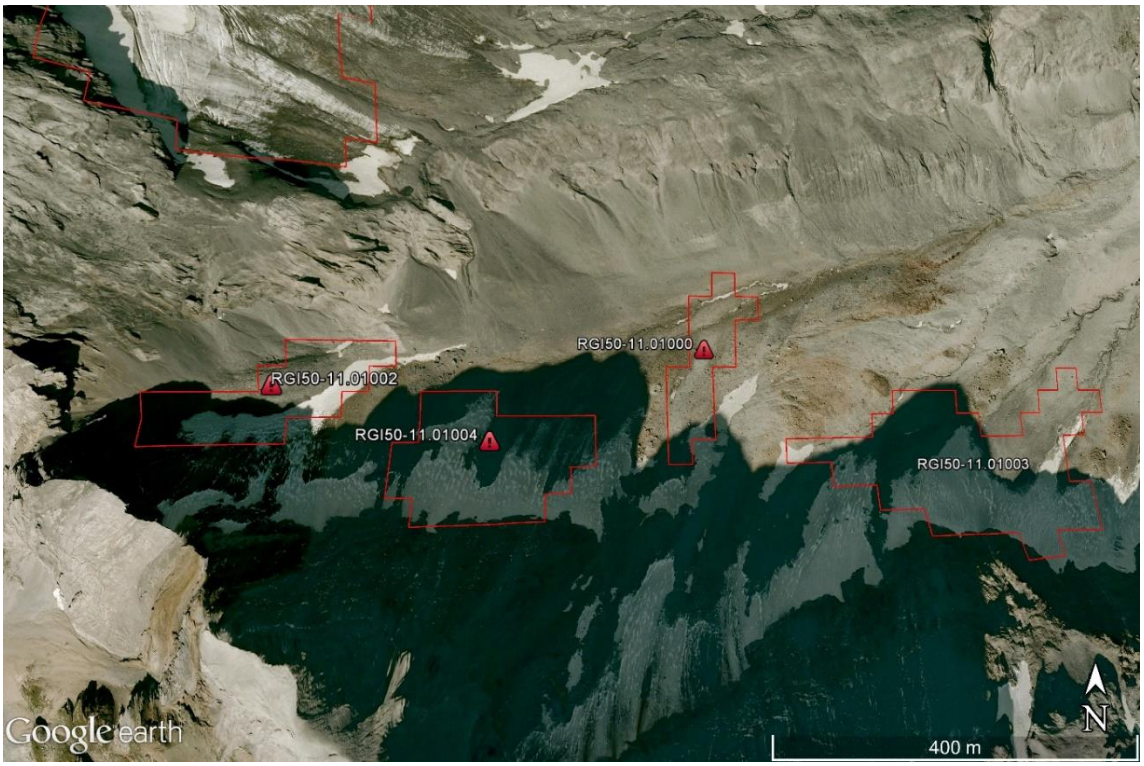

CH5 - Figure S3.3 | One glacier detected as multiple smaller glaciers. *Glaciers RGI50-11_01002, RGI50-11_01004, RGI50-11_01000 and RGI50-11_01003 have been detected as 4 separated glaciers when they appear to all belong to only one glacier. In this case, only the glacier RGI50-11_01003 (the largest) has been selected, and the others are considered "error" glaciers. Google Earth imagery from 30/06/2009 accessed on 02/09/2016.*

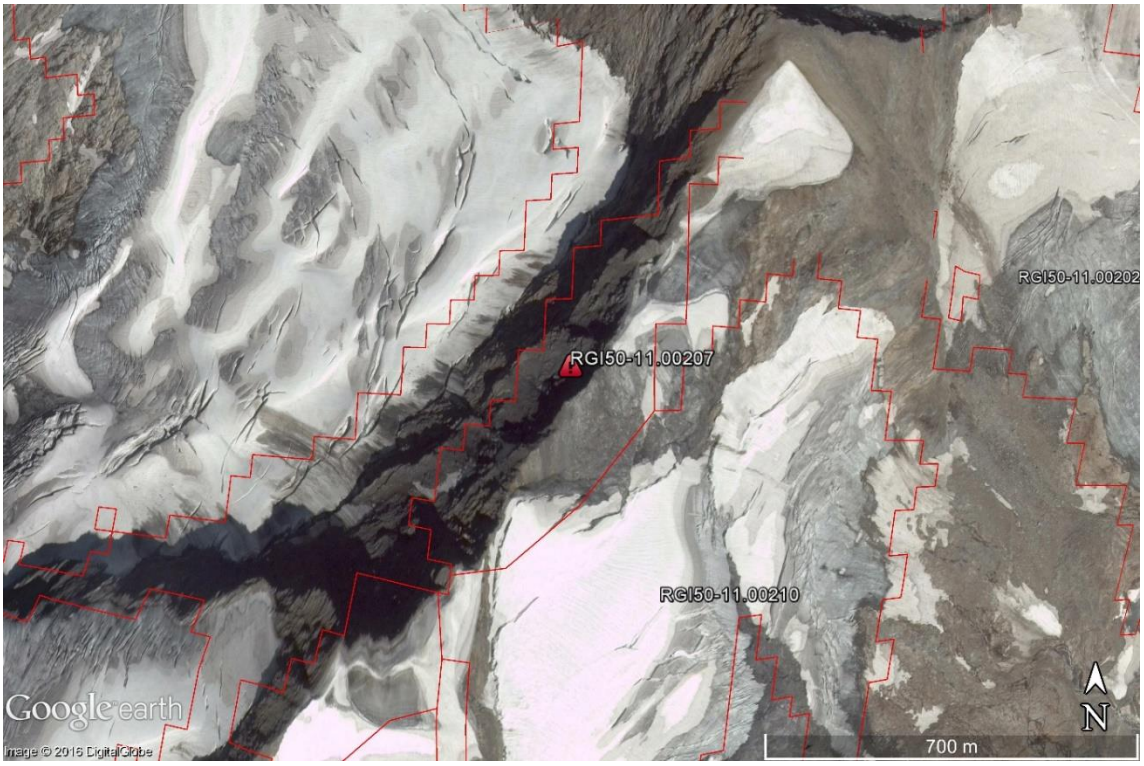

CH5 - Figure S3.4 | Glacier of the RGI created due to a problem in the DEM. *The glacier RGI50-11_00207 seems to be situated on the divide between two other glaciers. Consequently, this glacier has been considered as an "error" glacier. Google Earth imagery from 12/08/2015 accessed on 02/09/2016.*

Definition of a debris layer

To be considered as a debris-type glacier, a glacier should have a layer of identifiable rock debris and not simply a dust layer on its surface. A dust layer is not considered as a debris layer because it enhances the melting[4] of the underlying ice, contrary to a thicker rock debris layer.

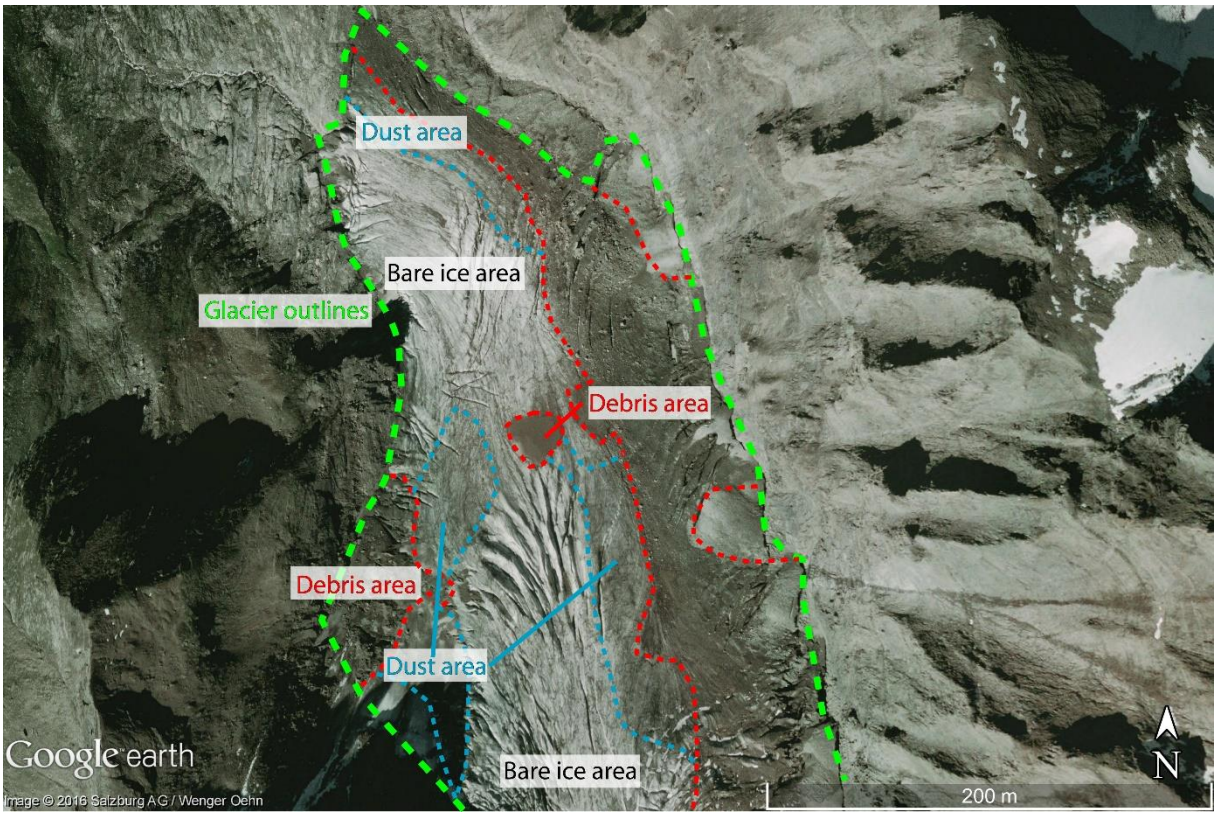

***CH5 - Figure S3.5 | Difference between a rock debris layer and dust layer**. Terminus of the debris-covered glacier RGI50-11_00047. Google Earth imagery from 30/12/2000 accessed on 02/09/2016.*

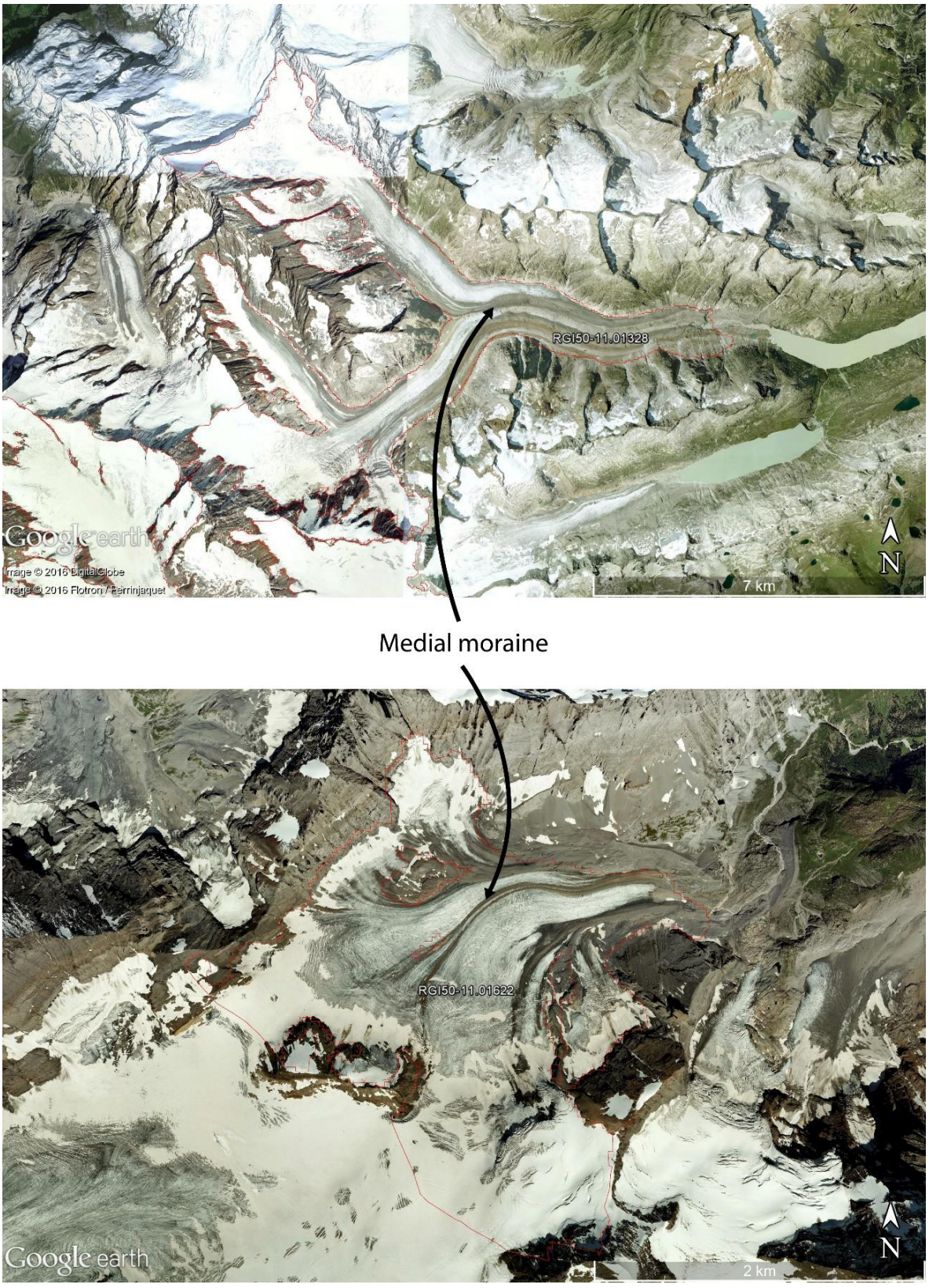

CH5 - Figure S3.6 | Examples of medial moraines forming the debris cover. *RGI50-11.01328 and RGI50-11.01622 are debris-covered glaciers with medial moraines reaching their terminus and forming most of the debris cover. These medial moraines have been included in the surface area of the debris layer of each glacier and are a case where the debris layer may not be fully inside the ablation area, as assumed in the methods section regarding the runoff modelling. Google Earth imagery from 31/12/2006 and 03/10/2009 accessed on 02/09/2016.*

Categories of glaciers

CH5 - Figure S3.7 | Examples of clean-ice glaciers and debris-covered glaciers. *RGI50-11.03618 (Glacier Blanc) is very good example of a clean-ice glacier. RGI50-11.03669 and RGI50-11.03686 (Glacier Noir and Glacier Noir Sud[5]) are good examples of debris-covered glaciers. Glacier Noir Sud was a tributary of Glacier Noir until 2009. Google Earth imagery from 03/10/2009 accessed on 12/09/2016.*

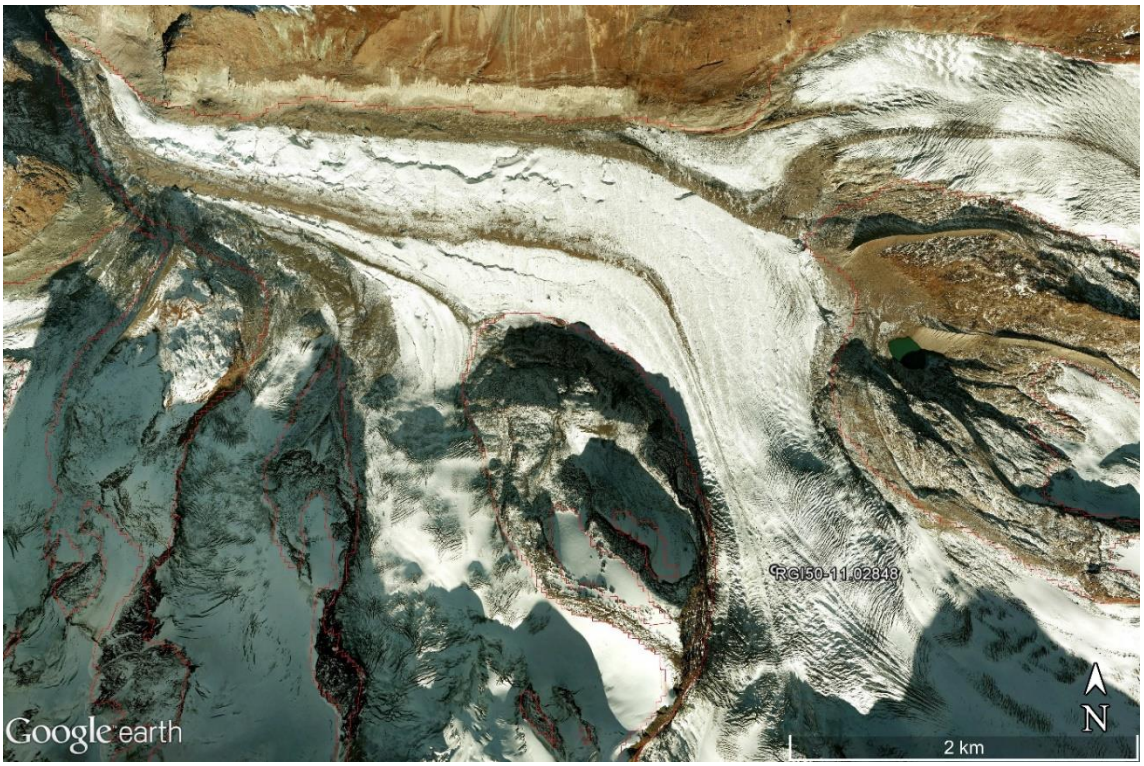

CH5 - Figure S3.8 | Example of a debris-influenced glacier. *RGI50-11.02848 displays medial moraines that reach the terminus of the glacier, without, however, fully covering the width of the glacier. Google Earth imagery from 29/10/2009 accessed on 12/09/2016.*

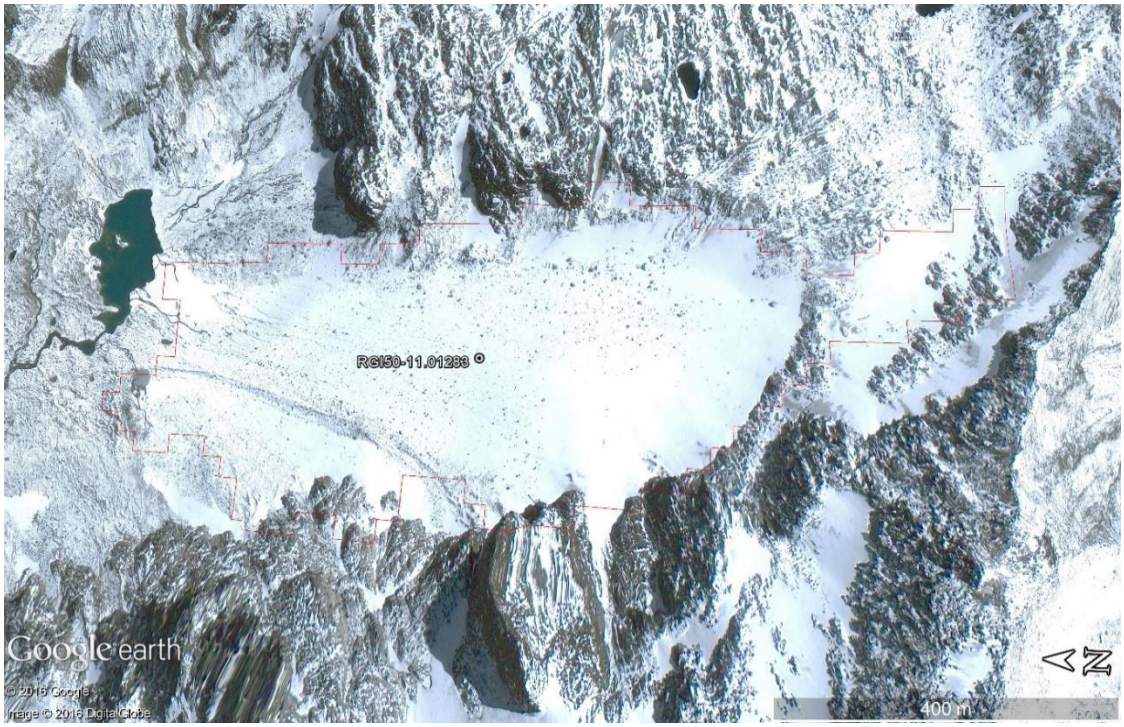

CH5 - Figure S3.9 | Example of an undetermined glacier. *The snow cover is too significant on this image to categorize RGI50-11.01283 as a debris-covered glacier, although there is a lot of debris apparent through the snow layer. This glacier is therefore categorized as an undetermined glacier. Other reasons for such a classification are: poor imagery, cloud cover, unclear glacier outlines and unclear debris layer outlines. Google Earth imagery from 31/08/2010 accessed on 12/09/2016.*

Debris-type glaciers outlines

As indicated in the Methods, it is known that the RGI underestimates glacier size when debris is present on the surface[6] due to the automatic detection technique.

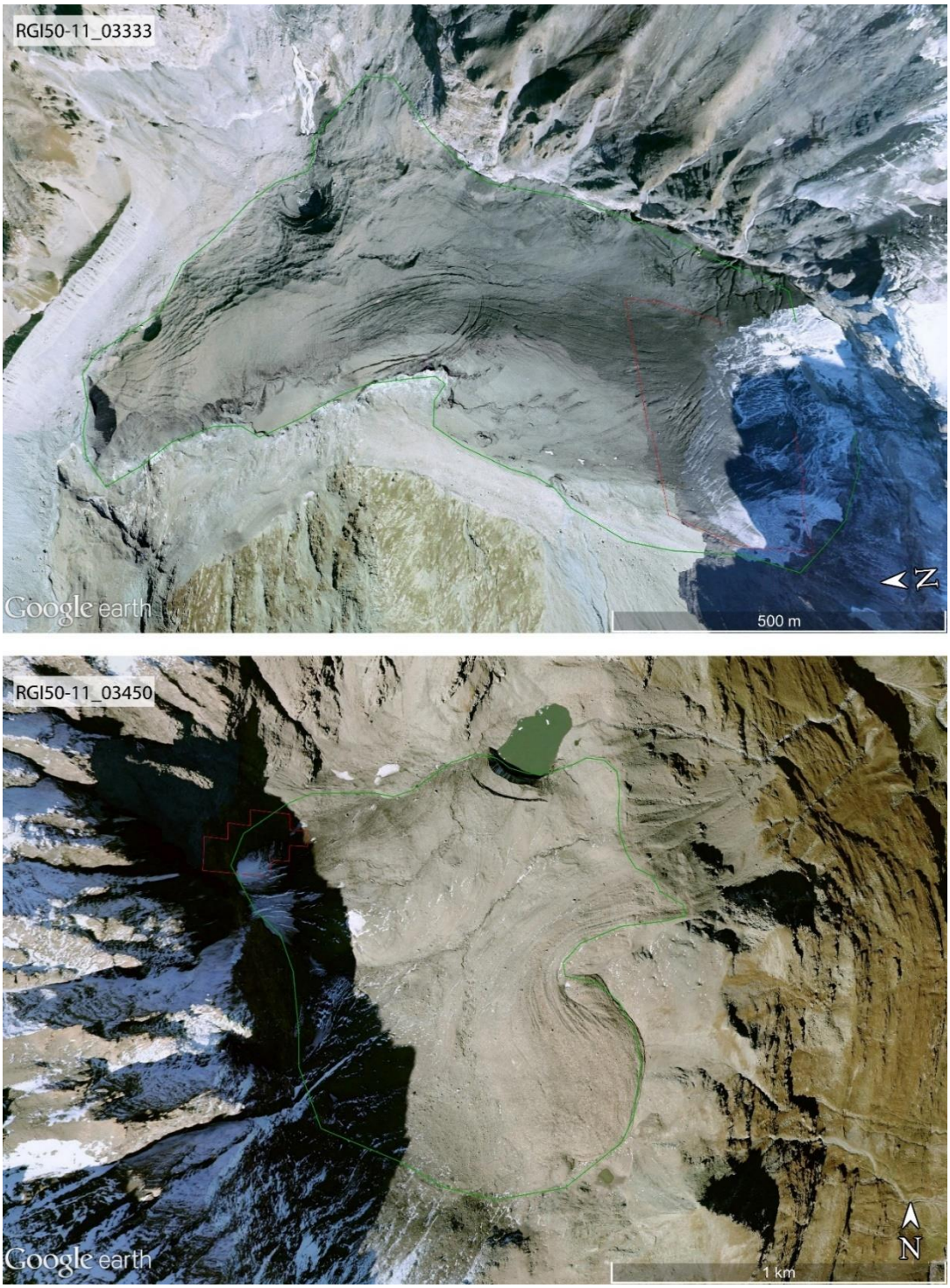

CH5 - Figure S3.10 | Example of two glaciers where the RGI strongly underestimates their size due to debris presence. *In red, the RGI outline. In green, the corrected outline. Google Earth imagery from 31/12/2005 accessed on 02/09/2016.*

Glacier distributions in the European Alps

Heatmaps

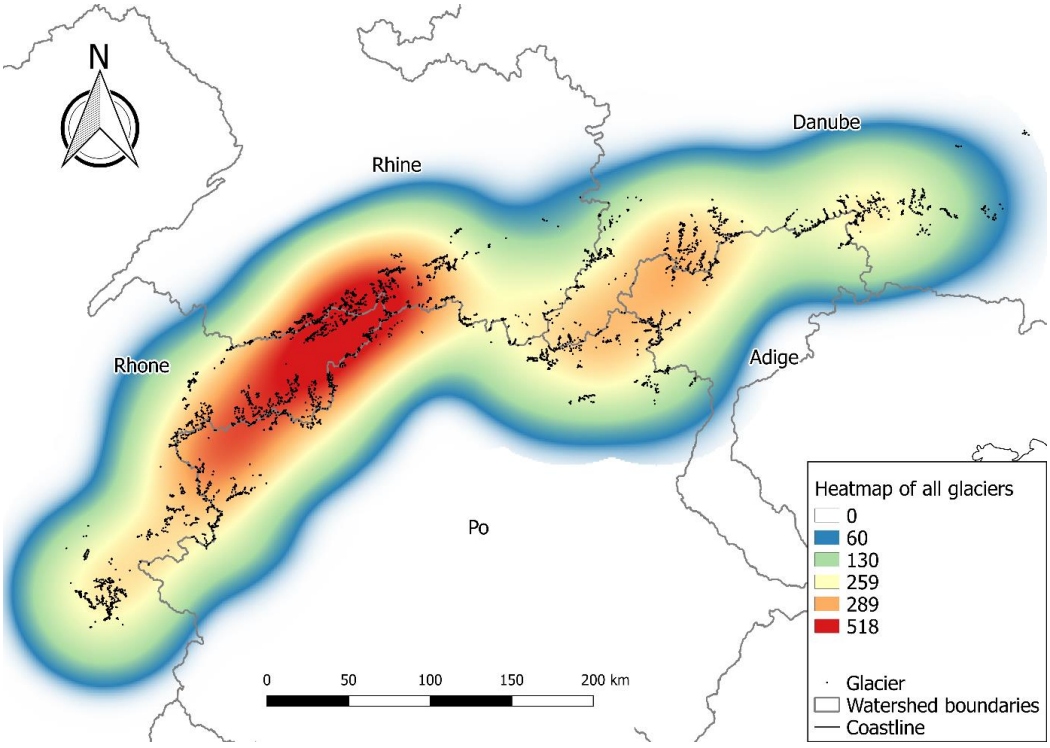

CH5 - Figure S4.1 | Heatmap of all glaciers in the Alps, using a search radius of 75 km.

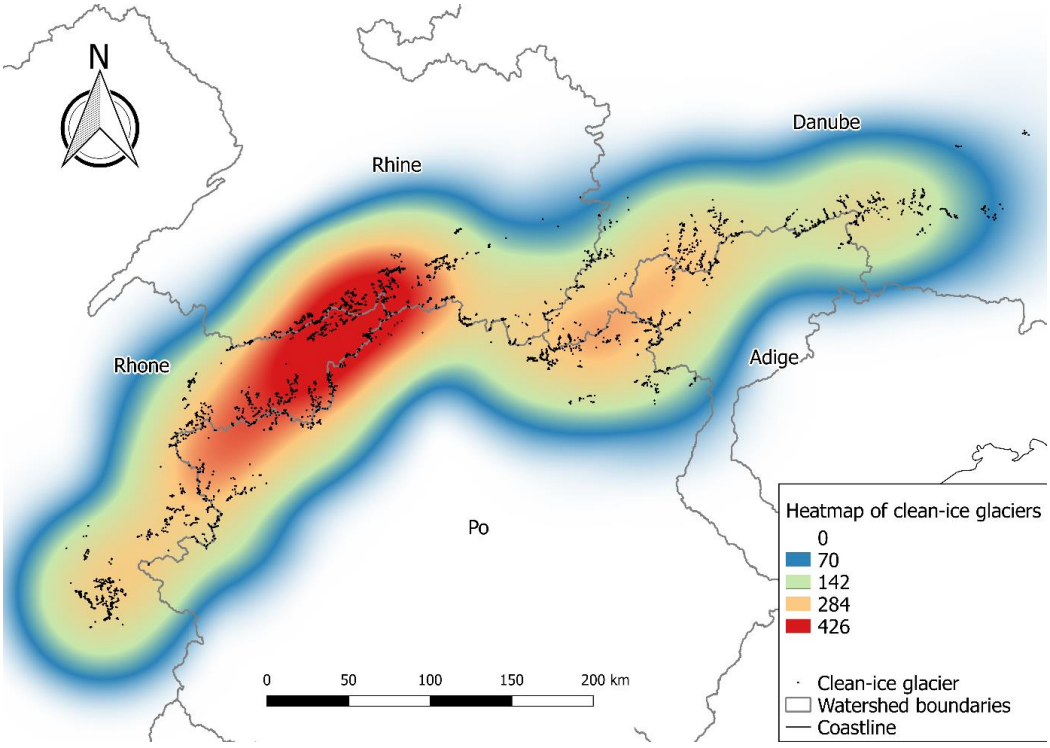

CH5 - Figure S4.2 | Heatmap of clean-ice glaciers in the Alps, using a search radius of 75 km.

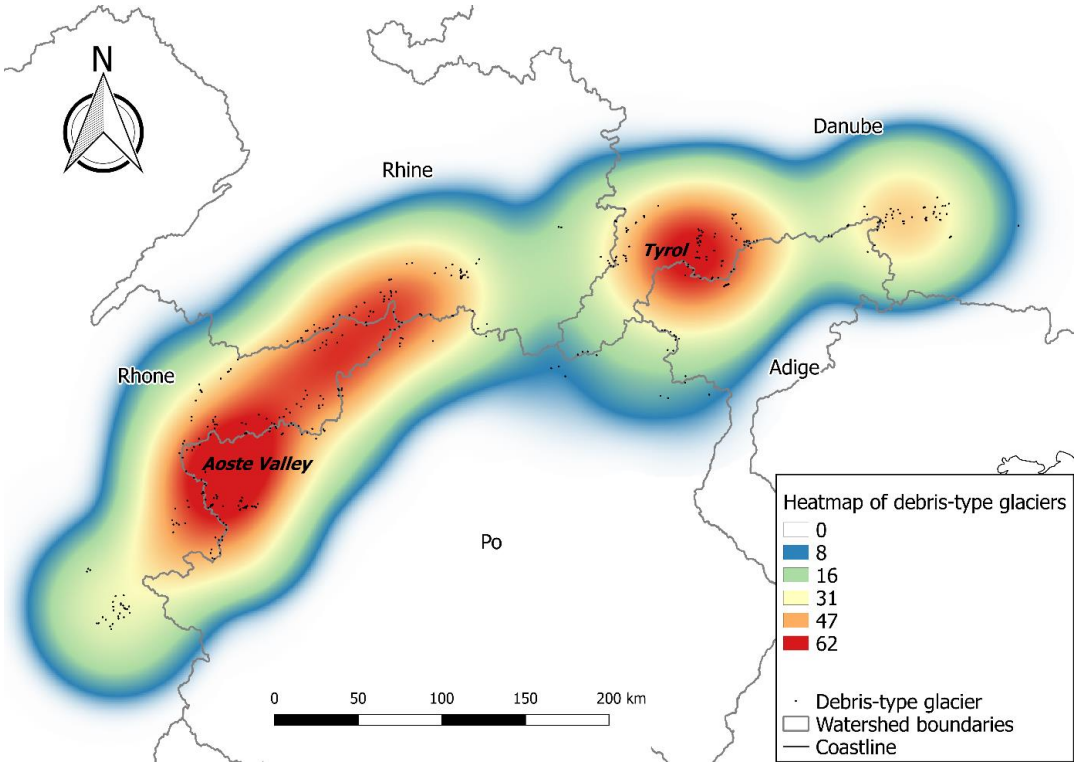

CH5 - Figure S4.3 | Heatmap of debris-type glaciers in the Alps, using a search radius of 75 km. *Debris-type glaciers are not equally spread across the Alps, in contrast to clean-ice glaciers. Debris-type glaciers are concentrated around the Aoste valley (Italy) in the west of the Alps, in the south-west Tyrol (Austria), and in lower concentration in the Eastern Alps.*

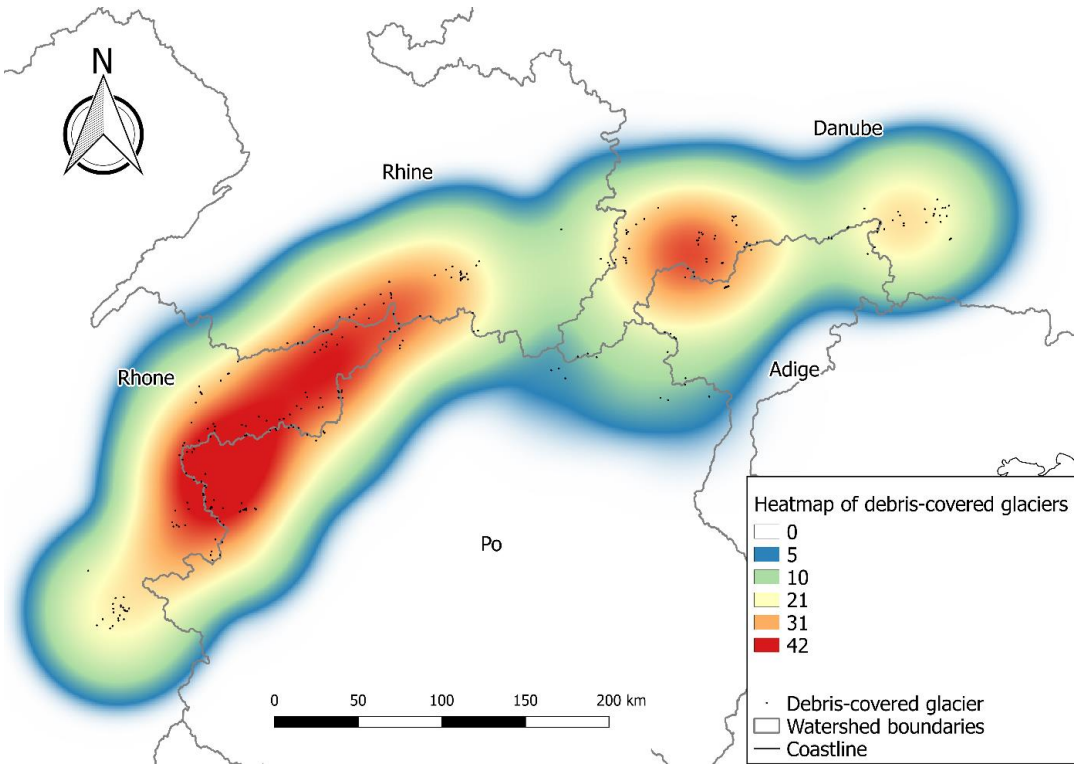

CH5 - Figure S4.4 | Heatmap of debris-covered glaciers in the Alps, using a search radius of 75 km.

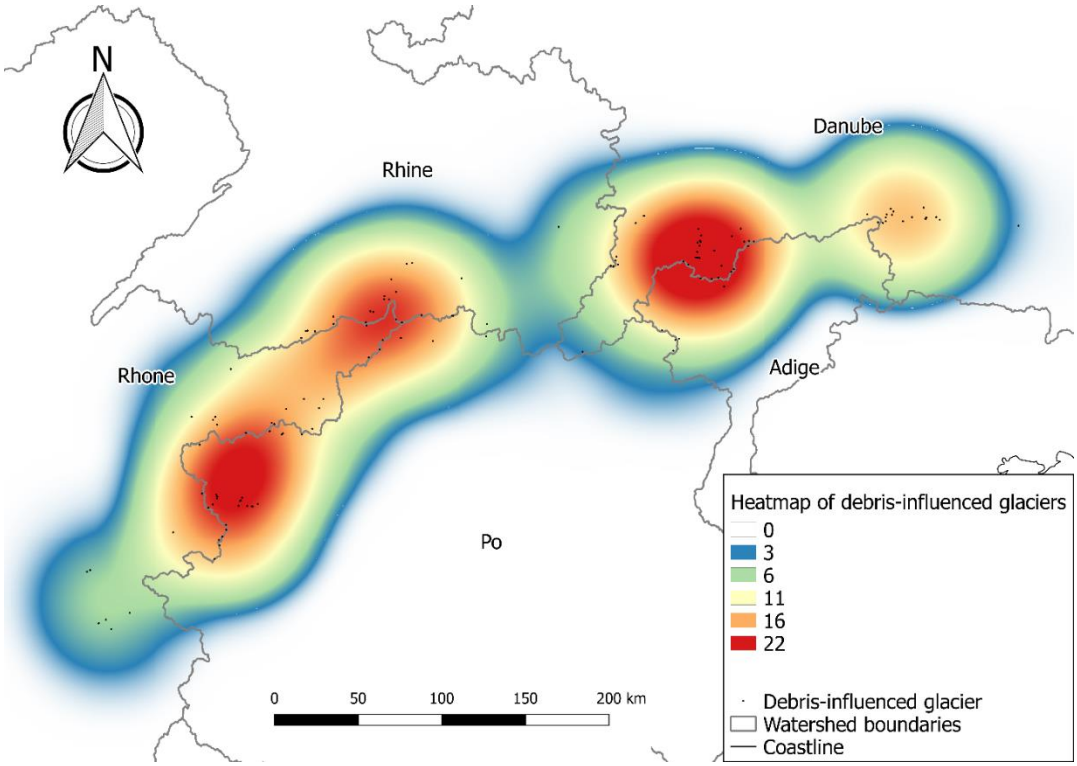

CH5 - Figure S4.5 | Heatmap of debris-influenced glaciers in the Alps, using a search radius of 75 km.

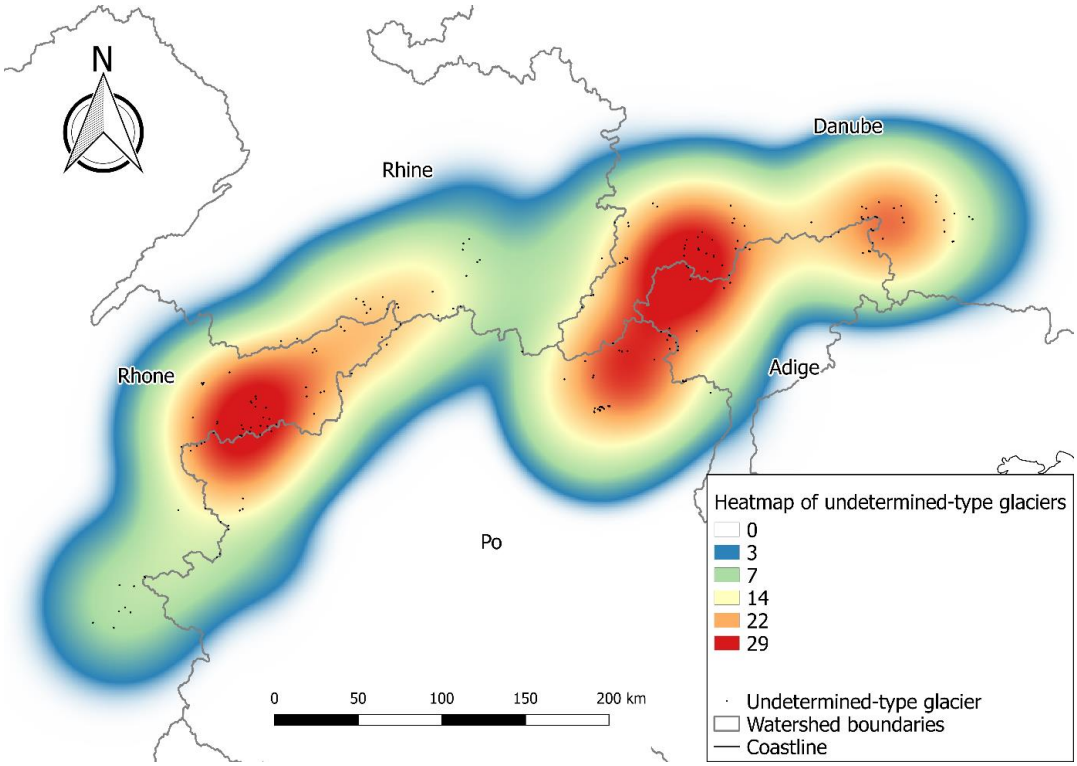

CH5 - Figure S4.6 | Heatmap of undetermined-type glaciers in the Alps, using a search radius of 75 km. *"Undetermined type" represent the determination uncertainty on the type of glacier. Taken together with Figure S4.3, this map shows that the larger the concentration of debris-type glaciers, the larger the uncertainty of the determination.*

Frequencies

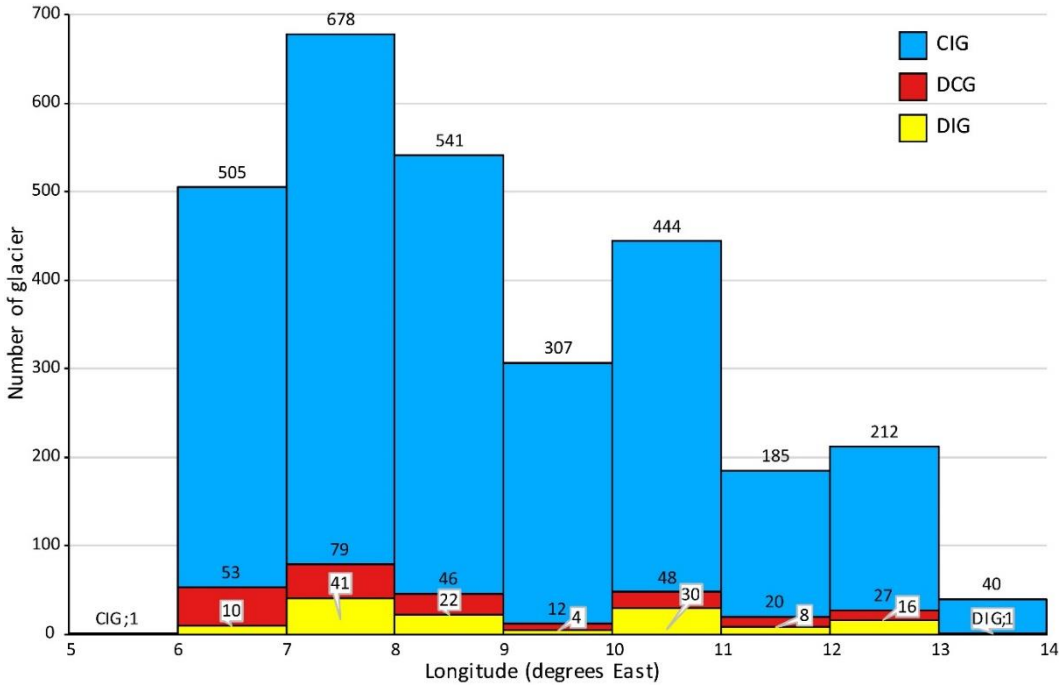

CH5 - Figure S4.7 | Occurrence of the different categories of glacier per longitude. *The number of glaciers is for every degree of longitude East covering the entire Alps. CIG: Clean-ice glacier. DCG: Debris-covered glacier. DIG: Debris-influenced glacier.*

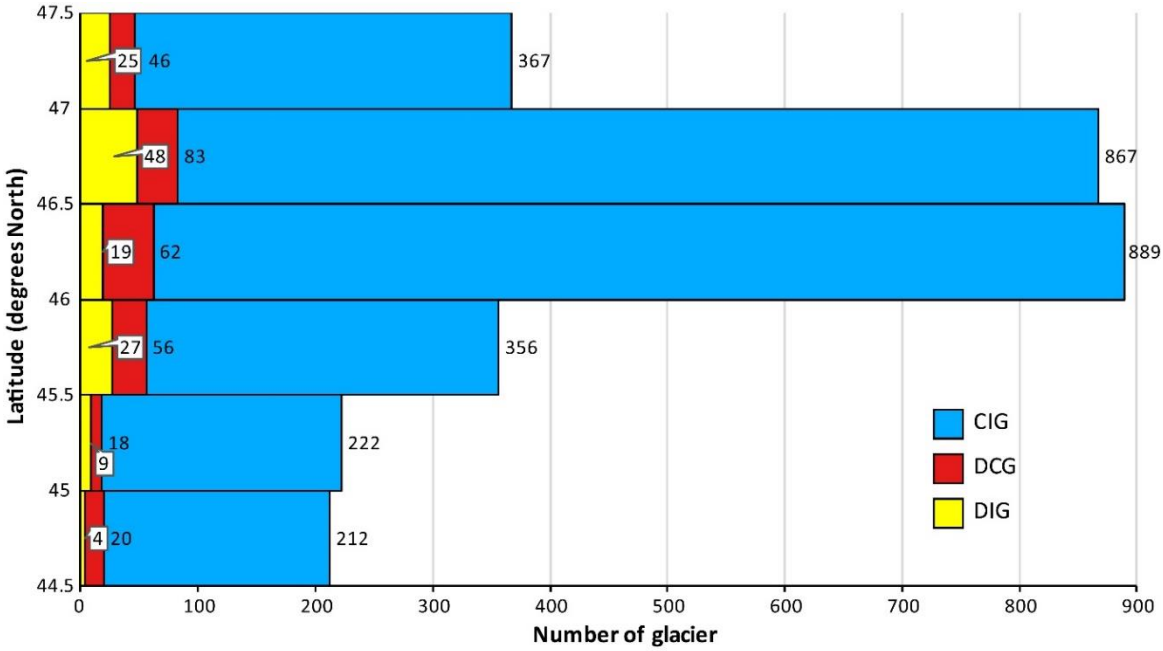

CH5 - Figure S4.8 | Occurrence of the different categories of glacier by latitude*. The number of glaciers is for every half degree of latitude North covering the entire Alps. CIG: Clean-ice glacier. DCG: Debris-covered glacier. DIG: Debris-influenced glacier.*

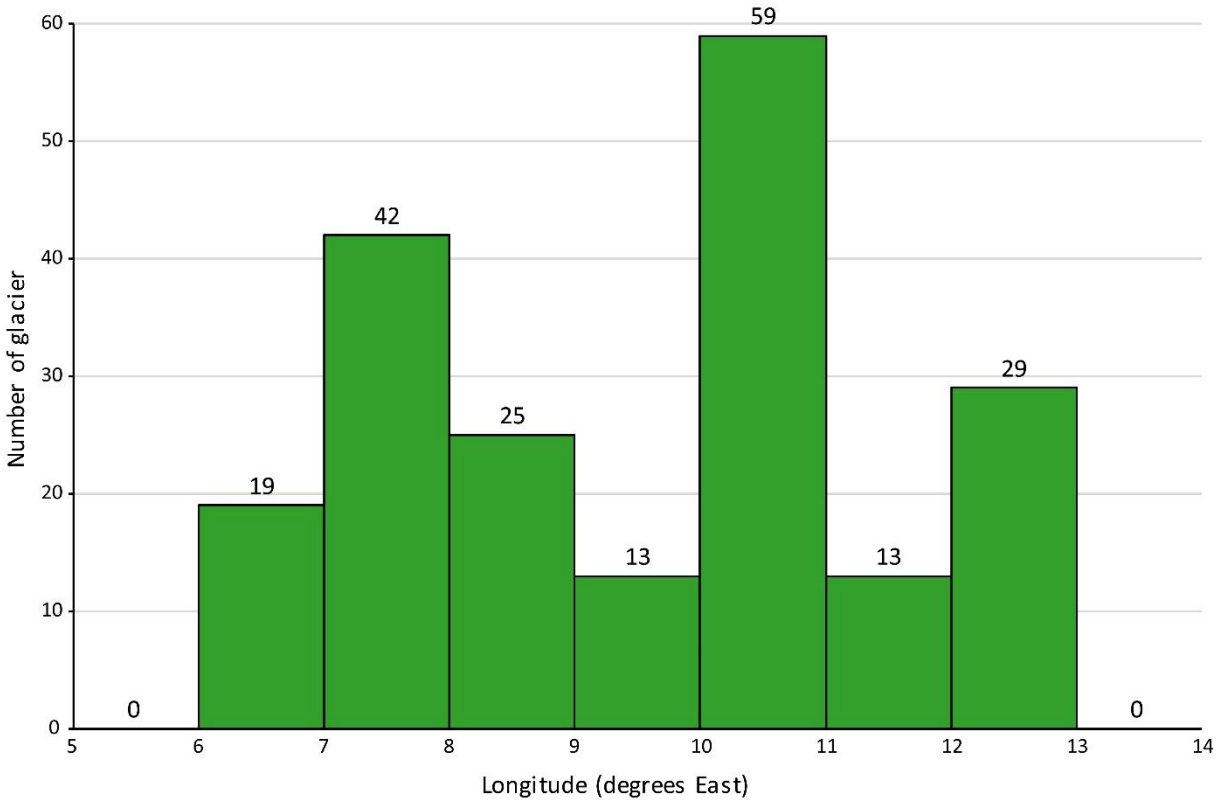

CH5 - Figure S4.9 | Occurrence of undetermined-type glaciers by longitude. *The number of glaciers is for every degree of longitude East covering the entire Alps.*

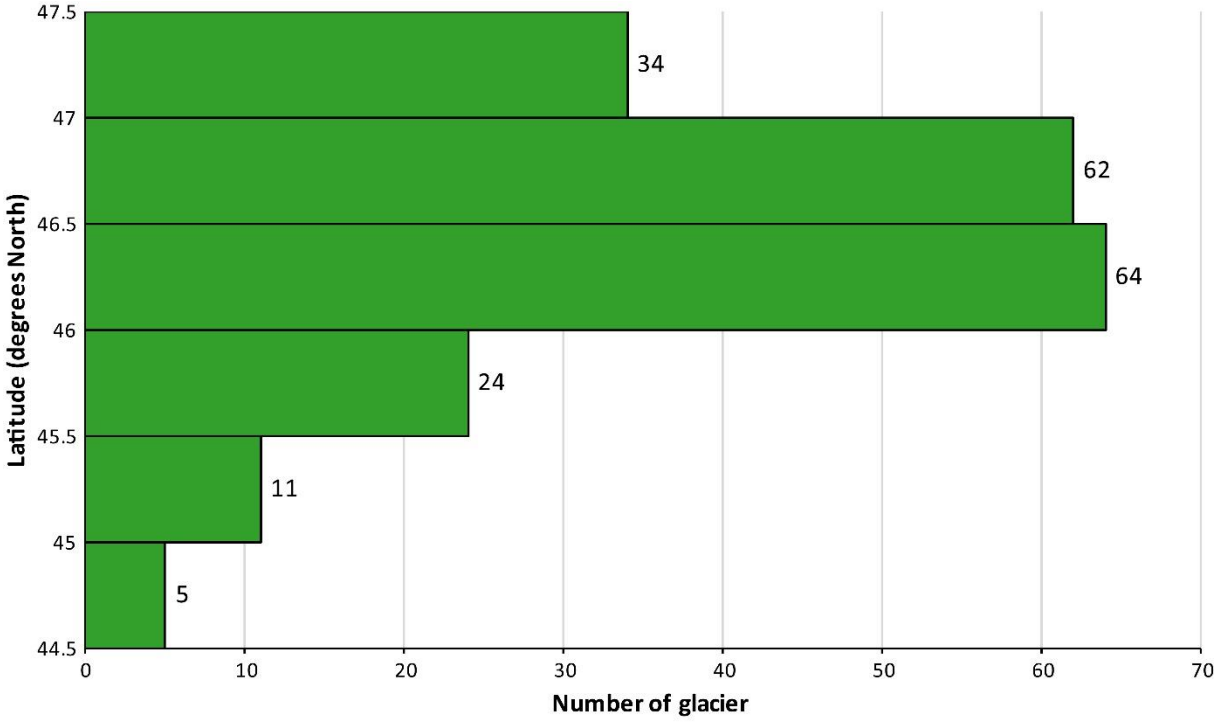

CH5 - Figure S4.10 | Occurrence of undetermined-type glaciers by latitude. *The number of glaciers is for every half degree of latitude North covering the entire Alps.*

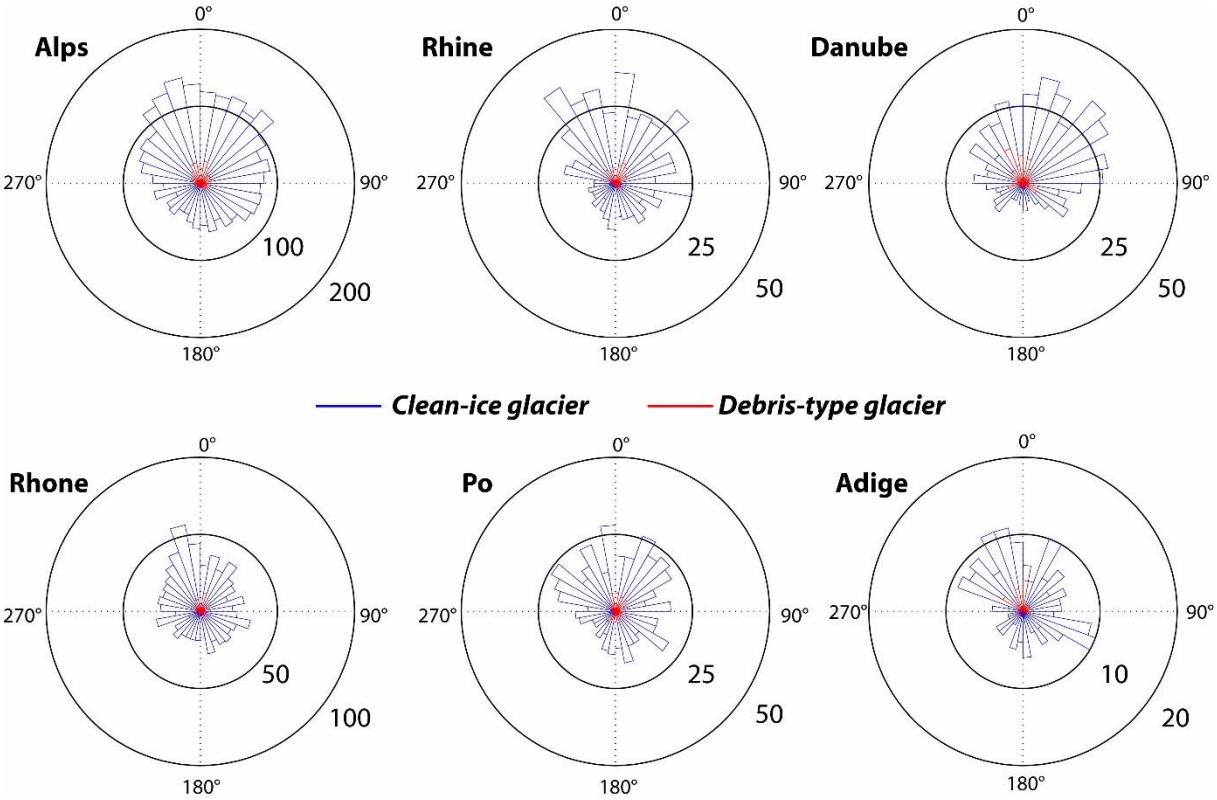

CH5 - Figure S4.11 | Frequency of clean-ice glacier and debris-type glacier dependent of their orientation, per bin of 10°.

ELA as a function of glacier orientation

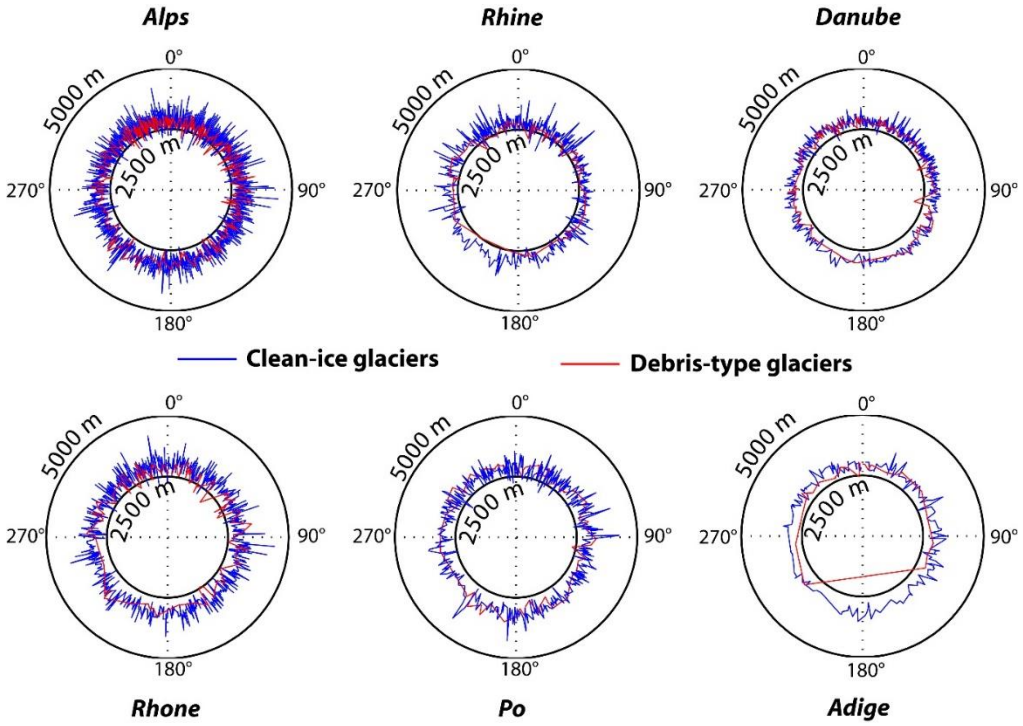

CH5 - Figure S5.1 | Polar representation of the equilibrium line altitude (ELA) as a function of the average orientation of the glacier per watershed*. As expected, clean-ice glaciers and debris-type glaciers present a lower ELA with northern orientation (both lines are closer to the 2500 m circle in the North-East orientation than in the South-West orientation). The two major differences between these two types of glaciers are the lower internal variation of debris-type glaciers compared to clean-ice glaciers and the more homogenous distributions of clean-ice glaciers compared to debris-type glaciers. For example, in the Adige basin, clean-ice glaciers can be found with any orientation, contrary to debris-type glaciers, which show no South or South-East orientations.*

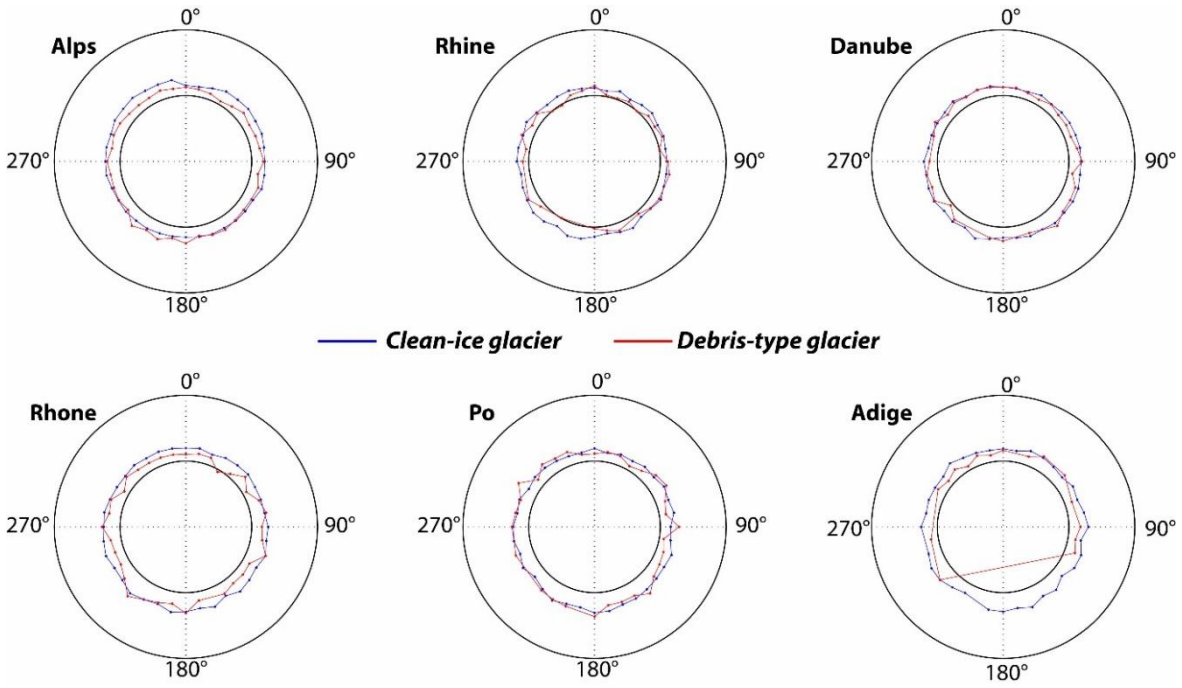

CH5 - Figure S5.2 | Polar representation of the equilibrium line altitude (ELA) as a function of the average orientation of the glacier per watershed, average per bin of 10°.

Sensitivity of runoff parametrization

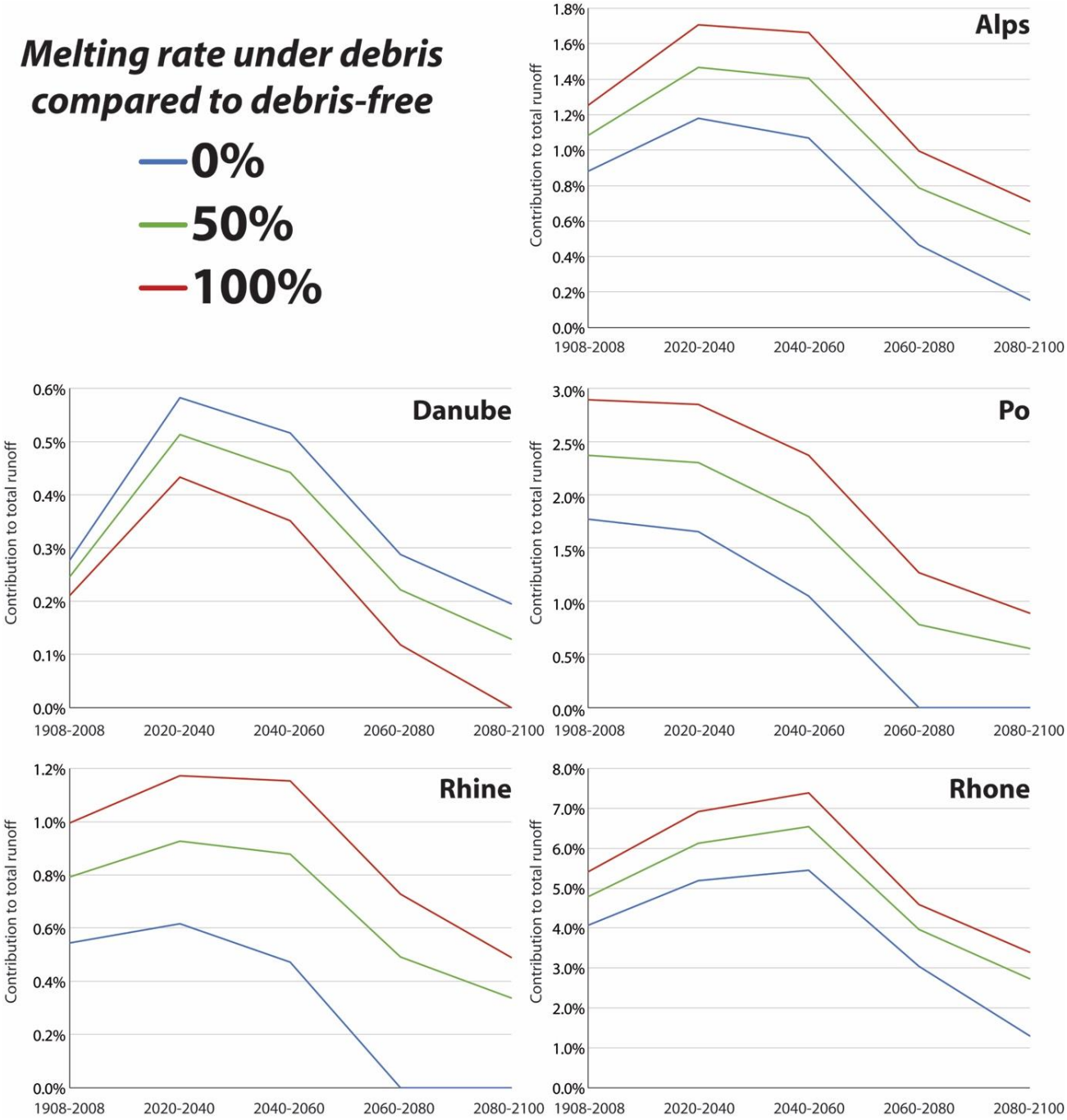

CH5 - Figure S6 | Sensitivity tests of the contribution to total runoff in volume of debris-type glaciers per basin. Here the parameter shown is the melt rate under the debris layer*. The contribution to total runoff is the most sensitive to this parameter, consequently all other sensitivity tests stand between the red line and the green line. The other tests are: variation of the transit time inside glaciers (following supplementary table S3 from Huss (2011)[7]), variation of the size of the ablation area for clean-ice and debris-type glaciers by 5%, and variation of the size of the debris layer for debris-type glacier by 5%. Note that the scale of the y-axis is different on each plot.*

The Volume/Area scaling method

The two parameters in the Volume/Area scaling equation are a source of debate and controversy, as indicated by the recent review article by Bahr et al. (2015)[8]. On one side, the γ parameter is fixed by the theory at a value of 1.375. One the other side, the c parameter depends on the location of the group of glaciers (in our case the European Alps), the typical size of glaciers in the group (in our case any size) and the climate at one particular time (in our case present time).

We choose to fix *c* at a value of 0.03 to be consistent with the literature. However, this value has been calculated with 149 glaciers around the world. In order to be more specific for the European Alps, we built a group of Alpine glaciers using Bahr et al. (1997)[9] and Chen & Ohmura (1990)[10] dataset to calculate a new value of *c*.

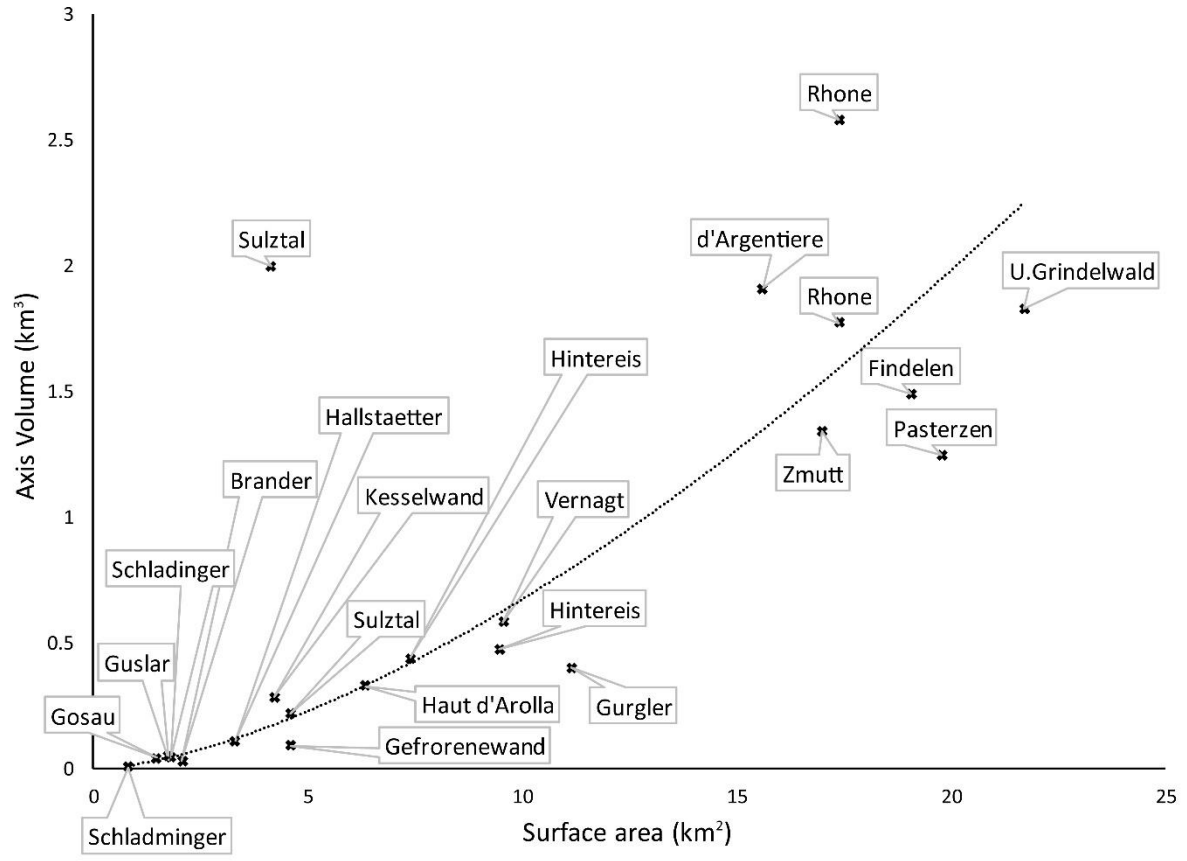

CH5 - Figure S7 | Plot establishing the relationship between the surface area of a glacier and its volume.

Relationship used for the AAR method

CH5 - Table S8 | Dataset used to establish the relationship between accumulation area ratio (AAR_0) and the surface area of a glacier for the AAR method. *All the glaciers chosen are situated in the European Alps.*

Extracted from Kern & Laszlo, 2010		Extracted from RGI v5.0	
Glacier name	**AAR0**	**RGIid**	**Surface Area (km2)**
Basodino	0.508	01987	2.09
Hintereisferner	0.659	00897	8.04
Jamtal Ferner	0.585	00781	3.82
Kesselwandferner	0.688	00787	3.97
Langtaler	0.575	00929	2.38
Limmern	0.512	00918	2.16
Maladeta	0.409	03818	0.26
Ochsentaler	0.653	00807	1.68
Sforzellina	0.332	02214	0.21
Silvretta	0.563	00804	2.88
Sonnblickkees	0.611	00080	1.19
Vernagtferner	0.660	00719	8.56
Wurtenkees	0.412	00306	0.19

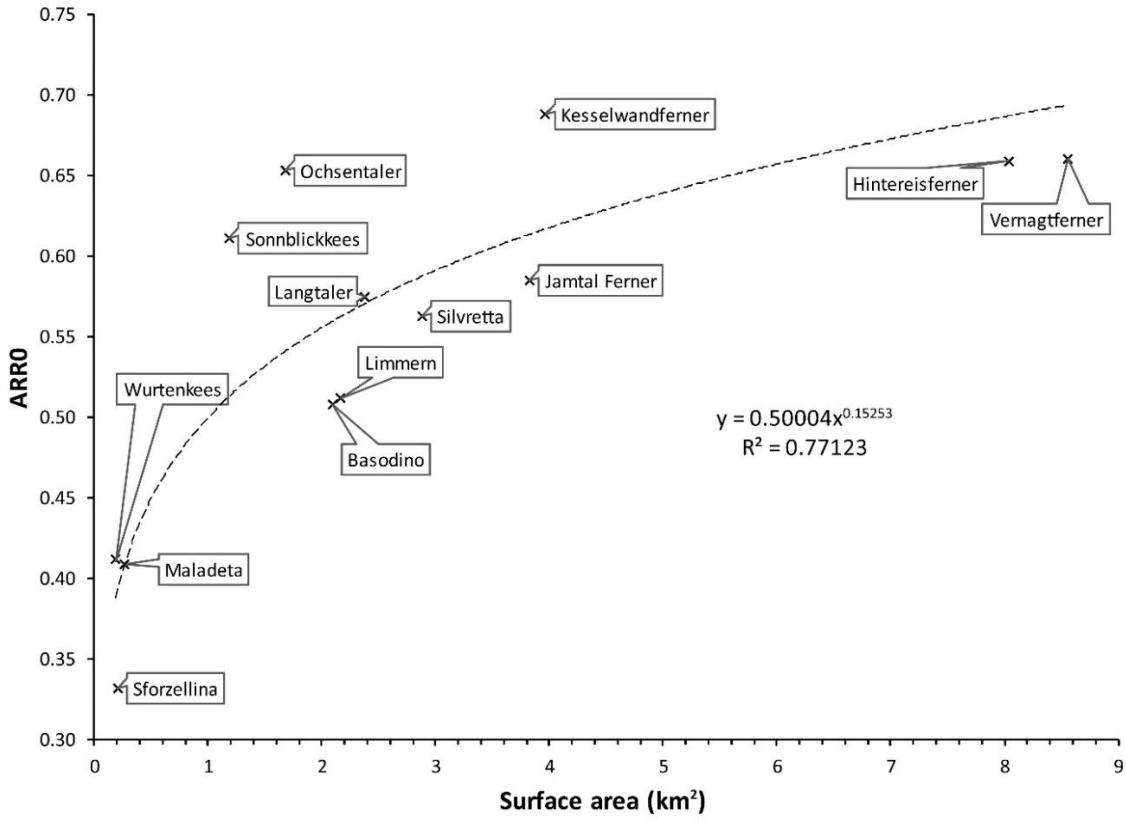

CH5 - Figure S8 | Plot establishing the relationship between AAR_0 and surface area of a glacier*. Each cross is a glacier from the dataset above (Table S8). The dashed line is a regression curve with its power law and regression coefficient displayed.*

The following relationship has been used for the calculation involved in the AAR method: $\boldsymbol{AAR = 0.50004 \times S^{0.15253}}$ where AAR is the accumulation area ratio for one particular glacier and S is its surface area in km^2.

References

1 Huss, M. & Farinotti, D. Distributed ice thickness and volume of all glaciers around the globe. *J Geophys Res-Earth* **117**, doi:10.1029/2012jf002523 (2012).

2 Arendt, A. *et al.* Randolph Glacier Inventory – A Dataset of Global Glacier Outlines: Version 5.0. (2015).

3 ©Google. Google Earth Imagery. Software available online at https://www.google.com/earth/ . Data accessed 07/09/2015 – 15/09/2015.

4 Reznichenko, N., Davies, T., Shulmeister, J. & McSaveney, M. Effects of debris on ice-surface melting rates: an experimental study. *Journal of Glaciology* **56**, 384-394, doi:10.3189/002214310792447725 (2010).

5 Lardeux, P., Glasser, N., Holt, T. & Hubbard, B. Glaciological and geomorphological map of Glacier Noir and Glacier Blanc, French Alps. *Journal of Maps*, 1-15, doi:10.1080/17445647.2015.1054905 (2015).

6 Pfeffer, W. T. *et al.* The Randolph Glacier Inventory: a globally complete inventory of glaciers. *Journal of Glaciology* **60**, 537-552, doi:10.3189/2014JoG13J176 (2014).

7 Huss, M. Present and future contribution of glacier storage change to runoff from macroscale drainage basins in Europe. *Water Resources Research* **47**, 14, doi:10.1029/2010wr010299 (2011).

8 Bahr, D. B., Pfeffer, W. T. & Kaser, G. A review of volume-area scaling of glaciers. *Reviews of Geophysics* **53**, 95-140, doi:Doi 10.1002/2014rg000470 (2015).

9 Bahr, D. B., Meier, M. F. & Peckham, S. D. The physical basis of glacier volume-area scaling. *J Geophys Res-Sol Ea* **102**, 20355-20362, doi:10.1029/97jb01696 (1997).

10 Chen, J. & Ohmura, A. Estimation of Alpine glacier water resources and their change since the 1870s. *IAHS Publ* (1990).

CHAPTER 6: Discussion and conclusions

The goal of this Chapter is to summarise the findings of each article and place them in the general context of the impact and importance of debris-covered glaciers in the European Alps.

Discussion

One of the key methods developed in this thesis is the application of SfM to historical images without specific fieldwork in order to answer questions about glacier change. In particular, this technique was used to answer Question A (comparing behaviour of debris-covered and clean-ice glaciers over the long term and the origins of the differences) presented in Chapter 1. Since this technique underpins much of the thesis, answering Question C (testing the viability of SfM with historical glacier images) forms the first element of this discussion.

Chapter 3 assessed the limitations and uncertainties linked to this usage of SfM in glaciology. Using this fast and inexpensive method, it is possible to achieve georeferencing within 10 m with only 2 images and 5 control points. However, the best results can be achieved with a minimum of 9 images and 10 control points on any given study area. The intrinsic limitations of the method (vertical resolution, image saturation, lack of camera calibration) does not allow it to be used alone for a study, as outlined in Chapter 4. Using SfM on historical images on the entire Glacier Noir/Glacier Blanc site allowed an orthoimage and DEM to be constructed for a time slice as early as 1952. This 'landscape scale' application of the method would have been improved by recovering old camera calibrations from the IGN, improving control points definition (mostly using fieldwork measurements) and more automation.

From a glaciological point of view, Chapters 3 and 4 demonstrated the ability of this method to provide glaciological measurements in areas not previously studied, making it a useful and complementary tool in the glaciology field.

Concerning the first part of question A (different behaviour between debris-covered glaciers and clean-ice glaciers), Chapter 4 showed that Glacier Noir and Glacier Blanc behaved differently over the course of 200 years in certain aspects (length and surface elevation). While both glaciers shrunk by the same area (~3km^2), Glacier Blanc receded by twice the linear distance of Glacier Noir. Additionally, the surface lowering of Glacier Blanc was in places twice that of Glacier Noir. Even in the absence of long-term surface velocity measurements, it appears that Glacier Noir flows much more slowly than Glacier Blanc.

As mentioned in Chapter 1, not all the controls regulating glacier behaviour over the long term can be resolved during this PhD project, leaving further questions to be answered about the second part of question A (the origins of difference in behaviour). With a similar climate and direct solar radiation, but different surface state (debris or not) and terminus bedrock topography, and unknown micro-climate and basal conditions, it remains difficult to conclude that the debris layer of Glacier Noir is solely responsible for the difference in behaviour. However, nuances in geometric changes experienced by both glaciers point toward a strong impact of the debris layer compared to the other controls, especially considering the following thought experiment. Assume that Glacier Noir and Glacier Blanc are both clean-ice glaciers. Even if both glaciers are very similar, Glacier Noir remains slightly smaller, lower and flatter, which should under the climatic conditions make Glacier Noir the fast retreating, shrinking and thinning glacier. However, the reverse is happening. It seems unlikely that the basal condition and micro-climate alone can produce such large differences. It should be noted that the recession rate difference is probably partially controlled by the bed topography at the terminus (local scale and not glacier-wide scale). The debris layer and its insulation effect is most probably the major control explaining the glacier-wide difference between Glacier Noir and Glacier Blanc.

Future work to confirm or refute this hypothesis would include extending fieldwork measurements, such as GNSS velocity and elevation measurements, full hydrological studies on both glaciers and conducting glaciological or geodetical mass balance studies. Additionally, these measurements should be repeated for several consecutive years and both glaciers should be observed extensively by surveying Glacier Noir Sud and the upper Glacier Blanc. To better understand the sub-range, i.e. the Pelvoux area, all these observations could be extended to the surrounding glaciers. Concerning the ablation stakes technique, it should be adjusted to cope with the specificities of debris-covered glaciers. For example, paint can be used to accurately mark the position of the stake relative to the supraglacial rocks (see Appendix [II]). The use of a time-lapse camera seems promising to study more finely the dynamics of Glacier Noir and Glacier Blanc, especially as the National Park already has one of these cameras pointing toward Glacier Blanc. An appropriate spot is needed for the same observation on Glacier Noir. More research in the archive of the National Park could help to complete the time-series of the glaciers' front position. Finally, full numerical modelling of

Glacier Noir with the debris layer and Glacier Blanc should be conducted with the latest available numerical models.

The inventory established in Chapter 5 demonstrated the glaciological importance of debris-covered glaciers in the European Alps, and thus helped to answer Question B (the importance of debris-covered glaciers at a mountain range scale). According to this new inventory and classification, debris-type glaciers represent 12% of the total number of glacier in the Alps, more than 40% of the glacial surface area and 50-60% of the ice volume. If only the debris is considered, 6% of the glacial surface area is covered, representing 6% of the ice volume. Even if the ice volume covered by debris remains small, the ice volume that is or will be affected and influenced by a debris layer represents half of all the Alpine ice. Additionally, the geometric characteristics of debris-covered glaciers set them clearly apart from clean-ice glaciers: they are on average larger, thicker and flatter.

There are still large uncertainties in understanding the hydrological (and thus the human) impact of debris-type glaciers in the European Alps, but the first approach described in Chapter 5 provided some insights into the present and future contribution of this type of glacier to the Alpine runoff. With only 1% of the total runoff for the 1908-2008 period, debris-type glaciers are not critical to the fresh water supply for the entire Alpine watershed. However, in mountain areas where the water supply relies on supraglacial melt, debris-type glaciers contribution represents 30% of the runoff. By 2100, the contribution to total runoff of all Alpine glaciers is expected to decrease dramatically. However, in proportion, the contribution of debris-type glaciers will rise to the point where they become the main source of supraglacial water for the entire Alpine watershed around the year 2114.

Overall the answer to Question B could be refined by improving the inventory (using images of the same year for the entire Alps to determine glacier surface area, resolving the undetermined glaciers, using a finer digital elevation model to improve the global hypsometry, re-digitising clean-ice glaciers that were counted in double or triple, running the ice thickness model considering the new outlines of glaciers and debris layer with their specificities) and decreasing the uncertainties on the runoff contributions (running the same hydrological model integrating specifically the debris-covered glaciers and also the Adige catchment) Model runs could also incorporate different climate scenarios, especially those developed by the Intergovernmental Panel on Climate Change (IPCC, 2013).

With the answers to question A and B, it is not currently possible to upscale the behaviour of Glacier Noir and Glacier Blanc to the entire European Alps. However, it is possible to compare them to the average Alpine glacier of their respective type. The case of Glacier Noir / Glacier Blanc (GNGB) shows mixed tendencies compared to the average debris-covered glacier (DCG) and clean-ice glacier (CIG) in the European Alps. DCG are generally longer than CIG and it is the contrary for GNGB. DCG are generally flatter than CIG which is true for GNGB (CH4 – Figure S5). DCG are generally larger in surface area (contrary for GNGB) and volume than CIG (no data for GNGB) but their elevation distribution is more balanced at each elevation range (true for GNGB). DCG are generally thicker (no data for GNGB). Finally, Glacier Noir is slower and is thinning less than Glacier Blanc but there are no data to demonstrate that this finding can be upscaled to the entire Alps.

Overall conclusion

Methodologically speaking, the viability of applying modern techniques such as SfM on old data such as historical glacier images without using new field data was demonstrated from an experimental point-of-view (Chapter 3) and an operational point-of-view (Chapter 4) to evaluate the evolution of Glacier Noir and Glacier Blanc. Some limitations of this variation in the established SfM technique were also shown, which need to be considered for future work. This method was complemented with others to balance the results with the reality of the field (GNSS measurements) and to cover a wider spectrum in the analysis (hydrological runoff modelling).

In conclusion, the impact and importance of debris-covered glaciers in the European Alps was approached from two different angles: the glacier-wide scale and the mountain range scale. Both scales provide different information: the local scale brings details on the individual behaviour of debris-covered glaciers, and at the same time, the regional scale brings a generalised understanding of the characteristics of this type of glacier. On the glacier scale, the evidence seems to correspond to what is expected with the insulation effect of the debris layer. There is individual variation, as demonstrated by Glacier Noir, but it is clear that debris-covered glaciers are distinguishable from clean-ice glaciers, even if they have similar geometries and evolve under the same climatic conditions, as in the case of Glacier Noir and Glacier Blanc. On the mountain range scale, debris-covered glaciers are more important in number, area and volume, than previously thought.

Overall, when considered at a larger scale than usual, debris-covered (and in general debris-type) glaciers are of first order importance for the cryosphere, hydrosphere and geosphere in the European Alps. The overall conclusion of this thesis is that, by the end of the 21st century, they will become critical to human societies as a major water resource.

REFERENCES

©GOOGLE Google Earth Imagery, 2015-2016.

AZZONI, R. S., SENESE, A., ZERBONI, A., MAUGERI, M., SMIRAGLIA, C. & DIOLAIUTI, G. A. 2016. Estimating ice albedo from fine debris cover quantified by a semi-automatic method: the case study of Forni Glacier, Italian Alps. *The Cryosphere,* 10**,** 665-679.

BANERJEE, A. & SHANKAR, R. 2014. Estimating the avalanche contribution to the mass balance of debris covered glaciers. *The Cryosphere Discussions,* 8**,** 641-657.

BENN, D. I., BOLCH, T., HANDS, K., GULLEY, J., LUCKMAN, A., NICHOLSON, L. I., QUINCEY, D., THOMPSON, S., TOUMI, R. & WISEMAN, S. 2012. Response of debris-covered glaciers in the Mount Everest region to recent warming, and implications for outburst flood hazards. *Earth-Science Reviews,* 114**,** 156-174.

BENN, D. I., WISEMAN, S. & HANDS, K. A. 2001. Growth and drainage of supraglacial lakes on debris-mantled Ngozumpa Glacier, Khumbu Himal, Nepal. *Journal of Glaciology,* 47**,** 626-638.

BROUGH, S., HUBBARD, B. & HUBBARD, A. 2016. Former extent of glacier-like forms on Mars. *Icarus,* 274**,** 37-49.

BRUN, F., BURI, P., MILES, E. S., WAGNON, P., STEINER, J., BERTHIER, E., RAGETTLI, S., KRAAIJENBRINK, P., IMMERZEEL, W. W. & PELLICCIOTTI, F. 2016. Quantifying volume loss from ice cliffs on debris-covered glaciers using high-resolution terrestrial and aerial photogrammetry. *Journal of Glaciology,* 62**,** 684-695.

CACCIANIGA, M., ANDREIS, C., DIOLAIUTI, G., D'AGATA, C., MIHALCEA, C. & SMIRAGLIA, C. 2011. Alpine debris-covered glaciers as a habitat for plant life. *The Holocene,* 21**,** 1011-1020.

CAPT, M., BOSSON, J. B., FISCHER, M., MICHELETTI, N. & LAMBIEL, C. 2016. Decadal evolution of a very small heavily debris-covered glacier in an Alpine permafrost environment. *Journal of Glaciology,* 62**,** 535-551.

CARRASCO, R. M., PEDRAZA, J., DOMÍNGUEZ-VILLAR, D., WILLENBRING, J. K. & VILLA, J. 2013. Supraglacial Debris Supply in the Cuerpo de Hombre paleoglacier (Spanish Central System): Reconstruction and Interpretation of a Rock Avalanche Event. *Geografiska Annaler: Series A, Physical Geography,* 95**,** 211-226.

CLARKE, G. K. C., JAROSCH, A. H., ANSLOW, F. S., RADIĆ, V. & MENOUNOS, B. 2015. Projected deglaciation of western Canada in the twenty-first century. *Nature Geoscience,* 8**,** 372-377.

DAVIES, B. J., GLASSER, N. F., CARRIVICK, J. L., HAMBREY, M. J., SMELLIE, J. L. & NÝVLT, D. 2013. Landscape evolution and ice-sheet behaviour in a semi-arid polar environment: James Ross Island, NE Antarctic Peninsula. *Geological Society, London, Special Publications,* 381**,** 353-395.

DE BLASIO, F. V. 2014. Friction and dynamics of rock avalanches travelling on glaciers. *Geomorphology,* 213**,** 88-98.

DELINE, P., HEWITT, K., REZNICHENKO, N. & SHUGAR, D. 2015. Rock Avalanches onto Glaciers. *In:* DAVIES, T. (ed.) *Landslide Hazards, Risks, and Disasters.* Elsevier.

ÉCRINS, P. N. D. 2005. Territoire Écrins - Les Cahiers Thematiques du Parc National: Les glaciers. *In:* ÉCRINS, P. N. D. (ed.).

EVATT, G. W., ABRAHAMS, D. I., HEIL, M., MAYER, C., KINGSLAKE, J., MITCHELL, S. L., FOWLER, A. C. & CLARK, C. D. 2015. Glacial melt under a porous debris layer. *Journal of Glaciology,* 61**,** 825-836.

FYFFE, C. L. 2012. *The hydrology of debris-covered glaciers.* PhD, University of Dundee.

FYFFE, C. L., REID, T. D., BROCK, B. W., KIRKBRIDE, M. P., DIOLAIUTI, G., SMIRAGLIA, C. & DIOTRI, F. 2014. A distributed energy-balance melt model of an alpine debris-covered glacier. *Journal of Glaciology,* 60**,** 587-602.

HALES, T. C. & ROERING, J. J. 2005. Climate-controlled variations in scree production, Southern Alps, New Zealand. *Geology,* 33**,** 701.

HAMBREY, M. J., QUINCEY, D. J., GLASSER, N. F., REYNOLDS, J. M., RICHARDSON, S. J. & CLEMMENS, S. 2008. Sedimentological, geomorphological and dynamic context of debris-mantled glaciers, Mount Everest (Sagarmatha) region, Nepal. *Quaternary Science Reviews,* 27**,** 2361-2389.

HAMILTON, S. J. & WHALLEY, W. B. 1995. Rock glacier nomenclature: A re-assessment. *Geomorphology,* 14**,** 73-80.

HARITASHYA, U. K., PLEASANTS, M. S. & COPLAND, L. 2015. Assessment of the Evolution in Velocity of Two Debris-Covered Valley Glaciers in Nepal and New Zealand. *Geografiska Annaler: Series A, Physical Geography,* 97**,** 737-751.

HUBBARD, B., SOUNESS, C. & BROUGH, S. 2014. Glacier-like forms on Mars. *The Cryosphere,* 8**,** 2047-2061.

HUSS, M. 2011. Present and future contribution of glacier storage change to runoff from macroscale drainage basins in Europe. *Water Resources Research,* 47**,** 14.

HUSS, M. & FARINOTTI, D. 2012. Distributed ice thickness and volume of all glaciers around the globe. *Journal of Geophysical Research: Earth Surface,* 117**,** n/a-n/a.

IMMERZEEL, W. W., KRAAIJENBRINK, P. D. A., SHEA, J. M., SHRESTHA, A. B., PELLICCIOTTI, F., BIERKENS, M. F. P. & DE JONG, S. M. 2014. High-resolution monitoring of Himalayan glacier dynamics using unmanned aerial vehicles. *Remote Sensing of Environment,* 150**,** 93-103.

IMMERZEEL, W. W., PELLICCIOTTI, F. & BIERKENS, M. F. P. 2013. Rising river flows throughout the twenty-first century in two Himalayan glacierized watersheds. *Nature Geoscience,* 6**,** 742-745.

IMMERZEEL, W. W., VAN BEEK, L. P. & BIERKENS, M. F. 2010. Climate change will affect the Asian water towers. *Science,* 328**,** 1382-5.

IPCC 2013. *Climate Change 2013: The Physical Science Basis. Contribution of Working Group I to the Fifth Assessment Report of the Intergovernmental Panel on Climate Change,* Cambridge, United Kingdom and New York, NY, USA, Cambridge University Press.

JACOB, T., WAHR, J., PFEFFER, W. T. & SWENSON, S. 2012. Recent contributions of glaciers and ice caps to sea level rise. *Nature,* 482**,** 514-8.

JUEN, M., MAYER, C., LAMBRECHT, A., WIRBEL, A. & KUEPPERS, U. 2013. Thermal Properties of a Supraglacial Debris Layer with Respect to Lithology and Grain Size. *Geografiska Annaler: Series A, Physical Geography,* 95**,** 197-209.

KERR, R. A. 2013. Glaciology. Melting glaciers, not just ice sheets, stoking sea-level rise. *Science,* 340**,** 798.

KIRKBRIDE, M. P. 2011. Debris-covered glaciers. *In:* SINGH, V. P., SINGH, P. & HARITASHYA, U. K. (eds.) *Encyclopedia of snow, ice and glaciers.* Dordrecht: Springer.

LARDEUX, P., GLASSER, N., HOLT, T. & HUBBARD, B. 2015. Glaciological and geomorphological map of Glacier Noir and Glacier Blanc, French Alps. *Journal of Maps,* 12**,** 582-596.

LE MEUR, E., GERBAUX, M., SCHÄFER, M. & VINCENT, C. 2007. Disappearance of an Alpine glacier over the 21st Century simulated from modeling its future surface mass balance. *Earth and Planetary Science Letters,* 261**,** 367-374.

LEJEUNE, Y., BERTRAND, J.-M., WAGNON, P. & MORIN, S. 2013. A physically based model of the year-round surface energy and mass balance of debris-covered glaciers. *Journal of Glaciology,* 59**,** 327-344.

LLIBOUTRY, L. 1965. *Traité de glaciologie - Glaciers, Variations du Climat, Sols Gelés*, Masson & Cie.

MARANGUNIC, C. 1972. Effects of a landslide on Sherman Glacier, Alaska. Columbus: Institute of Polar Studies.

MIHALCEA, C., MAYER, C., DIOLAIUTI, G., D'AGATA, C., SMIRAGLIA, C., LAMBRECHT, A., VUILLERMOZ, E. & TARTARI, G. 2008. Spatial distribution of debris thickness and melting from remote-sensing and meteorological data, at debris-covered Baltoro glacier, Karakoram, Pakistan. *Annals of Glaciology,* 48**,** 49-57.

MILES, E. S., WILLIS, I. C., ARNOLD, N. S., STEINER, J. & PELLICCIOTTI, F. 2016. Spatial, seasonal and interannual variability of supraglacial ponds in the Langtang Valley of Nepal, 1999–2013. *Journal of Glaciology,* 63**,** 88-105.

MILES, K. E., HUBBARD, B., IRVINE-FYNN, T. D. L., MILES, E. S., QUINCEY, D. J. & ROWAN, A. V. 2017. Review article: The hydrology of debris-covered glaciers – state of the science and future research directions. *The Cryosphere Discussions***,** 1-48.

NAGAI, H., FUJITA, K., NUIMURA, T. & SAKAI, A. 2013. Southwest-facing slopes control the formation of debris-covered glaciers in the Bhutan Himalaya. *The Cryosphere,* 7**,** 1303-1314.

NAKAWO, M., FOUNTAIN, A. & RAYMOND, C. F. 2000. Debris-covered glaciers. *Debris-covered Glaciers: Proceedings of an International Workshop Held at the University of Washington in Seattle, Washington, USA, 13-15 September 2000***,** 288.

NICHOLSON, L. & BENN, D. I. 2013. Properties of natural supraglacial debris in relation to modelling sub-debris ice ablation. *Earth Surface Processes and Landforms,* 38**,** 490-501.

ØSTREM, G. 1971. Rock Glaciers and Ice-Cored Moraines, a Reply to D. Barsch. *Geografiska Annaler. Series A, Physical Geography,* 53**,** 207.

PFEFFER, W. T., ARENDT, A. A., BLISS, A., BOLCH, T., COGLEY, J. G., GARDNER, A. S., HAGEN, J.-O., HOCK, R., KASER, G., KIENHOLZ, C., MILES, E. S., MOHOLDT, G., MÖLG, N., PAUL, F., RADIĆ, V., RASTNER, P., RAUP, B. H., RICH, J. & SHARP, M. J. 2014. The Randolph Glacier Inventory: a globally complete inventory of glaciers. *Journal of Glaciology,* 60**,** 537-552.

RADIĆ, V. & HOCK, R. 2011. Regionally differentiated contribution of mountain glaciers and ice caps to future sea-level rise. *Nature Geoscience,* 4**,** 91-94.

REZNICHENKO, N., DAVIES, T., SHULMEISTER, J. & MCSAVENEY, M. 2010. Effects of debris on ice-surface melting rates: an experimental study. *Journal of Glaciology,* 56**,** 384-394.

REZNICHENKO, N. V., DAVIES, T. R. H. & ALEXANDER, D. J. 2011. Effects of rock avalanches on glacier behaviour and moraine formation. *Geomorphology,* 132**,** 327-338.

RÖHL, K. 2008. Characteristics and evolution of supraglacial ponds on debris-covered Tasman Glacier, New Zealand. *Journal of Glaciology,* 54**,** 867-880.

ROUNCE, D. R., QUINCEY, D. J. & MCKINNEY, D. C. 2015. Debris-covered glacier energy balance model for Imja–Lhotse Shar Glacier in the Everest region of Nepal. *The Cryosphere,* 9**,** 2295-2310.

ROWAN, A. V., EGHOLM, D. L., QUINCEY, D. J. & GLASSER, N. F. 2015. Modelling the feedbacks between mass balance, ice flow and debris transport to predict the response to climate change of debris-covered glaciers in the Himalaya. *Earth and Planetary Science Letters,* 430**,** 427-438.

SAKAI, A., TAKEUCHI, N., FUJITA, K. & NAKAWO, M. Role of supraglacial ponds in the ablation process of a debris-covered glacier in the Nepal Himalayas. Debris-covered Glaciers: Proceedings of an International Workshop Held at the University of Washington in Seattle, Washington, USA, 13-15 September 2000, 2000. IAHS, 119-132.

SANTAMARIA TOVAR, D., SHULMEISTER, J. & DAVIES, T. R. 2008. Evidence for a landslide origin of New Zealand's Waiho Loop moraine. *Nature Geoscience,* 1**,** 524-526.

SASAKI, O., NOGUCHI, O., ZHANG, Y., HIRABAYASHI, Y. & KANAE, S. 2016. A global high-resolution map of debris on glaciers derived from multi-temporal ASTER images. *The Cryosphere Discussions***,** 1-24.

SCHAUWECKER, S., ROHRER, M., HUGGEL, C., KULKARNI, A., RAMANATHAN, A. L., SALZMANN, N., STOFFEL, M. & BROCK, B. 2015. Remotely sensed debris thickness mapping of Bara Shigri Glacier, Indian Himalaya. *Journal of Glaciology,* 61**,** 675-688.

SHEAN, D. E. & MARCHANT, D. R. 2010. Seismic and GPR surveys of Mullins Glacier, McMurdo Dry Valleys, Antarctica: ice thickness, internal structure and implications for surface ridge formation. *Journal of Glaciology,* 56**,** 48-64.

SHUGAR, D. H., RABUS, B. T., CLAGUE, J. J. & CAPPS, D. M. 2012. The response of Black Rapids Glacier, Alaska, to the Denali earthquake rock avalanches. *Journal of Geophysical Research: Earth Surface,* 117**,** n/a-n/a.

SHULMEISTER, J., DAVIES, T. R., EVANS, D. J. A., HYATT, O. M. & TOVAR, D. S. 2009. Catastrophic landslides, glacier behaviour and moraine formation – A view from an active plate margin. *Quaternary Science Reviews,* 28**,** 1085-1096.

STEINER, J. F., PELLICCIOTTI, F., BURI, P., MILES, E. S., IMMERZEEL, W. W. & REID, T. D. 2015. Modelling ice-cliff backwasting on a debris-covered glacier in the Nepalese Himalaya. *Journal of Glaciology,* 61**,** 889-907.

STOTT, T., MOUNT, N., BENBOW, R., BROOKMAN, C., HEDGES, M., MILES, C., PATTON, S. & WINTER, J. 2004. Field investigations in Hydrology, Fluvial Geomorphology and GIS in the Ecrins National Park, France, July 2004. Liverpool John Moores University.

STOTT, T., MOUNT, N., COLSON, O., HUNTER, T., MCCULLOCH, R., NICHOLSON, J. & WISEMAN, G. 2006. Solutes, Suspended Sediment, Bedload and Channel Change Studies in the Ecrins National Park, France, July 2005. Liverpool John Moores University.

STOTT, T., MOUNT, N., MOORE, S., MCGUFFIE, A., MISZKOWSKI, M. & HAMMOND, P. 2003. Field Investigations in Physical Geography at the Glaciers Noir and Blanc, Parc National des Ecrins, Southern France, July-August 2003. Liverpool John Moores University.

VINCENT, C., WAGNON, P., SHEA, J. M., IMMERZEL, W. W., KRAAIJENBRINK, P. D. A., SHRESTHA, D., SORUCO, A., ARNAUD, Y., BRUN, F., BERTHIER, E. & SHERPA, S. F. 2016. Reduced melt on debris-covered glaciers: investigations from Changri Nup Glacier, Nepal. *The Cryosphere Discussions***,** 1-28.

VIVIAN, R. 1967. Le glacier Noir. *Revue de géographie alpine,* 55**,** 733-736.

WESTOBY, M. J., GLASSER, N. F., HAMBREY, M. J., BRASINGTON, J., REYNOLDS, J. M. & HASSAN, M. A. A. M. 2014. Reconstructing historic Glacial Lake Outburst Floods through numerical modelling and geomorphological assessment: Extreme events in the Himalaya. *Earth Surface Processes and Landforms,* 39**,** n/a-n/a.

WIRBEL, A., JAROSCH, A. H. & NICHOLSON, L. 2017. Modelling debris transport within glaciers by advection in a full-Stokes ice flow model. *The Cryosphere Discussions***,** 1-22.

WU, Z., ZHANG, S. & LIU, S. 2013. Optimal antenna of ground penetrating radar for depicting the debris thickness and structure of the Koxkar Glacier, Tianshan, China. *Journal of Earth Science,* 24**,** 830-842.

APPENDIX

[I] – Published version of Glaciological and geomorphological map of Glacier Noir and Glacier Blanc, French Alps

Journal of Maps, 2015
http://dx.doi.org/10.1080/17445647.2015.1054905

SCIENCE

Glaciological and geomorphological map of Glacier Noir and Glacier Blanc, French Alps

Pierre Lardeux*, Neil Glasser, Tom Holt and Bryn Hubbard

Department of Geography & Earth Sciences, Centre for Glaciology, Llandinam Building, Penglais Campus, Aberystwyth University, Aberystwyth SY23 3DB, UK

(*Received 20 February 2015; resubmitted 8 May 2015; accepted 21 May 2015*)

This paper presents and describes a glaciological and geomorphological map of Glacier Noir and Glacier Blanc, French Alps. Glacier Noir is a debris-covered glacier and is adjacent to Glacier Blanc, a clean-ice (debris-free) glacier. The glaciological and geomorphological evolution of Glacier Blanc is well known, but the evolution of Glacier Noir is poorly understood, as is the case for many debris-covered glaciers globally, despite their importance in a number of mountain ranges around the world (e.g. European and Southern Alps, the Himalayas and the Rockies). The accompanying map was created by manually digitising aerial ortho-images and historical georeferenced photographs from 1952 to 2013. The main glacial and geomorphological features of both glaciers were mapped, including debris cover, crevasses, moraines, hummocky terrain and scree areas. Hydrological features (supra- and pro-glacial streams and meltwater ponds) were also mapped. The map illustrates the key differences between Glacier Noir and Glacier Blanc, and is important for understanding future glaciological and geomorphological changes.

Keywords: glaciology; geomorphology; hydrology; debris-covered glacier; Glacier Noir; Glacier Blanc

1. Introduction

Mountain glaciers are currently contributing ~27% of the observed global sea-level rise with a large uncertainty of more than 20% (Jacob, Wahr, Pfeffer, & Swenson, 2012). Although the contribution of debris-free or clean-ice glaciers is well known, debris-covered glaciers and their contribution are still poorly understood. Debris-covered or debris-mantled glaciers are those where part of the surface of the ablation area is covered by a layer of rock debris including dust, ash and boulders of various sizes (Cogley et al., 2011; Hambrey et al., 2008; Singh, Singh, & Haritashya, 2011).

Debris-covered glaciers represent ~5% of all mountain glaciers worldwide (WGMS & NSIDC, [1989] 2012) and the rate of sea-level rise attributed to them differs from clean-ice glaciers due to the insulating effect of the debris layer (Reznichenko, Davies, Shulmeister, & Mcsaveney, 2010). A better understanding of long-term glaciological processes on debris-covered glaciers is needed to reduce the uncertainty of their contribution to global sea level.

*Corresponding author. Email: pfl4@aber.ac.uk

The debris layer on debris-covered glaciers derives from a number of sources, most notably valley-side rockfalls (Deline & Kirkbride, 2009). These rockfalls can be significant at the glacier-scale, such as is the case for the Black Rapids Glacier (Shugar, Rabus, Clague, & Capps, 2012) and the Sherman Glacier (Marangunic, 1972). These rock avalanches form specific deposits characterised by the regular thickness of the debris layer and angular grains (Hewitt, 2009). Other sources of debris include collapsing lateral moraines (Hambrey & Ehrmann, 2004) and debris elevated from subglacial and englacial positions to supraglacial positions (Goodsell, Hambrey, & Glasser, 2005). The debris from these latter sources is more heterogeneous and may contain a mix of sub-angular to sub-rounded grains.

The supply of surface debris to the glacier's terminus has great control over the geomorphological processes occurring on and adjacent to that glacier (Reznichenko, Davies, & Alexander, 2011) and often results in the formation of very large geomorphological features, such as the Waiho Loop moraine in the Southern Alps, New Zealand (Tovar, Shulmeister, & Davies, 2008). From a glaciological perspective, the elevation of the snout of a debris-covered glacier would be lower than that of a similar clean-ice glacier. Specific glaciological and geomorphological dynamics of a debris-covered glacier are beginning to be considered in the interpretation of glaciated landscapes and landforms (Carrasco, Pedraza, Dominguez-Villar, Willenbring, & Villa, 2013; Reznichenko, Davies, Shulmeister, & Winkler, 2012). Accurate interpretation and attribution of features to debris-covered glaciers can lead to re-interpretation of palaeo-climatic conditions contributing to their formation (Shulmeister, Davies, Evans, Hyatt, & Tovar, 2009; Vacco, Alley, & Pollard, 2010).

Here, a detailed Main Map is presented in order to provide the basis for investigating the geomorphological context of, and relationships between, a debris-covered glacier (Glacier Noir) and an adjacent and morphometrically similar clean-ice glacier (Glacier Blanc). This map will also help the re-interpretation of palaeo-landforms where debris-covered glaciers may have contributed to their formation.

2. Study site

Located in the Haute Vallée de St Pierre in the 'Écrins' National Park (Parc National des Écrins) in the French Alps (Figure 1), Glacier Noir is a 4.5 km long debris-covered glacier with a surface area of 3.8 km^2. In contrast, the surface of adjacent Glacier Blanc is debris-free. Both glaciers were confluent in the Pré de Madame Carle field during the Little Ice Age (LIA, sixteenth to mid-nineteenth century, [Mann, 2002]). Pré de Madame Carle was a grazing field before it was transformed into an outwash plain by the advance of the combined glacier during the LIA (Letreguilly & Reynaud, 1989).

Glacier Noir (44°54′58″ N, 6°23′03″ E) has an elevation range of 2200–3600 m and comprises a main trunk (2200–2900 m in elevation) of 1.1 km^2 (2.6 km long), orientated WSW-ENE with a single tributary (2500–3600 m in elevation) of 2.7 km^2 (3.2 km long), orientated SSW-NNE. The tributary is now an independent glacier – named here Glacier Noir Sud – having separated from the main glacier between 2009 and 2013.

Glacier Blanc (44°56′25″ N, 6°22′42″ E) has an elevation range of 2500–4000 m and is 4.8 km^2 (5.5 km long), being orientated SW-NE in its upper section (3050–4000 m in elevation), which is relatively flat and then NW-SE in the steep crevassed area approaching its terminus (2500–3050 m in elevation). This main trunk is fed by six individual accumulation basins (cirques).

Both glaciers have attracted previous glaciological research, with Glacier Blanc being more widely studied (Allix, 1922, 1929; Letreguilly & Reynaud, 1989; Rabatel, Dedieu, & Reynaud, 2002; Rabatel, Dedieu, Thibert, Letreguilly, & Vincent, 2008; Rabatel, Letreguilly, Dedieu, &

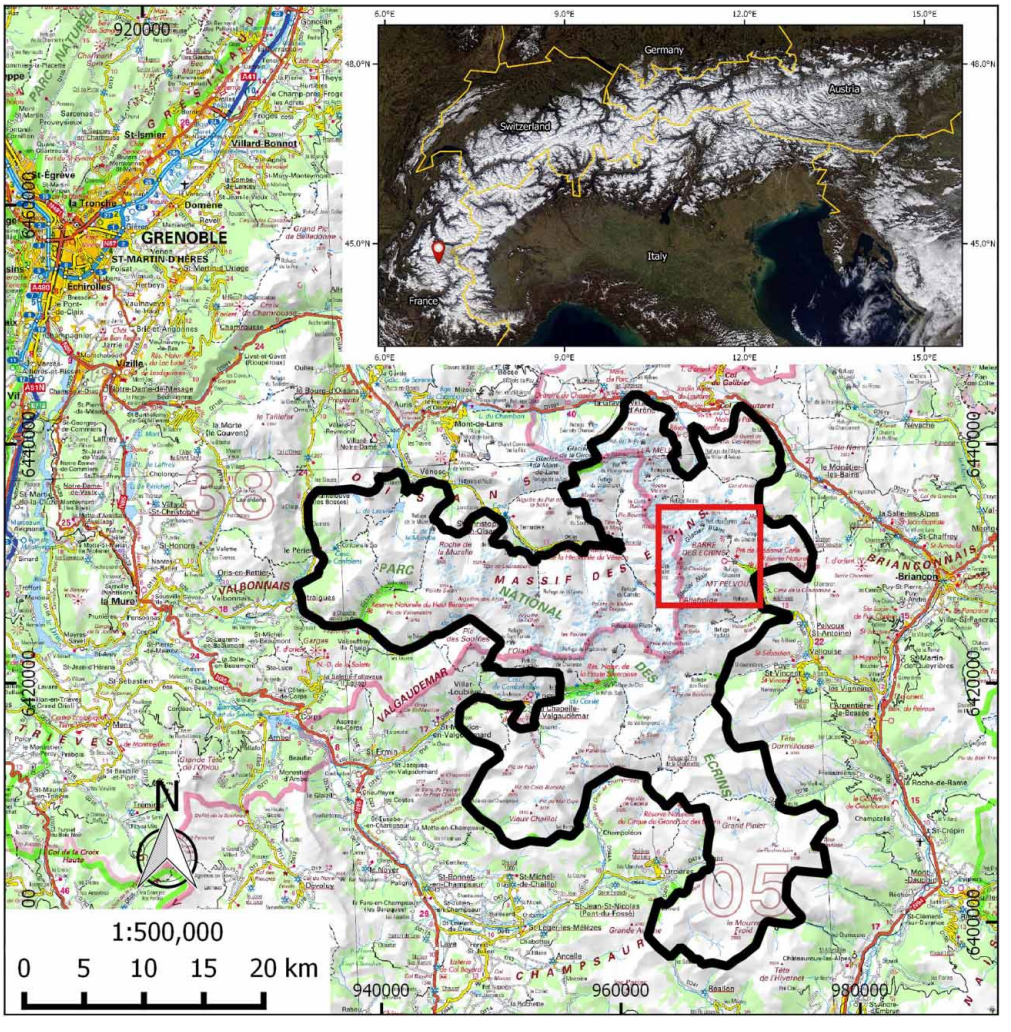

Figure 1. Overview map presenting the position of the study site (red rectangle) in 'Écrins' national park (solid black line). Background map: IGN ©SCANREGIONAL. Inset: location (red marker) of the study site in the European Alps. Background Image: ©NASA.

Eckert, 2013; Reynaud & Vincent, 2000, 2002; Thibert, Faure, & Vincent, 2005; Vivian, 1967a) than Glacier Noir (Allix, 1922, 1929; Cossart, Fort, Jomelli, & Grancher, 2006; Mount & Stott, 2008; Stott & Mount, 2007; Vivian, 1967b). The most recent studies have focused on sediment transport in the proglacial stream at Glacier Noir and on the variation of the equilibrium line altitude (ELA) at Glacier Blanc and its determination using optical remote sensing.

3. Data and methods

3.1. *Data sources*

Mapping was conducted by manually digitising aerial ortho-images (six RGB tiles of 5 km by 5 km with a 50 cm resolution) using QGIS software (Section 3.2). The National Institute of

Geographic and Forestry Information (IGN) provided the ortho-images. These images are part of the French national database, © BDORTHO, and were taken during summer 2013.

The topography is derived from the IGN topographical map (Meije-Pelvoux 3436 ET), which is included in the database SCAN25. The scale of the map is 1:25,000.

The dates of formation of the moraines are from various sources:

- A public engagement booklet edited by the 'Écrins' National Park (Écrins, 2005) on the glaciers present in the park.
- Unpublished historical and archive documents owned by the 'Écrins' National Park.
- Archived ortho-images and georeferenced aerial photographs extracted from the historical IGN database. This database is the compilation of previous versions of the © BDORTHO, grouping aerial scenes from 1952 to 2009.

The archived ortho-images were also used for the photo-interpretation of moraines, which are sensitive to the position of shadows (Otto & Smith, 2013).

The interpretation of the ortho-images was verified and refined by direct field observation between mid-August and mid-September 2014, particularly where the ortho-images have shadowed areas or other areas where misinterpretation is possible. All ground-based photographs presented in this article and on the map were taken during the same period.

3.2. *Software and digitising tools*

All mapping and digitising was conducted using the geographic information system QGIS (QGIS, 2014). Multiple versions of QGIS have been used (see Software Section below) as well as the updated versions of the following plugins:

- autoSaver plugin, for automatic saves of the work in progress.
- Digitizing Tools plugin, for additional digitising options.
- GdalTools plugin, for elevation data extraction.
- Georeferencer GDAL plugin, for the georeferencing of the aerial images.
- GPS Tools plugin, for the import of field data.
- Multipart Split plugin, for better management of multiple features in the same layer.

The map was designed using QGIS. The ground-based photographs presented on the map were modified using Adobe Illustrator CS2.

The digitisation of the ortho-images was conducted within a scale range of 1:1000–1:10,000, allowing a global view of each feature across the study site's large altitudinal range.

3.3. Map design

3.3.1. *General principles*

The mapped features are divided into four themes with additional background data: glaciological, geomorphological, hydrological and anthropogenic. The different colour schemes used are theme dependent. Glaciological features are depicted using only black and white colours. Geomorphological features are depicted in brown to yellow colours. In addition, vegetated features are presented in dark green. Hydrological features (ponds and streams) are depicted using different hues of blue. Although not essential to the map's principal purpose, anthropogenic features

which provide important context (e.g. buildings) are depicted in grey. To bring contrast to the map, the background contour lines are depicted in light green.

3.3.2. *Specific digitising cases*

Moraines have been digitised only as moraine ridges. Ridges are the best indicators of the position of a moraine and so help to develop understanding of the retreat history of glaciers. Moraine extent has not been digitised to not overload the map. From field observations, crevasses and crevasse traces represent the large majority of structural features on Glacier Blanc and Glacier Noir. However, due to ortho-image resolution and the heavily disturbed area in the curve of Glacier Blanc, the recognition of foliations and/or lineations was particularly difficult, and consequently, some may have been digitised as crevasses.

In addition to digitising active and relict meltwater ponds, their areas of topographic influence (see Section 4.3.1) was also mapped as separate features because of their importance in the melting of debris-covered glaciers (Sakai, Takeuchi, Fujita, & Nakawo, 2000).

4. Description of the mapped features

4.1. *Glaciological features*

4.1.1. *Glacier outlines*

Glaciers were identified using the following definition: 'mass of ice presenting active flow pattern', which is a simplified version of the GLIMS definition (Rau, Mauz, Vogt, Khalsa, & Raup, 2005). This definition was used as a guide to outline digitisation of both glaciers, although defining the lateral and frontal boundaries was easier for Glacier Blanc (i.e. between clean ice and proglacial debris) than for the ablation area of Glacier Noir, where the debris cover makes the identification of the glacier limit (Figure 2) and flow patterns more difficult (Cogley et al., 2011; Paul et al., 2013).

4.1.2. *Debris cover*

For this map, we defined debris cover as where no clean ice is visible. The precise limits of debris-covered areas are difficult to define because of the continuous variations in debris concentration that are encountered in the field. In addition, the debris cover must have been persistent, that is, appearing in images separated by at least one year. By these criteria, no debris cover was mapped on Glacier Blanc because the debris-covered areas are temporary and localised, and are rapidly buried by snow in the accumulation area, or removed from the surface through crevasses in the ablation area.

4.1.3. *Crevasses*

Crevasses form when the extensional strain exceeds a critical threshold (Vaughan, 1993), resulting in fields of fractures with distinctive lengths and orientations. A fractured area is particularly visible on the lower section of Glacier Blanc where the glacier changes direction and becomes steeper.

On Glacier Noir, most of the crevasses are filled by debris that only leave traces of the crevasses visible on the surface. These crevasse traces create only low relief perturbations and are consequently not visible by direct observation in the field.

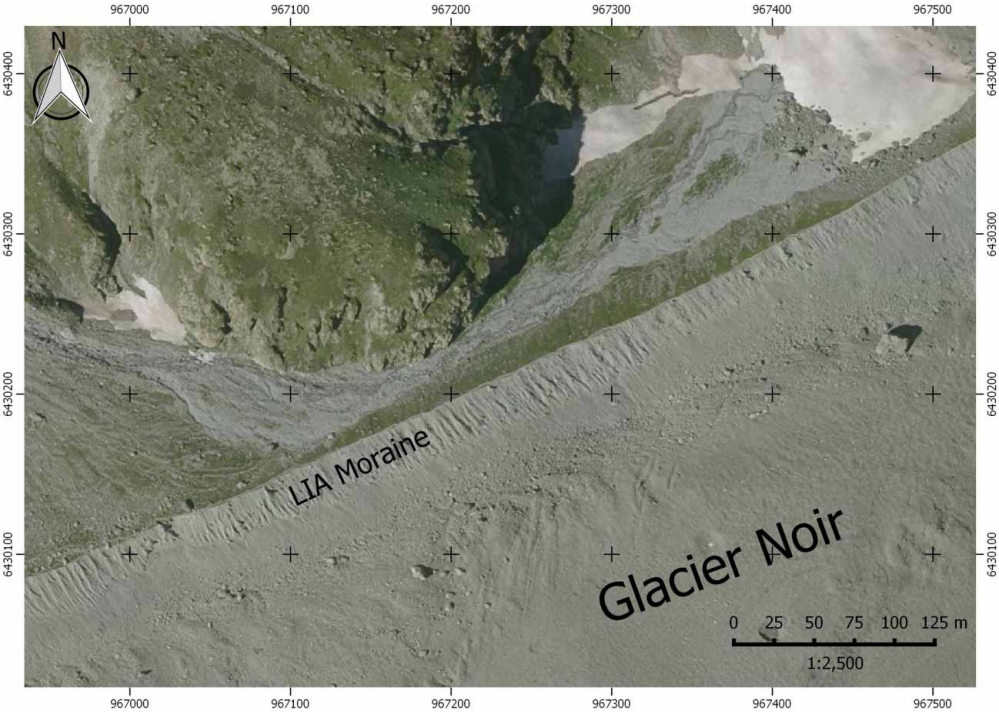

Figure 2. Extract of 2013 orthophotograph illustrating the difficulties in determining the edge of Glacier Noir, especially in the area between the northern border and the LIA moraine.

4.1.4. *Nunataks and bare-rock areas*

Nunataks are areas of glaciers where the bedrock is exposed (Singh et al., 2011). Nunataks and other bare-rock areas are mainly present on the south-facing side of Glacier Blanc. The locations of these rock exposures vary, as they are dependent on the ice thickness and ice flow. Consequently, the features mapped are only those present when the aerial images were acquired in 2013.

4.2. *Geomorphological features*

These features are all related to the former presence of a glacier.

4.2.1. *Moraines*

Moraines are landforms built by the deposition by glaciers of glacial sediments (Singh et al., 2011). There are many types of moraines (Bennett & Glasser, 2009); around Glacier Noir and Glacier Blanc, these are mostly frontal and lateral moraines and were mapped accordingly.

During the LIA, Glacier Noir and Glacier Blanc had a common terminus and produced a large moraine, like many other alpine glaciers. This LIA frontal moraine has been partially washed away by the proglacial stream, and currently, the only large LIA moraine intact is the lateral moraine of Glacier Noir. This moraine is recognisable because of its large size compared to the surrounding moraines (Figure 3).

Figure 3. Glacier Noir (white dotted line) and its LIA moraine (black dashed line). The LIA moraine is the largest geomorphological feature in the study site and its ridge is ~50–60 m above the surface of the glacier from the terminus to the headwall.

4.2.2. *Gullies*

Gullies are formed in areas of unconsolidated sediment where the runoff from rain and snowmelt creates micro-valleys. In the study site, most of the gullies are on the ice-proximal flanks of moraines.

The process of gullying is an active phenomenon (Figure 4) and was observed during heavy rainfall events during the fieldwork period. This process contributes widely to the erosion of moraines.

4.2.3. *Scree areas*

According to Singh et al. (2011), scree material (also called debris) is 'Unconsolidated sediment, larger than 1 mm, of angular or rounded angular fragments of boulders (clasts), predominantly

Figure 4. The new gullies (white arrows) created during a heavy rainfall event (26 August 2014) on the southern side of the LIA moraine of Glacier Noir.

originating from physical weathering'. Scree areas are steep zones of scree material. All the active scree areas around Glacier Noir and Glacier Blanc face SW to SE. Scree clast size is variable, ranging from pebble to boulder-size.

Three types of scree areas were mapped:

- Active scree areas where traces of rock falls are visible and where regular rock falls have been observed in the field. They are mainly located around the Glacier Noir catchment.

- Stabilised scree areas without traces of active rock falls located on the eastern side of the terminus of Glacier Blanc and above the outwash plain.
- Vegetated scree areas near the entrance of Haute Vallée de St-Pierre.

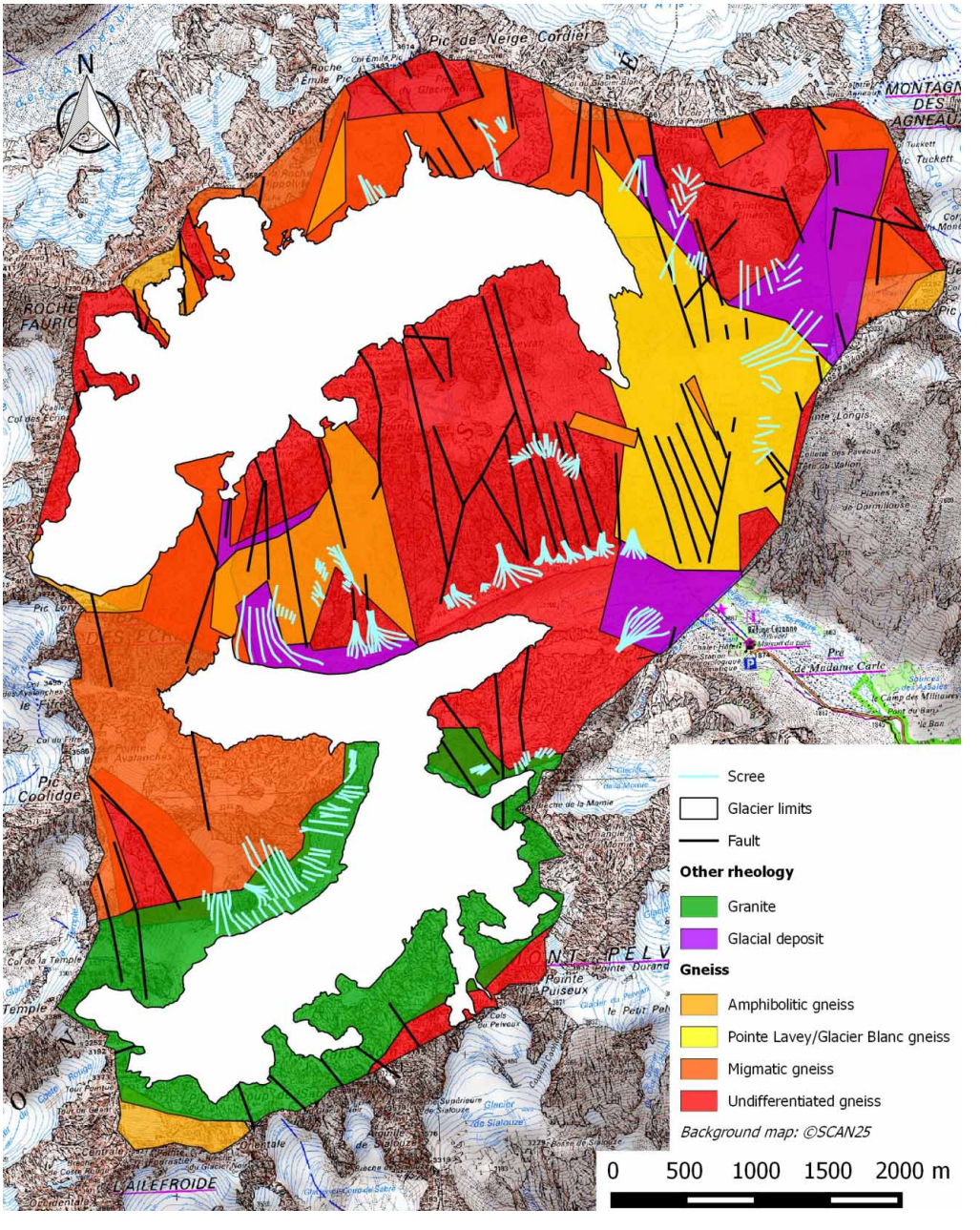

Figure 5. Geological map of the study site with superimposed scree areas. Geological variations (mainly gneiss except for Glacier Noir Sud with granite) in the study area cannot explain the origin of the scree areas. Slope orientation is the main factor in the scree production. Adapted from Bureau de Recherche Géologiques et Minières (BRGM) maps 0822N and 0823N.

Figure 5 presents the geological context for scree production. Production appears to be independent of lithology (gneiss or granite) and to be primarily driven by slope orientation (Nagai, Fujita, Nuimura, & Sakai, 2013).

4.2.4. *Hummocky terrain*

On the map, hummocky terrain (Figure 6) designates an assemblage of debris and glacial sediment pits and mounds including small, possibly ice-cored, moraines (Singh et al., 2011).

The hummocky terrain is located in the proglacial area of both glaciers and in a former lower accumulation cirque of Glacier Noir Sud. Like gullies, these areas are particularly active and their morphology evolves closely with the variation of the proglacial streams, especially during heavy rainfall events.

4.2.5. *Bedrock with incised channels*

Large areas of bedrock (gneiss) with incised channels are visible in front of Glacier Blanc, exposed as the glacier receded. Field observations confirm that some of the channels have subglacial origins and are probably Nye channels. Nye channels (or N-Channels) are subglacial channels directly carved into bedrock by meltwater discharge (Nye, 1973). Most of the visible channels are now abandoned except for those occupied by the glacier's main proglacial streams.

4.2.6. *Outwash plain*

An outwash plain is a large flat area covered with well-sorted glaciofluvial sediment. Braided rivers often develop widely in outwash plains, for example in Iceland where they are called 'sandur' because of the predominance of sand- and gravel-sized sediment across such plains. The proglacial streams of Glacier Noir and Glacier Blanc converge in the upper part of the outwash plain to form a dynamic braided stream system as shown in Figure 7 at two different dates.

Figure 6. Hummocky terrain in the proglacial area of Glacier Blanc. The hummocky moraines (green) are easily eroded by the proglacial stream. The frontal moraine (white) marks the lower limit of this hummocky area.

Figure 7. Outwash plain of Glacier Noir and Glacier Blanc. As a consequence of the heavy rainfall event of 26th August 2014, the proglacial stream shifted from the northern edge (left hand side image) of the outwash plain to the southern edge (right hand side image), illustrating this highly dynamic environment.

4.3. *Hydrological features*

4.3.1. *Meltwater ponds*

Meltwater ponds are depressions on the ice surface that are filled with water released by the melt of snow and ice. Numerous, often large, supraglacial meltwater ponds are a common feature on debris-covered glaciers. Indeed, such ponds form the basis of one key classification of the morphological evolution of debris-covered glaciers (Benn et al., 2012).

Meltwater ponds form by differential melting between debris-covered and clean-ice areas. Ablation of the latter is faster than the former, creating a depression – here called the area of topographic influence – where water can be stored. This process involves a positive feedback loop where the edge of the depression becomes steeper and so less debris-covered, inducing further melting and consequently steepening of the side. This feedback loop gradually expands the area of topographic influence of meltwater ponds.

However, these meltwater ponds are eventually drained supraglacially via a channel or englacially via crevasses. The drainage process creates relict/trace ponds (Figure 8) where the difference between the pond itself and the area of topographic influence is still visible.

4.3.2. *Streams*

Streams on the study site are produced by the melt of glaciers. They are found in two different positions: on the surface (supraglacial streams) and in front (proglacial streams) of both glaciers.

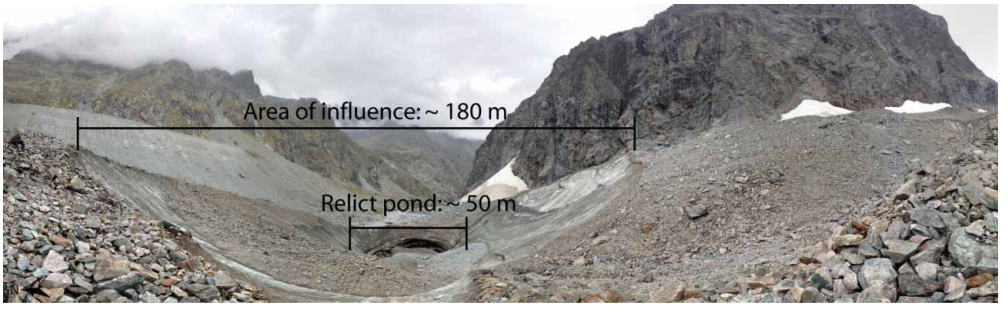

Figure 8. Relict meltwater pond and its area of influence at the terminus of Glacier Noir. The bottom of this pond collapsed into a subglacial channel between 2013 and 2014.

Due to the dynamics (water discharge, deposition of sediment) and ephemeral nature of proglacial streams, especially in the outwash plain, only principal active channels were mapped, illustrating the situation at the time the aerial images were acquired.

Supraglacial streams could only be observed on the debris-covered surface of Glacier Noir. Most of the mapped streams were restricted to the ablation area. No visual expression of supraglacial streams was found on aerial images of Glacier Blanc despite their presence in the field (Figure 9). Therefore, supraglacial streams were not mapped on Glacier Blanc.

4.4. *Anthropogenic features and elevation data*

The Glacier Noir and Glacier Blanc site is a tourist attraction in the 'Écrins' National Park and so buildings (three refuges, one visitor centre and public restroom facilities), roads and hiking trails were additionally mapped to provide context.

Contour lines from the IGN 1998 digital elevation model (DEM) were added as background information. To clarify the topographic context of the map, arête lines were added on to the DEM as well as some altitude points.

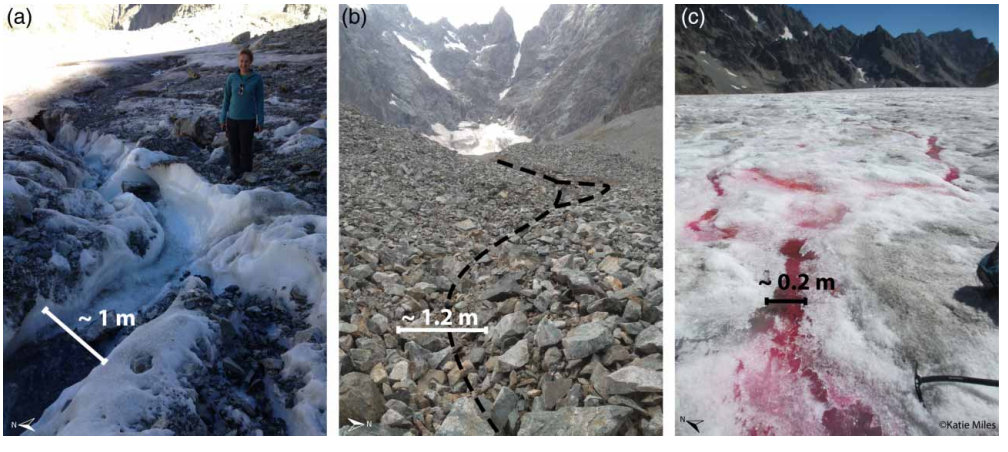

Figure 9. Various meltwater channels in the study area. (a) Active meltwater channel just below the accumulation area of Glacier Noir. (b) Trace of meltwater channels in the ablation area of Glacier Noir. (c) Active meltwater channels on Glacier Blanc highlighted by pink dye. Note the difference in scale between these images.

5. Conclusion

We describe here a new glaciological and geomorphological map of Glacier Noir and Glacier Blanc in the French Alps. The mapped features were divided into four different themes (glaciological, geomorphological, hydrological and anthropogenic) to facilitate the understanding of the map and future studies and comparisons. However, these four themes interact closely. Glacier Noir and Glacier Blanc are the main agents of sediment transport and deposition, creating a range of geomorphological features, from sand layers in the proglacial area to LIA moraines. The streams are, on the contrary, the main agents of erosion on the surface of Glacier Noir, acting to transfer sediment of the debris layer from the top of the glacier to the terminus, as well as eroding the proglacial terrain of both glaciers to create an outwash plain further downstream. Meltwater ponds are the perfect example of the interaction of glacial (melting of debris-free ice cliffs), geomorphological (back wasting of debris from the layer) and hydrological (storage and drainage of significant quantities of water) processes. Finally, anthropogenic features such as roads and bridges modify erosional/depositional patterns in a complex way, especially in the outwash plain.

Understanding these processes and their interactions is part of a larger research project on the impact of variations in supraglacial debris cover on glacier evolution and dynamic response to climatic forcing.

Software

Database development and map production were performed using QGIS 2.2, 2.4, 2.6, and 2.6.1. Additional QGIS plugins used include autoSaver, Digitizing Tools, GdalTools, Georeferencer GDAL, GPS Tools and Multipart Split. Figures on the map were edited using Adobe Illustrator CS2.

Acknowledgements

We would like to thank Stephen Jennings for his useful comments on the map and Patricia Gongal for her helpful comments on the manuscript.

Disclosure statement

No potential conflict of interest was reported by the authors.

Funding

The aerial images and orthophotographs were provided by the French National Institute of Geographic and Forestry Information under an education and research licence. The fieldwork season was possible, thanks to the ‘Ecrins’ National Park (activity authorisation 060/2014) and has been funded by the British Society for Geomorphology under the Postgraduate Research Grant programme and by the Department of Geography and Earth Sciences of Aberystwyth University under the Postgraduate Discretionary Research Fund programme.

ORCID

Pierre Lardeux http://orcid.org/0000-0001-7860-3053
Neil Glasser http://orcid.org/0000-0002-8245-2670
Bryn Hubbard http://orcid.org/0000-0002-3565-3875

References

Allix, A. (1922). Les glaciers des Alpes françaises en 1921. *Revue de géographie alpine*, *10*, 325–333.

Allix, A. (1929). Observations glaciologiques faites en dauphiné jusqu'en 1924. *Les Études rhodaniennes*, *5*, 185–186.

Benn, D. I., Bolch, T., Hands, K., Gulley, J., Luckman, A., Nicholson, L. I., … Wiseman, S. (2012). Response of debris-covered glaciers in the Mount Everest region to recent warming, and implications for outburst flood hazards. *Earth-Science Reviews*, *114*, 156–174.

Bennett, M. M., & Glasser, N. F. (2009). *Glacial geology: Ice sheets and landforms*. Chichester: John Wiley & Sons.

Carrasco, R. M., Pedraza, J., Dominguez-Villar, D., Willenbring, J. K., & Villa, J. (2013). Supraglacial debris supply in the Cuerpo de Hombre paleoglacier (Spanish Central System): Reconstruction and interpretation of a rock avalanche event. *Geografiska Annaler Series a-Physical Geography*, *95*, 211–226.

Cogley, J. G., Hock, R., Rasmussen, L. A., Arendt, A. A., Bauder, A., Braithwaite, R. J., … Zemp, M. (2011). *Glossary of glacier mass balance and related terms*. (IHP-VII Technical Documents in Hydrology No. 86, IACS Contribution No. 2). Paris: UNESCO-IHP.

Cossart, E., Fort, M., Jomelli, V., & Grancher, D. (2006). Les variations glaciaires en Haute-Durance (Briançonnais, Hautes-Alpes) depuis la fin du xix e siècle: mise au point d'après les documents d'archives et la lichénométrie. *Quaternaire*, *17*, 75–92.

Deline, P., & Kirkbride, M. P. (2009). Rock avalanches on a glacier and morainic complex in Haut Val Ferret (Mont Blanc Massif, Italy). *Geomorphology*, *103*, 80–92.

Ecrins, P. N. D. (2005). Territoire Écrins – Les Cahiers Thematiques du Parc National: Les glaciers. *In:* Écrins, P. N. D. (ed.).

Goodsell, B., Hambrey, M. J., & Glasser, N. F. (2005). Debris transport in a temperate valley glacier: Haut Glacier d'Arolla, Valais, Switzerland. *Journal of Glaciology*, *51*, 139–146.

Hambrey, M. J., & Ehrmann, W. (2004). Modification of sediment characteristics during glacial transport in high-alpine catchments: Mount cook area, New Zealand. *Boreas*, *33*, 300–318.

Hambrey, M. J., Quincey, D. J., Glasser, N. F., Reynolds, J. M., Richardson, S. J., & Clemmens, S. (2008). Sedimentological, geomorphological and dynamic context of debris-mantled glaciers, Mount Everest (Sagarmatha) region, Nepal. *Quaternary Science Reviews*, *27*, 2361–2389.

Hewitt, K. (2009). Rock avalanches that travel onto glaciers and related developments, Karakoram Himalaya, Inner Asia. *Geomorphology*, *103*, 66–79.

Jacob, T., Wahr, J., Pfeffer, W. T., & Swenson, S. (2012). Recent contributions of glaciers and ice caps to sea level rise. *Nature*, *482*, 514–518.

Letreguilly, A., & Reynaud, L. (1989). Past and forecast fluctuations of glacier Blanc (French Alps). *Annals of Glaciology*, *13*, 159–163.

Mann, M. E. (2002). *Little ice age. Encyclopedia of global environmental change*. Chichester: John Wiley & Sons.

Marangunic, C. (1972). *Effects of a landslide on Sherman glacier*. Columbus, OH: Institute of Polar Studies.

Mount, N., & Stott, T. (2008). A discrete Bayesian network to investigate suspended sediment concentrations in an Alpine proglacial zone. *Hydrological Processes*, *22*, 3772–3784.

Nagai, H., Fujita, K., Nuimura, T., & Sakai, A. (2013). Southwest-facing slopes control the formation of debris-covered glaciers in the Bhutan Himalaya. *The Cryosphere*, *7*, 1303–1314.

Nye, J. F. (1973). *Water at the bed of a glacier. Hydrology of Glaciers*. Cambridge: IASH Publisher.

Otto, J.-C., & Smith, M. J. (2013). Geomorphological mapping. In L. Clarke (Ed.), *Geomorphological techniques* (Online Edition). London: British Society for Geomorphology.

Paul, F., Barrand, N. E., Baumann, S., Berthier, E., Bolch, T., Casey, K., … Winsvold, S. (2013). On the accuracy of glacier outlines derived from remote-sensing data. *Annals of Glaciology*, *54*, 171–182.

Qgis, D. T. (2014). *QGIS Geographic Information System* [Online]. http://www.qgis.org/ Open Source Geospatial Foundation Project. Retrieved June 9, 2015, from http://qgis.osgeo.org.

Rabatel, A., Dedieu, J. P., & Reynaud, L. (2002). Reconstitution des fluctuations du bilan de masse du Glacier Blanc (Massif des Écrins, France) entre 1985 et 2000, par télédétection optique (imagerie Spot et Landsat). *La Houille Blanche*, *6*, 64–71.

Rabatel, A., Dedieu, J. P., Thibert, E., Letreguilly, A., & Vincent, C. (2008). 25 years (1981–2005) of equilibrium-line altitude and mass-balance reconstruction on Glacier Blanc, French Alps, using remote-sensing methods and meteorological data. *Journal of Glaciology*, *54*, 307–314.

Rabatel, A., Letreguilly, A., Dedieu, J. P., & Eckert, N. (2013). Changes in glacier equilibrium-line altitude in the western Alps from 1984 to 2010: evaluation by remote sensing and modeling of the morpho-topographic and climate controls. *The Cryosphere*, *7*, 1455–1471.

Rau, F., Mauz, F., Vogt, S., Khalsa, S., & Raup, B. (2005). *Illustrated GLIMS glacier classification manual*, Version 1.0. GLIMS Regional Centre, 'Antarctic Peninsula', GLIMS (Global Land Ice Measurement from Space), NSIDC.

Reynaud, L., & Vincent, C. (2000). Relevés de fluctuations sur quelques glaciers des Alpes françaises. *La Houille Blanche*, *5*, 79–86.

Reynaud, L., & Vincent, C. (2002). Histoire des fluctuations des glaciers en remontant le Petit Age de Glace. *La Houille blanche*, *8*, 16–19.

Reznichenko, N., Davies, T., Shulmeister, J., & Mcsaveney, M. (2010). Effects of debris on ice-surface melting rates: an experimental study. *Journal of Glaciology*, *56*, 384–394.

Reznichenko, N. V., Davies, T. R. H., & Alexander, D. J. (2011). Effects of rock avalanches on glacier behaviour and moraine formation. *Geomorphology*, *132*, 327–338.

Reznichenko, N. V., Davies, T. R. H., Shulmeister, J., & Winkler, S. (2012). Influence of rock avalanches upon the formation of moraines and their subsequent palaeoclimatic interpretation: a critical appraisal. *Zeitschrift Fur Geomorphologie*, *56*, 37–54.

Sakai, A., Takeuchi, N., Fujita, K., & Nakawo, M. (2000, September 13–15). *Role of supraglacial ponds in the ablation process of a debris-covered glacier in the Nepal Himalayas*. Debris-covered Glaciers: Proceedings of an International Workshop Held at the University of Washington in Seattle, Washington, USA, IAHS, pp. 119–132.

Shugar, D. H., Rabus, B. T., Clague, J. J., & Capps, D. M. (2012). The response of black rapids Glacier, Alaska, to the Denali earthquake rock avalanches. *Journal of Geophysical Research-Earth Surface*, *117*, 1–14.

Shulmeister, J., Davies, T. R., Evans, D. J. A., Hyatt, O. M., & Tovar, D. S. (2009). Catastrophic landslides, glacier behaviour and moraine formation – a view from an active plate margin. *Quaternary Science Reviews*, *28*, 1085–1096.

Singh, V. P., Singh, P., & Haritashya, U. K. (2011). *Encyclopedia of snow, ice and glaciers*. Dordrecht: Springer.

Stott, T., & Mount, N. (2007). Alpine proglacial suspended sediment dynamics in warm and cool ablation seasons: Implications for global warming. *Journal of Hydrology*, *332*, 259–270.

Thibert, E., Faure, J., & Vincent, C. (2005). Bilans de masse du Glacier Blanc entre 1952, 1981 et 2002 obtenus par modèles numériques de terrain. *La Houille Blanche*, *2*, 72–78.

Tovar, D. S., Shulmeister, J., & Davies, T. R. (2008). Evidence for a landslide origin of New Zealand's waiho Loop moraine. *Nature Geoscience*, *1*, 524–526.

Vacco, D. A., Alley, R. B., & Pollard, D. (2010). Glacial advance and stagnation caused by rock avalanches. *Earth and Planetary Science Letters*, *294*, 123–130.

Vaughan, D. G. (1993). Relating the occurrence of crevasses to surface strain rates. *Journal of Glaciology*, *39*(132), 255–266.

Vivian, R. (1967a). Le glacier Blanc. *Revue de géographie alpine*, *55*, 729–732.

Vivian, R. (1967b). Le glacier Noir. *Revue de géographie alpine*, *55*, 733–736.

WGMS & NSIDC. ([1989] 2012). *World glacier inventory.* Compiled and made available by the World Glacier Monitoring Service, Zurich, Switzerland, and the National Snow and Ice Data Center, Boulder, CO.

Glaciological and geomorphological map of Glacier Noir and Glacier Blanc, French Alps

Pierre Lardeux
Neil Glasser
Tom Holt
Bryn Hubbard

Centre for Glaciology
Aberystwyth University
Wales, UK

Datum: RGF93
Projection: Lambert 93
Altitude Datum: NGF-IGN69

Glaciological features
- Glacier outline
- Debris cover
- Crevasses
- Nunatak and bare-rock areas

Geomorphological Features

Sediment Related
- Moraine Ridge (Formation)
- Gullying Area
- Scree Area
- Stabilised Scree Area
- Vegetated Scree Area
- Hummocky Terrain

Water Related
- Main Nye Channel
- Nye Channel Area
- Outwash Plain (Sandur)

Hydrological Features

Pond Related
- Meltwater Pond
- Pond Impact Area
- Snow-filled Pond
- Relict Pond
- Relict Pond Impact Area

Stream Related
- Supraglacial Meltwater Channel
- Stream

Anthropogenic Features
- Building
- Hiking Trail
- Road
- Parking Area

Background
- Photographs (direction)
- Altitude Point (m)
- Aretes
- Major Contour Line (500 m)
- Contour Line (100 m)

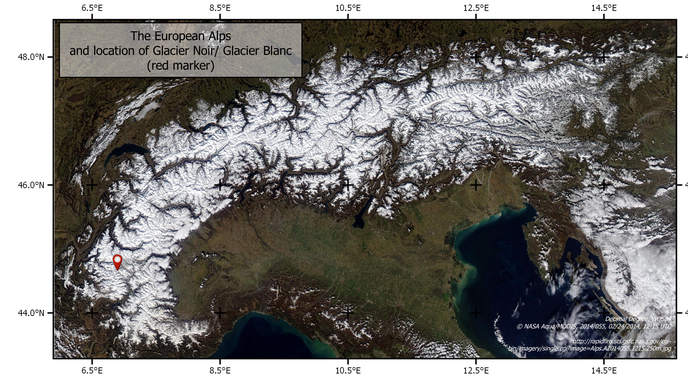

A: 1950's lateral moraine of Glacier Noir (dashed)

B: Meltwater pond and impact area (dashed), Glacier Noir

C: Crevassed area in the ablation zone, Glacier Blanc

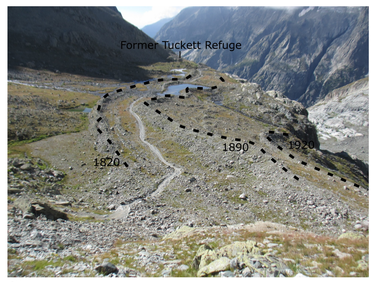

D: Lateral moraines (dashed) and decade of formation, Glacier Blanc

[II] – Fieldwork results

This appendix groups the first analysis of the results of most of the fieldwork measurements. No interpretation or discussion is provided as these results are presented only for informational purposes. Only the results where I processed the data myself are shown here.

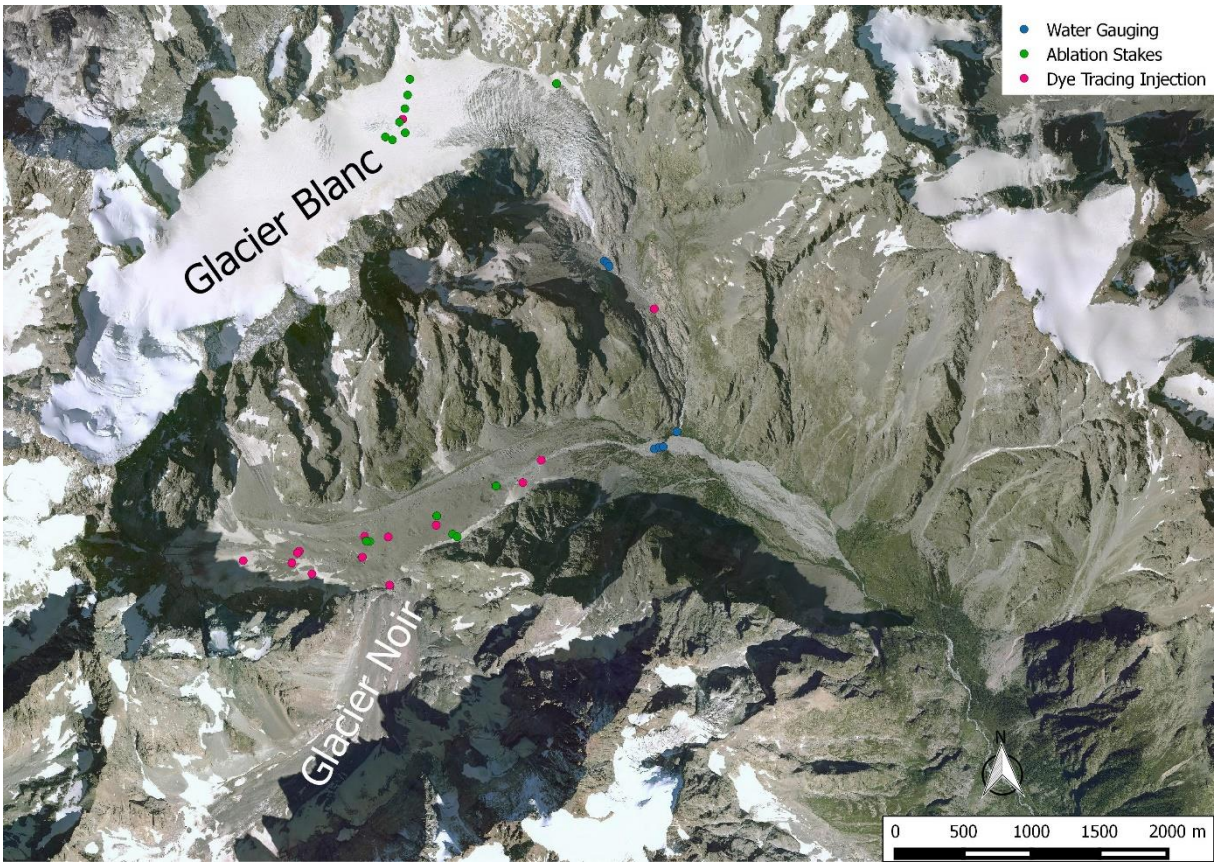

Appendix II – Figure 1: Location of the different fieldwork measurements.

Debris thickness

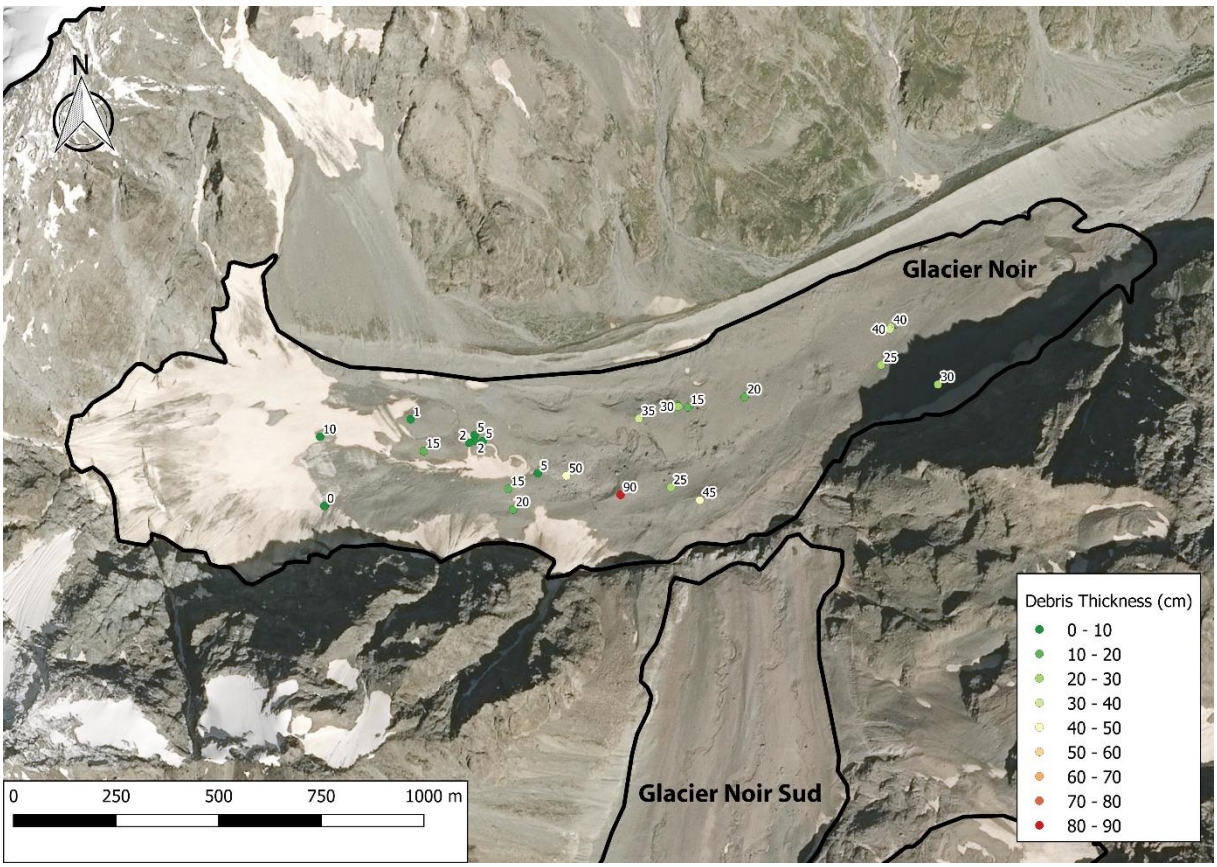

Appendix II – Figure 2: Debris thickness on Glacier in August / September 2014. *See Chapter 4 – page 97 for measuring technique. Background image: Spot 6, Summer 2014.*

Temperature

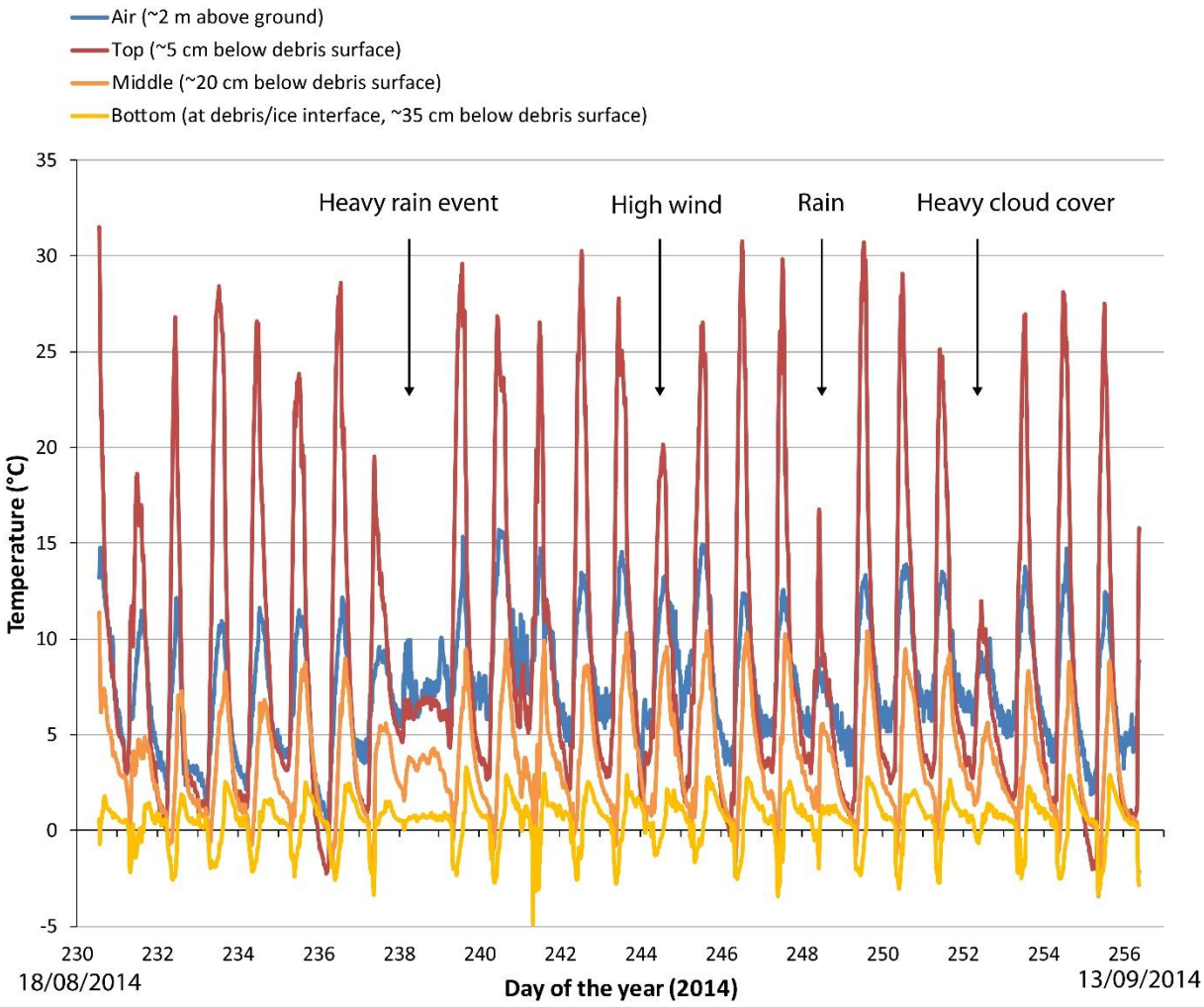

Appendix II – Figure 3: Temperature recorded at 4 different levels between 18/08/2014 and 13/09/2014.

Ablation stakes

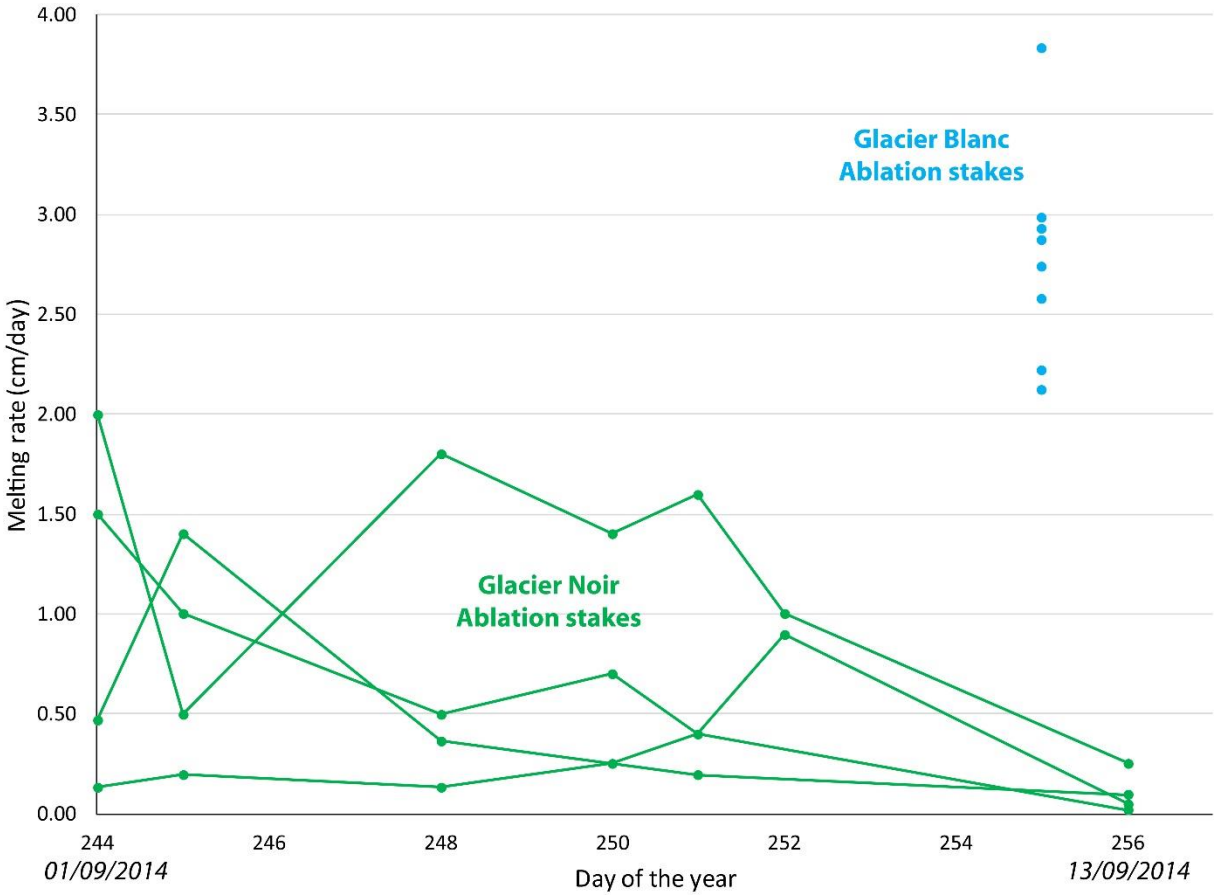

Appendix II – Figure 4: Melting rate for Glacier Noir and Glacier Blanc. *Only the period when the measurements have been verified is shown here. Ablation stakes on Glacier Blanc have been measured only twice, explaining the sole data point. Glacier Blanc shows a melting rate 2-4 times higher than Glacier Noir.*

Discharge, Electrical conductivity, Suspended sediment concentration

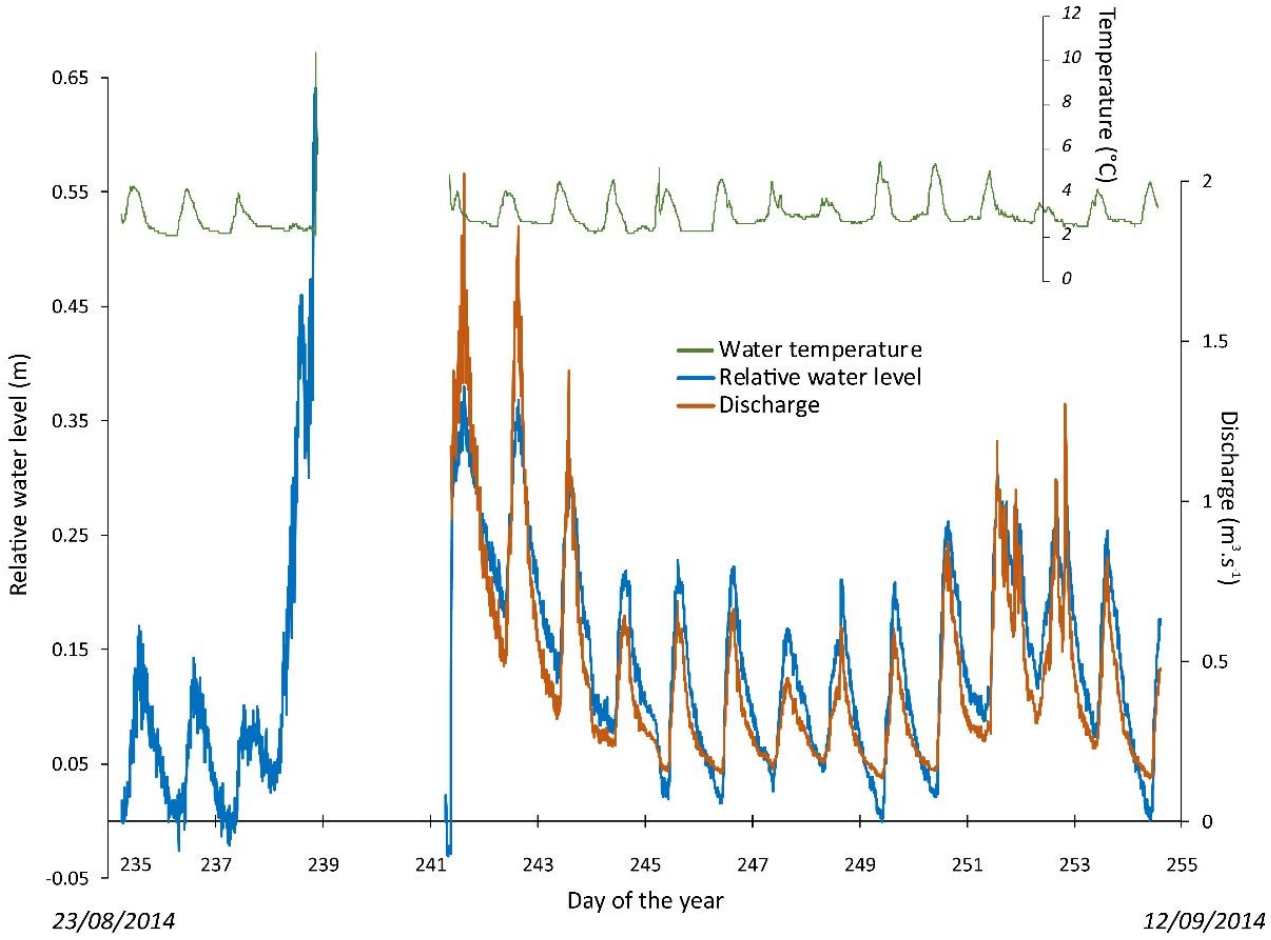

Appendix II – Figure 5: Relative water level, discharge and water temperature of the Glacier Noir proglacial stream*. All time-series were interrupted during a heavy rain event, which destroyed the gauging station. Before the gauging station destruction, the water level was more than 70 cm higher than the lowest level recorded.*

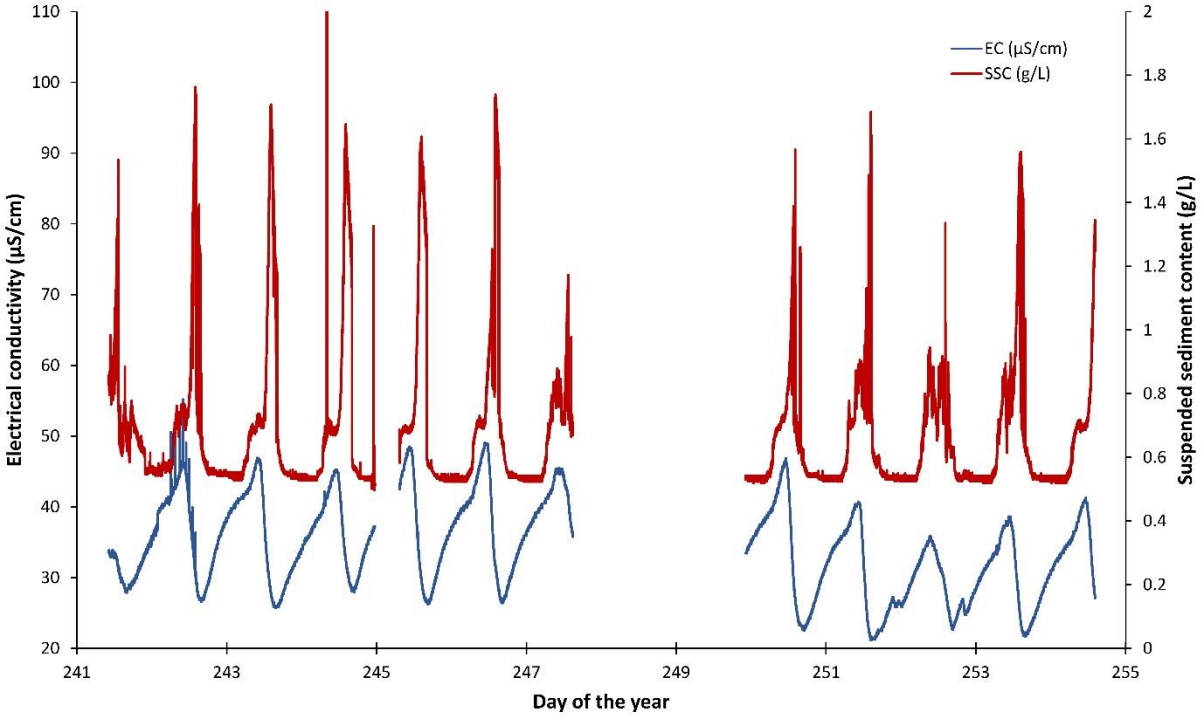

Appendix II – Figure 6: Electrical conductivity and suspended sediment content for a Glacier Noir proglacial stream. *Both time-series were interrupted during a sensor failure. The recording started after the heavy rain event, as before that the readings were extremely noisy.*

[III] – Early modelling results

In the early stages of the project, modelling was considered as a viable tool to compare Glacier Noir and Glacier Blanc. However, after the first results, presented hereafter, and the disappearance of support for the 2.5D model (Figure 2), this part of the project was discontinued.

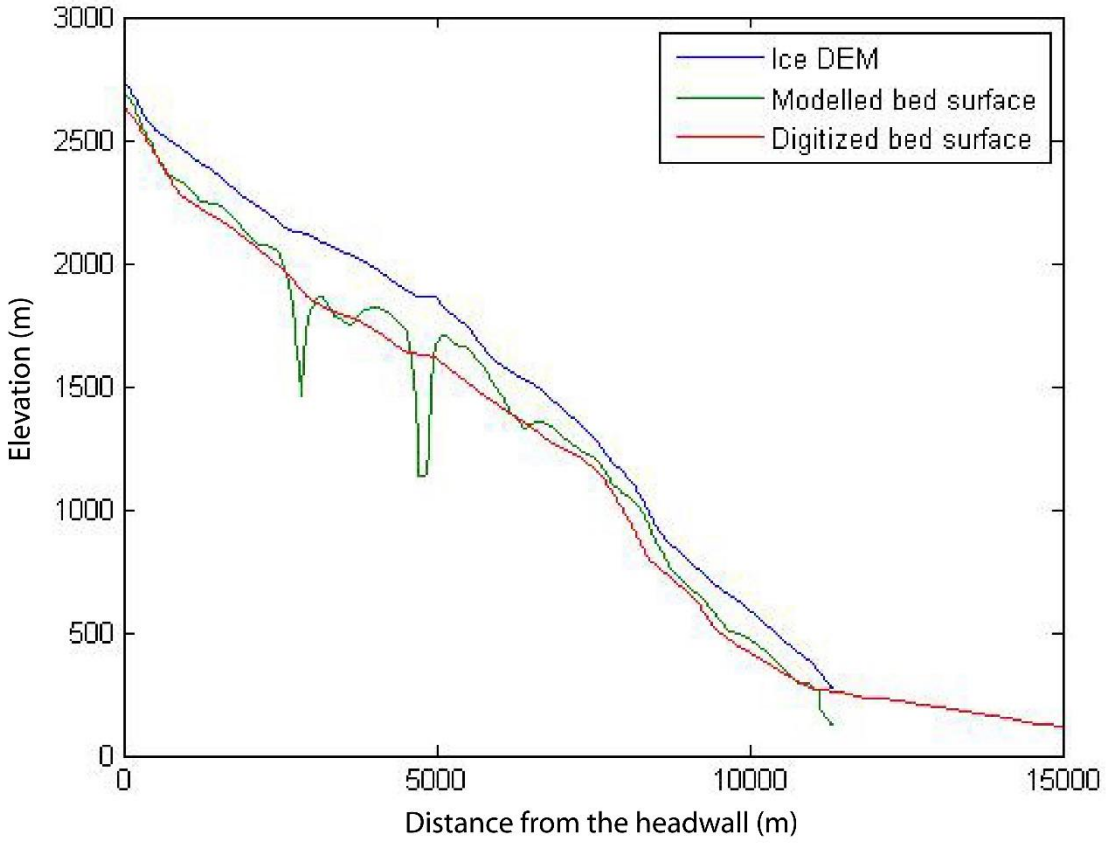

Appendix III – Figure 1: 2D model results. *To test the feasibility of a 2D model using the perfect plasticity principle, we used the study by Alexander et. Al. (2011)[1] on the Franz Joseph Glacier, New Zealand. The blue line is the ice surface as describe in the article, the red line is the bedrock surface and the green line is our modelled bedrock surface. A threshold angle was introduced in the model to prevent minus infinity elevation for the bedrock when the ice surface is close to the horizontal. However, some problems subsisted.*

[1] ALEXANDER, D. J., DAVIES, T. R. & SHULMEISTER, J. 2011. A Steady-State Mass-Balance Model for the Franz Josef Glacier, New Zealand: Testing and Application. *Geografiska Annaler Series a-Physical Geography,* 93A**,** 41-54.

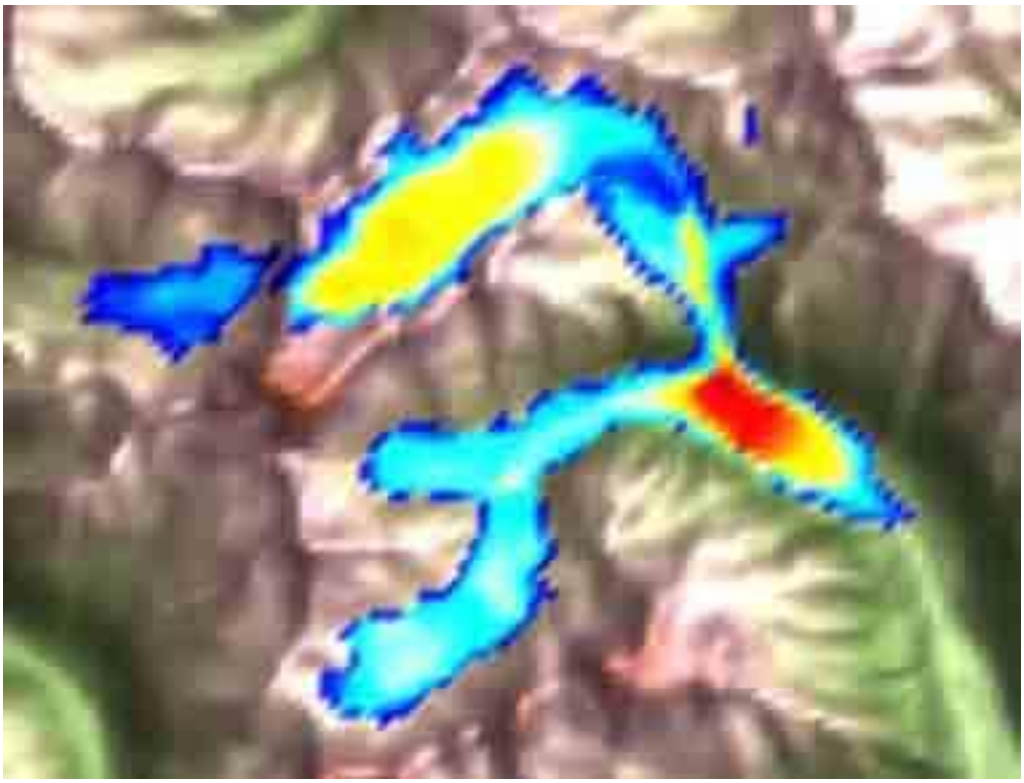

Appendix III – Figure 2: 2.5D model results. *Using the iSOSIA model*[2] *with the default parameter, we succeeded to have Glacier Noir and Glacier Blanc grow at the same time with a resolution of 100 m over 200 year only. Multiple problems appear: it was impossible to stop the common front to advance endlessly and the poor resolution combined with an over-estimation of the ice thickness of Glacier Blanc, made the glacier flow in another valley.*

[2] EGHOLM, D. L., KNUDSEN, M. F., CLARK, C. D. & LESEMANN, J. E. 2011. Modeling the flow of glaciers in steep terrains: The integrated second-order shallow ice approximation (iSOSIA). *Journal of Geophysical Research: Earth Surface (2003–2012),* 116.